Optimization of refinery preheat trains undergoing fouling: control, cleaning scheduling, retrofit and their integration

By:

Federico Lozano Santamaría

A thesis submitted for the degree of *Doctor of Philosophy* in Chemical Engineering

Imperial College London

Department of Chemical Engineering

June 2020

Declaration of originality

This is to certify that the content presented in this thesis is the product of work of the author carried out in the Department of Chemical Engineering at Imperial College London between October 2016 and March 2020. This thesis, or parts of it, have not been submitted for a degree in any other university.

Federico Lozano Santamaría

Copyright declaration

Acknowledgements

First, I would like to express my sincere gratitude to my supervisor, Professor Sandro Macchietto, for his guidance and support during these years. I greatly appreciate the independence and many opportunities he granted me as well as the insights on conducting and applying top research.

I also want to thank Dr. Francesco Coletti and Dr. Emilio Dias-Bejarano for the very fruitful discussions, the practical inputs on industrial perspective of various projects and for welcoming in Hexxcell ltd for a short internship.

Many thanks to my friends in London and those back home in Colombia for their constant support and all the good times.

Finally, I want to express my gratitude to my girlfriend, Giorgia, my mom, Nhora, and my grandparents for always believing in me. This thesis would not have been possible without your constant and unconditional support.

Abstract

Crude refining is one of the most energy intensive industrial operations. The large amounts of crude processed, various sources of inefficiencies and tight profit margins promote improving energy recovery. The preheat train, a large heat exchanger network, partially recovers the energy of distillation products to heat the crude, but it suffers of the deposition of material over time – fouling – deteriorating its performance. This increases the operating cost, fuel consumption, carbon emissions and may reduce the production rate of the refinery.

Fouling mitigation in the preheat train is essential for a profitable long term operation of the refinery. It aims to increase energy savings, and to reduce operating costs and carbon emissions. Current alternatives to mitigate fouling are based on heuristic approaches that oversimplify the representation of the phenomena and ignore many important interactions in the system, hence they fail to fully achieve the potential energy savings. On the other hand, predictive first principle models and mathematical programming offer a comprehensive way to mitigate fouling and optimize the performance of preheat trains overcoming previous limitations.

In this thesis, a novel modelling and optimization framework for heat exchanger networks under fouling is proposed, and it is based on fundamental principles. The models developed were validated against plant data and other benchmark models, and they can predict with confidence the main effect of operating variables on the hydraulic and thermal performance of the exchangers and those of the network.

The optimization of the preheat train, an MINLP problem, aims to minimize the operating cost by: 1) dynamic flow distribution control, 2) cleaning scheduling and 3) network retrofit. The framework developed allows considering these decisions individually or simultaneously, although it is demonstrated that an integrated approach exploits the synergies among decision levels and can reduce further the operating cost. An efficient formulation of the model disjunctions and time representation are developed for this optimization problem, as well as efficient solution strategies. To handle the combinatorial nature of the problem and the many binary decisions, a reformulation using complementarity

constraints is proposed. Various realistic case studies are used to demonstrate the general applicability and benefits of the modelling and optimization framework. This is the first time that first principle predictive models are used to optimize various types of decisions simultaneously in industrial size heat exchanger networks.

The optimization framework developed is taken further to an online application in a feedback loop. A multi-loop NMPC approach is designed to optimize the flow distribution and cleaning scheduling of preheat trains over two different time scales. Within this approach, dynamic parameter estimation problems are solved at frequent intervals to update the model parameters and cope with variability and uncertainty, while predictive first principle models are used to optimize the performance of the network over a future horizon. Applying this multi-loop optimization approach to a case study of a real refinery demonstrates the importance of considering process variability on deciding about optimal fouling mitigation approaches. Uncertainty and variability have been ignored in all previous model based fouling mitigation strategies, and this novel multi-loop NMPC approach offers a solution to it so that the economic savings are enhanced.

In conclusion, the models and optimization algorithms developed in this thesis have the potential to reduce the operating cost and carbon emission of refining operations by mitigating fouling. They are based on accurate models and deterministic optimization that overcome the limitations of previous applications such as poor predictability, ignoring variability and dynamics, ignoring interactions in the system, and using inappropriate tools for decision making.

Contents

List of figures

List of tables

Nomenclature

Symbols

Symbol	Units	Description
A	m^2	Cross sectional area
C	-	Matrix used in heuristics to define arrangement of HEX to clean simultaneously
Cp	kJ/kgK	Specific heat capacity
d	mm	Outer tube diameter
d_I	mm	Inner tube diameter
dir	-	Variable indicating the axial direction of the flow
E	J/mol	Activation energy
f	-	Fanning friction factor
F_M	-	Price correction factor due to material
F_P	-	Price correction factor due to pressure
F_{CEPCI}	-	Price correction factor to date – CEPCI index ratio
G	kg/m^2s	Mass flux
h	W/m^2K	Convective heat transfer coefficient
HTA	m^2	Heat transfer area
I	-	Schedule instability
k	day^{-1}	Frequency factor in ageing kinetics
l	-	Terminal cost or penalty in the objective function of MPC
L	m	Tube length
m	kg/s	Mass flow rate
N_D	-	Number of time discrete points (columns) in a schedule representation
N_U	-	Number of units (rows) in a schedule representation
N_0	-	Number of variables in a parameter estimation problem
N_{HEX}	-	Maximum number of cleanings per exchanger over the time horizon
N_m	-	Number of measurements of a variable
N_T	-	Number of tubes / Maximum number of simultaneous cleanings
N_P	-	Number of tube passes / Number of periods
N_z	-	Number of periods in the FPH to freeze scheduling decisions
NTU	-	Number of transfer units
p	m	Wet perimeter in tube or shell
P	-	Effectiveness factor of a heat exchanger

P	bar	Pressure
P_ϵ	$	Threshold in heuristics to define cleanings based on potential savings
P_{cap}	$	Capital cost of a heat exchanger
P_f	$/MW	Cost of fuel burnt in the furnace
P_{CO}	$/ton	Cost of carbon emissions
P_{cl}	$	Cost of cleaning actions
P_m	$/kg	Profit per crude processed
P_{tube}	$	Cost of a single tube - $ 25/m
P_{x-HTA}	$	Area retrofit cost
Pr	-	Prandtl number
q	W/m^2	Heat flux
Q	MW	Heat duty
$\hat{Q}$	MW	Approximation of heat duty as an explicit function of time
r	m	Radial direction
$\tilde{r}$	-	Dimensionless radial direction
R	J/molK	Universal gas constant
Rc	-	Ratio of heat capacities tube:shell
Re	-	Reynolds number
R_f	m^{2}K/W	Fouling thermal resistance
s	-	Slack variable
s_x	-	Split fraction
t	day	Time
t^*	day	Current time of the operation
$\bar{t}$	-	Dimensionless time [0, 1]
t_{EH}	day	Estimation horizon for parameter estimation
T	K	Temperature
u	m/s / -	Flow velocity / Manipulated variable in a MPC scheme
U	W/m^{2}K	Overall heat transfer coefficient
v	-	Parameters to be estimated in a parameter estimation problem
V	-	Running cost in the MPC objective function
x	-	Mass fraction composition in the deposit layer / any continuous variable
x_r	-	Heat exchanger area retrofit variable
$\tilde{x}$	-	Measured variable
y	-	Binary variable for cleanings {0, 1}
y_I	-	Binary variables used in a general representation of scheduling problems {0, 1}
y_r	-	Binary variable for heat exchanger retrofit {0, 1}

Y	-	Logic variable {TRUE, FALSE}
z	- / m	Binary variable for the overall state of a period / Axial direction

Greek letters

Symbol	Units	Description
α	m^2K/J	Deposition constant in Ebert-Panchal model
β	-	Duration of a cleaning action in a discrete time representation
γ	m^5K/J^2	Removal constant in Ebert-Panchal model
δ	mm	Deposit thickness
ε	-	Tolerance
ϵ	mm	Deposit roughness – Friction factor calculation
ΔP	bar	Tube side pressure drop
η	-	Efficiency of heat transfer
λ	W/mK	Thermal conductivity
μ	Pa.s / -	Viscosity / Mean
π	-	Irrational number (3.14159)
ρ	kg/m^3 / -	Density / Penalty parameter in an objective function
σ	-	Standard deviation
τ	Pa	Shear stress on the tube side
φ	-	Complementarity function between two variables
T	day	Length of a time period
T^*	day	Update interval – sampling time of a control loop
T_{cl}	day	Cleaning time

Subscripts

Symbol	Description
C	Control feedback loop
f	Variable of the furnace / Referring to a fouling variable / Final time
i	Index in a set referring to nodes
in	Variable evaluated at inlet conditions
j	Index in a set referring to nodes
k	Index in a set referring to streams
l	Index in a set referring to nodes
out	Variable evaluated at outlet conditions
ov	Related to overall schedule instability

ovw	Related to time weighted overall schedule instability
r	Related to a retrofit variable
sch	Related to the evaluation (optimization) of schedules in an online approach
S	Scheduling feedback loop
t	Index in a set referring to discrete time
ts	Related to task timing schedule instability
T	Related to task allocation schedule instability

Superscripts

Symbol	Description
0	Inlet condition of a source node in a network / Initial condition / Cleaned conditions
a	Variable evaluated at the aged deposit or ageing kinetics
aw	Variable evaluated at the interface between the aged deposit and the inner tube wall
B	Variable evaluated at the bypass streams
D	Variable evaluated at the deposit (continuous domain)
f	Variable evaluated at the fresh deposit
fa	Variable evaluated at the interface between the fresh deposit and the aged deposit
F	Variable evaluated at the internal tube wall (flow) conditions of an exchanger
LB	Lower bound
S	Variable evaluated at the shell side of an exchanger
tf	Variable evaluated at the interface between the tube side and the fresh deposit
T	Variable evaluated at the tube side of an exchanger
UB	Upper bound
W	Variable evaluated at the external tube wall conditions of an exchanger
ws	Variable evaluated at the interface between the outer tube wall and the shell side

Acronyms

Symbol	Description
A	Arcs / Set of arcs in a network
AAE	Absolute average error
CDU	Crude distillation unit
CFD	Computational fluid dynamics
DAE	Differential algebraic equations
DEA	Data envelop analysis
FPH	Future prediction horizon

HEN	Heat exchanger network(s)
HEX	Heat exchanger / Set of heat exchangers
HTA	Heat transfer area
LMTD	Logarithm mean temperature difference
MHE	Moving horizon estimator
MINLP	Mixed integer nonlinear program
Mx	Mixer node / Set of mixer nodes
N	Set of all nodes in a network
NM	No mitigation operation strategy for HEN. No cleanings and constant flow splits
NMPC	Nonlinear model predictive control
NLP	Nonlinear program
NTU	Number of transfer units
OT-FPH	Overlapping time of the future prediction horizons of two consecutive schedule evaluations
PEH	Past estimation horizon
PDAE	Partial differential algebraic equations
PC	Principal component in PLS method
PLS	Partial least squares
RHS	Right hand side of an equation or constraint
S	Set of streams in a network
SCH	Optimal cleaning scheduling solution for a HEN under fouling
SE	Set of schedule evaluations over the operating time
Si	Sink node / Set of sink nodes
So	Source node / Set of source nodes
Sp	Splitter node / Set of splitter nodes
T	Set of discrete time points independent of the discretization approach

Chapter 1

Introduction

The energy sector is undergoing a shift from traditional fossil fuels to highly efficient, low carbon emission and sustainable alternatives. The focus has been driven to a more energy efficient operation of energy intensive industries, such as refining and chemical, because of stringent environmental policies, a competitive market, and tighter production margins (Coletti et al. 2015). Industry accounts for approximately 40% of energy use in the world and refinery operations represents almost 10% of it. Refinery is one of the most energy intensive operations and it produces carbon emissions that represents 12% of the total man-made emissions (U.S. Energy Information Administration 2016; International Panel on Climate Change IPCC 2014). The high impact of this industry on the economy and environment has motivated intensive research on how to reduce the energy demand, and how to make refinery operations more efficient. Making refinery processes more energy efficient helps to reduce carbon emissions and energy consumption, and to increase the process profitability of the operation. For instance, an increase of 1.0 MW in the duty of a furnace in a small refinery processing 100 kbbl / year represents an increase of 90 tons CO_2 emitted per year and an additional cost of $300.000 USD / year– assuming average cost of 2017 for fuel, and standard carbon and energy content (Nategh, Malayeri, and Mahdiyar 2017; Abdul-Manan, Arfaj, and Babiker 2017). Most of the additional costs due to energy inefficiencies in a refinery come from the operation of the preheat train and crude distillation unit (CDU).

All crude processed in a refinery must go through the CDU where the different cuts, such as lights olefins, naphtha, diesel, and gas oil, are obtained. Because of the high energy demand of operating the CDU, the energy of its products – hot streams – is partially recovered in the preheat train – large heat exchanger network – where they heat up the crude stream from storage conditions up to 350°C – 370°C. The large flow rates of crude and the high temperatures of the operation make the preheat train a key section for improving the overall

energy efficiency and profitability of the refinery as it can recover up to 70% of the energy contained in product streams of the CDU (Panchal 2000). The preheat train is divided in three sections according to the temperature ranges at which crude is processed: cold end, intermediate section, and hot end. A desalter is usually located after the cold end to remove the inorganic material in the crude, and a flash drum before the hot end to remove the light components and ensure that a saturated liquid enters the CDU. Also, a furnace after the hot end supplies the extra energy necessary to satisfy a constant inlet temperature to the CDU. When the efficiency of the preheat train decreases, the duty of this furnace increases to compensate for the energy lost, which increases the operating cost and the carbon emissions of the refinery.

The deposition of unwanted material – fouling – in process surfaces reduces the heat transfer efficiency, and it is almost ubiquitous to all heat transfer operations (Coletti and Hewitt 2015). Refining operations, and specially the preheat train, are dramatically affected by crude oil fouling due to the high temperatures at which crude is processed, the high energy demand of the operation, and the varying composition of crude oil. Crude oil fouling is not yet well and fully understood, but it is known that it can be caused by the presence of impurities in the crude oil, thermal decomposition, and oxidation reactions of fuel oil constituents (Diaby et al. 2012; Coletti, Crittenden, and Macchietto 2015). For instance, the presence and concentration of asphaltenes in the crude has been associated with its fouling propensity and deposition rates (Yang et al. 2015; Ho 2016a). Contrary to the crude oil fouling mechanisms, its effect and consequences are well known in the operation of refineries and preheat trains. The two main consequences of fouling are: reduction of the heat transfer rate as an additional thermal resistance is built in the heat exchanger – thermal impact – and increment of the pressure drop due to partial blockage of the flow area – hydraulic impact. Both have important economic implications in the operation of preheat trains such as:

- Capital cost: when fouling is considered at the design stage of heat exchangers following TEMA guidelines, the actual heat transfer area is ~30% higher than the one required (TEMA 2007), although this approach ignores the dynamics of fouling and assume a unique and constant fouling resistance for the worst case scenario. Other capital costs arise from exploring retrofit options such as the use of tube inserts, heat transfer enhancement technology, or modifying the network

structure (Nguyen et al. 2010; Tjoe and Linnhoff 1986). Most of these decisions are often still made based on practical observations and ignore the fouling mechanisms and dynamics.

- Fuel and energy cost: burning extra fuel in a furnace or boiler or using more electricity for pumping to compensate the effects of fouling leads to additional operational cost that, considering a global perspective, may represent 1% to 5% of the energy consumed by the industrial sector (Muller-Steinhagen and Zettler 2011; Sheikh et al. 2000).
- Maintenance cost: during the operation of preheat trains it is common to schedule maintenance actions – cleanings – to recover partially or completely the thermo-hydraulic performance of key units. While units are taken out of service the energy recovery capacity of the preheat train drops increasing the energy cost. There is also a maintenance cost – due to chemicals, utilities, commissioning – which is case dependent, based on the size of the exchanger, the degree of fouling, and the type of cleaning (Lachas-Fuentes 2015).
- Production loss cost: when operational constraints are reached, like the furnace firing limit or the maximum pressure drop, the CDU throughput is reduced or in drastic cases an unplanned shut-down is necessary. This leads to a significant reduction of the production rate and, depending on the length of this low production period, the production loss cost may represent 60% of the total cost associated with fouling (Muller-Steinhagen and Zettler 2011; Coletti and Macchietto 2011).

Alternatives for fouling mitigation in refining operations are needed and of major importance to reduce the operational cost, increase energy efficiency, and reduce carbon emissions. Mitigation strategies can be broadly classified as proactive strategies, which aim is to reduce the consequence of fouling before it happens such as the use of antifoulant agents (Ho 2016a) or tube inserts (Muller-Steinhagen and Zettler 2011); or reactive strategies, which aim is to restore the efficiency of the heat exchangers after fouling has occurred, such as periodic cleanings, network retrofit, or flow control. There is a great potential in using predictive models, which provide a good understanding of the physical and chemical

phenomena of heat exchange and fouling for analysing, monitoring and provide insights of the operation considering all interactions, trade-offs and long term effects on the system.

This thesis focuses on the model based optimization of preheat trains under fouling using mathematical programming as the tool to define fouling mitigation strategies including flow control, network retrofit, and cleaning scheduling. It aims to provide efficient and practical solutions to the problem of fouling in preheat trains so that carbon emissions are reduced, and energy efficiency increased. This works builds on previous research done at Imperial College on modelling heat exchangers networks under fouling to analyse their performance and suggest fouling mitigation actions from different perspectives (Georgiadis, Rotstein, and Macchietto 1998; Coletti and Macchietto 2011; Diaz-Bejarano, Coletti, and Macchietto 2016).

1.1. Motivation and objectives

A model based solution for the operation of preheat trains under fouling should be able to: i) represent accurately the thermal and hydraulic behaviour of heat exchangers and their interactions in a network, ii) capture the fouling dynamics and how it is affected by the main operating variables of each unit, iii) predict the effect of various fouling mitigation alternatives on the thermo-hydraulic performance of the network, iv) quantify all elements of the operating cost of the preheat train, v) cope with process variability and disturbances, and vi) provide optimal operating conditions and fouling mitigation actions that are feasible in the long term operation. This ideal solution allows to automate optimal decisions regarding fouling mitigation in preheat trains considering all interactions, synergies, trade offs, and dynamic effects over long periods of operations. These features are desirable from a practical perspective, but there is no a single platform or approach that is successful in all of them.

Heat exchanger models used for this purpose can range from simple heat transfer calculations – LMTD – to complex CFD simulations. Each captures different time and length scales of the heat transfer process. Similarly, to model crude oil fouling, completely empirical models that ignore the effect of operating conditions have been proposed, as well as phenomenological models that accounts for the effects of interfacial mass transfer, particle diameter, and crude composition. In the context of providing optimization based solutions to the problem of crude oil fouling, it is necessary to find the right balance between model

complexity and model accuracy so they are suitable for optimization purposes – this is understood as models that can be solved in a reasonable computational time with standard computational power – and their solution represents the actual behaviour observed. Hence, modelling approaches such as CFD for the flow distribution inside heat exchangers, or molecular dynamics for the force interactions that lead to crude deposition are very challenging to include in a deterministic optimization framework, although they can provide great details on the local phenomena.

On the other side of the spectrum, optimization based approaches that have been used for the operation and cleaning scheduling of preheat trains typically rely on simplified models whose accuracy is questionable. For instance, using completely empirical models for the deposition rate and linearized models for the heat exchangers define a MILP formulation that can be easily solved with current commercial solvers, but its solution may not reflect the economic benefits claimed or may even be infeasible. In that case, the predicted models used ignore the effect of operating conditions in various phenomena, and their applicability is restricted around a nominal operating point and short periods of operation (Diaby et al. 2012). More accurate and representative models for the heat exchangers and fouling can be included in the problem formulation, but the resulting optimization problem, an MINLP, may require alternative solution strategies –different from those used in commercially available solvers such as branch and bound or outer approximation. Nevertheless, those approaches have only considered one fouling mitigation option at a time so they either deal with the flow distribution problem, the cleaning scheduling problem, or the network retrofit problem. A holistic and comprehensive approach is better so that the synergies among the different fouling mitigation alternatives are exploited to maximize energy recovery. Here the challenge is to efficiently solve a mathematical programming problem that defines multiple fouling mitigation strategies – flow distribution, cleaning schedule, network retrofit – over long periods of operation for preheat trains under fouling using an accurate representation of the units and their interactions.

An important aspect that is usually ignored during the optimization of the preheat train, is the variability of the operation. Most of the current optimization approaches assume constant operating conditions over long operating periods – from 1 to 5 years. In refineries the crude flow rates, crude blends, and operating conditions change dynamically at high

frequency, almost daily, reacting to changes in market conditions, demand, and availability of crude. This dynamic behaviour has an important effect on the efficiency and performance of the preheat train because changes in flow rates affect the deposition rates, and different blends have different fouling propensity. For example, refineries that process heavy crudes and that have a high yield of heavy products tends to be more efficient and have lower carbon emissions than those that process light crude because the unit operations are less energy intensive (Han et al. 2015). Also, changes in the crude blends processed can promote deposition, inhibit it, or contribute to removal of existing deposit (Wiehe and Kennedy 2000). Accounting for the effect of process variability and uncertainty enhance the optimal decisions regarding fouling mitigation in preheat trains because it improves the accuracy of the predictive model, and those actions react to the observed changes in the operation to maximize the energy recovery.

This thesis aims to develop a deterministic optimization framework that overcomes the pitfalls faced by previous approaches. In this way, an accurate representation of the preheat train under fouling among various time scales is used to minimize the operating cost, considering dynamic flow distribution, cleaning scheduling, and network retrofit simultaneously, and under variable operating conditions. The time scales of the problem range from hours and days for the flow distribution, to months and years for the cleaning scheduling and network retrofit. Specific objectives of this work are:

1. To develop accurate predictive models based on first principles that are suitable for optimising the operation, cleaning scheduling, and retrofit of HEN under fouling in off-line and on-line applications.
2. To develop efficient algorithms and solution strategies for the large scale MINLP problems that arise from the formulation of the integrated – and individual – optimal control, cleaning scheduling, and/or retrofit problems of HEN under fouling.
3. To develop an online fouling mitigation methodology able to optimally determine the HEN operation and its cleaning schedule, while updating the prediction models based on current and past data to monitor the operation, and ensuring closed loop stability. Note that because of the time scale of fouling which is a slow process,

what is defined as an online or real-time application in this case correspond to one with updates in the order of hours or days.

4. To demonstrate the benefits and validate the application of optimization based fouling mitigation strategies using the models and algorithms developed in real refinery applications.

This thesis focuses on crude oil fouling and its mitigation in the operation of the preheat train, although most of the contributions presented here can be extended to other types of fouling in heat transfer applications. For instance, fouling due to protein denaturation and aggregation is a major problem in milk pasteurization processes, and daily cleanings are necessary to maintain the desired operating conditions (Prakash, Kravchuk, and Deeth 2015; Georgiadis, Papageorgiou, and Macchietto 2000). Fouling is also an important source of inefficiencies in the power generation industry, cosmetic industry, food industry and in some chemical facilities (Chen et al. 2017; Laouini et al. 2014). Therefore, the findings presented in this thesis can be extrapolated to provide model based and optimization solutions to the fouling problem in those applications.

1.2. Thesis structure

Chapter 2 presents a literature review of modelling approaches for heat exchangers and fouling in crude oil preheat trains, the various formulation of optimization problems related to fouling mitigation, model simplifications, and solution strategies covering from heuristic approaches to deterministic optimization.

In Chapter 3, a general and rigorous mathematical formulation for optimizing HEN under fouling is developed. It uses a radially distributed first principle model for the exchangers, and a semi empirical model for the deposition rate. Various time discretization approaches are proposed, and their performance evaluated. The main complicating factors of solving the associated MINLP optimization problem are identified, and the simultaneous optimal cleaning schedule and flow distribution is defined for realistic case studies under a wide range of operating conditions, constraints and limitations in the operation.

The formulation developed is validated in Chapter 4 against a more rigorous and previously validated model of HEN under fouling. A set of case studies, including a total of 37 exchangers, is used for validation under clean conditions and under dynamic operation.

In addition, a parameter estimation and model validation approaches are developed to determine the optimal set of parameters that make the two modelling approaches equivalent in terms of predicting the overall performance of the system. Finally, actual measurements from a refinery are used to validate the model developed, and to test the validation approach.

In Chapter 5, an efficient solution strategy is presented for the large scale combinatorial MINLP problem associated with the optimal cleaning scheduling and flow distribution of HEN under fouling. The theoretical framework of a mathematical reformulation, its assumptions and limitations are presented. Several case studies are used to demonstrate the validity of the reformulation approach, its computational advantages and its impact on the economics of the process.

In Chapter 6, the formulation presented is expanded to include retrofit decisions. Heat transfer area and network retrofit decisions are included in the problem formulation which make it more complex, but they are represented in a way that the solution strategy proposed in Chapter 5 is still effective. Its application to realistic case studies demonstrates the important trade-off and interactions among the three fouling mitigation alternatives considering capital cost in the operation of the network.

Chapter 7 introduces process variability, uncertainty and disturbances in the optimization of preheat trains. It develops an online optimization approach based on two MHE/NMPC loops to cope with different time scales and fouling mitigation decisions occurring at those scales – flow distribution for short time scales, and integration of flow distribution and cleaning scheduling for long time scales. A realistic case study is used to demonstrate the advantages of this approach when the preheat train operates dynamically, under large disturbance in the inputs, and the prediction models are not perfect.

Chapter 8 deals with the issue of closed loop scheduling stability which is a practical problem that arise in online implementations. In this chapter novel and general measurements to quantify closed loop schedule instability are developed, and alternative to reduce it without compromising the closed loop performance are evaluated. The trade-offs between closed loop performance – operational cost – and closed loop schedule stability are analysed in two realistic case studies, one under nominal operating conditions and other under variable and uncertain conditions.

Chapter 9 presents the main conclusions and findings of this thesis. It also presents recommendations and future directions of research.

Table 1.1. Descriptions and abbreviations for the different solution strategies and cases considered in this thesis for HEN under fouling.

Short notation(s)	**Description**	**Optimization variables**			
		Scheduling	**Flow control**	**Network retrofit**	**Area retrofit**
NM	No mitigation. There are no cleanings and the flow in all parallel branches of the network is constant	X	X	X	X
SCH Opt. Sch Opt. S	Optimal cleaning scheduling. The only decision variables are those associated with the cleaning schedule (cleaning time and cleaning sequence). The flow distribution in the network is constant	O	X	X	X
SP Opt. Sp Opt. C	Optimal flow distribution. The only decision variables are the dynamic flow rates through the network. There are no cleanings.	X	O	X	X
Seq. Opt Opt SCH → Sp	Sequential optimization of the cleaning scheduling and dynamic flow distribution in the network. First the cleaning schedule is optimized with constant flow rates (constant at 50% for all parallel branches), and then the dynamic flow distribution is optimized for that cleaning schedule.	O	O	X	X
Opt. Sp + Sch Opt. C + S	Simultaneous optimization of the dynamic flow distribution and the cleaning schedule.	O	O	X	X
HEN Retrofit	Optimal network retrofit. Optimal allocation or removal of exchangers in a network without any fouling mitigation actions.	X	X	O	X
HEN Retrofit + SCH	Optimal network retrofit and fouling mitigation. Optimal allocation or removal of exchangers in a network considering optimal cleanings and optimal dynamic flow distribution in the time horizon.	O	O	O	X
HEN-HTA Retrofit	Optimal network and heat exchanger area retrofit. Optimal allocation or removal of exchangers in a network, and retrofit of their heat transfer area without any fouling mitigation actions.	X	X	O	O
HEN-HTA Retrofit + SCH	Optimal network and heat exchanger area retrofit and fouling mitigation. Optimal allocation or removal of exchangers in a network, and retrofit of their heat transfer area considering optimal cleanings and optimal dynamic flow distribution in the time horizon.	O	O	O	O
ΔP-X	Suffix applied to the short notation of other solution strategies to indicate that the crude oil flow is pressure driven through the parallel branches of the network. X = {NM, SCH, SP, SP+SCH}	-	-	-	-

One of the key aspects of this thesis is the integration of multiple decisions levels under the same framework, so that in many instances and for various cases, problems of optimal control, scheduling, retrofit and different combinations of them are solved for HEN under fouling. Table 1.1 presents a summary of abbreviations and descriptions used extensively in various chapters, which aim to facilitate the understanding of the combinations and solution

strategies considered. The reader is referred to this table when solution strategies are compared to demonstrate the advantages of integrating multiple decision levels.

The appendices of this thesis contain supporting information for a better understanding of the discussion and developments presented here. They present in detail all case studies and their operating conditions, the fundamental equations of a distributed model for shell and tube heat exchangers, and a heuristic algorithm developed for the online cleaning schedule of HEN under fouling.

Finally, throughout this thesis many optimization problems are solved, either NLPs or MINLPs, and their computational time is reported in order to compare different approaches or algorithms. All optimization problems are modelled in Python using the Pyomo environment (Hart, Watson, and Woodruff 2011) and solved in an Intel Core i7 computer, 3.40 GHz, 16.0 GB RAM. Also, all the NLPs are solved using IPOPT, an interior point algorithm (Wächter and Biegler 2006).

Chapter 2

Optimizing preheat trains under fouling: a review

This chapter presents a review of model based optimization solutions for fouling mitigation in preheat trains. It reviews the models, assumptions, and solution strategies of the optimization problem of preheat trains under fouling considered as fouling mitigation alternatives: flow distribution in the network, cleaning scheduling, and network retrofit. In this review, gaps in the literature and important areas that require improvement are identified which set the fundamental drivers and motivation for this thesis.

2.1. Introduction

The aim of this literature review is to provide an overview of the current modelling approaches for HEN under fouling and on how they have been used to optimize their operation. The optimization problems reviewed here focus on the optimal definition of fouling mitigation action such as flow distribution, cleaning scheduling, and network retrofit. This review identifies various optimization opportunities in the operation of refinery preheat trains, their numerical difficulties, solution approaches, and their potential impact on the operation of the system.

It is well known that there are other approaches than mathematical optimization that are useful to define fouling mitigation approaches, or to design heat exchangers or HEN considering fouling. The TEMA standards provide practical guidelines for the design and operation of heat exchanger, and include heuristics related to fouling (TEMA 2007). The TEMA guidelines have been used for a long time in industry and offer a practical approach for operating and designing shell and tube heat exchangers, although when fouling is considered it is in the way of safety factors or oversizing of the units. Also, pinch technology

has proven to be very useful for HEN synthesis and retrofit, as it provides a systematic methodology based on thermodynamic principles to maximize energy savings (Flower and Linnhoff 1980; Kemp 2006). Pinch technology has been used to design and retrofit heat exchangers and networks including fouling propensity minimization as an additional goal to energy recovery maximization (Brodowicz and Markowski 2003; Markowski 2000). These alternatives are useful for practical purposes. They provide relatively quick diagnostics of the system and solutions, but they rely on many assumptions limiting their applicability to more realistic and dynamic scenarios. For these reasons, alternatives different from mathematical programming for defining fouling mitigation strategies are not reviewed further in this thesis. The limitations of those alternatives can be overcome with a more rigorous model based approach for the problem, hence mathematical programming approaches are preferred.

This review does not cover in detail the nature, mechanisms and causes of crude oil fouling. The reader is referred to specialised books and reviews on that subject (Deshannvar et al. 2010; Coletti et al. 2015; Epstein 1983; Bott 1995; Macchietto et al. 2011; Müller-Steinhagen 2011; Bennett 2012; Watkinson and Wilson 1997; Coletti, Crittenden, and Macchietto 2015). A more comprehensive description of fundamental models developed for crude oil fouling, their assumptions, and phenomena captured can also be found in other sources (Wang et al. 2015; Wilson, Polley, and Pugh 2005; Wilson, Ishiyama, and Polley 2017; Diaz-Bejarano, Coletti, and Macchietto 2017; Diaz-Bejarano et al. 2017).

2.2. Problem definition and challenges

The core problem addressed in this thesis is fouling in refinery preheat trains, its economic consequences, and how to optimally define mitigation actions using first principle models. Figure 2.1 shows a simplified representation of a preheat train, and illustrates its three main sections: cold end, intermediate section, and hot end. It has been reported that exchangers in the cold end exhibit minimum to no fouling because of the low wall temperatures (Muller-Steinhagen 2000), while severe fouling is commonly observed in the intermediate section and in the hot end. Fouling in the intermediate section is characterized by the deposition of inorganic material, and that in the hot end by organic material (Muller-Steinhagen 2000; Mozdianfard and Behranvand 2015). The hot end usually exhibits the

highest levels of fouling characterized by decomposition of organic material and chemical reactions. The high wall temperatures in this section promotes a faster deposition than that in other sections of the preheat train – usually the hot streams in the hot end correspond to the residue of the CDU or to the bottoms of the vacuum distillation unit which are the products with the highest temperature. Because of this, most of the operational problems and difficulties are observed in this section. Also, the hot end recovers the largest fraction of the energy of the CDU products so fouling mitigation actions here are advantageous and have great potential to reduce operational costs.

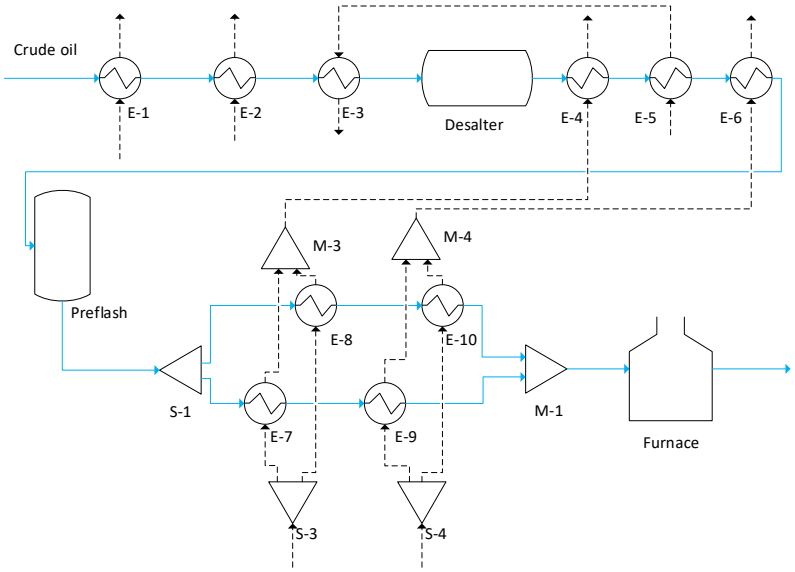

Figure 2.1. General (simplified) representation of a refinery preheat train.

Fouling mitigation actions commonly performed in the preheat train, their advantages and disadvantages are summarized in Table 2.1. In practice, these fouling mitigation actions are defined in a reactive manner. After observing a significant decrease in the preheat train performance, or after reaching operational limits such as the firing limit of the furnace or the pressure drop limit of the network some actions are taken immediately to move the system to better operating conditions. Most of these decisions are often based on heuristics, engineering knowledge of the specific refinery, or simplified calculations. However, not all alternatives can be defined in a reactive manner. For example, surface coating or heat transfer enhancement modifications require long planning times and are implemented during turnarounds – proactive fouling mitigation. A purely reactive approach to fouling – for instance regarding the cleaning decisions – is risky as it eclipses the economic benefits of the

mitigation strategies and in the long term it can produce large economic losses when operational limits are reached, and production rates must be reduced. A proactive approach that considered the current and future implications and impacts of mitigation actions will be beneficial for the overall operation.

Table 2.1. Fouling mitigation actions commonly performed in HEN.

Fouling mitigation	Description	Advantages	Disadvantages
1.Antifoulant agents	Chemical additives added directly to the crude to prevent fouling.	Prevent agglomeration of large particles, inhibits fouling reactions, or act as chain terminator agent (Bott 1990; Müller-Steinhagen, Malayeri, and Watkinson 2011).	Costly, need to be constantly restored, effective only for a short time (Coletti et al. 2015).
2.Surface treatment	Inhibits fouling by altering the interaction forces between surface and fluid.	Prevent fouling from occurring altering its mechanism (Banerjee, Pangule, and Kane 2011)	Costly, do not prevent fouling in the long term, its effectiveness deteriorates over time.
3.Chemical cleaning actions	Use of detergents, dispersers, basic solutions or acid solution to remove the deposit layer.	Performed in place and on-line in a short time	Difficult matching between cleaning agent and deposit type, no guarantee of complete removal (Müller-Steinhagen, Malayeri, and Watkinson 2011).
4.Mechanical cleaning actions	Use of water jets, projectiles, drilling, blasting and high pressure water to remove the deposit	Highly effective, almost complete removal	Off-line, unit out of service, long maintenance time (Müller-Steinhagen, Malayeri, and Watkinson 2011; Muller-Steinhagen 2000).
5.Heat transfer enhancement	Heat transfer maximization by modifying the flow pattern – helicoidal baffles, tube inserts, twisted tube.	Increase of heat transfer and shear stress promoting deposit removal (Somerscales and Bergles 1997)..	Increase in pressure drop, capital investment (Master, Chunangad, and Pushpanathan 2003; Pahlavanzadeh, Nasr, and Mozaffari 2007).
6.Flow velocity control	Dynamic control of flow distribution and velocity using bypasses and parallel branches.	Promote deposit removal (Rodriguez and Smith 2007; Wang, Zhan, and Feng 2015).	Complex interactions in large networks hinder its application
7.Network retrofit	Adding or removing exchangers in a network, or changing their connectivity.	Cheaper than purchasing new units, increase of heat transfer.	May promote faster fouling, or lower heat transfer in the long term (Ishiyama et al. 2013; Pan, Bulatov, and Smith 2016)

Accurate predictive models for the operation of preheat trains under fouling have a great potential to improve the performance of the system by defining proactive fouling

mitigation approaches. When mitigation actions are defined in advance and their benefits quantified properly, a long term feasible and profitable operation of the preheat train is more likely without the need of drastic reactive measures to recover the system performance.

For some of the fouling mitigation alternatives, (1,2,3) described in Table 2.1, it is challenging to predict their effectiveness, their interaction across the system and to quantify their potential benefits. This hinders the use of predictive models for smart decision making and proactive fouling mitigation. To quantify the effectiveness of antifoulant agents (1) and coated surfaces (2) it is necessary a deep understanding of the chemical reactions causing crude oil fouling, the interaction forces among the particles, the crude composition and how it changes dynamically. Including these features in a high level techno-economic model of a complete preheat train is not practical considering that these mitigation alternatives are expensive, their effectiveness last for short periods, and the mechanistic models are poorly understood (Gomes da Cruz et al. 2015). In the case of chemical cleanings (3), similar features, in addition to a detail characterization of the deposit, are required to quantify their performance and cost. Although models for chemical cleanings have been developed (Lanchas-Fuentes et al. 2016), they have not been validated and rely on empirical factors; hence the insights obtained through them can be inaccurate. For these reasons, these three fouling mitigation alternatives are not reviewed further and are excluded from the mitigation actions that can be defined proactively using a predictive model.

The fouling mitigation alternatives that have been optimized using predictive models are: time and allocation of mechanical cleaning, flow control in a network to modify the flow velocity, network retrofit options, and using heat transfer enhancement technology. Only the first three alternatives are considered in this thesis and reviewed further from the point of view of optimal fouling mitigation. Heat transfer enhancement decisions – which exchanger to retrofit with a certain technology – have been studied, and optimization methods have been used for that purpose, although their application is limited to a single type of technology, HiTRAN®, and a rather simple modification of the shear stress and heat transfer coefficient is used (Pan, Bulatov, and Smith 2016, 2013b; Wang and Smith 2013). It is also unclear how different technologies affect fouling rates at different time scales or in a wide range of operating conditions. Therefore, this approach is limited to certain technologies and

applications, thus defying the purpose of this thesis to have a general modelling and optimization framework for preheat trains under fouling.

Finally, a single fouling mitigation alternative may not be enough to guarantee a feasible and profitable operation of the preheat train. The interactions among the various mitigation alternatives, the operating conditions of the system, and variability of the crude processed are important to maximize energy recovery. Mathematical programming offers a robust framework to optimize the cleaning schedule, the flow distribution, and retrofit decisions of preheat trains under fouling, although the size of the problem and number of possibilities may be a limitation for its application. The rest of this chapter reviews modelling approaches for preheat trains under fouling that have been used to optimally define these three fouling mitigation actions, the solution strategies employed, their assumptions and limitations.

2.3. Optimization alternatives for preheat trains under fouling

This section revises and classifies optimization approaches and formulations, based on the fouling mitigation strategy they use to minimize the operating cost or maximize the energy recovery of preheat trains. Mathematical programming has been used to individually define: i) the flow distribution in the preheat train, ii) the cleaning schedule of the network, and iii) network retrofit alternatives. The models and assumptions used in these formulations are different as they serve different purposes, although they share a common goal of mitigate the effects of fouling and reduce the operating cost. Table 2.2 presents a summary and comparison of key contributions in these areas. The contributions are classified according to the fouling mitigation alternative used to optimize the preheat train operation, and this defines the nature of the optimization problem. The preheat train optimization can be formulated as an NLP when flow or velocity distributions – continuous variables – are considered, and as a MINLP or MILP when cleaning or retrofit decisions – integer variables – are included to mitigate fouling. Therefore, the complexity of the optimization problem is dictated by the decision variables defining the fouling mitigation strategies.

Table 2.2. Mathematical programming applications on fouling mitigation alternatives

Reference	Fouling mitigation alternative	HEX model*	Fouling model+	Key assumptions	Decision variables	Objective	Problem classification
(Rodriguez and Smith 2007)	Flow velocity	P-NTU	Semi-empirical threshold model	Thin layer No variability No pressure drop	Bypass fraction per HEX	Total operating cost	NLP
(Assis et al. 2013)	Flow velocity	P-NTU	Constant R_f	No dynamics Steady state No pressure constraints	Flow in parallel branches	CIT	NLP
(Wang, Zhan, and Feng 2015)	Flow velocity	P-NTU	Semi-empirical threshold model	Thin layer No variability	Pumping power New pumps	Annual total cost	NLP
(Assis et al. 2015)	Flow velocity	P-NTU	Semi-empirical threshold model	No variability No pressure constraints	Flow in parallel branches	Utilities cost	NLP
(Georgiadis, Papageorgiou, and Macchietto 2000)	Cleaning schedule	LMTD	Empirical linear model	Linearized models Constant U_{cl} No pressure drop	Cleaning time HEX to clean	Total operating cost	MILP
(Lavaja and Bagajewicz 2004, 2005a, 2005b)	Cleaning schedule	LMTD	Empirical linear model	Linearized models Constant U_{cl}	HEX to clean	Total operating cost	MILP
(Ishiyama, Paterson, and Wilson 2011)	Cleaning schedule	LMTD	Empirical linear model	Constant U_{cl} No pressure drop Cyclic operation	Cleaning cycle time	Total operating cost	MINLP
(Pogiatzis, Wilson, and Vassiliadis 2012)	Cleaning schedule	LMTD	Empirical linear model	Thin layer Constant U_{cl} No pressure drop Single HEX	Cleaning times Number of cleanings	Total operating cost	MINLP
(Pan, Bulatov, and Smith 2013a, 2013b)	Retrofit	LMTD	Semi-empirical threshold model or no fouling	Linearized models No variability No pressure drop	HTA retrofit Network retrofit Tube inserts	Total cost	MILP

*P-NTU: number of transfer units and P effectiveness. LMTD: model based on $Q = U(HTA)(LMTD)$ to calculate duties and temperatures

+ Empirical models define the fouling resistance as an explicit function of time, $R_f = f(t)$.

Threshold models define the rate of change of the fouling resistance as function of the deposition and removal rates, $\frac{dR_f}{dt} = n_{deposition} - n_{removal}$

The first optimization alternative aims to define the flow distribution in parallel branches, velocities in the exchangers, and potential bypass flow rates. It uses lumped models, simple representations of the deposit, and ignores the variability of the operation. These optimization problems are relatively easy to solve with respect to the other optimal fouling mitigation problems. There are cases where the optimal flow distribution and optimal cleaning scheduling have been integrated, such as those of Rodriguez and Smith (2007); and Tian, Wang, and Feng (2016) where the bypass flows or the velocity of the cold stream in each exchanger are defined simultaneously with the cleaning scheduling of the preheat train.

The second optimization alternative aims to define the cleaning schedule of a HEN, and it includes the starting time of the cleanings, the allocation of the cleanings to units, and, in some cases, the type of cleaning. This is a challenging MINLP problem because of the large number of feasible solutions and the nonlinearities present in the model. Here, it is common to find approaches that simplify the predictive models – linearizing the heat transfer models and using empirical linear fouling models – so that the optimization problem can be solved with commercial tools. These simplifications compromise the accuracy of the models and the validity of the solutions achieved with them.

The optimal cleaning scheduling problem of HEN has been widely research and there are several approaches to solve this problem which range from simple reactive heuristics to deterministic optimization algorithms. This is reviewed in detail in Section 2.5 because these approaches differ significantly in their modelling assumptions and solution strategies.

The research on the final optimization alternative – optimal retrofit – is not as abundant as that in the other fields. The work of Pan, Bulatov, and Smith (2013a, 2013b), Table 2.2, deals with the optimal heat transfer area retrofit of exchangers under fouling in a preheat train. The optimization variables in that case are continuous and define the additional area required in certain units, but they proposed a separate algorithm – iterative MILP – to optimally define network modifications such as the introduction of new exchangers or new connections in the network at steady state conditions. Mathematical programming methods have not been used extensively to optimize these retrofit decisions for preheat trains under fouling. However, they have been used in retrofit problems at steady state conditions ignoring fouling (Ciric and Floudas 1989; Yee and Grossmann 1991). Also, there are alternative methods to mathematical programming for the retrofit of HEN without fouling. Those

methods can be based on pinch analysis (Lal et al. 2018) or on heuristic algorithms that consider the improvement in energy recovery (Walmsley et al. 2018). Despite the extensive research on HEN retrofit, there is still a need to include the effects of fouling, fouling mitigation, and system dynamics. The benefits of a retrofit option can be diminished by higher deposition rates, constrained operating points, and higher energy cost in the long term.

Current optimal retrofit approaches maximizing steady state energy recovery without considering fouling have serious limitations. An increase of the heat transfer area or of the heat transfer rate in a given network will increase the fouling rates because the wall temperature increases, hence the deposition rate increases and the performance of the retrofitted network decays much faster than that of the original network (Bott 1990). The same pattern is observed when heuristics, such as *match the hottest stream with the cold stream at its hottest point*, or retrofit approaches based on pinch analysis are used (Bott 1990). Even allowing for extra area at the design stage to prepare for future effects of fouling is not a good approach, as the higher wall temperatures reached increases the fouling rate. Improvements in energy recovery using these retrofit approaches are most likely observed during the initial operation of the retrofitted network, and then fouling effects overtake those benefits. On the other hand, an optimal retrofit approach that considers fouling may not maximize the energy recovered at steady state, but it will maximize the overall energy recovered during the whole operation of the network. Considering fouling, and fouling mitigation alternatives at the retrofit level is important to ensure that the retrofitted network operates at its maximum efficiency possible over long times.

The fouling mitigation alternatives discussed in this section have typically been considered independently. The interactions among various mitigation actions have been ignored so the potential to exploit synergies among them has not been considered. These alternatives are usually considered in a sequential manner, first the network retrofit, then the cleaning scheduling for the resulting network, and finally the flow distribution optimization, hence important information about the interactions is lost in this process.

2.4. Problem formulation and modelling considerations

While the previous section reviewed the instances in which mathematical programming has been used to tackle the problem of fouling in preheat trains, this section reviews the

models used to represent the operation of the heat exchangers, networks, and fouling phenomena. These models are an important component of the mathematical optimization formulation. An accurate and realistic representation of the preheat train operation is paramount to ensure the real benefits and potential of fouling mitigation actions, and to assess the performance of the system.

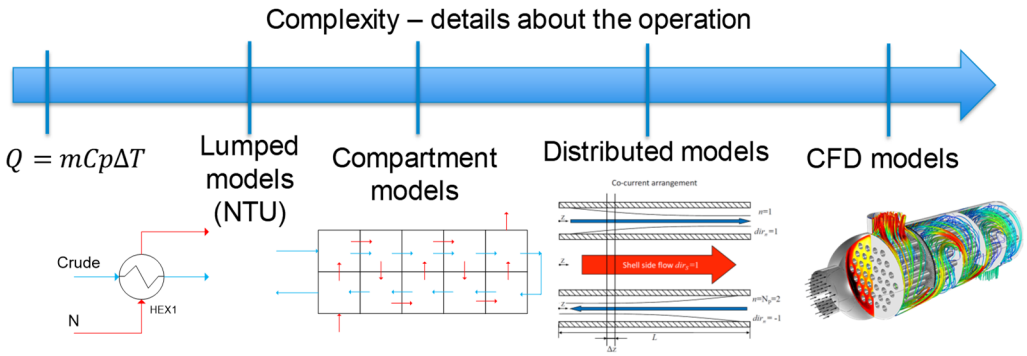

Figure 2.2. Schematic representation of the modelling approaches for shell and tube heat exchangers

There are many models for describing the operation of shell and tube heat exchanger covering a wide range of applications, and each captures in more detail than the others a specific part of the problem. The models can be classified according to their complexity or amount of information provided about the operation of a unit, and this is summarized in the scheme of Figure 2.2. Only first principle models are considered here because of their prediction and extrapolation capabilities, while data driven model are ignored. The first kind of models are simple macroscopic models based on the overall energy balance around the exchanger to estimate the outlet temperate of the streams. Then, there are the models that define an overall efficiency term (e.g. P-NTU) lumping all the phenomena that occurs inside the unit in a single term (Thulukkanam 2013; Hewitt, Shires, and Bott 1994). The next kind of models arise from the combination of various lumped models in a given arrangement such that the exchanger is divided in interconnected cells or compartments, and an efficiency term is defined for each (Varbanov, Klemeš, and Friedler 2011). If instead of defining a discrete partition of the exchanger, a continuous domain is used, the resulting model is distributed in the axial and/or radial direction of the exchanger. These distributed models do not need to define an efficiency term as they consider the local heat transfer phenomena explicitly (Coletti and Macchietto 2011). The last kind of models are those based on CFD that consider

in detail the hydrodynamics and heat transfer in all domains of the exchanger and provide a more realistic representation of the problem.

Table 2.3. Applications of shell and tube heat exchanger models

	Macroscopic energy balance	**Lumped models (NTU)**	**Cell models**	**Distributed models**	**CFD models**
Duty calculations	O	O	O	O	O
Control	X	O	O	O	X
Data reconciliation	O	O	O	O	X
Optimal cleaning scheduling	X	O	~	X	X
Identify flow patterns	X	X	~	~	O
Hydraulic design	X	X	X	~	O
Fouling diagnostic	X	~	~	O	~
Fouling monitoring	O	O	O	O	X
Unit retrofit	X	~	~	O	O
Network retrofit	X	O	O	O	X

O: the model has been used successfully for the application
X: the model cannot be used for the application because it cannot predict the relevant variables
~: the model can be used for the application with limited prediction capabilities

Each of the previous models have been used in different applications, and do not aim to solve the same problem, nor a single model can be used to solve all possible problems in heat transfer applications. Table 2.3 summarizes some key applications or problems in the operation of heat exchangers and their networks. Simple macroscopic models are useful for quick calculations of the heat duty in energy integration, but they do not provide any other practical information for the operation of the system. Lumped models are the most commonly used in different applications including control, cleaning scheduling of networks under fouling (Diaby et al. 2012; Wilson, Ishiyama, and Polley 2017; Assis et al. 2015; Lemos et al. 2015), and retrofit of the network or exchangers (Wang and Smith 2013; Pan, Bulatov, and Smith 2016). Similarly, cell or compartment models can be used for the same applications as lumped models, although poor understanding on how to define the compartments of a unit hinder their application. The compartmental approach gives insights about the state of the variables inside the unit, and distributions along the axial direction – it serves to identify areas of high fouling limiting the operation – but is subject to the accuracy of each individual model and the definition of the compartments. On the other hand, distributed models do not require to define arbitrary divisions in the unit to capture the spatial variability of the key variables (Diaz-Bejarano, Coletti, and Macchietto 2016;Coletti and Macchietto 2011). They define continuous domains that are representative for each region of

the exchanger – tube, wall, shell, deposit – although the representation of the shell side is rather simple and do not consider the actual flow patterns. Finally, CFD approaches give a detailed representation of the flow patterns in the tube and shell sides, but to couple them with fouling models is a complex task that demands high computational power.

There are two other modelling approaches that could be used to represent the operation of heat exchangers, but they have not been explored in sufficient detail. In the first category are surrogate models. These models are simplified representations of a more complex model or an approximation of experimental data that still capture the effect of the inputs on the outputs of the model within a range of validity. For example, a surface response can be a surrogate model of CFD model of an exchanger which is developed using the information of multiple runs. This modelling approach has been used for the design of heat exchangers in other applications different from refining (Wansaseub, Pholdee, and Bureerat 2017; Qian et al. 2005). In the second category are hybrid models. These models integrate first principle modelling with data driven models. The data driven part is usually employed to represent a complex phenomenon for which experimental data is available or for which a different approach, such as CFD or molecular dynamics, is the correct way to represent it. This modelling approach has been used to represent the fouling state of a single heat exchanger, while macroscopic energy balance characterized its performance (Navvab Kashani et al. 2012).

Similar to heat exchanger models, there also have been many models developed for crude oil fouling. The simplest modelling approach consist of defining the fouling resistance as an explicit function of time. These models are empirical models fitted from experimental or plant data and mainly used for quick engineering calculations on the field (Scarborough et al. 1979; Yong Wang et al. 2015). On the contrary, deterministic models for fouling try to capture the mechanistic driving forces of the phenomena such as mass transfer and molecular forces. However, this is a complex task because the large number of components present in the crude can deposit at different rates following different mechanism. Salts, asphaltenes and heavy component in the crude can deposit because of corrosion, chemical reactions, thermal decomposition, precipitation or adhesion (Wilson, Polley, and Pugh 2005; Paterson and Fryer 1988). The lack of understanding of crude oil fouling mechanisms and the poor prediction

capabilities of deterministic models have hindered their application at a refinery level operation (Yong Wang et al. 2015; Alimohammadi, Zendehboudi, and James 2019).

Semi-empirical models for the deposition or fouling rate have been proposed to overcome the disadvantages of the previous two models – completely empirical or completely deterministic – so that they can provide meaningful insights about the operation and fouling mitigation of the preheat train. Threshold models are semi-empirical models that try to encompass all the parameters and effects leading to fouling in a simple and practical expression. The fouling rate is a function of two competing mechanism, deposition and suppression or removal. Although there are many variations of the threshold fouling model, in general the deposition rate is a function of the Reynolds and Prandtl numbers, the temperature effect is captured in an Arrhenius expression, and the removal or suppression rate is function of the shear rate (Wilson, Polley, and Pugh 2005). Good compilations of threshold fouling models, their different assumptions, and simplifications can be found in (Wilson, Ishiyama, and Polley 2017; Wang et al. 2015). The main advantage of this type of models is that they capture the effect of the operational variables on the deposition rate, and after they are fitted against experimental or plant data, their predictions can be sufficiently accurate to assess the preheat train performance and the effect of mitigation actions.

Additional approaches to model crude oil fouling are: a) data driven models and neural networks, which may have good prediction capabilities but lack to capture the physical meaning of the operation and cannot be extrapolated to other exchangers (Aminian and Shahhosseini 2009; Kashani et al. 2012); b) molecular models, which give insights to distinguish among different fouling mechanism and the interactions between the foulant and the surface. However, this approach requires significant computational effort, limiting its applicability to model complete heat exchangers (Müller-Steinhagen 2011; Puhakka, Riihimäki, and Keiski 2007); and c) CFD models where the fouling layer is modelled either as a very viscous fluid, a moving interface, or as particles disperse in a fluid that interact with a surface (Yang et al. 2015; Emani, Ramasamy, and Shaari 2019; Gounder and Emani 2017). These models are not suitable for optimizing the operation of preheat trains and to decide on optimal mitigation actions because they require a large computational effort to solve or they cannot be generalized in terms of heat exchangers configurations and range of operating conditions.

Table 2.4. Review of heat exchanger and fouling models used in preheat train operation

Reference(s)	HEX model*	Fouling model	Hydraulic effects	Variability	Purpose and use	Special considerations
(Georgiadis, Papageorgiou, and Macchietto 2000)	LMTD	Empirical lineal model	Critical deposit thickness	Constant conditions	Optimal cleaning schedule	Pseudo steady state Constant U_{cl}
(Smaïli, Vassiliadis, and Wilson 2001)	NTU-ε	Empirical lineal and asymptotic models	Pressure drop	Constant conditions	Cleaning scheduling	Pseudo steady state Constant U_{cl} Heuristic algorithm for cleanings
(Lavaja and Bagajewicz 2004, 2005a, 2005b)	LMTD	Empirical lineal and asymptotic models	None	Constant conditions	Optimal cleaning schedule	Pseudo steady state Constant U_{cl} Linearization of all models
(Ishiyama, Paterson, and Wilson 2009; Ishiyama et al. 2010)	NTU-ε	Semi-empirical threshold model	Pressure drop	Constant conditions	Cleaning schedule Control	Pseudo steady state Constant U_{cl} Thin layer assumption Heuristic algorithm for cleanings
(Coletti and Macchietto 2011; Diaz-Bejarano, Coletti, and Macchietto 2016)	Distributed	Local semi-empirical threshold model	Local pressure drop	Variable input streams condition§ Constant conditions	Conditioned cleaning Performance assessment Retrofit Diagnostic	Dynamic model Moving boundary condition Large PDAE system
(Assis et al. 2015)	P-NTU	Semi-empirical threshold model	None	Constant conditions	Optimal flow and velocity distribution	Pseudo steady state Constant U_{cl} Thin layer assumption
(Trafczynski et al. 2016)	Cell NTU-ε	Data driven	None	Noise and variable input streams conditions	Regulatory control	Pseudo steady state Constant U_{cl}
(Emani, Ramasamy, and Shaari 2019)	CFD	Discrete particles	Full hydraulic profiles	Constant conditions	Performance assessment	Dynamic model Model of inter particle forces Short operation time
(Ismaili et al. 2019)	LMTD	Empirical asymptotic model	None	Variable input streams conditions	Optimal cleaning schedule	Stochastic optimization Pseudo steady state Constant U_{cl}

*P/ε -NTU: number of transfer units and P/ε effectiveness. LMTD: model based on $Q = U(HTA)(LMTD)$ to calculate duties and temperatures.
Distributed: first principle models based on heat balances in axial and radial directions of the exchanger
§ Variable conditions are only used for performance assessment and in all other situations constant conditions applied

Table 2.4 summarizes key contributions on modelling shell and tube heat exchanger integrated with crude oil fouling and their uses. The models used cover a wide range of approaches to represent the heat transfer and fouling phenomena, but models of different complexity are used for different purposes. The simplest models – only a few algebraic equations – are used to optimize the cleaning schedule of preheat trains and in some cases those models are linearized to simplify even further the optimization problem, so that it can be solved with commercial MINLP/MILP solvers and algorithms. Such models have also been used for control and optimal flow distribution in HEN, but their limitations are recognized and other approaches that represented better the heat transfer – distributed or compartment models – offer more accurate representations.

The process variability arising from changes in the input stream conditions have been ignored in the modelling approaches and in the optimization of preheat trains. The distributed model proposed in Coletti and Macchietto (2011); and Diaz-Bejarano, Coletti, and Macchietto (2016) has been tuned with actual variable plant data, and used to assess the performance of preheat trains under dynamic operating conditions. However, it has not been employed to optimally define fouling mitigation actions. On the other hand, Ismaili et al. (2019) consider the effect that the variability in the input streams has on the expected operating cost and on the optimal cleaning schedule, although each scenario of the optimization formulation assumes constant conditions over time. The large scale and many combinatorial alternatives of the MINLP formulation lead to big assumptions and simplifications on the fouling and heat exchanger models that make the solution less representative of the actual performance of the system.

The main aspects of the optimal fouling mitigation problems in preheat trains that have not been widely research and have a significant impact on the process performance are: i) the use of accurate and detailed models in the formulation and solution of the optimization problem, and ii) accounting for the effects of variable operating conditions on the optimal fouling mitigation actions and network performance. For the first aspect, the main challenge is to solve large scale MINLP problem where the model representing the preheat train may include a large number of nonlinear constraints, differential equations and discontinuities. Whereas the second aspect is a practical problem related to ways to include variability and

uncertainty in a deterministic optimization formulation while allowing the process to react and adapt to changing conditions.

2.5. Mathematical considerations and solution strategies

Optimal fouling mitigation actions in crude preheat trains have been addressed using mathematical programming. The flow distribution problem in large networks has been formulated as an NLP which, despite its large scale, can be easily solved with current commercial solvers. On the other hand, cleaning scheduling and network retrofit problems have been formulated as MINLPs with large number of binary decisions and nonlinearities which hinder their solution with current strategies – branch and bound, outer approximation. This section reviews the solution strategies and algorithms that have been applied to solve: 1) the optimal cleaning scheduling problem, 2) the optimal network retrofit problem, and 3) the optimal integration of control and scheduling decisions in general applications.

The main decision variables of the optimal cleaning scheduling problem are the starting time of the cleanings – continuous decisions – and the assignment of cleanings to exchanges – binary decisions. The large number of binary variables – there are many exchangers (10 – 30) in a preheat train and it operates for long periods (2 – 6 years) – defines a combinatorial problem which makes it impossible to evaluate all feasible schedules. Also, different schedules can have the same or very similar objective function values introducing degeneracy and multiplicity in the solution (Lavaja and Bagajewicz 2005a; Georgiadis, Papageorgiou, and Macchietto 2000). Another complicating factor is the presence of discontinuities and disjunctions that arise from the cleaning decisions that model the state of the exchangers, and the nonlinear models representing their operation. To address these difficulties heuristic algorithms, stochastic optimization algorithms, and algorithms based on deterministic optimization have been proposed.

Table 2.5 summarizes the evolution of different approaches and algorithms developed to solve the optimal cleaning scheduling problem of HEN. All formulate the optimization problem as an MINLP or MILP, but their assumptions and solution strategies are different. Those formulations that use simplified models – linear models for the exchanger and empirical fouling models – and ignore the effect of operating conditions are often solved to optimality using standard MILP solvers, or an outer approximation / equality relaxation

algorithm implemented in the solver DICOPT in the case of MINLP problems. These problems are solved to local optimality without major computational effort, although they representation of the problem is not accurate and oversimplified. In addition, the nonlinear representation of the problem are usually nonconvex – the heat exchanger models and heat transfer correlations are nonconvex – and the solvers used assumes nonconvexity so that the solution found is only locally optimal. Using global optimization algorithms such as BARON or ANTIGONE has not been explored for this MINLP instances, but it is expected that because of the large size of the problem the computational time required to find a solution will be a limitation. Despite their limitations, global optimization algorithms can still be used to find good feasible solutions to bound the objective function. On the other hand, formulations that use more realistic models – threshold fouling models and nonlinear representations of the exchangers – cannot be solved to optimality with standard MINLP solvers because a prohibitively large computational time is required. In these cases global optimization solvers are not an option. To solve those problems either stochastic optimization algorithms or heuristic algorithms are used. The stochastic algorithms rely on a partially random or pseudo random search that does not guarantee optimality. Also, these algorithms demand high computational effort as each new alternative or iteration requires a complete simulation of the system, which may be infeasible.

The performance of stochastic optimization algorithms applied to the cleaning scheduling problem is not guaranteed. It has been shown that multiple stochastic algorithms – genetic algorithms, particle swarm optimization, simulated annealing – provide different solutions to the same cleaning scheduling problem (Rennard 2006; Deka and Datta 2017) and that their performance is extremely sensitive to the initialization of the problem (Tian, Wang, and Feng 2016). Also, different solutions to the same problem have been observed even under constant operating conditions and assuming perfect models. Since it is expected that the uncertainty in crude operation – due to varying conditions of input streams and properties of the crude or blends processed – will have a significant effect on the optimal fouling mitigation actions, a solution algorithm that increases the uncertainty and variability on the solution is detrimental to the operation.

Table 2.5. Review of solution strategies and formulation of the optimal cleaning scheduling problem of preheat trains

Reference	HEX / fouling models	Formulation	Time discretization	Simplifications	Solutions strategy
(Georgiadis, Papageorgiou, and Macchietto 2000)	LMTD / Empirical	MINLP and MILP	Fixed grid, 1 month step	Linearization of models Simple exchanger models Constant conditions	DICOPT for MINLP OSL for MILP
(Smaïli, Vassiliadis, and Wilson 2001)	LMTD / Empirical	MINLP	Fixed grid, 1 month step Periods divided in cleaning + operation	Threshold cost for definition of cleanings U_{cl} constant	Moving window optimizing one period at the time
(Smaïli, Vassiliadis, and Wilson 2002)	LMTD / Empirical	MINLP	Fixed grid, 1 month step Periods divided in cleaning + operation	Simple exchanger models U_{cl} constant	DICOPT
(Lavaja and Bagajewicz 2004, 2005a, 2005b)	LMTD / Empirical	MILP	Fixed grid, 1 month step Periods divided in cleaning + operation	U_{cl} constant Linearization of models	1) Deterministic + 2) Moving window 3) Heuristic sequential
(Rodriguez and Smith 2007)	P-NTU / Threshold	MINLP	Fixed grid, 1 month step	U_{cl} constant	Simulated annealing
(Ishiyama et al. 2010)	NTU- ε / Threshold	MINLP	Fixed grid, 1 month step Periods divided in cleaning + operation	U_{cl} constant	Moving window Economic heuristic
(Pogiatzis, Wilson, and Vassiliadis 2012)	LMTD / Threshold	MINLP	Fixed grid, 1 month step Periods divided in cleaning + operation	Cyclic operation	DICOPT multiple initializations
(Gonçalves et al. 2014)	NTU- ε / Empirical	MINLP	Fixed grid, 1 month step	Sequential solution of model Simple U models	Heuristic based on random search
(Lemos et al. 2015)	P-NTU / Empirical	MILP	Fixed grid, 0.25 month step	Linearization of models U_{cl} constant	Solution of MILP in a moving window
(Biyanto et al. 2016)	LMTD / Empirical	MINLP	Fixed grid, 1 month step	Max. one cleaning per HE U_{cl} constant	Stochastic algorithms: Genetic, Imperialist competitive, Duellist, Particle swarm
(Diaby et al. 2016)	NTU- ε / Threshold	MINLP	Continuous integration, 1 day step	U_{cl} constant	Heuristic Conditional cleanings
(Diaby, Miklavcic, and Addai-Mensah 2016)	NTU- ε / Threshold	MINLP	Double time grid for integer decisions 1 month major step 1 day minor step	U_{cl} constant	Genetic algorithm
(Ismaili et al. 2018)	P-NTU / Empirical	MINLP / MIOCP	Multiperiod variable length	U_{cl} constant Relax and round up integer variables	Multiperiod optimal bang-bang control

There are two types of heuristic algorithms that have been applied to solve the cleaning scheduling problem. The first type uses predictive models and an extensive search to evaluate potential benefits of cleanings, and define cleanings based on a threshold criteria over a moving window (Ishiyama et al. 2010; Diaby et al. 2016). The second type also uses a moving window to define the cleaning actions, but at each instance a deterministic optimization problem – MILP or MINLP – is solved (Lemos et al. 2015). This type of heuristics aims to reduce the problem size, but they are still based on simplified models assuming constant operating conditions

Regardless of the solution approach adopted for the cleaning scheduling problem, all above references use a similar simplification to represent the time horizon. Most of the works reviewed use a fixed time step to discretize the operating horizon, and this is usually set as one month, although some divide the discretized time step in two, one for cleaning and other for normal operation. Using this coarse grid to integrate DAE models compromises the accuracy of the solution and completely ignores the dynamic effects and changes on shorter time scales. For instance, it is not possible to capture the variability of the flow rates and temperature of the input streams to the network, which occur on a time scale of days. Another limitation of this discretization approach is the pre-assignment of intervals or time instances at which cleanings are possible. This limits the number of possible cleaning schedules and restricts the starting time of the cleanings.

In summary, to solve the cleaning scheduling problem of HEN either the prediction model is simplified and accuracy is lost, but the optimization is done with deterministic algorithms; or more representative models are used together with heuristics that does not guarantee optimality. Also, a better and more precise representation of the time horizon is needed to capture the fast dynamics in the system.

In contrast to the optimal cleaning scheduling of HEN under fouling, the optimal retrofit problem including fouling has not received as much attention. True, the optimal synthesis and retrofit of HEN have been widely studied for a long time using mathematical programming approaches (Yee and Grossmann 1990; Papoulias and Grossmann 1983a, 1983b; Floudas and Grossmann 1987), but they are based on steady state models that ignore the process dynamic and fouling.

Addressing the problem of HEN retrofit while including fouling mitigation alternatives in the optimization problem is challenging because of the dynamic effects, the many possibilities of network retrofits, and the large number of binary decisions involved. Regarding network retrofit – where to include a new heat exchanger, or which one to remove from the network – the most common approaches used are pinch technology methods, and mathematical programming. Pinch technology uses thermodynamic principles to compute the minimum heating and cooling duties in the network, and to identify in the enthalpy-temperature space possible matches for the cold and hot streams (Tjoe and Linnhoff 1986). This approach has been used to identify possible streams splits and where to add new exchangers to an existing network (Lal et al. 2018; Li and Chang 2010), although it only considers the heat duty and area of the units without any more level of detail about the operation of the network. Mathematical programming approaches arise from the optimal HEN synthesis problem (Papoulias and Grossmann 1983a, 1983b), and define an MILP or MINLP problem to decide where to include additional heat exchangers. The retrofit problem is usually formulated using the stage-wise model of Yee and Grossmann (1990) and adapting it to fix certain units in the network while deciding where additional area is required and beneficial for the operation; or using a superstructure model for the network with all possible connections between existing and new exchangers (Floudas, Ciric, and Grossmann 1986; Ciric and Floudas 1989). These problems are usually solved using decomposition approaches based on an iterative solution of two subproblems: a MILP and an NLP. The stage-wise model is used for retrofitting in Liu, Luo, and Ma (2014) where the MINLP problem is solved using stochastic optimization algorithms, while the same problem is addressed by Angsutorn, Siemanond, and Chuvaree (2014) using a hybrid approach between pinch technology and mathematical programming. All these approaches for network retrofit assume steady state operation, fix inlet and outlet streams temperature, and ignore fouling.

In some HEN retrofit applications fouling has been considered. Using detailed and distributed dynamic models (Coletti, Macchietto, and Polley 2011) or dynamic simulations with lumped models (Yeap et al. 2004, 2005), retrofit approaches and fouling have been simulated, although the network retrofit– modifying the network structure, or adding new units – is defined ad hoc or based on pinch technology analysis. These works proved that a retrofitted network maximizing energy recovery at steady state is not always the best

alternative for long time operation under fouling. However, the retrofit alternatives considered are few and limited to the criteria of the analyst, therefore optimization based solutions will be beneficial to explore all possible network retrofit alternatives and define the best structure with minimum operating cost over time. Optimization based approaches have been used to retrofit HEN considering fouling, but they are limited to the use of heat transfer enhancement technology (Pan, Bulatov, and Smith 2016; Wang and Smith 2013) and ignore possible network modifications. Even if fouling is considered within the HEN retrofit problem, the possibility of performing fouling mitigation actions, such as cleanings, is ignored at this decision level, and at best their effect is evaluated a-posteriori, after retrofitting the network (Ishiyama et al. 2013). This fails to capture the compromise between extra energy recovered, and operation cost due to fouling and frequent cleanings.

The final group of solution strategies reviewed here is related to the integrated optimization of control and scheduling in general applications. This set of problems is important in the operation of preheat trains under fouling since there are two time scales involved: one for the fast dynamics associated with changes in the operation and optimization of the flow distribution of the network, and another for the slow dynamics of fouling and the long term effects of optimal cleanings. Also, this is a highly dynamic process prone to disturbances where the decisions at different time scales have important interactions. Some attempts to integrate these two levels of decisions have been performed for the refining application of interest. In Tian, Wang, and Feng (2016) and Rodriguez and Smith (2007) the velocity distribution and the bypass flow rates are simultaneously optimized with the cleaning schedule. However, the same coarse grid used for the scheduling problem is also used in the control problem, which limits the ability of the continuous manipulated variables to react faster to changes in the operation – they use a time step of one month, and it is not realistic to assume that the split fraction in parallel branches change once a month. Better integration approaches have been proposed in other applications and the optimal operation of preheat trains under fouling could benefit from them.

There are two general philosophies for integrating scheduling and control decisions: i) a top-down approach where the scheduling formulation is attained and control elements included, and ii) a bottom-up approach where scheduling elements are included in the dynamics of the control problem (Baldea and Harjunkoski 2014). Inevitable in each approach

some key elements of control or scheduling are left out because of the complexity of the problem.

Top-down approaches aim to include the dynamic representation and control of the system in the scheduling problem. The dynamic model of the system or PID controllers have been directly included in the formulation of the optimal scheduling problem and applied to a multiproduct CSTR and batch polymerization reactors (Nie et al. 2015; Flores-Tlacuahuac and Grossmann 2006). These approaches are equivalent to open loop control as they ignore the effect of feedback in the system. An alternative for closed-loop integration of control and scheduling following a top-down approach was proposed where the KKT conditions of an MPC controller are directly included in the optimal scheduling problem of a multiproduct batch reactor (Simkoff and Baldea 2019). However, the integrated problem is only solved once assuming perfect knowledge of the disturbances – product demand and prices.

Bottom-up approaches aim to include the objectives of the scheduling problem in the control layer and the feedback control loops. The most common way of doing so is using an economic objective in (N)MPC control loop (Ellis and Christofides 2014; Subramanian, Rawlings, and Maravelias 2014). This formulation inherits the benefits of the control loops in handling large variability, uncertainties, and disturbances in a closed-loop, but it is usually limited to continuous decisions. It is a complex task to include integer decisions, which are characteristic of a scheduling problem, in a feedback control loop. To overcome this issue parametric MPC strategies (Pistikopoulos and Diangelakis 2016) or online rescheduling – solving a scheduling problem in a receding horizon or when large disturbances are observer – have been proposed (Dias and Ierapetritou 2016). More recently "grey box" optimization which combines first principle models with data driven models has been proposed for the integration of control elements at the scheduling layer (Dias and Ierapetritou 2020b, 2020a).

Economic (N)MPC has been successfully used to integrate the operational optimization layer – real time optimization – and the advanced control layer in process operations, so it has great potential to also include decisions of the scheduling layer as the time scale divisions become less evident. Economic (N)MPC uses a general objective function defining the performance of the operation instead of the common tracking function of regulatory control applications, and it can include performance constraints – for instance, average concentration of the product or total production (Rawlings, Angeli, and Bates 2012). Another advantage

of economic (N)MPC is that it optimizes dynamic trajectories of the variables and not steady state conditions, which can perform better for an operation that is dynamic and subjected to time varying disturbances (Ellis, Liu, and Christofides 2017). However, desirable properties of tracking (N)MPC formulations such as closed-loop stability and convergence cannot always be guaranteed with an economic oriented controller, and modifications of the formulation are needed – introducing, for example, terminal constraints, terminal costs, periodic constraints (Ellis and Durand 2014; Ellis, Durand, and Christofides 2016).

From a control perspective, a dual loop control approach allows to integrate decisions over two-time scales and its principles can be applied on the integration of scheduling and control decisions. In this case, two time scales of the system are identified, control loops are designed for each one, and solved at their own frequency, although they interact to ensure consistency of the decisions (Kadam et al. 2003). Usually, the control loops are solved at asynchronous frequency to keep the division between the two time scales, and the outer layer correspond to a controller with economic objectives or a dynamic real time optimization procedure (Kadam et al. 2002). In some instances the two layers has been defined as economic (N)MPC controllers to maximize the close loop performance – economic profit – of the process over all time scales (Ellis, Liu, and Christofides 2017; Ellis and Christofides 2014). The dual loop control approach is versatile enough that the control models of each layer can have different levels of complexity and do not need to have the same structure, although it can be desirable for consistency of the decisions, and they can potentially include binary decision variables (Marquardt 2002) – assuming that the computational time is not a limitation for their application. For these reasons, a dual control approach can potentially integrate scheduling and control decisions for dynamic system operating under high variability and disturbances, which is the case of HEN under fouling, although their application has been limited to process with only continuous decision variables.

The interaction of control and scheduling has usually been ignored for fouling mitigation in HEN, but their integration becomes attractive when: i) the system is subject to large fluctuations so that the time scale of scheduling and control decisions overlap, and ii) the process is highly dynamic and prone to frequent disturbances. The operation of preheat trains have all these features, so the online integration of flow control and cleaning scheduling decisions should, in principle, improve the overall performance of the system (Shi, Chu, and

You 2015). Most alternatives that integrate control and scheduling decisions are done offline and are equivalent to operating the system in open loop, ignoring the variability of the system and the effect of disturbances. Although they may include PID (Chu and You 2012) or MPC controllers (Simkoff and Baldea 2019), disturbances are not considered explicitly. On the other hand, integration approaches that uses feedback to cope with the process variability cannot handle efficiently discrete decisions like those related to scheduling (Ellis and Christofides 2014; Subramanian, Rawlings, and Maravelias 2014). In the case of HEN under fouling Pitarch et al. 2017 have proposed an online approach to monitor and optimize the performance of an evaporation system considering the cleanings of the units. However, it is done sequentially as first the state of the system is estimated and its operation optimized, and then the cleaning cycle is defined for each individual unit without considering the interactions in the network.

The integration of scheduling and control decisions at the same decision level has proven to be more efficient and better able to reduce the operational cost in various applications than the common sequential optimization and operation. However, most of the applications and case studies have involved small systems with a single multiproduct reactor or few units with multiple variable targets. Another simplification of these integration approaches is assuming a perfect knowledge of the variability and disturbances. The closed-loop performance and online application of integrated scheduling and control have not been analysed. Finally, the optimal operation and fouling mitigation of crude preheat trains can benefit from the optimal integration of scheduling and control decisions as long as closed loop performance is considered, due to the large variability observed in the process.

2.6. Concluding remarks

Fouling mitigation is paramount for a reliable and profitable operation of crude preheat trains. There are many mitigation strategies, but among those the most studied and effective are cleaning periodically the exchangers, controlling the flow distribution in the network, and design retrofits. Mathematical models and optimization approaches have been used to individually define these three mitigation alternatives, although most of the progress and work have been focused on the optimal cleaning scheduling problem. Not much attention has

been directed to the optimization of the flow distribution, the optimal network retrofit, or the optimal integration of various mitigation actions.

To efficiently determine optimal fouling mitigation actions in crude preheat trains, two elements are necessary: 1) an accurate predictive dynamic model of the network performance, and 2) an efficient solution approach. The most descriptive and detailed models of heat exchangers and fouling have proved to be accurate and useful to assess the performance of preheat trains, but their large scale hinder their use in optimization algorithms for real industrial applications. From a modelling perspective significant progress has been made to model heat exchangers and crude oil deposition. There is a vast range of models developed under different assumptions that capture different parts of the problem. However, the models used for optimization purposes have been restricted to lumped models coupled with empirical or semi-empirical models for fouling. These simplified models compromise the accuracy of the predictions and ignore the effect of important variables in the system. Despite the simplification of the models, the optimal cleaning scheduling problem and optimal retrofit problem are still challenging, and the use of heuristics and linearization of the models has typically been necessary to achieve feasible solutions and explore alternatives.

Even though mathematical programming solutions have been proposed to optimize the operation and to define fouling mitigation strategies of crude preheat trains, there are key aspects that need to be addressed to achieve a better representation of the actual problem, or to improve the quality of the solution:

1. The use of more accurate, descriptive and predictive models of fouling and heat transfer within the optimization– flow distribution, cleaning scheduling, retrofit – of preheat trains.
2. The simultaneous optimization of multiple fouling mitigation actions to exploit their interactions and synergies.
3. The time representation and discretization of the cleaning scheduling problem should be refined to consider the influence of fast dynamics and disturbances occurring at shorter time scales.
4. Accounting for the effect of variability and uncertainty in the operation and optimization of preheat trains – variable input stream conditions and changes in the properties of crude oil.

5. Efficient algorithms to solve the deterministic optimization problem associated with the cleaning scheduling and/or retrofit of preheat trains under fouling when they are represented using rigorous models.
6. Validation of the predictive models under the varying operating conditions observed in industrial preheat trains.
7. A closed-loop implementation that optimally defines fouling mitigation actions – flow distribution and cleanings – considering the process variability.

These aspects are addressed in this thesis. New modelling approaches, solution strategies, algorithms to integrate multi-scale decisions, and online practical applications are developed.

Chapter 3

Optimizing preheat trains under fouling: general mathematical formulation

This chapter presents the models developed to represent the elements of HEN, their interactions, and the heat transfer, mass transfer, and deposition phenomena. These models are used in the formulation of the optimal cleaning scheduling and flow distribution problem (MINLP) along with operational constrains. The generality and flexibility of the models, and the benefits of optimally integrating control and scheduling decisions, are demonstrated in small but realistic case studies covering a wide range of conditions observed in refining operations. In addition, an efficient representation of the logic disjunctions and time discretization is proposed to reduce the number of complicating variables of the problem.

3.1. Introduction

One of the objectives of this thesis is to develop predictive models that accurately capture the behaviour of HEN under fouling in refining applications with the purpose of optimising their operation. The predictive models should capture all important interactions of the system, including the main physical phenomena such as heat transfer, deposition, changes in the streams temperature, and in the pressure drop of the exchangers. These features represent the equality constraints of an optimization problem formulation. Also, these models should provide insights about the key performance indicators of the operation – energy consumption, total cost – and they should allow to quantify the effect and benefits of possible fouling mitigation actions such as cleaning units of the network. These key performance indicators are part of the objective function of the optimization problem.

In this chapter a flexible and general mathematical model is introduced to represent the operation of HEN under fouling. It has the right balance between complexity and accurate

representation of the phenomena making it suitable for optimization purposes. The model is used to formulate and solve the optimal cleaning scheduling and flow distribution problem of HEN under fouling. Different formulations, time representations, and solutions strategies are evaluated and applied to realistic case studies.

3.2. Model building blocks

The model developed to represent heat exchangers is specific to shell and tube heat exchangers as they are the most commonly found in refinery preheat trains. The model considers the radial heat transfer and temperature distribution, and it includes a detailed representation of the deposit layer, but it does not consider axial effects. Instead, it only considers the average effects between inlet and outlet conditions of the exchanger to characterize the heat transfer, pressure drop, and their interactions with the deposition mechanisms.

The following are the constituent equations and additional considerations of the model.

3.2.1. Network representation

The HEN is represented as a directed multigraph, in which each stream type or fluid corresponds to a graph, and the connections between two nodes defines an arc. The nodes of the network are: heat exchangers, sources, sinks, mixes, splitters, and furnace. Figure 3.1 shows an example of a network that illustrates each node. The network used in this example has two stream types: crude oil and naphtha defining two directed graphs. All the nodes in the network are considered adiabatic except the furnace where additional heat is provided as fuel is burnt to increase the temperature of the crude oil stream before entering the CDU. All nodes satisfy mass and energy balances, and only in the heat exchanger nodes two graphs interact as heat is transferred from one stream to the other.

To define the HEN model in a compact mathematical representation the following sets and indexes are used:

- $HEX = \{1,2,\dots,n_{HEX}\}$. Set of heat exchangers in the network.
- $Sp = \{1,2,\dots,n_{Sp}\}$. Set of splitters in the network.
- $Mx = \{1,2,\dots,n_{Mx}\}$. Set of mixers in the network.
- $So = \{1,2,\dots,n_{So}\}$. Set of source nodes

- $Si = \{1,2,\dots,n_{Si}\}$. Set of sink nodes
- $N = HEX \cup Sp \cup Mx \cup So \cup Si$. Set of all nodes in the network.
- $S = \{1,2,\dots,n_S\}$. Set of stream types (e.g. crude, naphtha) in the network, where each type is a different fluid.
- $A = \{(i,j,k)|\exists(i,j,k) \in N \times N \times S\}$. Set of arcs that define the connection between nodes for a given stream type.
- $T = \{1,2,\dots,n_T\}$. Set representing time. It is represented as a sorted sequence of discrete points. Its structure can change depending on the way time is represented and on the discretization technique. This is discussed in more detail in Section 3.3.

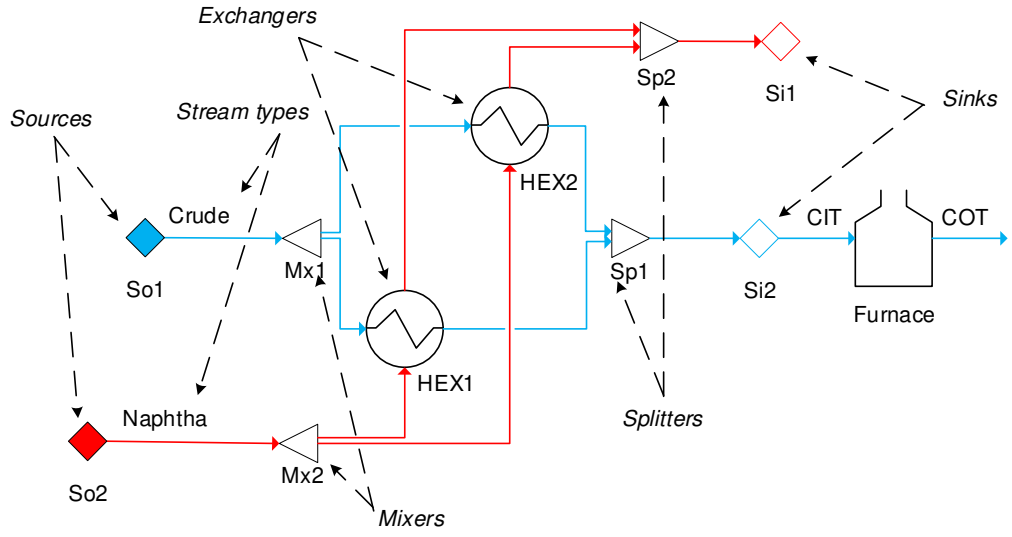

Figure 3.1. Representation of a HEN as a graph showing all the nodes and arcs.

The arcs are defined in terms of the node of origin, node of destination, and stream type. A stream type refers to the fluid that flows through the network – single graph – and defines the physical properties of those streams. The physical properties of each stream are function of temperature, and a linear relation is used for the specific heat capacity, the density, and the thermal conductivity, while an exponential relation is used for the viscosity. These functions are fitted either from data or from more rigorous correlations depending on the case study. In most of the cases the crude oil and CDU product streams physical properties correlations are fitted from API relations (Riazi 2005). Appendix A presents the temperature dependent functions for calculating the physical properties of the fluids in refinery preheat trains, and the various sources from where data is acquired.

The mass balances for all the nodes are defined in Eq. (3.1) – (3.2) , and the energy balances in Eq. (3.3) – (3.5). Note that the mass flow rate, and the inlet temperature of the source nodes are additional degrees of freedom, or they can be fixed depending on the scenario. Also, for the splitter nodes an additional constraint is imposed to ensure that the temperature of all outlet streams is the same.

$$\sum_{j\in N|(i,j,k)\in A} m_{i,j,k,t} = \sum_{j\in N|(j,i,k)\in A} m_{j,i,k,t}\,, \qquad \forall i \in N\backslash\{So \cup Si\}, k \in S, t \in T \tag{3.1}$$

$$\sum_{j\in N|(i,j,k)\in A} m_{i,j,k,t} = m_i^0, \qquad \forall i \in So, k \in S, t \in T \tag{3.2}$$

$$\sum_{j\in N|(i,j,k)\in A} m_{i,j,k,t} Cp_{k,t} T_{i,j,k,\mathrm{t}} = \sum_{j\in N|(j,i,k)\in A} m_{j,i,k,\mathrm{t}} Cp_{k,t} T_{j,i,k,\mathrm{t}}\,, \qquad \forall i \in \{Mx \cup Sp\}, k \in \mathrm{S}, t \in T \tag{3.3}$$

$$\sum_{j\in N|(i,j,k)\in A} T_{i,j,k,t} = T_i^0, \qquad \forall i \in So, k \in S, t \in T \tag{3.4}$$

$$\sum_{i'\in N|(i',i,k)\in A} T_{i',i,k,t} = T_{i,j,k,t}, \qquad \forall i \in Sp, j \in N, k \in S, t \in T(i,j,k) \in Arcs \tag{3.5}$$

The mass and energy balances assume steady state operation, although fouling is a dynamic process. The fouling rate is much slower than the heat transfer rate, so that a pseudo steady state assumption is valid. The time evolution of the system follows a series of steady states and the only dynamic behaviour is given by the deposition rate. While the time scale of the heat transfer is in the order of seconds – a fast process –, that of the deposition rate is in the order of days and months – a slow process. The energy balance for the heat exchanger is defined later in this section considering the interaction between two streams.

Finally, the furnace is considered as an additional node in the network for which the mass balance is trivial, and the energy balance, Eq. (3.6), defines the furnace duty. The inlet temperature to the furnace – coil inlet temperature, CIT – varies because of fouling and operational changes in the network, but its outlet temperature – coil outlet temperature – is fixed based on the operation of the atmospheric distillation unit. The COT target is usually ~ 350°C, but it is a controlled variable to ensure the quality and production targets of the refinery. Hence, to maintain a constant COT, the furnace duty must react to the changes in the CIT, and because of the performance decay of the heat exchanger due to fouling, the furnace duty increases as well as the operating cost of the network.

$$\sum_{j\in N|(i,j,k)\in A} m_{i,j,k,\mathrm{t}} Cp_{k,t} T_{i,j,k,\mathrm{t}} = \eta_f Q_{f,t} + \sum_{j\in N|(j,i,k)\in A} m_{j,i,k,\mathrm{t}} Cp_{k,t} T_{j,i,k,\mathrm{t}}\,, \quad \forall i = Furnace, k \in \mathrm{S}, t \in T \tag{3.6}$$

3.2.2. Heat exchanger model

The heat exchanger model adopted here is the P-NTU model for shell and tube exchangers (Thulukkanam 2013; Hewitt, Shires, and Bott 1994). It is based on the definition of the temperature effectiveness P to quantify the ratio of temperature change of the tube side with respect to that of the shell side. The effectiveness is a function of the flow patterns of the shell and tube side. The most common configuration is: counter current flow, single shell, multiple tube passes exchangers for which the effectiveness is defined by Eq. (3.7), where its dimensionless terms are defined in Eq. (3.8) for the number of transfer units, and Eq. (3.9) for the ratio of heat capacities. From this exchanger configuration others more complex can be built. Exchangers with multiple shell passes are modelled using two or more single shell pass exchanger with the appropriate connections for the streams. All the physical properties are temperature dependent, so for all calculations they are averaged between inlet and outlet conditions of the exchanger.

$$P_{i,\mathrm{t}} = 2\left\{1 + Rc_{i,\mathrm{t}} + \left(1 + Rc_{i,\mathrm{t}}^2\right)^{1/2}\left[\frac{1+\exp\left(-NTU_{i,\mathrm{t}}\left(1+Rc_{i,\mathrm{t}}^2\right)^{1/2}\right)}{1-\exp\left(-NTU_{i,\mathrm{t}}\left(1+Rc_{i,\mathrm{t}}^2\right)^{1/2}\right)}\right]\right\}^{-1}, \quad \forall i \in HEX, t \in T \tag{3.7}$$

$$NTU_{i,t} = \frac{U_{i,t}(HTA_i)}{m_{i,t}^T Cp_{i,t}^T}, \quad \forall i \in HEX, t \in T \tag{3.8}$$

$$Rc_{i,\mathrm{t}} = \frac{m_{i,\mathrm{t}}^T Cp_{i,t}^T}{m_{i,\mathrm{t}}^S Cp_{i,t}^S}, \quad \forall i \in HEX, t \in T \tag{3.9}$$

The number of transfer units (NTU) is a function of the overall heat transfer area, and of the overall heat transfer coefficient. The overall heat transfer coefficient, defined in Eq. (3.10), represents the inverse of the total resistance to heat transfer from the shell side to the tube side, and it includes the convective heat transfer coefficient of the tube side and of the shell side; the conductive heat transfer coefficient of the tube wall and of the deposit layer, and the fouling resistance. The convective heat transfer coefficient on the tube side is calculated using the McAdams correlation for convection in tubes in turbulent regime (McAdams 1954), and that on the shell side is calculated using the Bell-Delaware method (Bell 1963, 1981). The additional terms in Eq. (3.10) are correction factors so that all the heat

transfer resistances are defined with respect to the external area of the tubes of the exchanger, Eq. (3.11).

$$\frac{1}{U_{i,t}} = \frac{1}{h_{i,t}^{S}} + \frac{d_i}{2\lambda_i^{W}} Ln\left(\frac{d_i}{d_{I,i}}\right) + \frac{d_i}{d_{i,t}^{F}} \frac{1}{h_{i,t}^{T}} + R_{f,i,t}, \qquad \forall i \in HEX, t \in T \tag{3.10}$$

$$HTA_i = \pi d_i L_i (N_{T,i}), \qquad \forall i \in HEX \tag{3.11}$$

The main key performance indicators of heat exchangers are their duty, outlet streams temperature, and pressure drop. All of them are affected by fouling, so they change dynamically as material deposits over the surface. The first two performance indicators are estimated using the temperature effectiveness, Eq. (3.12) – Eq. (3.14), while the pressure drop is a function of the friction factor and the flow diameter. Only the changes in the tube side pressure drop due to fouling are considered in the model, while those of the shell side pressure drop are neglected. It is assumed that fouling only takes place inside the tubes of the exchangers because generally the fouling propensity of crude oil – which flows on the tube side most of the times – is much higher than that of heating streams which are products of the CDU. Crude distillation products have a low fouling propensity as much of the fouling agents – asphaltenes – deposit on the preheat train or are carried away in the bottoms of the column to the vacuum distillation unit (Coletti et al. 2015; Jones and Pujado 2006). As deposition takes place inside the tubes, the flow diameter decreases, and the surface roughness increases, which affects significantly the pressure drop and may compromise the feasibility of the operation. Eq. (3.15) defines the tube side pressure drop as a function of the Fanning friction factor, surface roughness, and tube length. Although crude oil deposition changes the surface roughness, it is assumed to be constant for simplicity and because it has been proven to reach an asymptotic level relatively fast, and its evolution to have a negligible effect on the overall performance of the unit (Coletti and Macchietto 2011).

$$Q_{i,t} = P_{i,t} m_{i,t}^{T} Cp_{i,t}^{T} \left(T_{i,t}^{S,in} - T_{i,t}^{T,in}\right), \qquad \forall i \in HEX, t \in T \tag{3.12}$$

$$T_{i,t}^{T,out} = T_{i,t}^{T,in} + P_{i,t} \left(T_{i,t}^{S,in} - T_{i,t}^{T,in}\right), \qquad \forall i \in HEX, t \in T \tag{3.13}$$

$$T_{i,t}^{S,out} = T_{i,t}^{S,in} - P_{i,t} Rc_{i,t} \left(T_{i,t}^{S,in} - T_{i,t}^{T,in}\right), \qquad \forall i \in HEX, t \in T \tag{3.14}$$

$$\Delta P_{i,t} = \frac{\left(G_{i,t}^{T}\right)^2}{2\rho_{i,t}^{T}} \left[\frac{f_{i,t} L_i}{d_{i,t}^{F}} \left(\frac{\mu_{i,t}^{T}}{\mu_{i,t}^{W}}\right)^{0.25}\right] N_{P,i}, \qquad \forall i \in HEX, t \in T \tag{3.15}$$

In summary, this is a lumped model to predict the heat transfer and outlet conditions of each exchanger, and to have a complete representation of the preheat train it must be linked with a fouling model that considers the radial effects, and with a network model.

3.2.3. Fouling model

The deposition rate, and the deposit properties define the additional thermal resistance, the flow diameter, and their time evolution. Also, changes of the deposit structure due to long exposure to high temperature affect the heat transfer in the exchangers as they can change the nature and properties of the deposit such as its thermal conductivity. Ageing or coking is of interest in crude oil fouling, and it refers to the structural change of a fresh gel-like deposit, to an aged hard coke-like deposit that has a higher thermal conductivity and that is more difficult to remove from the surface (Ishiyama et al. 2010; Coletti et al. 2010). Figure 3.2 shows a schematic representation of all the domains involved in the radial heat transfer. It shows the various resistances: shell side, tube wall, aged deposit, fresh deposit, and tube side, and the expected temperature profiles along the radial direction indicating the labels of the variables at the boundaries of the domains. These boundary temperatures can be calculated by solving explicitly an energy balance in the radial direction, assuming steady state – the fouling dynamics characterize the system evolution – and using the heat transfer coefficients of each section.

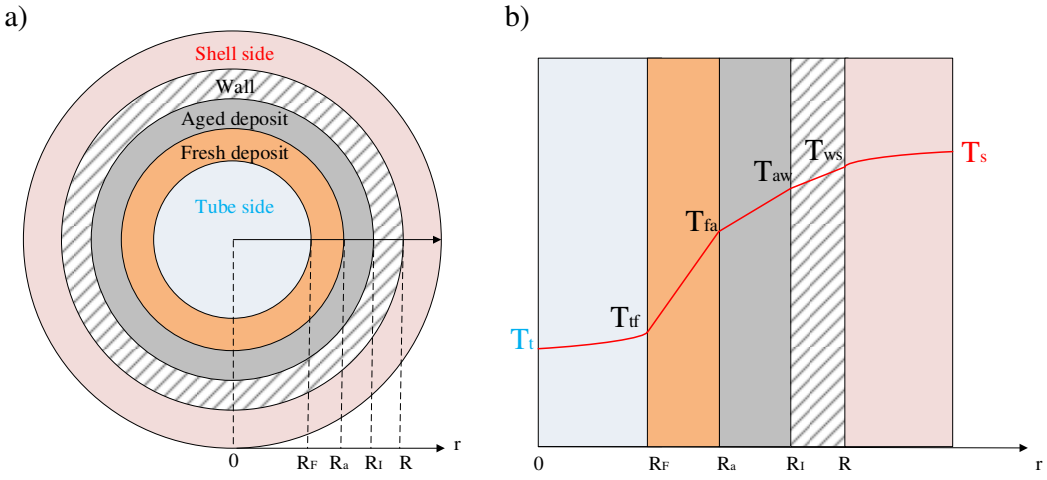

Figure 3.2. Multi-layer representation for the heat transfer in the radial direction of a shell and tube heat exchanger. a) frontal view for a tube, b) representative temperature profile and notation.

Eq. (3.16) – Eq. (3.19) are the solution of steady state energy balances in the radial direction, used to calculate the temperature at the boundaries. They are function of the overall heat transfer coefficient, and of the thickness of each deposit layer or fouling resistance of the layer. Note that this energy balance is solved at the inlet and outlet conditions of the exchange assuming a counter current flow. In this model, it is assumed that the deposit is a discrete domain with two compartments that do not mix, one for the fresh deposit and other for the aged deposit as proposed by Ishiyama, Paterson, and Wilson (2010). In contrast to a continuous representation of the deposit in which its evolution and composition is defined at every point in the radial direction (Diaz-Bejarano, Coletti, and Macchietto 2018), the approach adopted here does not require additional differential equations to model the deposit; and it is still capable of predicting with reasonable accuracy the average effect of the deposit and its composition on the operation of the exchangers. The compactness of the model is a desired feature for optimization purposes.

$$T_{i,t}^{ws,k} = \begin{cases} T_{i,t}^{T,in} + \dfrac{U_{i,t}}{h_{i,t}^{S}}\left(T_{i,t}^{S,out} - T_{i,t}^{T,in}\right), k = in \\ T_{i,t}^{S,in} + \dfrac{U_{i,t}}{h_{i,t}^{S}}\left(T_{i,t}^{T,out} - T_{i,t}^{S,in}\right), k = out \end{cases}, \quad \forall i \in HEX, t \in T, k \in \{in, out\} \tag{3.16}$$

$$T_{i,t}^{aw,k} = \begin{cases} T_{i,t}^{tf,k} + U_{i,t}R_{f,i,t}\left(T_{i,t}^{S,out} - T_{i,t}^{T,in}\right), k = in \\ T_{i,t}^{tf,k} + U_{i,t}R_{f,i,t}\left(T_{i,t}^{T,out} - T_{i,t}^{S,in}\right), k = out \end{cases}, \quad \forall i \in HEX, t \in T, k \in \{in, out\} \tag{3.17}$$

$$T_{i,t}^{fa,k} = \begin{cases} T_{i,t}^{tf,k} + U_{i,t}R_{f,i,t}^{f}\left(T_{i,t}^{S,out} - T_{i,t}^{T,in}\right), k = in \\ T_{i,t}^{tf,k} + U_{i,t}R_{f,i,t}^{f}\left(T_{i,t}^{T,out} - T_{i,t}^{S,in}\right), k = out \end{cases}, \quad \forall i \in HEX, t \in T, k \in \{in, out\} \tag{3.18}$$

$$T_{i,t}^{tf,k} = \begin{cases} T_{i,t}^{T,in} + \dfrac{U_{i,t}d_i}{h_{i,t}^{T}d_{i,t}^{F}}\left(T_{i,t}^{S,out} - T_{i,t}^{T,in}\right), k = in \\ T_{i,t}^{S,in} + \dfrac{U_{i,t}d_i}{h_{i,t}^{T}d_{i,t}^{F}}\left(T_{i,t}^{T,out} - T_{i,t}^{S,in}\right), k = out \end{cases}, \quad \forall i \in HEX, t \in T, k \in \{in, out\} \tag{3.19}$$

Fouling is a local phenomenon, and it is function of the local conditions at which the deposition or the changes in the deposit occur. The deposition of asphaltenes that generates the fresh layer of the deposit takes place at the thermal boundary layer between the tube side and the deposit surface. Hence, the deposition rate is function of the film temperature, which is calculated in Eq. (3.20) as a weighted average between the tube side temperature and the temperature at the boundary between the tube bulk and the deposit (Ebert and Panchal 1995). In the case of ageing or coking reactions that take place in the aged deposit layer, they are assumed to be function of the average temperature of that layer at the inlet and outlet

conditions of the exchanger, Eq. (3.21). The average temperature is calculated from the solution of the steady state temperature profile in the aged deposit layer.

$$T_{i,t}^{f,k} = \begin{cases} T_{i,t}^{T,in} + 0.55\left(T_{i,t}^{tf,k} - T_{i,t}^{T,in}\right), k = in \\ T_{i,t}^{S,in} + 0.55\left(T_{i,t}^{tf,k} - T_{i,t}^{S,in}\right), k = out \end{cases}, \quad \forall i \in HEX, t \in T, k \in \{in, out\} \tag{3.20}$$

$$T_{i,t}^{a,k} = T_{i,t}^{fa,k} + \left(T_{i,t}^{aw,k} - T_{i,t}^{fa,k}\right)\left[\frac{d_{I,i}}{2\delta_{i,t}^{a}} + \frac{1}{\ln\left(1 - 2\delta_{i,t}^{a}/d_{I,i}\right)}\right], \quad \forall i \in HEX, t \in T, k \in \{in, out\} \tag{3.21}$$

The explicit solution of the radial temperature profiles and the definition of the thermal resistance considering the curvature effects is a novelty of this work. The thermal resistance of the deposit has been usually defined applying a thin layer assumption which restrict the application and validity of the model to small deposits ($\delta \ll d_I$) (Ishiyama, Paterson, and Wilson 2010, 2014). Using a rigorous radial representation of the deposit allows to accurate represent the operation of exchanger with large obstructions of the tubes and high thermal resistances.

The Ebert-Panchal model, Eq. (3.22), is used to characterize the deposition rate, and in this case it defines directly the total fouling resistance (Ebert and Panchal 1995). It is a semi empirical model that defines the deposition rate as the competition of the processes of deposition and removal. The deposition is function of the tube side Reynolds number, tube side Prandtl number, and of the film temperature following an Arrhenius expression, while the removal rate is assumed to be proportional to the shear stress. The film temperature is calculated at the inlet and outlet conditions of the exchanger, so each extreme has a different fouling rate. Because the heat exchanger model is lumped in the axial direction the effective fouling rate is defined as the average fouling rate between those calculated at the inlet and outlet conditions.

$$\frac{dR_{f,i,t}}{dt} = \left\langle \alpha_i Re_{i,t}^{-0.66} Pr_{i,t}^{-0.33} \exp\left(-\frac{E_{f,i}}{RT_{i,t}^{f}}\right) - \gamma_{i,t}\tau_{i,t} \right\rangle, \qquad \forall i \in HEX, t \in T \tag{3.22}$$

The fouling model parameters: deposition constant (α), removal constant (γ), and activation energy (E_f) can be calculated based on experimental observation or on operational plant data and are adjustable tuning parameters. This model can be adapted to different applications depending on the conditions observed, while still being able to predict the effect of the process variables such as flow rates and temperature on the deposition rate.

There are other models in the literature for crude oil fouling beyond the Ebert-Panchal one. They can be of three types: completely empirical, semi empirical, or based on fundamental principles. The empirical ones are simple linear or exponential relations of the fouling resistance and time, they require a large data set, and do not capture the effect of the process variable on the deposition rate. The semi empirical models are usually variations of the Ebert-Panchal model with additional terms to consider the effect of geometry in more detail (Wilson, Polley, and Pugh 2005), different values for the exponents of the dimensionless number, or ignoring the removal rate (Wang et al. 2015). They present the same characteristics of the Ebert-Panchal model, although the number of tuning parameters may vary. The final type of models is based on the fundamental principles behind the deposition of asphaltenes and their attachment to the surfaces. These models consider mass transfer processes, and some may be as detail as to introduce molecular dynamic approaches (Yang et al. 2015; Bennett 2012). The main limitations of these models are the large number of parameters to determine (e.g. mass transfer coefficients), the still lack of understanding of crude oil fouling mechanisms, and their limited accuracy for predicting macroscopic effects of fouling in the operation of heat exchangers. Considering these features, and with the goal of developing a model suitable for optimization purposes the Ebert-Panchal model has a good compromise between prediction capabilities, and model complexity.

To model the effects of deposit ageing or coking a first order kinetic approach is used, Eq. (3.23). Because the ageing rate changes from inlet to outlet conditions of the exchanger, the effective ageing rate is defined as the average rate between those conditions. It has been previously reported that a first order kinetics best represents the ageing process in crude oil fouling, but there is still a need to fit the model parameters using data (Ishiyama et al. 2010). The ageing model defines the age of the deposit using a "youth" variable which represents the mass fraction of fresh deposit in the overall deposit layer. Ageing changes the physical properties of the deposit affecting the total fouling resistance. The higher the coke fraction – low values of the "youth" variable – the higher the thermal conductivity of the deposit which can be wrongly interpreted as reduction in fouling as the deposit thickness is still increasing, and no deposit has been removed (Ishiyama, Paterson, and Wilson 2014). Not considering this in the predictive model may lead to wrong decisions, and even compromise the operation of a HEN by delaying cleaning actions and causing blockages of the tubes. For these reasons

it is important to consider the pressure drop caused by the flow diameter reduction in the performance analysis of the system.

$$\frac{dx_{i,t}^{f}}{dt} = \langle -k_i^a \exp\left(-\frac{E_i^a}{RT_{i,t}^a}\right) x_{i,t}^{f} \rangle, \qquad \forall i \in HEX, t \in T \tag{3.23}$$

Using the "youth" variable the total deposit thickness, which affects the pressure drop, can be calculated as well as the individual fouling resistance of each layer. Eq. (3.24) – Eq. (3.28) are a set of implicit algebraic equations that define the individual layer and total thicknesses and fouling resistances. Each of the individual fouling resistance considers the radial effects of heat transfer, and their expressions are derived from solving an energy balance in the radial direction. This overcomes the thin layer assumption (Ishiyama, Paterson, and Wilson 2010) that restrict the application and accuracy of the model to situations with small deposits. In addition, Eq. (3.29) defines the free flow diameter which affects directly the tube side pressure drop. These set of variables are used as the key indicators of the performance decay of each heat exchanger.

$$x_{i,t}^{f} = \frac{\left(d_{I,i} - \delta_{i,t}\right)\delta_{i,t}^{f}\rho^{f}}{\left(d_{I,i} - \delta_{i,t}\right)\delta_{i,t}^{f}\rho^{f} + \left(d_{I,i} - \delta_{i,t}^{a}\right)\delta_{i,t}^{a}\rho^{a}}, \qquad \forall i \in HEX, t \in T \tag{3.24}$$

$$\delta_{i,t} = \delta_{i,t}^{f} + \delta_{i,t}^{a}, \qquad \forall i \in HEX, t \in T \tag{3.25}$$

$$R_{f,i,t}^{f} = \frac{d_i}{2\lambda^{f}} \ln\left(\frac{d_{I,i} - 2\delta_{i,t}^{a}}{d_{I,i} - 2\delta_{i,t}}\right), \qquad \forall i \in HEX, t \in T \tag{3.26}$$

$$R_{f,i,t}^{a} = \frac{d_i}{2\lambda^{a}} \ln\left(\frac{d_{I,i}}{d_{I,i} - 2\delta_{i,t}^{a}}\right), \qquad \forall i \in HEX, t \in T \tag{3.27}$$

$$R_{f,i,t} = R_{f,i,t}^{f} + R_{f,i,t}^{a}, \qquad \forall i \in HEX, t \in T \tag{3.28}$$

$$d_{i,t}^{F} = d_{I,i} - 2\delta_{i,t}, \qquad \forall i \in HEX, t \in T \tag{3.29}$$

Overall the fouling model consists of a set of differential algebraic equations that are linked to the model of a heat exchanger. The presence of differential equations requires the definition of consistent initial conditions for the problem, but they may vary depending on the case. For instance, the initial state of some networks may be cleaned so that $R_f = 0$ and $x^f = 1$, but for other cases some exchangers may exhibit some initial deposit. Also, differential equations add complexity to the problem because they need an appropriate discretization scheme, and the optimization decision variables become a function of time

(e.g. when to clean a unit). The time discretization alternatives and dynamic optimization are discussed later in the chapter.

3.2.4. Operating mode disjunctions

Two possible states are defined for a heat exchanger in a network: "operating" or "idle". The idle state is defined as an exchanger taken out of operation for cleaning. These two states are associated with a logic variable $Y_{i,t} \in \{True, False\}\ \forall i \in HEX, t \in T$ which is True (1) when the exchanger is idle or being cleaned, and False (0) when the exchanger is operating normally. Each of these states are associated with a set of equations defining the operation of the exchanger. For the operating state the models defined in Sections 3.2.2 and 3.2.3 characterize the normal operation of the units, whereas for the idle state a new set of equations is required to model the behaviour of the network.

To model the idle state of the heat exchangers bypass streams are included in the network representation so that the flow can be diverted when the unit is being cleaned while ensuring the complete connectivity of the network. Figure 3.3 shows the additional bypass streams for the tube and shell sides of a single heat exchanger which are included in the HEN representation. These streams are defined for all the units and are only active – mass flow rate greater than zero – when the unit is idle, otherwise there is no flow in those streams. Besides the bypass streams, splitters and mixers are introduced in the network representation around each exchanger – Figure 3.3b – to model correctly the switching of the flow streams between changes of state. These elements introduce more variables and constraints as each additional node must satisfy mass and energy balances, although they are simple linear constraints.

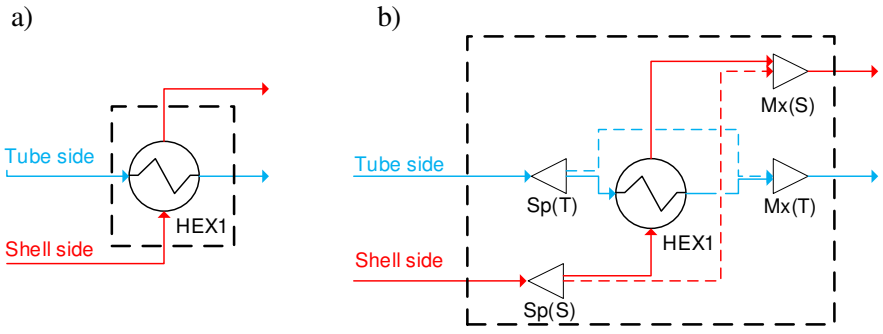

Figure 3.3. Representation of a heat exchanger in a network (a), and the addition of bypass streams for idle state (b).

Considering the introduction of bypass streams and additional nodes around each exchanger, the disjunctions in Eq. (3.30) define the two possible states of each unit at every time. In the "operating" state the heat transfer, fouling, and pressure drop models are active and the bypass flow rates are zero, while in the "idle" state the bypass flow rates are equal to the inlet flow rates of the exchangers. Hence, in the idle state the actual inlet flow rates to the exchanger are zero, which leads to a trivial solution of the mass and energy balances – no heat transfer – and it forces the tube side pressure drop to be zero as it is proportional to the mass flux of the tube side. In addition, during the "idle" state there is no fouling nor ageing of the deposit. When the unit is back in the operating state after a cleaning, the exchanger is at cleaned conditions – no deposit, no ageing – or, depending on the effectiveness of the cleaning, it may still have a small deposit thickness. In this thesis, only mechanical cleanings that can completely remove the deposit are considered, although the modelling approach can easily incorporate other type of cleanings, such as chemical cleanings, that partially remove the deposit and have shorter cleaning times and lower cleaning cost. This assumption does not diminish the generality of the mathematical formulation.

$$\begin{bmatrix} Y_{i,t} \\ Q_{i,t} = 0 \\ \Delta P_{i,t} = 0 \\ R_{f,i,t} = 0 \\ x^{a}_{i,t} = 1 \\ \delta_{i,t} = 0 \\ m^{T,B}_{i,t} > 0 \\ m^{S,B}_{i,t} > 0 \end{bmatrix} \vee \begin{bmatrix} \neg Y_{i,t} \\ \text{Eq. (3.7)} - \text{(3.15)} \\ \text{Eq. (3.22)} - \text{(3.29)} \\ m^{T,B}_{i,t} = 0 \\ m^{S,B}_{i,t} = 0 \end{bmatrix}, \qquad \forall i \in HEX, t \in T \tag{3.30}$$

This set of logic disjunctions is introduced as constraints in the model. They are translated into equality constraints using a BigM reformulation, and the M parameter is chosen independently for each equation based on the variable bounds. The BigM formulation is preferred because of the linear nature of the additional constraints that facilities the converge of standard MINLP solution algorithms. Additional considerations, like introducing slack variables, are necessary in some of the nonlinear equations to avoid numerical inconsistencies such as divisions by zero when a unit is idle.

To introduce the disjunctions into the mathematical model the logic variable $Y_{i,t}$ is replaced by the binary variable $y_{i,t} \in \{0,1\}\ \forall i \in HEX, t \in T$. All the BigM constraints are defined with respect to this binary variable to indicate the state of each exchanger over time.

3.2.5. Operational constraints

The main decision variables of the optimal operation and cleaning scheduling of HEN under fouling are: the flow rates of the network, continuous variables, and the timing and allocation of the cleaning actions, integer variables. The two types of variables are time dependent, and they have strong interactions. The flow rates of the network respond dynamically to maximize the energy recovery at each time instant, and when the state of the unit change – from idle to operating or vice versa – they also change.

One of the main factors that make the cleaning scheduling problem complex and difficult to solve is the large number of binary variables – of the order $n_{HEX}n_T$ – that generates many feasible combinations and solutions with similar objective function values. Inequality constraints related to the binary variables and the structure of the cleaning schedule are introduced to reduce the size of the search space. For instance, Eq. (3.31) is a constraint that avoids consecutive cleanings of the same exchanger, which is well known to be an inefficient strategy, Eq. (3.32) is a constraint to fix the state of all exchanger at the end as operating because cleanings are not profitable towards the final time, Eq. (3.33) defines the maximum number of simultaneous cleanings, and Eq. (3.34) the maximum number of cleanings per unit over the operating time. In the case of heat exchangers with multiple shells, the various shells must be cleaned at the same time, and this is ensured using Eq. (3.35). Other scenarios involving simultaneous cleanings or exclusive cleanings are modelled with similar constraints, but they are case specific depending on the HEN, the requirements of the refinery, or the layout of the units in the plant. This set of constraints help to discard a priori cleaning schedules that are known to be non-optimal or infeasible.

$$y_{i,t} + y_{i.t-1} \leq 1, \qquad \forall i \in HEX, t \in T\backslash\{1\} \tag{3.31}$$

$$y_{i,t} = 0, \qquad \forall i \in HEX, t \in \{n_T\} \tag{3.32}$$

$$\sum_{t \in T} y_{i,t} \leq N_{HEX}, \qquad \forall i \in HEX \tag{3.33}$$

$$\sum_{i \in HEX} y_{i,t} \leq N_T, \qquad \forall t \in T \tag{3.34}$$

$$y_{i,t} = y_{j,t}, \qquad \forall i \in HEX' \subseteq HEX, j \in HEX'' \subseteq HEX, t \in T \tag{3.35}$$

Besides the constraints related with the binary variables, the HEN is also constrained by the operating limits and capacity of the system. Common constraints of this type are: a

firing limit that indicates the maximum duty of the furnace, Eq. (3.36); the minimum and maximum throughput of the distillation column, Eq. (3.37); the minimum pressure, or maximum pressure drop, allowed at the end of the network based on the pumping capacity, Eq. (3.38). If the HEN has parallel branches, additional constraints are required to capture the correct operation of that specific section. The split fraction of the branches can be constrained, Eq. (3.39); and if the flow thought the branches is pressure driven, an equality constraint must ensure that the outlet pressure of each branch is balanced to avoid backflow, Eq. (3.40). These constraints represent possible operational limitation of HEN under fouling observed in real refineries, but they are case specific so that only some may apply.

$$Q_{f,t} \leq Q_f^{max}, \qquad \forall t \in T \tag{3.36}$$

$$m^{min} \leq \sum_{j \in N | (i,j,k) \in A} m_{i,j,k,\mathrm{t}} \leq m^{max}, \qquad \forall i = Furnace, k \in S, t \in T \tag{3.37}$$

$$P^{min} \leq \sum_{j \in N | (i,j,k) \in A} P_{i,j,k,\mathrm{t}}, \qquad \forall i = Furnace, k \in S, t \in T \tag{3.38}$$

$$s_x^{LB}\left(\sum_{j \in N | (j,\mathrm{i},k) \in A} m_{j,\mathrm{i},k,\mathrm{t}}\right) \leq m_{i,j,k,\mathrm{t}} \leq s_x^{UB}\left(\sum_{j \in N | (j,\mathrm{i},k) \in A} m_{j,\mathrm{i},k,\mathrm{t}}\right), \tag{3.39}$$
$$\forall i \in Sp, j \in N, k \in S, t \in T | (i,j,k) \in A$$

$$\sum_{i \in HEX^{B1} \subseteq HEX} \Delta P_{i,t} = \sum_{i \in HEX^{B2} \subseteq HEX} \Delta P_{i,t}, \qquad \forall t \in T \tag{3.40}$$

Most of the above operational constraints are linear equalities or inequalities that do not represent a significant increase in the complexity of the problem, instead they help to reduce its combinatorial nature. The only nonlinear operational constraint is the equality of pressure drop in parallel branches – the pressure drop calculation is a nonlinear expression – but it is only one additional nonlinear constraint among many others from the heat transfer and fouling models.

3.2.6. Objective function

The objective of optimizing the operation and cleaning scheduling of HEN under fouling is the maximization of the economic benefits: minimal operational cost, and maximum profit. The objective function is mathematically represented in Eq. (3.41). The operational costs are: cost of energy, cost of carbon emissions, and cost of cleanings, while the only source of profit is the production rate. The cost of energy is proportional to the

furnace duty, as well as the cost of carbon emissions. The cleaning cost is specific to each exchanger, and it may vary depending on the type of cleaning, location and size of the exchanger. Another possible operational cost is the electricity cost that arise from the power of pumps used to move the crude through the network. However, this cost is negligible compared to the others and it can be neglected (Coletti and Macchietto 2011a).

$$J = \min\left(P_f \int_0^{t_f} Q_f dt + P_{CO} K_{CO} \int_0^{t_f} Q_f dt + \sum_{i \in HEX} P_{cl,i} \sum_{t \in T} y_{i,t} - P_m \int_0^{t_f} m_f dt\right) \tag{3.41}$$

This objective function only considers the operational costs, and it ignores any capital cost. Capital cost should be included in the objective function if retrofit alternatives decisions are part of the optimization problem. This is discussed in Chapter 6 of this thesis.

3.3. Time representation: discrete and continuous formulation

The time representation is key for a successful integration of scheduling and control decision in the operation of HEN under fouling. The requirements of any time representation approach are: to represent accurately the differential equations of the model, and to be able to model scheduling decisions such as task assignment, task sequencing, and timing of the tasks. In addition, it should accurately capture the slow long-term dynamics – scheduling decisions – and fast dynamics – control decisions – of the process without additional complexity. The difficulty of finding a solution to the optimization problems addressed in this thesis comes from the number of binary variables which are indexed in time, so that a time representation that requires many discrete time instances increases the combinatorial aspect of the problem (Bassett, Pekny, and Reklaitis 1996).

There are two alternatives for representing time and time events for the integrated scheduling and control problem of HEN: a discrete time formulation, and a continuous time formulation. Depending on the time discretization approach, the time related events are modelled differently, and it may be necessary to introduce additional binary variables and constraints. Figure 3.4 shows a schematic representation of the two discretization approaches. In both alternatives the time domain is divided in a fixed number of intervals. For the discrete approach the length of the intervals is set, while for the continuous one it is variable, and it is assumed to be global – the same for all the units. The specifications of the formulation, variables, and constraints associated with each discretization alternative are described in the

following sections. In addition, in this continuous time representation, the time events in a scheduling problem can be modelled based on the precedence of the task executed in the units – immediate precedence relationships or general precedence relationships – but this is not suitable for the HEN cleaning scheduling problem because they have limitations to model inventory constraints (Méndez et al. 2006). A HEN has a high level of connectivity among the nodes, they interact through the flow rates at every single point in time, and the mass and energy balances – inventory – must be satisfied.

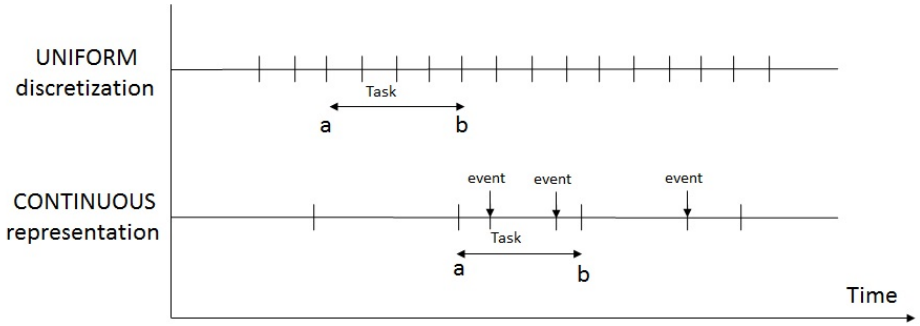

Figure 3.4. Time domain discretization for scheduling problems, adapted from (Pinto and Grossmann 1998).

3.3.1. Discrete time approach

Using the discrete time approach the time horizon is divided in n_T periods of equal length, T, defining a uniform grid. Then the set representing time is defined as $T = \{1,2,\dots,n_T\}$, which elements correspond to equally distributed fixed points in the time horizon. The fixed time grid of this approach limits the occurrence of time events to the discrete points specified, although an event can occur at more than one event point. The length of the periods should capture all relevant time dependent events of the scheduling problem, and it is usually defined as the greatest common factor of the characteristic time of the problem (Floudas and Lin 2004). In the cleaning schedule problem of HEN, the length of the periods is defined as the minimum factor of the cleaning times. For instance, if all the mechanical cleanings last 10 days, then this defines the length of the periods. However, shorter period lengths can be used for a more accurate representation of the time events – also in the case of units with different cleaning times – and integration of the differential equations. The more periods used to represent the time horizon, the larger the number of binary variables, making the optimization problem more challenging.

In this time representation, the binary variables of the problem, $y_{i,t}$, represent the starting time of the cleaning actions. Cleanings that last more than one discrete period are modelled by Eq. (3.42), where β_i is the fixed duration of the cleaning expressed in terms of number of periods. In this modelling approach all cleaning times must be a factor of the length of the period, T.

$$\sum_{t'=t}^{t+\beta_i-1} y_{i,y'} - 1 \leq \beta_i(1 - y_{i,t}), \qquad \forall i \in HEX, t \in T \tag{3.42}$$

The differential equations of the model are discretized using a backward finite difference approach. They are transformed into a set of algebraic constraints given by Eq. (3.43) and Eq. (3.44). Here, x indicates a differential variable that could be the fouling resistance or the composition of the deposit in the fouling problem; RHS is a short notation for the right-hand side of the corresponding differential equation, and s is a slack variable which is active when the unit is idle and the differential equations of the model are not active. The accuracy of the integration of the set of equations depends on the value of T used in the discretization of the time horizon.

$$x_t = x^0, \qquad \forall t \in \{1\} \tag{3.43}$$

$$x_t - x_{t-1} = \mathrm{T}(RHS_t) + s_t, \qquad \forall t \in T\backslash\{1\} \tag{3.44}$$

The discrete time representation of the scheduling problem allows an easy formulation of the scheduling decisions, although it has shortcomings such as the large number of binary variables required, and the inherit inaccuracy of the solution.

3.3.2. Continuous time approach

Using a continuous time representation the timing, sequence, and duration of events are represented by continuous variables, while the change of states are represented by binary variables (Floudas and Lin 2004). This reduces the number of binary variables needed in the model and provides more flexibility and accuracy to define the starting time of the cleaning actions. Comparing this representation with the discrete time one, it generates a better and more realistic abstraction of the problem, but the relaxation of the MINLP formulation is not as tight, which may compromise its solution (Sundaramoorthy and Maravelias 2011).

The continuous time representation used defines the events at global time points, so that all the units in the network share the same time scale and the mass and energy balances are satisfied at every time point. Continuous time representations in which the events are unit specific or defined based on the precedence of tasks are not suitable for the HEN cleaning scheduling problem because of the generality of the networks and the high level of connectivity among the nodes at all times, although they are can be advantageous for batch production scheduling problems (Mouret, Grossmann, and Pestiaux 2011; Méndez et al. 2006).

In this approach, the time horizon is divided in a fixed number of periods N_P of variable length T_p. The length of the period is an additional decision variable, but it is bounded between a minimum and maximum value. Including realistic bounds for the period length allows to retain the same solution accuracy through all the time horizon. In addition, each period is further discretized using orthogonal collocation in finite elements, and for all applications in this thesis a Radau scheme with three collocation points is used, although other discretization alternatives can be used (Biegler 2010). The internal points of the periods help to increase the accuracy of the integration of the differential equations. Considering this, the set representing time is defined as $T = \{(1,1), (1,2), \dots, (N_p, N_c)\}$, where each pair element represent a point in the time horizon, and the first element of the pair correspond to the period, while the second to the discretization point within that period.

Figure 3.5 shows a schematic representation of the continuous time discretization approach, and how each period is divided in discrete points to improve the accuracy with which the differential equations are integrated. Each period only has one state for each exchanger, so that changes in the state of the units are only allowed in the transition from one period to the other. Hence, the binary variables indicating the state of the units are only indexed in the number of periods and not in all the time points. This reduces significantly the number of binary variables as the periods are much fewer than the elements of the time set.

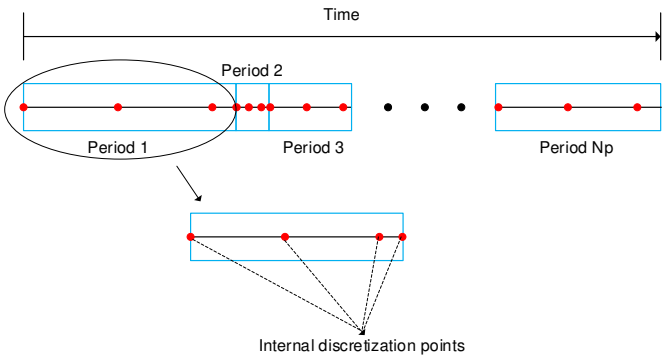

Figure 3.5. Representation of the time horizon using a continuous time approach

The continuous time representation introduces additional variables to the problem formulation: $z_p \forall p \in \{1,2,\dots,N_p\}$ which is a binary variable indicating whether one or more units are at an idle state, and $\mathrm{T}_p \forall p \in \{1,2,\dots,N_p\}$ which is the length of each period. In addition, constraints to model correctly the time evolution, and time dependent events are required in this approach. For instance, Eq. (3.45) defines the cleaning time, Eq. (3.46) defines the lower and upper bounds for the length of each period depending on the states of the exchangers, Eq. (3.47) defines the actual time at the end of each period, and Eq. (3.48) is the constraint that ensure completion of the operation and reaching the final time. Note that the cleaning time is defined as the maximum cleaning time of the units, so that when two or more are cleaned simultaneously all of them are idle for their maximum cleaning time. The maximum expression used in this constraint is approximated using a smooth function based on the logarithm of the exponential of each element (log-sum-exp function), but for simpler cases, when the cleaning time of all units is the same or when there are no simultaneous cleanings, it can be expressed as a linear constraint. Hence, the cleaning time expression is defined accordingly to the specific case, and the constraint is simplified if possible.

$$\mathrm{T}_{cl,p} = \max\{t_{cl,i} y_{i,p} \; \forall i \in HEX\}, \qquad \forall p \in \{1,2,\dots,N_p\} \tag{3.45}$$

$$\mathrm{T}_{cl,p} + (1 - z_p)\mathrm{T}^{min} \leq \mathrm{T}_p \leq \mathrm{T}_{cl,p} + (1 - z_p)\mathrm{T}^{max}, \qquad \forall p \in \{1,2,\dots,N_p\} \tag{3.46}$$

$$t_p = \sum_{p'=1}^{p} \mathrm{T}_{p'}, \qquad \forall p \in \{1,2,\dots,N_p\} \tag{3.47}$$

$$t_p = t_f, \qquad \forall p \in \{N_p\} \tag{3.48}$$

$$z_p \leq \sum_{i \in HEX} y_{i,p} \leq z_p N_T, \qquad \forall p \in \{1,2,\dots,N_p\} \tag{3.49}$$

$$y_{i,p} \leq z_p, \qquad \forall i \in HEX, p \in \{1,2,\dots,N_p\} \tag{3.50}$$

These additional time constraints in the continuous time discretization approach are defined with respect to the new binary variable z_p because in this case is not possible to individually track the time evolution of the states of each unit. Eq. (3.49) and Eq. (3.50) represent the logic implications of the original binary variables, $y_{i,t}$, on the new one, z_p, so that the cleanings are properly represented.

The differential equations of the model are discretized for each period using a dimensionless time, and equality constraints are introduced to ensure continuity of the differential variables between consecutive periods. Eq. (3.51) represents the initial conditions of the problem, Eq. (3.52) represents the continuity condition of the differential variables between two periods, and Eq. (3.53) the discretization of the differential equations. Here, x indicates any differential variable, RHS the right-hand side of the differential equations, $\frac{dx}{d\bar{t}}$ is the dimensionless derivative of the variable which is approximated by orthogonal polynomials in finite elements, and s is a slack variable for when the units are idle and the differential constraints of the model are inactive. This discretization approach is applied to all differential equations in the model.

$$x_{(p,t)} = x^0, \qquad \forall (p,t) \in \{(1,1)\} \tag{3.51}$$

$$x_{(p,1)} = x_{(p-1,N_c)} + s_p, \qquad \forall p \in \{2, \dots, N_p\} \tag{3.52}$$

$$\frac{dx}{d\bar{t}}_{(p,t)} = \mathrm{T}_p\left(RHS_{(p,t)}\right) + s_{(p,t)}, \qquad \forall (p,t) \in \{(1,2), \dots, (N_p, N_c)\} | t > 1 \tag{3.53}$$

When the differential equations are discretized using a continuous time representation a bilinear term arises, the multiplication of the period length and the right-hand side of the differential equation. This introduces complexity into the problem because as the length of the period tends to zero, the problem becomes ill conditioned (Biegler 2010), but this is avoided including realistic bounds for the length of the period.

3.3.3. Scalability and comparison of time representations

So far, the formulation of the discrete and continuous time representations has been presented in the context of HEN under fouling and cleaning scheduling problem, also their advantages and disadvantages have been discussed. Now, a quantitative comparison of the scalability of the problem using each formulation is presented.

Consider a hypothetical HEN of 20 units to compare the scalability of the two discretization approaches. This number of units is sufficiently large to be representative of most academic examples and industrial applications. To enable a realistic scenario for the comparison some parameters of the operation are fixed: the maximum number of units that can be cleaned simultaneously is two, the time horizon is set as one year, the maximum number of cleanings per unit per year is two, and the cleaning time of each unit is 10 days. These parameters are used to estimate the feasible number of cleanings and structure of the cleaning schedule for different scenarios.

Table 3.1. Scenarios to define problem size and scalability using the continuous time discretization

Scenario	Max. number of cleanings	Simultaneous cleanings	Sequence of network states
Worst-case	N_T	No	Operating > Cleanings > Operating
Normal-case	1	No	Operating > Cleanings > Operating
Best-case	1	Yes	Operating > Cleanings > Operating

Three scenarios are defined based on the number of periods required to correctly capture the sequence of cleanings. In all the scenarios it is assumed that all the exchangers are cleaned the maximum number of times within the time horizon which is a worst-case assumption as there may exist exchangers in a network with low fouling rates that do not need to be cleaned at all. Table 3.1 summarizes the scenarios considered, and they are labelled according to the number of cleanings expected and periods required to define correctly that schedule. It is also assumed that there are no cleanings at the beginning of the operation, neither at the end.

Figure 3.6 compares the number of periods or time events (a) and the number of binary variables (b) estimated for the stated problem. While the number of time events is constant in the discrete time approach, it increases linearly using a continuous time approach. Also, the complexity of the problem – measure as the number of binary variables – increases linearly for the discrete time approach, and quadratically for the continuous time approach. However, for most networks the number of periods and problem size is lower when the continuous time discretization is used than when the discrete one is used. For example, a network of 5 heat exchangers requires 105 binary variables for the “worst-case” scenario

with the continuous time discretization and 185 binary variables with the discrete time approach. There is a critical point in the number of units after which the discrete time approach may be favoured over the continuous one – specifically for the wort case scenario – but only under the conditions considered to define the three cases of the continuous time discretization.

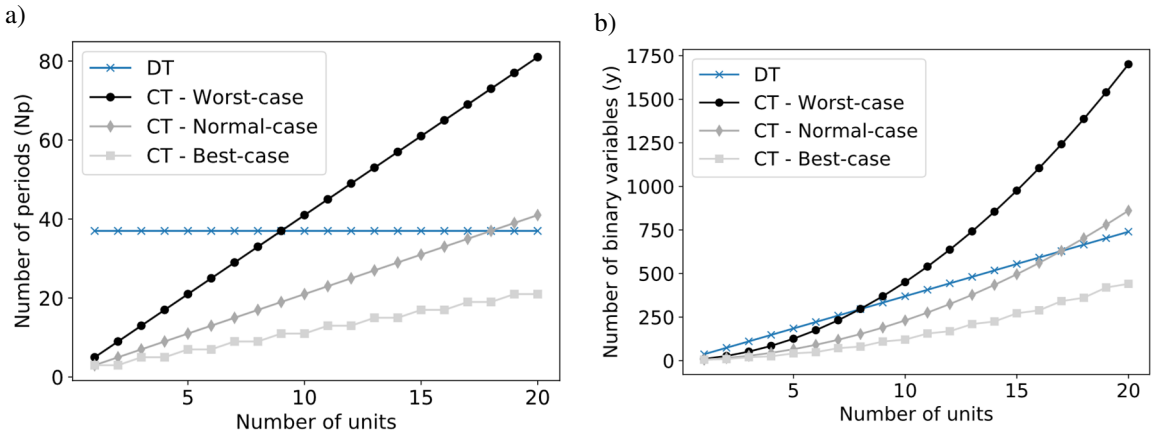

Figure 3.6. Problem size comparison and scalability for time discretization approaches. a) Number of time events, b) total number of integer variables. (CT: continuous time, DT: discrete time).

The estimation of the problem size for the continuous time approach is based on the assumptions that all units are cleaned within the time horizon, and that there is an operating period between two cleaning periods. These assumptions are not general, and there are cases in practice where the fouling rate of exchangers is negligible or mitigated by shear stress alone and cleanings are not necessary; or other cases where consecutive or simultaneous cleanings of units are possible. In those cases, an optimal solution may require fewer periods. In addition, depending on the number of units, the number of periods of the continuous time approach have a wide range, so it is a good strategy to start solving the optimization problem with the lowest number of periods possible, and increase it systematically until there is no improvement in the objective function. This strategy avoids dealing with complex unsolvable problems in some situations.

General purpose MINLP solvers can typically handle hundreds of variables and based on this scalability analysis it will be difficult to use them to solve to optimality problem with more than 3 units that have over 100 binary variables. In addition, in the problem formulation there are not many constraints among the binary variables increasing the number of feasible

combinations. Equality and inequality constraints on the decision variables are helpful when solving large scale MINLP problem because reduce the size of the search space – for instance in branch and bound approaches those constraints are essential to prune nodes because of feasibility. The computational time required for the sort of problems addressed in this thesis may become prohibitive, and for realistic applications more efficient solution are necessary.

3.4. Optimal integration of cleaning scheduling and control

The mathematical formulation introduced here for the optimal cleaning scheduling and control problem of HEN under fouling is tested with four case studies, and both time discretization approaches are compared. All the case studies used in this thesis are presented in detail in Appendix A, including all operating conditions and unit specifications, and those used in this chapter are: 1HE, 2HE-S, 2HE-B, and 4HE-S. For completeness, the network structure of each case is shown in Figure 3.7. These cases are small networks that range from one to four heat exchangers, but they include all the elements found in industrial preheat trains, such as interaction of the exchangers though the hot streams, parallel branches, mixers, and flow splitters, as well as commonly found operational constraints.

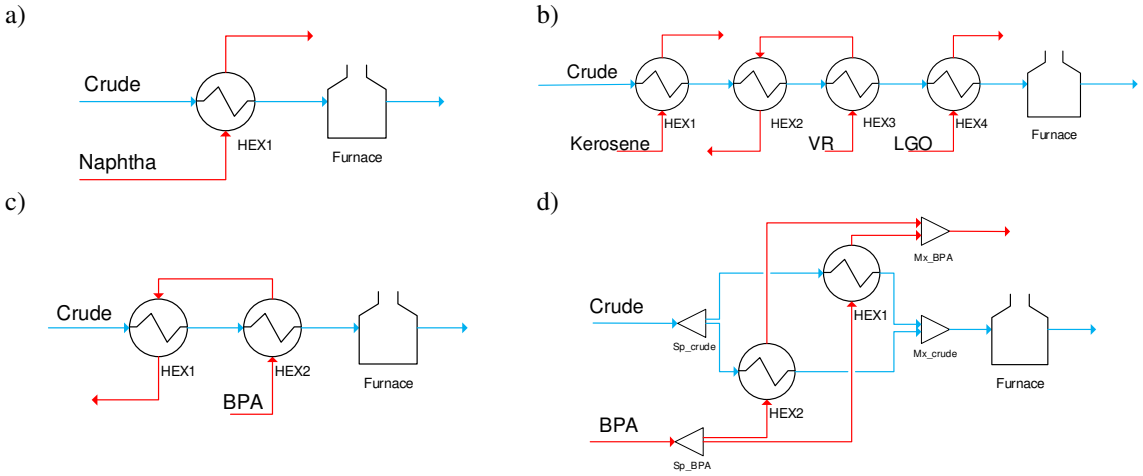

Figure 3.7. HEN representation of the case studies of this chapter. a) Case 1HE, b) Case 4HE-S, c) Case 2HE-S, d) Case 2HE-B.

These networks are utilized for different purposes. First, cases 1HE, 2HE-S, and 2HE-B are used to compare the efficiency of both time discretization approaches when the optimization problem is solved with standard MINLP solvers based on branch and bound algorithm. Second, case 4HE-S is used to illustrate the advantages of using a continuous time

formulation to optimize a partially pre-set cleaning schedule, which is not possible with a discrete time formulation (Section 3.4.2). Third, the fouling parameters, such as ageing rate, of case 1HE are modified to analyse their effect on the optimal cleaning schedule. This case study is also used to demonstrate the prediction capabilities of the model, and the phenomena it can capture (Section 3.4.3). Fourth, the operational conditions and limiting constraints of case 2HE-S are modified to analyse their effect on the optimal cleaning schedule (Section 3.4.4). Finally, the synergies of simultaneously optimizing the flow distribution and the cleaning schedule are evaluated defining different instances of case "2HE-B" (Section 3.4.5).

For all the optimization problems the same initialization procedure is followed and it is described in Appendix A. For those problems involving scheduling decisions, all the binary variables are initialized at 0.5, and the length of the periods is initialized with the same value for all assuming they are evenly distributed.

3.4.1. Summary of problem formulation

The overall optimal cleaning scheduling and flow distribution problem of HEN under fouling can be summarized in Eq. (3.54). It shows, in a short notation, all elements included in the problem formulation, and all the aspects of the operation considered. The time related constraints, number of binary variables, and disjunction formulation change depending on the type of time discretization approach used. This is a large scale nonconvex MINLP problem which is solved to local optimality in this case as only local solvers – sequential branch and bound – are used. The nonconvexities of the problem arise from the heat exchanger and fouling models, and from the integer nature of the decisions which define discontinuities in the search space. Global optimization solvers such as BARON or ANTIGONE have strong limitations to be applied in this case because of the large scale of the problem, and the large number of binary decision variables.

$$
\begin{aligned}
&\min_{y_{i,t}, m_{a,t}} \ Total\ operating\ cost - Eq.(3.41) \\
&s.t. \\
&Network\ representation - Section\ 3.2.1 \\
&Heat\ exchanger\ model - Section\ 3.2.2 \\
&Fouling\ model - Section\ 3.2.3 \\
&Operating\ mode\ disjunctions - Section\ 3.2.4 \\
&Operational\ constraints - Section\ 3.2.5 \\
&Time\ representation\ and\ time\ related\ constraints - Section\ 3.3.1\ OR\ 3.3.2
\end{aligned}
\qquad (3.54)
$$

This mathematical formulation is general, and it applies to all case studies considering that there are constraints that are case specific and that the network connectivity and number of units dictates the set dimension, hence the size of the optimization problem. The decision variables for all cases are the timing and allocation of cleaning actions regardless of the time discretization approach, and additional control decision variables arise for those networks that have parallel branches.

The constraints in the formulation are derived from the specifications of the case studies presented in Appendix A, and if some of them are modified, or parameters of the case study changed, it is mentioned explicitly during the analysis of the results in the following sections.

3.4.2. Comparison of time discretization approaches

The mathematical model and the optimal cleaning scheduling formulation presented in this chapter are used to compare the two discretization approaches: discrete (DT) and continuous (CT) for three case studies, 1HE, 2HE-S, and 2HE-B. The models implemented can predict all important variables of the performance of the network such as the CIT, furnace duty, and overall pressure drop; they can also predict those specific to each heat exchanger such as deposit thickness, temperature radial distribution, duty, and outlet temperatures. For the goal of this section of comparing the performance of two discretization approaches, the analysis is limited to the overall performance of the network and the computational resources required to find a solution. In the following sections various scenarios are analysed in which the individual performance variables of the exchangers are more relevant, and they show the broad prediction capabilities of the model.

The optimal cleaning scheduling problem is solved for the three case studies, and Table 3.2 presents the results for case 1HE, while Table 3.3 present those of cases 2HE-S and 2HE-B. For each case the optimization problem is solved using the discrete time approach, and the continuous time approach with two different number of periods. These results include the problem size, computational load, optimal cost and profit of the operation, optimal cleaning schedule, and optimality gap. In addition to the optimal solution of each scenario, the no mitigation (NM) case is included – see Table 1.1. This scenario serves as a reference point to compare the potential benefits of optimizing the operation of a given HEN.

Table 3.2. Computational results and optimal solution of cleaning scheduling problem for case: 1HE

Case	**1HE**			
Discretization*	**DT**	**DT**	**CT**	**CT**
Mode **	**NM**	**SCH**	**SCH**	**SCH**
n_T +	37	37	5	10
Continuous variables	1218	1218	702	1407
Binary variables	0	37	10	20
Equality constraints	992	992	565	1130
Inequality constraints	2697	2697	1409	2819
CPU time [min]	0.03	65.71	2.6	32.86
Total energy [MW-h]	4.092×10^5	4.078×10^5	4.076×10^5	4.077×10^5
Production profit [$]	6.617×10^8	6.617×10^8	6.617×10^8	6.617×10^8
Fuel cost [$]	1.105×10^7	1.101×10^7	1.101×10^7	1.101×10^7
Carbon cost [$]	1.866×10^6	1.859×10^6	1.859×10^6	1.859×10^6
Cleaning cost [$]	0	30000	30000	30000
Cleaning schedule (HEX#, time [days]) x	None	(1, 180)	(1, 182)	(1, 180)
Lower bound (cost)	1.123×10^7	1.123×10^7	1.122×10^7	1.122×10^7
Upper bound (cost)	1.123×10^7	1.123×10^7	1.122×10^7	1.122×10^7
Optimality gap [%]	0.00	0.00	0.00	0.00

* DT: discrete time approach, CT: continuous time approach

** NM: no mitigation operating mode (no cleanings considered), SCH: optimal cleaning scheduling problem solved

+ Number of time steps for DT, and number of periods for CT

x Cleaning time rounded to the closest integer value for the CT approach

Table 3.3. Computational results and optimal solution of cleaning scheduling problem for cases: 2HE-S and 2HE-B.

Case	**2HE-S**				**2HE-B**			
Discretization*	**DT**	**DT**	**CT**	**CT**	**DT**	**DT**	**CT**	**CT**
Mode **	**NM**	**SCH**	**SCH**	**SCH**	**NM**	**SCH**	**SCH**	**SCH**
n_T +	37	37	9	13	37	37	9	13
Continuous variables	2284	2284	2362	3414	2740	2740	2794	4038
Binary variables	0	74	27	39	0	74	27	39
Equality constraints	1908	1908	1962	2834	2288	2288	2322	3354
Inequality constraints	4824	4824	4517	6525	6040	6040	5669	8189
CPU time [min]	0.08	3000.00	548.64	3000.00	0.12	3000.00	374.38	3000.00
Total energy [MW-h]	$3.873\text{x}10^5$	$3.804\text{x}10^5$	$3.800\text{x}10^5$	$3.801\text{x}10^5$	$3.982\text{x}10^5$	$3.914\text{x}10^5$	$3.910\text{x}10^5$	$3.910\text{x}10^5$
Production profit [$]	$6.617\text{x}10^8$	$6.617\text{x}10^8$	$6.617\text{x}10^8$	$6.617\text{x}10^8$	$6.617\text{x}10^8$	$6.617\text{x}10^8$	$6.617\text{x}10^8$	$6.617\text{x}10^8$
Fuel cost [$]	$1.046\text{x}10^7$	$1.027\text{x}10^7$	$1.026\text{x}10^7$	$1.026\text{x}10^7$	$1.075\text{x}10^7$	$1.057\text{x}10^7$	$1.056\text{x}10^7$	$1.056\text{x}10^7$
Carbon cost [$]	$1.766\text{x}10^5$	$1.735\text{x}10^5$	$1.733\text{x}10^5$	$1.733\text{x}10^5$	$1.816\text{x}10^5$	$1.785\text{x}10^5$	$1.783\text{x}10^5$	$1.783\text{x}10^5$
Cleaning cost [$]	0	90000	90000	90000	0	90000	90000	90000
Cleaning schedule (HEX#, time [days]) x	None	(2, 120) (1, 190) (2, 250)	(2, 115) (1, 182) (2, 250)	(2, 114) (1, 182) (2, 250)	None	(1, 80) (2, 180) (1, 270)	(1, 88) (2, 180) (1, 278)	(1, 80) (2, 172) (1, 261)
Lower bound (cost)	$1.063\text{x}10^7$	$1.033\text{x}10^7$	$1.052\text{x}10^7$	$1.039\text{x}10^7$	$1.093\text{x}10^7$	$1.067\text{x}10^7$	$1.083\text{x}10^7$	$1.074\text{x}10^7$
Upper bound (cost)	$1.063\text{x}10^7$	$1.054\text{x}10^7$	$1.052\text{x}10^7$	$1.052\text{x}10^7$	$1.093\text{x}10^7$	$1.084\text{x}10^7$	$1.083\text{x}10^7$	$1.083\text{x}10^7$
Optimality gap [%]	0.00	2.02	0.00	1.29	0.00	1.57	0.00	0.83

* DT: discrete time approach, CT: continuous time approach

** NM: no mitigation operating mode (no cleanings considered), SCH: optimal cleaning scheduling problem solved

+ Number of time steps for DT, and number of periods for CT

x Cleaning time rounded to the closest integer value for the CT approach

In terms of problem size, the number of binary variables is lower in the continuous time representation than that in the discrete one. Reducing the number of binary variables while having the same representation of the problem is advantageous because it reduces the size of the search space. In these cases, the reduction of binary variables ranges from 47% to 73% depending on the case study, which reduces exponentially the number of possible schedules. On the other hand, the number of continuous variables and equality constraints are greater in the continuous time representation than those in the discrete time representation as there are unique variables and constraints related to the variable length of the periods, and because the inner discretization of each period introduces more variables to the problem. Most of the equality constraints are those related with the heat exchanger, fouling, and mass and energy balance models, while the inequality constraints represent operational limits. In the cleaning scheduling problem, there are few constraints among the binary decision variables – assignment of periods of no cleanings, no consecutive cleanings, simultaneous cleanings – which would be useful to reduce the search space and facilitate the solution, and they scale in the same way as the binary variables regardless of the time discretization approach. The number of continuous variables and constraints in the problem is not a limitation, and current NLP solvers can handle problems of these sizes and much larger ones efficiently.

Under the same conditions the continuous time approach reaches an optimal solution much faster than the discrete time approach. The computational time is reduced by 84% - 96% depending on the case study using the number of periods of the "worst-case" (Section 3.3.3). When the number of periods of the continuous time approach is increased to 10 for the "1HE" case and to 13 for the others, a significant reduction in the computational load is still observed. For the "1HE" case the computational time is reduced by 50%, while for the other no optimal solution is found after 3000 min of computation, but the optimality gap is smaller – solution closer to optimality – using the continuous time representation than the discrete one. Besides these computational advantages of the continuous time approach, it improves the time resolution of the cleaning actions. While in the discrete time approach cleanings can only start at the discrete time intervals – every 10 days for these cases – in the continuous one they can start at any time with a resolution of hours. This improves the accuracy of the models as the duration of the cleanings may vary from one exchanger to another, and it provides more precise solutions and quantification of the operation costs than

in most previous approaches that use a discrete time approach with a resolution of one month (Rodriguez and Smith 2007; Gonçalves et al. 2014).

There are no significant differences between the optimal solutions obtained with both time discretization approaches. The production profit and operating cost of all cases only differ by few thousands of dollars which is negligible based on the order of magnitude of the problem. Also, the differences in the starting time of the cleaning actions is lower than 10 days in all cases, and this corresponds to the time resolution used in the discrete time approach. Figure 3.8 shows the optimal profiles for the CIT and the furnace duty of each case study solved with two discretization approaches including the two scenarios of the continuous time using different number of periods (CT-#N). The cleaning actions are observed as a sudden decrease in the CIT followed by a drastic increase; the opposite is observed in the furnace duty. Both variables are measurements of the network performance, but the duty is directly related to the operating cost. There are no observable differences in those profiles, only those introduce by the differences in starting cleaning time. Both alternatives predict the same number of cleanings for each exchanger of the networks, one for the "1HE" case, and three total cleanings for each of the other cases. During the cleanings the CT approach provides a better representation of the evolution of the network than the DT one because it captures what happens during the cleaning, although it is a short time. During long operating times the CT start losing accuracy in the integration of problem equations – see CT-5N for the 1HE case – but this is easily solved by increasing the number of periods and tightening the bounds used to define the period length.

It is observed in Figure 3.8 that the optimal cleaning actions improve the performance of each network with respect to the NM case. In all cases, the CIT achieved in the optimal operation is greater than that of the NM scenario during most of the operating time, and the opposite is observed for the furnace duty. Despite the cleaning cost, and the temporary increase of the furnace duty during the cleanings, an optimal allocation and timing of cleanings in a network brings benefits to the operation and helps to mitigate fouling. For these cases of small networks, the savings achieved range from $\$12x10^3$ - $\$110x10^3$ and they can escalate rapidly for larger networks and longer operating times.

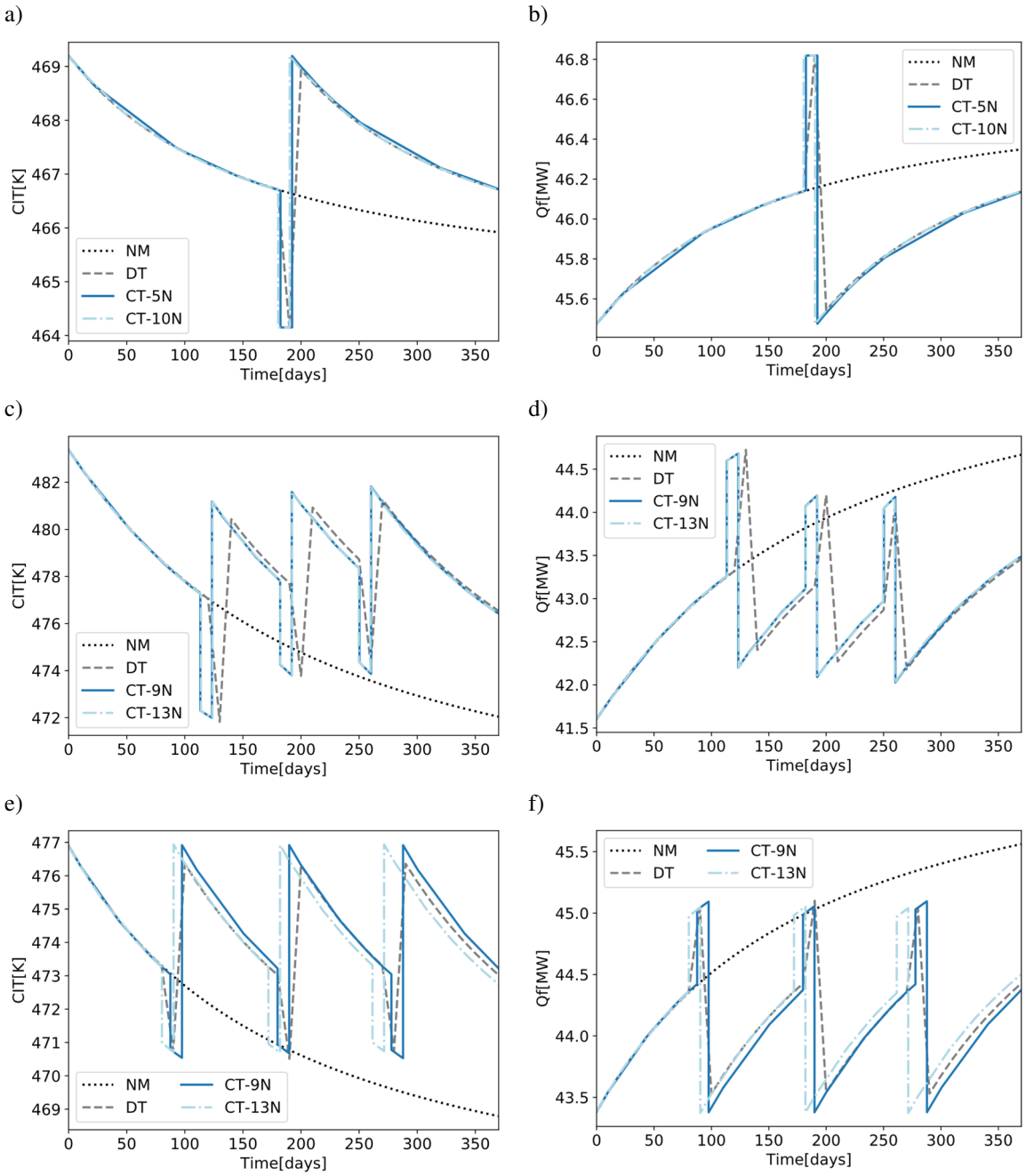

Figure 3.8. Optimal CIT (a, c, e) and furnace duty (b, d, f) profiles for the cleaning scheduling problem of cases: 1HE (a, b), 2HE-S (c, d), and 2HE-B (e, f).

One important advantage of the continuous time discretization approach over the discrete time approach is that it can optimize partially defined cleaning schedules. Partially define or pre-set schedules arise, for example, from expert criteria or knowledge of plant engineers and constraints of the refinery based on long term planning and budgets. In these cases, an approach that can improve those decision is advantageous. Consider the case study

4HE-S, where based on external knowledge a partial cleaning schedule is set as follows: *clean HEX2 and HEX3 twice, HEX2 must be clean immediately after HEX3; clean once all other exchangers; the cleaning sequence should be HEX3-HEX2-HEX4-HEX1*. The continuous time approach can be used here considering those statements as additional constraints for the problem, so that the cleaning times are optimized (Opt. A). In another scenario the cleaning times of all units and the cleaning actions of HEX4 are optimized (Opt. B). Note that the Opt. A scenario is formulated as an NLP problem because the decision variables are the cleaning times and all binary variables are fixed, while the Opt. B is formulated as an MINLP problem that included the binary variables associated with the cleanings of HEX4 only. In addition to these two scenarios, the no mitigation case (NM) is included for comparison purposes.

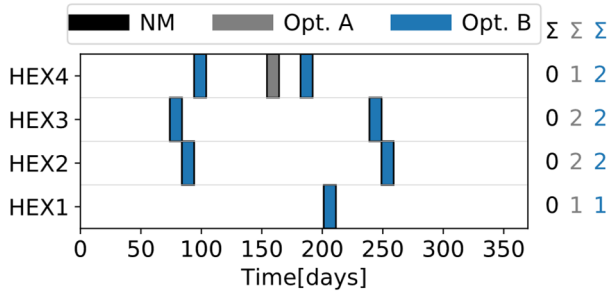

Figure 3.9. Partially optimized cleaning schedule for case 4HE-S. A) Optimal cleaning times, B) Optimal cleaning times and cleaning schedule of HEX4.

Figure 3.9 shows the optimal cleaning schedule obtained for the case 4HE-S under the cleaning sequence specifications when the cleaning times are optimized (Opt. A) and when the cleaning sequence of HEX4 is also optimized (Opt. B). The total number of cleanings is displayed on the right-hand side for each scenario. The optimal cleaning schedule satisfies the number of cleanings and the cleaning sequence predefined. The cleaning actions of both optimization cases overlap for all exchangers but HEX4. When the cleaning sequence of HEX4 is optimized together with the cleaning time of all cleaning actions, the optimal solution involves two cleanings of this unit instead of one. The optimization of pre-set cleaning schedules is a novelty and an advantage of the continuous time discretization approach as this kind of problems were not addressed before and they are relevant to the industry. In addition, they can be solved efficiently in short computational times. The Opt. A

problem is solved in 3.2 min of CPU time as it only involves continuous variables, while the Opt. B problem is solved in 448.6 min of CPU time because of the binary variables included.

Optimizing partially specified cleaning schedules reduces the operating cost significantly. Figure 3.10 shows the CIT and the furnace duty profiles for the optimized schedules of case 4HE-S. When cleanings are introduced and their timing optimized the CIT is greater than that of the NM case during most of the operation, and the furnace duty is lower than that of the NM case. Note that all the cleanings are lumped towards the middle of the operation because the initial state of the network is clean, so early cleanings are not necessary, and cleanings towards the end of operation are not profitable. All scenarios have the same production profit as the crude flow rate is always at its maximum, but their operating cost changes. The Opt. A scenario reduces the operating cost from $\$11.667 \times 10^6$ of the NM case to $\$11.338 \times 10^6$ which translates in savings of $\$329.2 \times 10^3$ during one year of operation. The savings of the Opt. B scenario ($\$329.5 \times 10^3$) are marginally larger than those of the Opt. A scenario because of the different cleaning sequence. Comparing the performance of scenarios Opt. A and Opt. B, it is observed that the former has a higher furnace duty during most of the operation, while the later have a higher cleaning cost. These two factors generate the overall trade off for the network performance.

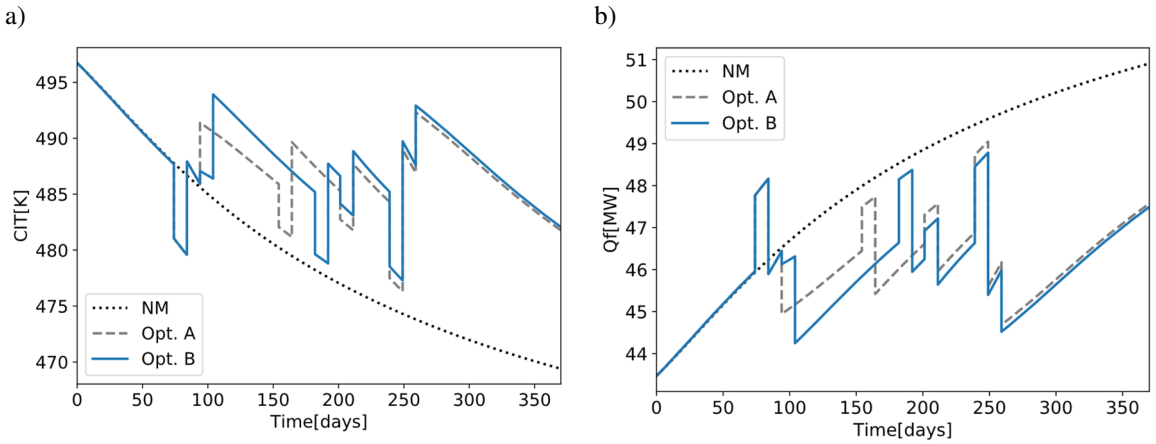

Figure 3.10. Optimal CIT (a) and furnace duty (b) profiles for the partially optimize cleaning schedule of case 4HE-S.

In summary, the model and problem formulation developed allows to solve the optimal cleaning scheduling of relevant HEN under fouling using two discretization approaches. The

continuous one proved to be more efficient in terms of computational effort, while guaranteeing the same optimal solution and allowing to optimize pre-set cleaning schedules.

3.4.3. Optimal cleaning scheduling considering deposit ageing

The 1HE case study is extensively used in this section to demonstrate the effects of deposit ageing, and the main trends on the key performance variables of a single exchanger. The no mitigation scenario (NM) and the optimal cleaning scheduling scenario (SCH) are compared for various ageing rates. The continuous time representation approach with five periods is used in all the optimization scenarios as this was proved to be sufficient and accurate for this case.

To analyse the effects of ageing in the performance of the network, the NM and SCH scenarios are solved for the cases of no ageing ($k^a = 0\ day^{-1}$), and three ageing frequency factors of: 500 day^{-1}, 1500 day^{-1}, and 3000 day^{-1}.

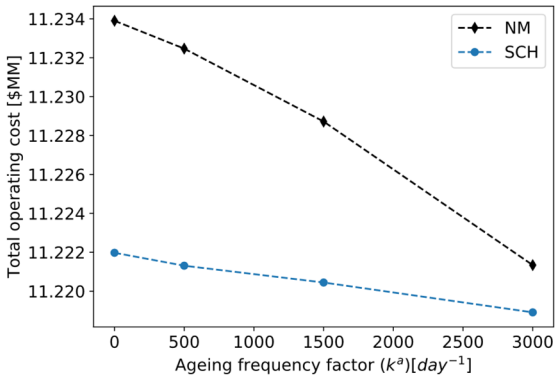

Figure 3.11. Total operating cost of the optimal cleaning scheduling (SCH) of case 1HE for various ageing scenarios.

This case study is not constrained by furnace or hydraulic limits, so the production rate is always at is maximum, and only the operating cost varies. Figure 3.11 shows the operating cost of the network for the scenarios of NM and SCH varying the ageing frequency factor. The optimal cleaning schedule of all scenarios involves only one cleaning. As the ageing rate increases, the optimal total cost decreases because of the higher thermal conductivity of the deposit and lower furnace duty required. However, the difference in cost between the scenarios NM and SCH becomes smaller as the ageing rate increases, so it is expected that for higher ageing rates, cleanings will not reduce the operation cost, and the optimal policy will be one of no cleanings. On the opposite end, optimal cleanings allocation has a greater

potential when the fouling rate is high and there is no ageing than when ageing rates are high. It is necessary to analyse individual variables of the exchanger to understand the effects of ageing on the operation, and on the optimal cleaning schedule.

The most important performance indicators of the network are the furnace duty – thermal performance – and the overall tube side pressure drop – hydraulic performance – and both are affected by deposit ageing. Figure 3.12 shows the furnace duty for the NM and SCH scenarios varying the ageing rate. The thermal performance of the network improves as the ageing rate increases, although it reaches its asymptotic point faster. Contrarily, the hydraulic performance deteriorates as the ageing rate increases, as observed in Figure 3.13. In some cases, such an increase in the pressure drop may constrained the network operation as the pumping limit can be reached and production rate must be reduced. Regardless of the effect of ageing on the performance of the network, the optimal cleaning schedule is always a single cleaning after 180 days of operation, and the cleaning time only changes in the order of magnitude of hours with respect to the ageing rate. The optimal cleaning action starts when there are no significant differences on the network thermal performance for all the ageing rates. It is the thermal performance and its trade-off with the cleaning cost which defines the optimal solution, not the hydraulic performance of the network, unless it is constrained.

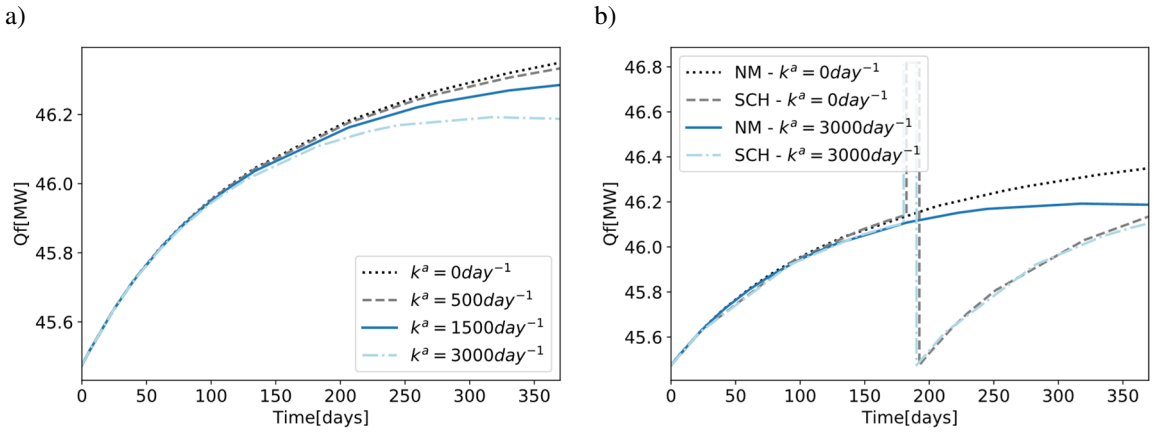

Figure 3.12. Furnace duty for various ageing scenarios of case 1HE. a) no mitigation operation, b) optimal cleaning scheduling solution.

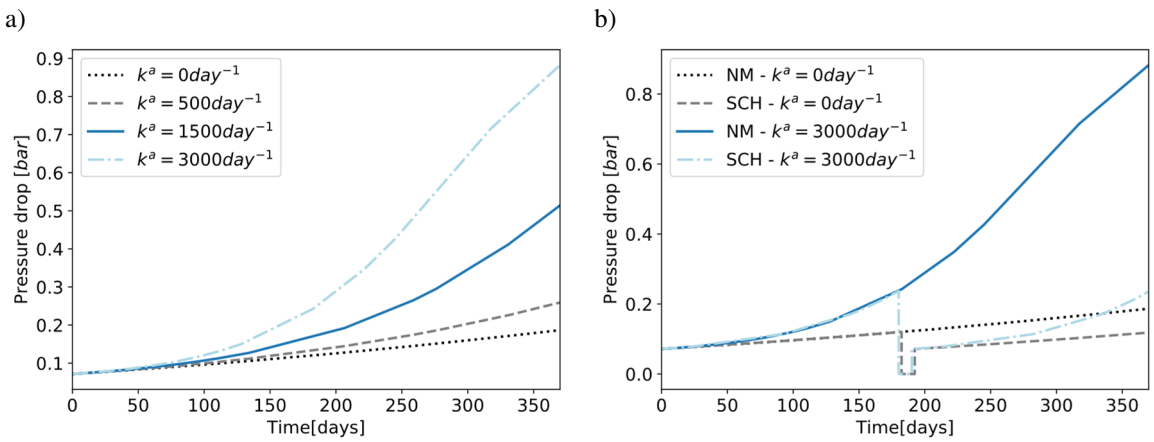

Figure 3.13. Tube side pressure drop for various ageing scenarios of case 1HE. a) no mitigation operation, b) optimal cleaning scheduling solution.

The pressure drop of the system considering ageing is much larger than that when there is no ageing, and these differences are still observed when the cleaning schedule is optimized. The pressure drop is function of the thickness of the deposit, and the deposit grows faster when there is ageing because of the changes in composition. Figure 3.14 shows the evolution of the deposit thickness for various ageing rates. This variable, as well as the fouling resistance and the deposit composition, are an axial average due to the abstraction and assumptions of the model, but in reality, they change in the axial direction of the exchanger according to the operating conditions. There is no difference on the optimal cleaning time for the cases with and without ageing, but before the cleaning starts the deposit thickness is 1.1 mm larger with ageing than without it.

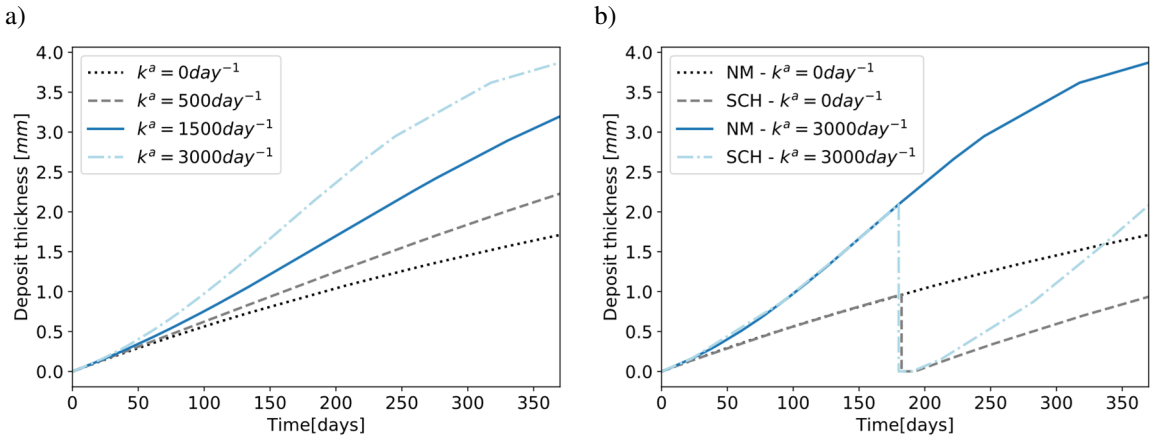

Figure 3.14. Deposit thickness for various ageing scenarios of case 1HE. a) no mitigation operation, b) optimal cleaning scheduling solution.

High ageing rates improve the thermal performance because the fouling resistance decreases as the coke fraction in the deposit increases. The coke deposit has a higher thermal conductivity than the fresh deposit. Figure 3.15 presents the time evolution of the total fouling resistance of the deposit for various ageing rates, which decreases when the ageing rate increases. Also, when the cleaning schedule is optimized, there is no significant difference in the fouling resistance because the cleaning time is defined based on the thermal performance of the system. However, the deposit removed in those cleanings is significantly different: while in the case of no ageing the deposit is only a fresh gel-like deposit, that of the high ageing rate scenario has a coke fraction of 0.8 and a fresh deposit fraction of 0.2, as observed in Figure 3.16. The deposit composition changes dynamically, and in some cases, it may be mainly coke towards the end of the operation. The deposits removed during the cleanings – no ageing, and high ageing rate –have different attachment properties, and, in principle, aged deposit should be harder to remove so the cleaning cost and cleaning time for those may be higher. Including these features in the model and objective function is complex as those deposits are rarely characterized before and during the cleanings – collecting samples is a difficult and expensive task that most of the time changes the composition of the deposit – nor the cleaning costs are reported as a function of the deposit composition or cleaning method in the open literature. These features are beyond the scope of this thesis, and to include them many assumptions must be made that cannot be validated with the scarce data available.

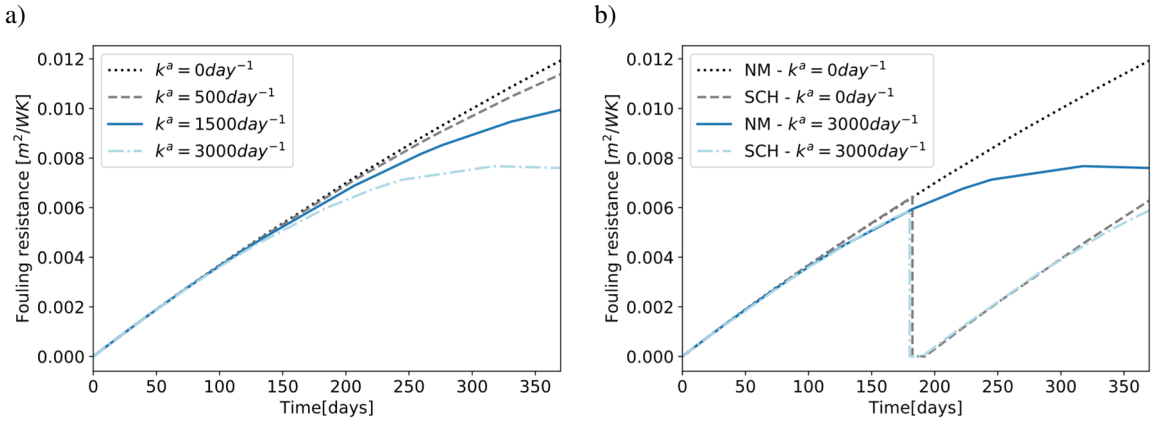

Figure 3.15. Fouling resistance for various ageing scenarios of case 1HE. a) no mitigation operation, b) optimal cleaning scheduling solution.

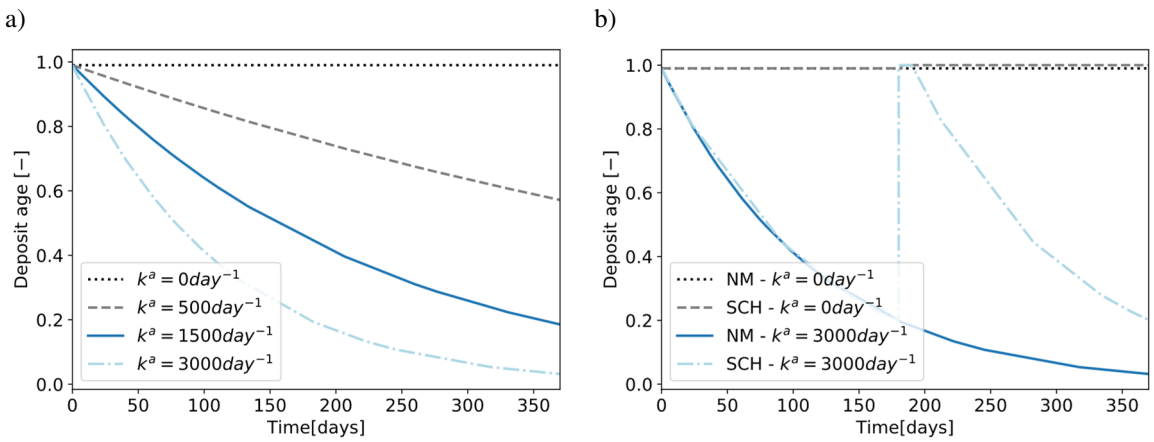

Figure 3.16. Deposit age for various ageing scenarios of case 1HE. a) no mitigation operation, b) optimal cleaning scheduling solution.

Ageing affects the thermal and hydraulic performance of HEN, but the optimal cleaning schedule is usually defined only based on the long-term thermal performance for which ageing does not make a significant difference. Only in cases where the network is hydraulically limited ageing can play an important role on deciding optimal cleaning actions.

3.4.4. Optimization of HEN with constrained operation

Fouling in HEN can limit the operation by two factors: i) increasing the furnace duty until it reaches the firing limit and no more fuel can be burnt in the furnace to provide additional energy – thermal limit (TL) –, and ii) increasing the overall pressure drop of the system until the pump cannot supply the required head to make the crude flow through the whole network – hydraulic limit (HL). To continue the operation of the network in any of these limiting scenarios, the production rate or the CDU throughput must be reduced which translates into large economic losses. These are practical problems found in a refinery when fouling is severe, and they must be avoided at all cost.

The 2HE-S case study is used to analyse the operation of the network for the thermal and hydraulic limiting scenarios, and a no limited (NL) scenario is included for reference and comparison. It is assumed that the firing limit is 44 MW and that the maximum allowed pressure drop is 0.25 bar. These limits are defined based on the order of magnitude for the operation of the small network considered. They could also be defined as bounds on equivalent variables such as minimum CIT or maximum pumping power. For each scenario

the no mitigation case (NM) and the optimal cleaning scheduling problem (SCH) are solved to demonstrate the advantages of the formulation when the HEN is constrained.

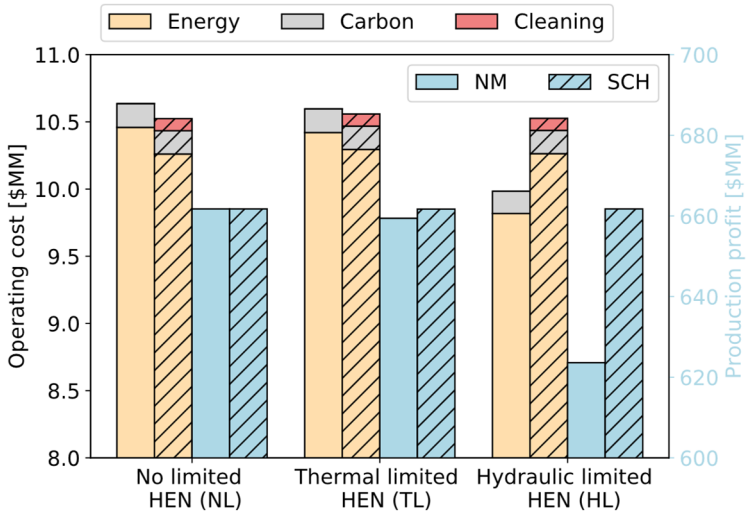

Figure 3.17. No mitigation (NM) and optimal cleaning scheduling (SCH) operating cost (left) and production profit (right) for the case 2HE-S when the network operation is limited.

Figure 3.17 is a bar plot showing the total operating cost (left) and the production profit (right) for each of the limited scenarios, and for the no mitigation (no hashed bars) and optimal cleaning schedule cases (diagonal hashed bars). The optimal cleaning schedule for the not limited operation reduces the operating cost by $ $112x10^3$ while the production profits are constant. On the other hand, when the network operation is limited, the main benefits arise from the increase of the production rate to its maximum level, hence reaching a much higher production profit. Figure 3.18 shows the evolution of the CDU throughput, and how it decreases when a constraint is reached, while it remains almost constant at its maximum when optimal cleaning actions are performed. The thermally limited operation of the network causes a reduction of the production rate that translates into $ $2.3x10^6$ losses in profit, but when this constraint is included in the problem formulation, the production rate is almost fully recovered, the operating cost is reduced, and the profit increases. During the cleaning actions of the thermally limited operation the production rate decreases slightly – less than 0.2 kg/s for 1 day of operation – because the additional energy required cannot be supplied without the exchanger that is out of operation so that the firing limit is reached. Similarly, the hydraulically limited operation of the network reduces the production rate, hence the

profit by \$ 38.1x10^6, although it reduces the operating cost by \$ 652x10^3. The optimal cleaning scheduling of the hydraulically limited scenario allows to recover those losses in profit, but more energy and cleaning actions are necessary. The increase in operating cost associated with the cleanings or additional energy is negligible compared to the profit achieved by debottlenecking the operation of the network.

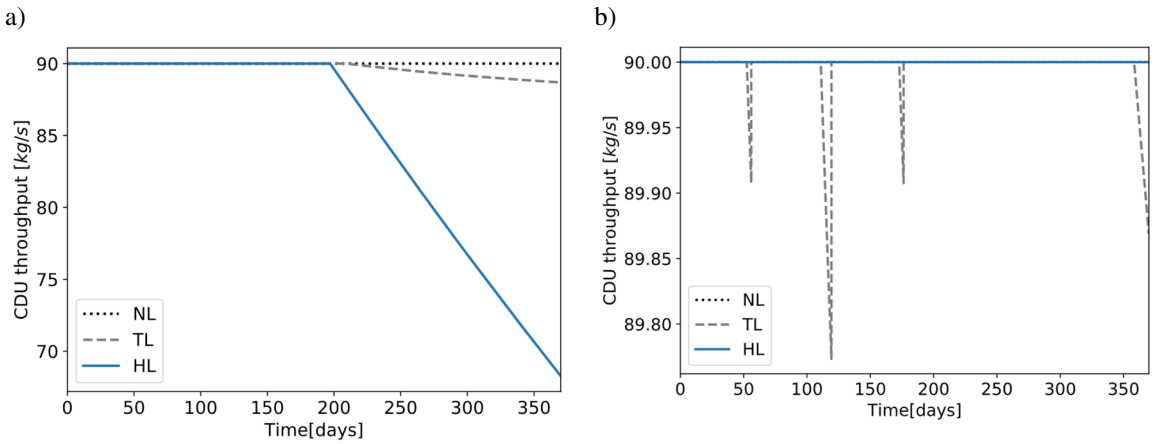

Figure 3.18. CDU production throughput of the case 2HE-S when the network operation is limited. a) No mitigating actions, b) optimal cleaning scheduling.

The general formulation of the optimal cleaning scheduling problem copes well with scenarios where the operation of the network is limited. Including this kind of constraints changes the optimal cleaning schedule because the cleanings are defined so that the operating limits are avoided, and the profits maximized. Figure 3.19 presents the optimal cleaning schedule for the three operating scenarios of the case study and the total number of cleanings. The optimal cleaning schedule of the hydraulic limited scenario is similar to that of the not limited operation, but all the starting cleaning times are move forward in time. Figure 3.20 shows the time evolution of the overall pressure drop of the system. If no mitigating actions are performed the hydraulic limit becomes active after 190 days of operation and then the production rate decreases, while under the optimal cleaning schedule operation policy this limit is never reached, and cleanings are performed in a proactive way.

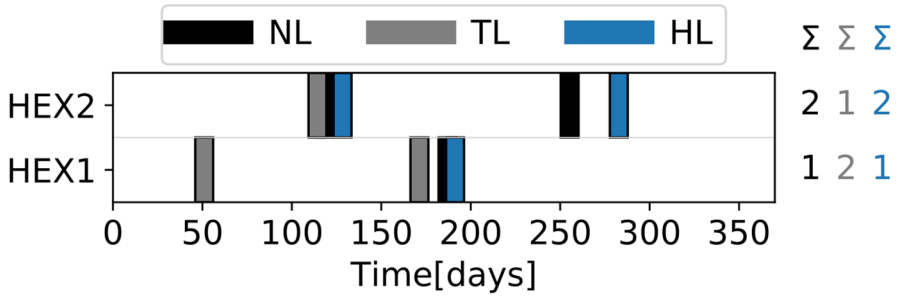

Figure 3.19. Optimal cleaning scheduling for the case 2HE-S when the network is thermally limited (TL), hydraulically limited (HL), and not limited (NL).

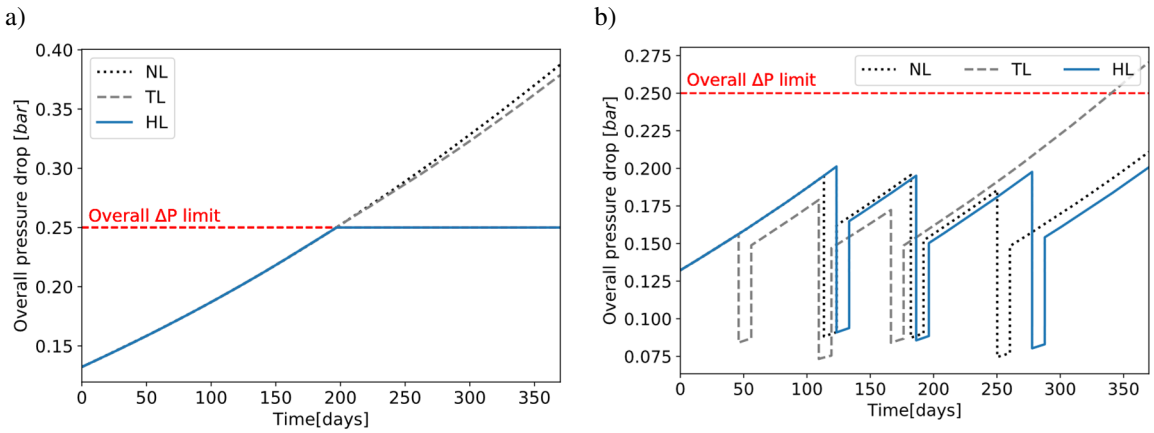

Figure 3.20. Overall tube side pressure drop of the case 2HE-S when the network operation is limited. a) No mitigating actions, b) optimal cleaning scheduling.

Contrary to the hydraulically limited scenario, the optimal cleaning schedule of the thermally limited scenario changes drastically as cleanings occurs earlier during the operation, and HEX1 is cleaned twice instead of HEX2. This cleaning sequence is necessary to avoid reaching the firing limit during the operation and during the cleanings when the furnace duty increases temporarily. Figure 3.21 shows the time profiles of the furnace duty for all scenarios comparing the no mitigation and optimal cleaning scheduling cases. In the thermal limited operation, the firing limit is reach after 200 days of operation when there are no cleanings, and after that the furnace duty is held constant while the production rate decreases. In addition, the optimal cleanings occur early during the operation to avoid reaching the firing limit during the cleanings, although it is reached during a short time towards the end of the cleanings and the production rate is reduced. Towards the end of the operation the furnace duty also reaches the furnace limit, but at this point it is not convenient to perform a cleaning of any unit as the cost is higher than the future savings.

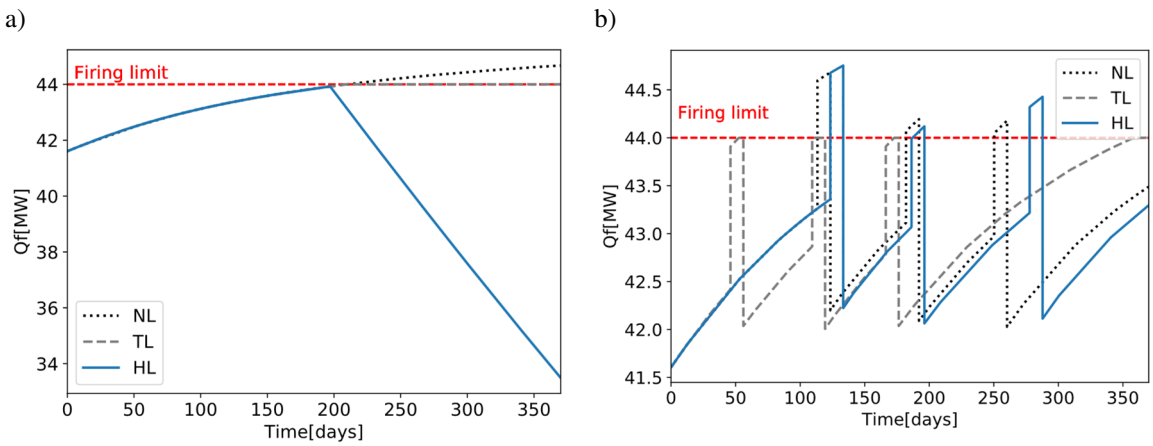

Figure 3.21. Furnace duty of the case 2HE-S when the network operation is limited. a) No mitigating actions, b) optimal cleaning scheduling.

The additional constraints that are included in the optimal cleaning scheduling problem formulation for the thermal and hydraulic limited cases do not increase the complexity of finding a solution. While the not limited case is solved in 548 min of CPU time using a continuous time formulation with nine periods, the thermally limited case is solved in 335 min, and the hydraulic limited case in 570 min using the same time discretization parameters.

3.4.5. Optimal integration of cleaning scheduling and control

The "2HE-B" case study is used to investigate the operation of networks with parallel branches. This configuration – with more exchangers in each branch – is commonly found in practice to supply large thermal requirements and to give more flexibility to the operation (Assis et al. 2015). Here the exchangers are identical, but it is assumed that at the initial time HEX1 has a fouling resistance of 0.005 m^2K/W and HEX2 is clean. The shell side flow rate of the exchangers is also distributed in parallel branches and it is considered as a control degree of freedom. All the split fractions are bounded between 20% and 80%.

Various scenarios are defined according to the policy with which the tube side flow rate is distributed in the branches and the degrees of freedom of the optimization problems. The solution strategies and abbreviations defined in Table 1.1 are used here. These scenarios are: 1) a no mitigation scenario (NM) with fixed flow rates of all parallel branches at 50%, 2) a pressure driven flow scenario for the tube side flow, while the shell side flow is free (ΔP-NM), 3) an optimal flow split scenario for all the branches (Opt. Sp), 4) optimal cleaning schedule (Opt. Sch), 5) sequential optimization of the cleaning schedule and the flow

distribution (Seq. Opt), 6) optimal cleaning schedule for pressure driven flow (ΔP-Opt), and 7) simultaneous optimization of the cleaning schedule and the flow distribution through all parallel branches (Opt. Sp + Sch). The scenarios in which only the cleaning schedule is optimized – 4 and 5 –, the flow distribution in the parallel branches is fixed at 50% and constant over time. All these scenarios cover all common operating modes found in industry, and they include the interactions of control and scheduling variables. The goal is to compare all different flow distribution policies, and to demonstrate the advantages of simultaneously optimizing scheduling and control for fouling mitigation in HEN.

Table 3.4 presents the problem size summary, the operating cost, and the optimal cleaning schedule of each of the scenarios considered here. Scenarios 1 is a simulation case with no degrees of freedom to optimize, scenarios 2, 3 and 5 are NLP problems where the optimization variables are the flow distribution through the parallel branches – shell side, tube side, or both – and scenarios 4, 6, and 7 are MINLP problems including the cleaning schedule decisions. All the scenarios are formulated using the continuous time discretization approach with nine periods which introduces 27 binary variables in the MINLP problems. The optimal flow distribution problems or flow constrained problems formulated as NLPs are solved in less than 1 min of CPU time, while the optimal cleaning scheduling problems are challenging and solved in 330 min of CPU time average. Regardless of the flow distribution policy through the parallel branches of the network, the complexity of the problem arises from the large number of feasible cleaning schedules.

Table 3.4. Optimal cleaning solution and computational results of case 2HE-B for the integration of scheduling and control decisions

Case number	**1**	**2**	**3**	**4**	**5**	**6**	**7**
Case ID	**NM**	**Δ*P*-NM**	**Opt. Sp**	**Opt. Sch**	**Seq. Opt**	**ΔP-Opt**	**Opt. Sp+Sch**
Operating mode**	**NM**	**NM**	**NM**	**SCH**	**Fixed SCH**	**SCH**	**SCH**
Branches flow	**Fixed**	**Δ*P***	**Free**	**Fixed**	**Free**	**Δ*P***	**Free**
Continuous variables	2758	2794	2794	2758	2758	2794	2794
Binary variables	0	0	0	27	0	27	27
Equality constraints	2322	2358	2322	2322	2322	2358	2322
Inequality constraints	5669	5741	5669	5669	5669	5741	5669
CPU time [min]	0.06	0.12	0.09	329.51	0.26	288.15	374.38
Total energy [MW-h]	$3.990\text{x}10^5$	$3.987\text{x}10^5$	$3.983\text{x}10^5$	$3.934\text{x}10^5$	$3.912\text{x}10^5$	$3.943\text{x}10^5$	$3.910\text{x}10^5$
Production profit [$]	$6.617\text{x}10^8$	$6.617\text{x}10^8$	$6.617\text{x}10^8$	$6.617\text{x}10^8$	$6.617\text{x}10^8$	$6.617\text{x}10^8$	$6.617\text{x}10^8$
Fuel cost [$]	$1.077\text{x}10^7$	$1.077\text{x}10^7$	$1.075\text{x}10^7$	$1.062\text{x}10^7$	$1.056\text{x}10^7$	$1.065\text{x}10^7$	$1.056\text{x}10^7$
Carbon cost [$]	$1.829\text{x}10^5$	$1.818\text{x}10^5$	$1.816\text{x}10^5$	$1.794\text{x}10^5$	$1.784\text{x}10^5$	$1.798\text{x}10^5$	$1.783\text{x}10^5$
Cleaning cost [$]	0	0	0	90000	90000	60000	90000
Total cost [$]	$1.096\text{x}10^7$	$1.095\text{x}10^7$	$1.093\text{x}10^7$	$1.089\text{x}10^7$	$1.083\text{x}10^7$	$1.089\text{x}10^7$	$1.083\text{x}10^7$
Cleaning schedule (HEX#, time [days]) [x]	None	None	None	(1, 81) (2, 173) (1, 226)	(1, 81) (2, 173) (1, 226)	(1, 167) (1, 167)	(1, 88) (2, 180) (1, 278)

[**] NM: no mitigation operating mode (no cleanings considered), SCH: optimal cleaning scheduling problem solved

[x] Cleaning time rounded to the closest integer value for the continuous time discretization approach

All the scenarios of the 2HE-B case that have some mitigation action – flow control, cleaning scheduling, or both, scenarios 2 to 7 – present a reduction of the total operational cost relative to the NM case, with fuel consumption representing the highest contribution (>90%). The scenarios in which the only mitigation action is the flow distribution, either free or pressure driven, achieve a cost reduction lower than 0.1%. Despite this small benefit, controlling the flow distribution in the network is advantageous to recover more energy in branches that have low fouling resistance. There is an important compromise between the flow rate and the fouling rate in parallel branches. While low flow rates favour high outlet temperature, they also increase the fouling rate. Figure 3.22 shows the fouling resistance of each branch for the scenarios that consider flow distribution without cleanings. The fouling resistance of the branches at a fixed flow rate or pressure driven flow are similar, but HEX1 has a higher fouling resistance than HEX2 when the flow split is optimized. This trend is the best possible trade-off between energy recovery rate and fouling rate of the exchangers in the branches, and a faster fouling rate in one of the branches does not imply a bad operation.

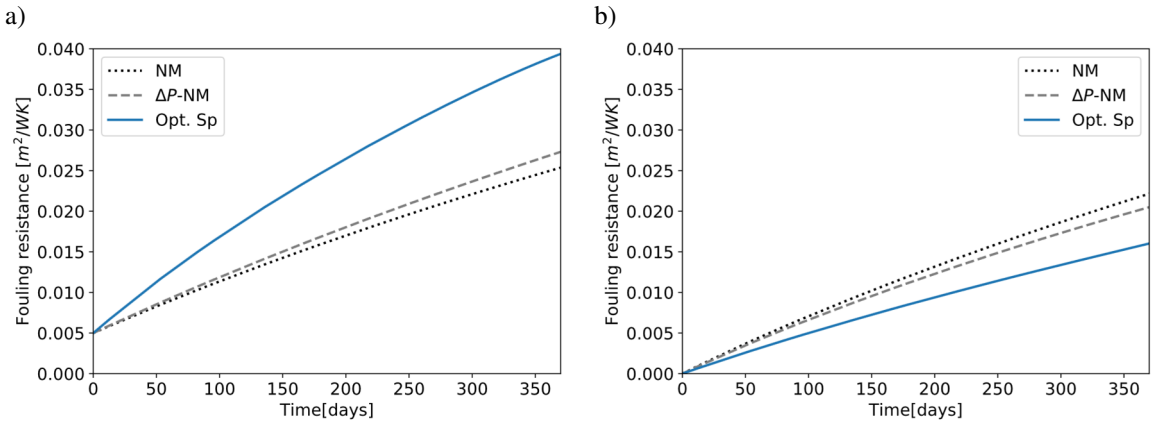

Figure 3.22. Fouling resistance of HEX1 (a) and HEX2 (b) of case "2HE-B" under different flow split scenarios when there are no cleanings.

On the contrary to the scenarios that only consider flow distribution, those that optimize the cleaning schedule reduce significantly the operating cost as they allow to restore the thermal and hydraulic performance of the network periodically. The optimal cleaning schedule alone – scenario 3 – provides a cost reduction of \$ 65x10^3 with respect to the NM scenario, and when it is integrated with control decisions, the cost reduction is \$ 125x10^3 for the sequential case – scenario 5 – and \$ 131x10^3 for the simultaneous case – scenario 7. The main difference between scenarios 5 and 7 is the starting time of the cleanings. The total

number of cleanings of each exchanger and the cleaning sequence is the same for both scenarios, but the operating time between two consecutive cleanings is larger in the simultaneous approach than that in the sequential approach. A longer operating time is achieved by optimally distributing the flow through the parallel branches recovering more energy overall. Although the individual effect on the heat exchangers may be an increase in the fouling resistance or decreasing the heat duty, the overall effect on the network is a reduction of the total operating cost.

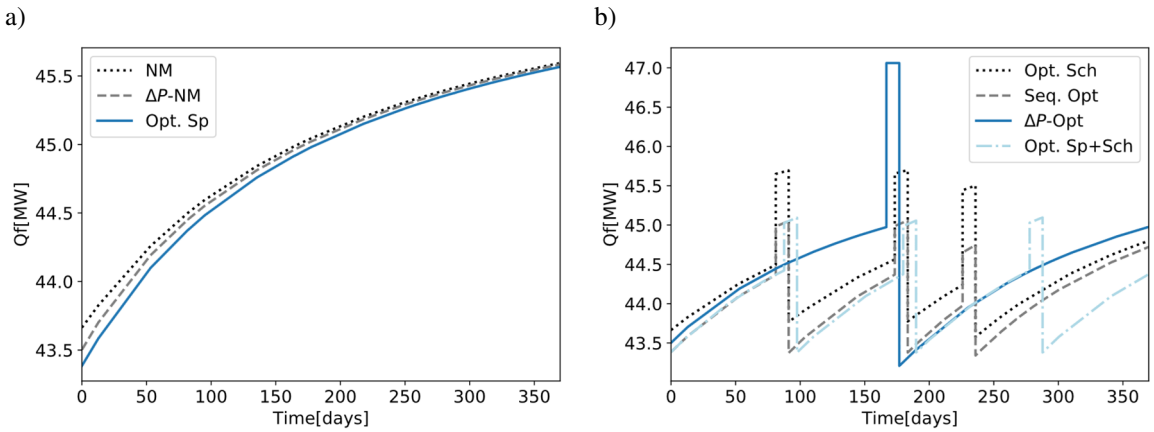

Figure 3.23. Furnace duty for the case 2HE-B under different flow split scenarios. a) no cleanings, b) optimal cleaning scheduling.

Figure 3.23 shows the furnace duty for all the scenarios with and without cleanings. The effect of the flow distribution is marginal in reducing the furnace duty, and the optimal flow distribution defines a duty that is always lower than the others, although the pressure driven flow scenario still improves the operation. There is an important synergy when the flow distribution is integrated with the cleaning scheduling decisions. For instance, the furnace duty of the sequential optimization case – scenario 5 – shows that the duty during the cleanings decreases as the flow is distributed towards the branch that is operating and diverted from the branch that is being cleaned. The crude flow rate distributed towards HEX1 is displayed in Figure 3.24 for all the scenarios. The flow is shifted during the cleanings towards the branch that remains operating, and towards the cleaned unit just after the cleaning finishes. The dynamic flow distribution also contributes to reducing the fouling rate as it modifies the shear stress on the tube side, hence increasing the removal rate of the deposit. These interactions increase the economic benefits of the operation when both decisions are

considered sequentially or simultaneously, although a simultaneous optimization exploits all synergies and provides the greatest benefits.

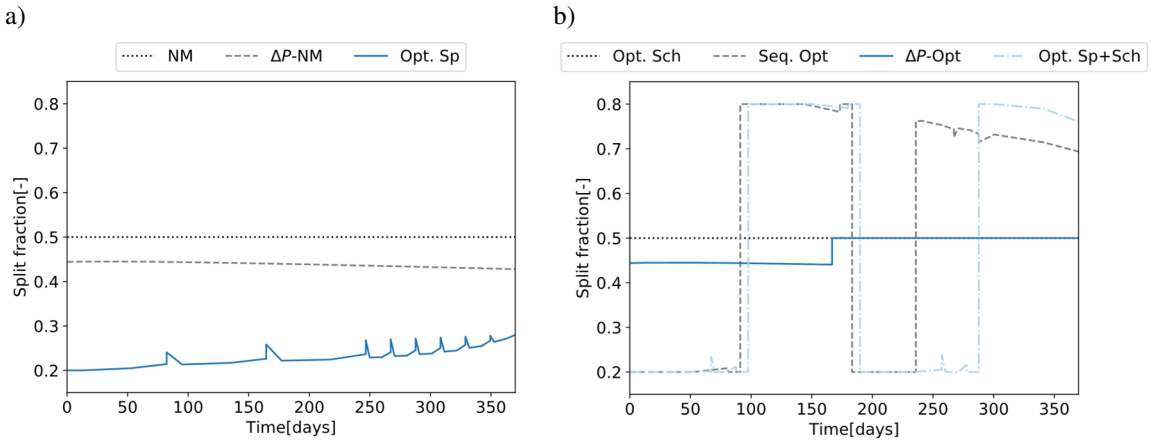

Figure 3.24. Split fraction towards HEX1 branch on the tube side of case 2HE-B under different flow split scenarios. a) no cleanings, b) optimal cleaning scheduling.

The optimal cleaning schedule of the case study when the flow distribution is free or fixed consist of cleaning HEX1 twice – it has an initial deposit – and HEX2 once. This pattern changes when the flow distribution of the crude stream is pressure driven. In this case, the optimal cleaning schedule is to clean both exchangers simultaneously after 167 days of operation. This ensure that the pressure of the branches is balanced at all time, although when only one branch is active during an individual cleaning this constraint is relaxed. After the simultaneous cleaning of the two exchangers the split fraction is fixed at 50% for the tube and shell side because both units follow the same evolution.

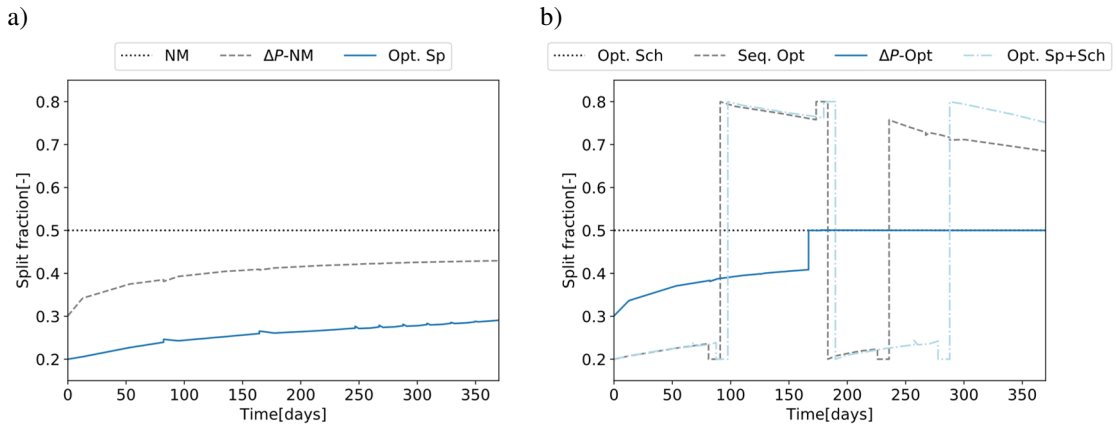

Figure 3.25. Split fraction towards HEX1 branch on the shell side of case 2HE-B under different flow split scenarios. a) no cleanings, b) optimal cleaning scheduling.

The pressure driven flow scenarios still have a control degree of freedom which is the flow distribution of the shell side, and it is shown in Figure 3.25 for all the scenarios. The hot stream flow is distributed to the exchangers so that a higher flow rate is sent to the unit with a lower fouling resistance and more energy is recovered. The additional constraint introduced in the formulation to equalize the pressure of the crude oil branches reduces the possibilities of improving the operation, and the cost reduction achieved is lower than that of scenarios where the flow distribution is completely free.

3.5. Concluding remarks

A general and novel mathematical formulation for the simultaneous optimization of cleaning scheduling and dynamic flow distribution of HEN under fouling is presented. This formulation exploits the synergies between scheduling and control decisions, which previous studies have only considered individually. The optimal integration of control and scheduling decisions for fouling mitigation in HEN outperforms any other mitigation alternative including the sequential optimization of first the cleaning schedule and then the flow distribution. The HEN model used in the formulation is based on fundamental principles, and it has an ideal trade-off between prediction capabilities, and complexity for optimization purposes. The heat exchanger model includes the radial heat transfer effects explicitly – overcoming the common thin slab assumption – and averages the axial effects. The generality of the formulation allows to modify or change any of the building blocks that constitute the overall model, to include more than one cleaning alternative, to introduce control elements, and to add/remove case specific operational constraints.

The main challenges for solving the optimal cleaning scheduling and control problem of HEN are the large number of binary variables, and the many feasible solutions with similar performances. A continuous time representation is proposed to reduce the complexity of the problem, while retaining prediction accuracy and quality of the solution. It performs better than the commonly used discrete time approach as it allows solving relevant optimization problems much faster. In addition, this modelling approach allows to optimize scenarios not considered before such as the optimal timing of known cleanings, and the optimization of a partially defined cleaning schedules. Both scenarios arise in refining applications where some of the decisions are done by experts and all others can be optimized by computer algorithms.

Various small but realistic case studies and scenarios are evaluated to test the prediction capabilities of the model proposed, and to determine their effect on the optimal cleaning scheduling. The optimal cleaning scheduling problem is solved for a heat exchanger with different ageing rates, and it is shown that, for that case, the optimal solution is independent of the ageing rate, although the operating cost changes significantly. It is also shown, through the case studies, that optimally cleaning the units of a network can avoid bottlenecks in the operation that generate a large operating cost and production losses. No previous studies can include all these features in the same problem formulation for optimizing the cleaning schedule of HEN.

The mathematical formulation presented here can be extended to include retrofit decisions (Chapter 6), and it can also be used for the online monitoring and optimization of HEN (Chapter 8). Despite the successful application of the problem formulation, it is still challenging to solve larger networks of industrial relevance. An efficient solution strategy for this problem is described in Chapter 5, which significantly reduces the computational time. Finally, validating the prediction models is necessary for any real application, which is done and discussed in great detail in Chapter 4.

Chapter 4

Optimizing preheat trains under fouling: model validation

The mathematical model developed in the previous chapter (lumped model) for HEN under fouling is validated using two approaches. In the first one, it is directly compared against a more detailed and previously validated model that considers the axial distribution of the variables in the exchanger (distributed model). The fouling parameters are determined based on the predictions of the detailed model. In the second one, real refinery data is used to fit the fouling parameters of the model, and the prediction error is quantified. A model fitting and validation procedure is established to improve the prediction capabilities of the lumped model using, simultaneously, the distributed model and plant measurements. It is demonstrated that the prediction accuracy of the lumped model is not different from that of the distributed model, that it predicts the variability observed in the actual measurements, and that it can be used for optimization purposes.

4.1. Introduction

Accurate heat exchanger and fouling models are paramount for understanding the operation of large HEN, their limiting conditions, causes of fouling, effects of the main variables, and how to improve their efficiency over time. The validity and efficiency of any proactive mitigation action depends on the accuracy of the model used to support the decision making.

This chapter aims to validate the model developed previously using as benchmark a detailed and previously validated model. Also, actual plant measurements (e.g. flow rates, temperature, pressure) are used in a separate validation test. In all instances, the data – either simulated, or measured – is used to fit the fouling parameters of the model using a novel

estimation procedure. This chapter will demonstrate that the model developed previously can capture accurately the behaviour of all performance indicators in a HEN, and that it can efficiently be used for optimizing their operation and to define their optimal cleaning scheduling.

4.2. Summary of heat exchanger models used for validation

Among the heat exchanger models reviewed in Section 2.4 of this thesis, lumped and distributed models are suitable for optimizing the operation and the cleaning scheduling of large HEN. One lumped, and one distributed model are analysed here. The model developed in Chapter 3 is a lumped model that includes explicitly the radial distribution effects in a more complete way than other lumped models. For the rest of this chapter this model will be referred to as model A for simplicity. The model developed by Coletti, and later revised by Diaz-Bejarano is a distributed model that has been previously tested and validated for real applications (Coletti and Macchietto 2011; Diaz-Bejarano, Coletti, and Macchietto 2016). This model is commercially available as *Hexxcell Studio*^{TM} (Hexxcell Ltd. 2016), and the software is used for all cases analysed in this chapter. Appendix B presents the fundamental assumptions, considerations, and model equations of this distributed model. For simplicity, this model is referred to as model B for the rest of the chapter.

Models A and B, when coupled with an appropriate fouling model, for instance the Ebert-Panchal model which is used in this thesis, predict the key performance indicators of individual units and overall networks needed to optimally define fouling mitigation strategies. However, they differ significantly in their complexity, number and type of constraints. Table 4.1 shows a comparison of the two models, the axially lumped one (A) and the fully distributed one (B), indicating the main equations, and an estimation of the model size. This estimation assumes that all the differential equations, including the time derivatives, are fully discretized, although for simulation purposes a forward integration technique – Runge-Kutta methods for example – can be used reducing the number of equations solved at every time step.

Table 4.1. Model size comparison and estimation of the number of equations and variables.

	Lumped model (A)		Distributed model (B)	
	Algebraic (A) or differential (D)	**Estimated number after discretization*.**	**Algebraic (A) or differential (D)**	**Estimated number after discretization*.**
VARIABLES				
Temperature - shell	A	$(N_{HEX})N_T$	D	$(N_{HEX}*N_Z)N_T$
Temperature - tube	A	$(N_{HEX})N_T$	D	$(N_{HEX}*N_Z*N_P)N_T$
Temperature (wall and deposit)	A	$(2N_{HEX})N_T$	D	$2(N_{HEX}*N_Z*N_P*N_R)N_T$
Flow rates	A	$(2N_{HEX})N_T$	A	$(2N_{HEX})N_T$
Pressure	A	$(N_{HEX})N_T$	D	$(N_{HEX}*N_Z*N_P)N_T$
Fouling resistance	D	$(N_{HEX})N_T$	D	$(N_{HEX}*N_Z*N_P)N_T$
Deposit thickness	A	$(N_{HEX})N_T$	A	$(N_{HEX}*N_Z*N_P)N_T$
Heat duty	A	$(N_{HEX})N_T$	A	$(N_{HEX}*N_Z*N_P)N_T$
Total		$(10N_{HEX})N_T$		$N_{HEX}(2+N_Z(1+N_P(5+2N_R)))N_T$
EQUATIONS				
Mass balance	A	$(2N_{HEX})N_T$	A	$(2N_{HEX})N_T$
Energy balance	A	$(2N_{HEX})N_T$	D	$(N_{HEX}*N_Z*(1+N_P*(2N_R+1)))N_T$
Fouling model	D	$(N_{HEX})N_T$	D	$(N_{HEX}*N_Z*N_P)N_T$
Deposit thickness	A	$(N_{HEX})N_T$	D	$(N_{HEX}*N_Z*N_P)N_T$
Heat transfer	A	$(3N_{HEX})N_T$	A	$(N_{HEX}*N_Z*N_P)N_T$
Pressure drop	A	$(N_{HEX})N_T$	D	$(N_{HEX}*N_Z*N_P)N_T$
Total		$(10N_{HEX})N_T$		$N_{HEX}(2+N_Z(1+N_P(5+2N_R)))N_T$

*N_{HEX}, number of heat exchangers in the networks (≥ 1).

N_T, number of discretization points in time (≥ 2).

N_Z, number of discretization points in the axial direction (≥ 5).

N_R, number of discretization points in the radial direction (≥ 20).

N_P, number of tube passes (≥ 1).

It is observed that while the lumped parameter model size is only a function of the number of exchangers in the network and the number of time discretization points, the distributed model size also depends on the mesh size of the axial and radial domains, and on the number of tube passes. The additional features included in the distributed model increase its size rapidly, as for an accurate integration of the variables at least 10 discretization points are required in the axial coordinate, and 20 in the radial coordinate. Hence, the distributed model size can be more than hundred times larger than that of the lumped model. Another key difference between the models is that while model A has mainly algebraic constraints and the only differential equations come from the fouling model, model B uses partial differential equations for the energy balance of each domain, and the fouling model is a differential equation solved at every discrete point in space. Special considerations must be taken for solving the large set of PDAE of model B because of the moving boundary condition in the radial deposit domain – see Appendix B for the detail assumptions and equations. Despite these numerical difficulties, model B is able to simulate large networks of industrial importance in a reasonable computational time, and to use plant data over long periods of operation for parameter estimation and validation, and then for simulation-based assessment of flow control and cleaning schedules (Coletti and Macchietto 2011b; Diaz-Bejarano, Coletti, and Macchietto 2016; Diaz-Bejarano, Coletti, and Macchietto 2017).

Aiming to solve the optimal cleaning scheduling and control problem formulated in Chapter 3 with a realistic and accurate heat exchanger model, the lumped model (A) is advantageous over model (B). The number of binary variables and logic disjunctions, which are the main complicating factors, are function of the problem size and the discrete time points. The continuous time approach discussed in Chapter 3 cannot be used in model B because the solution of all the differential domains, especially the radial distribution of the deposit, are very sensitive to the time step of integration. However, model B has been successfully validated, and its accuracy proven while model A has not. Also, the features of model B may be necessary for monitoring in detail the development, nature and location of the deposit formed in a heat exchanger (Diaz-Bejarano, Coletti, and Macchietto 2018). A good balance between the two models is therefore necessary, but first it is necessary to establish that valid and accurate predictions can be achieved with model A for optimization. In the following section, a novel combined strategy for model validation and parameter

estimation is described that integrates the two models to improve the prediction capabilities of the lumped one.

4.3. Model validation approach and parameter estimation problem

The lumped model (A) described in Chapter 3 must be validated before using to support decision making. Figure 4.1 presents a flowchart describing the data collection, model fitting, and validation procedure designed for this application. It starts with the primary measurements from the plant which can be flow rates, streams temperature, and pressure, although pressure measurements are rarely available. The data is used to fit the fouling parameters of the distributed model (B) as described in previous works (Coletti and Macchietto 2011; Diaz-Bejarano, Coletti, and Macchietto 2016). Then, model B acts as a soft sensor to predict additional variables of the system including intermediate stream conditions and pressure drops that are not measured during the operation or included in the data set. The new and enhanced data set generated using the simulation results of model B are the inputs for the parameter estimation and validation of the lumped model A. This data set is filtered and divided in two groups: one for estimation and other for validation, and because of the dynamic nature of the problem this partition is based on the time horizon, by defining an estimation horizon (t_{EH}) – steps 2 and 3 in Figure 4.1. All data points between $t = 0$, and $t = t_{EH}$ belong to the estimation data set, and all other points ($t > t_{EH}$) belong to the validation data set. Only the estimation data set is used within the parameter estimation problem – described later in this section – to determine the fouling parameters of model A that best explain the behaviour predicted by model B based on the plant observations. The validation data set is also used to calculate and evaluate the prediction error of the model after fitting. Finally, once the lumped model is validated it can be used with adequate confidence to analyse different aspects of the operation of HEN under fouling, and to support decision-making to mitigate fouling and increase energy efficiency, such as optimal flow distribution and optimal cleaning scheduling decisions.

The only parameters that are considered for estimation in both models are those of the Ebert-Panchal fouling model. They are the deposition constant α, and the removal constant γ, while the activation energy E_f is assumed fixed. These are referred in general as fouling model parameters, although they are not necessary the same for model A and model B.

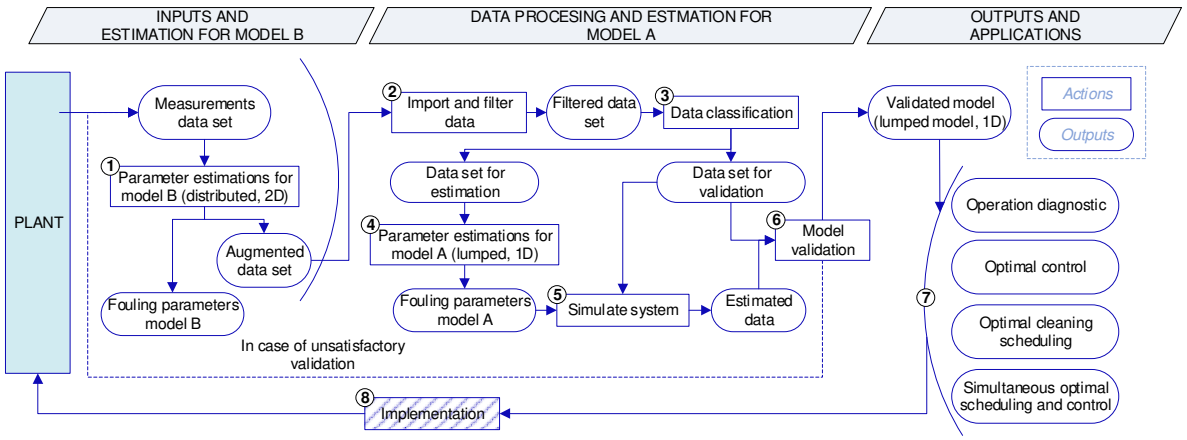

Figure 4.1. Flowchart of model validation procedure using 2D distributed model as benchmark

The procedure developed to estimate the parameters of the lumped model is indirect because it does not use directly the plant measurements available. The main motives to implement this procedure are: i) for the purpose of this thesis, the scarcity of good quality plant data in the open literature, and confidentiality policies that prohibit refinery operators to share data or information about the operation, ii) the typical lack of complete measurements in a whole HEN, where key pressure or temperature measurements required for the estimation procedure may be missing, and iii) the 2D distributed model available in *Hexxcell Studio*^{TM} has been previously validated, and used with real refineries for commercial purposes. This model has shown to accurately predict the main performance variables of the heat exchangers such as outlet streams temperature, pressure drop, and heat duty in real applications (Coletti and Macchietto 2011; Diaz-Bejarano, Coletti, and Macchietto 2015). In Coletti and Macchietto (2011); and Diaz-Bejarano, Coletti, and Macchietto (2017) it has been reported that model B has a prediction error within +/- 2.0°C for the streams temperature, and within +/- 1.5% for the heat duty and pressure drop of the heat exchangers. These prediction errors are within acceptable ranges considering the large time scales of the operation, the errors in the measurements, and the large variability of the flow rates and crude blends. Hence, an indirect validation approach for the lumped model is deemed suitable and enables overcoming the lack of data and measurements.

Under these considerations for model validation, and assuming that the distributed model (B) accurately represents the operation of any HEN, the validation of the lumped model (A) will depend on how well it captures the phenomena and dynamics predicted by

model B. A direct comparison of the predictions of the two models will indicate whether they capture the same phenomena observed and under which conditions.

During the first stages of the validation procedure, a parameter estimation problem is solved using the primary plant data – tube and shell side temperature, flow rates, and pressure drop if available – to estimate the fouling model parameters in the 2D distributed model B – step 1 in Figure 4.1. The maximum likelihood estimation problem is presented in Eq. (3.6). It is a constrained optimization problem which solution is the optimal model parameters, v – used as a general notation. The objective function of this problem includes the variance of the measurements to standardize all quadratic errors between the observed and predicted variables. Also, the error is calculated for all variables measured. This parameter estimation problem can only be solved, in a reasonable time, for individual heat exchangers because of the scale of model B, and the large computational load required to solve the partial differential and algebraic system of equations at every iteration. For large networks, an estimation problem is solved for every exchanger, isolating the measurements around it. For multiple shell exchangers intermediate measurements are not available, so that the same fouling parameters are assumed for all the shells. The parameter estimation process for model B is automated using *Hexxcell Studio*^{TM}.

$$\min_{v} \left\{ \frac{N_0 N_m}{2} \ln(2\pi) + \frac{1}{2} \sum_{i=1}^{N_0} \sum_{j=1}^{N_m} \left[\ln\left(\sigma_{i,j}^2\right) + \frac{\left(\tilde{x}_{i,j} - x_{i,j}\right)^2}{\sigma_{i,j}^2} \right] \right\}$$
$$s.t. \tag{4.1}$$
$$Model\ B\ (Distributed\ heat\ exchanger\ model)$$
$$Fouling\ model$$
$$Pressure\ drop\ calculations$$

The second parameter estimation problem solved – step 4 in Figure 4.1 – estimates the parameters of the lumped model (A), based on the predictions generated using the fitted distributed model (B). This problem is presented in Eq. (4.2), where the "measured" variables are those predicted using model B including any soft-measurements. In this case the estimation problem is solved for the whole network instead of individual units by minimizing the quadratic error observed on the tube side temperature, the shell side temperature, and the tube side pressure drop of each exchanger. The parameters w in the equation correspond to relative weights among the different errors, and they are assigned as: $1x10^2$ for the shell and tube side temperature errors and $1x10^{-3}$ for the pressure drop error. The errors – differences

between the two models – are summed using weights defined by the analyst which are not standardized using the variance as in the previous problem. Contrary to the parameter estimation problem for the distributed model – step 1 – this formulation includes all three key performance indicators of each exchanger and of each shell because, regardless whether they are measured or not, they can be predicted using model B.

$$\begin{aligned}
&\min_{v} \sum_{i=1}^{N_{HEX}} \sum_{j=1}^{N_m} \left[w_T \left(\widetilde{T^T}_{i,j} - T^T_{i,j} \right)^2 + w_T s \left(\widetilde{T^S}_{i,j} - T^S_{i,j} \right)^2 + w_P \left(\widetilde{\Delta P}_{i,j} - \Delta P_{i,j} \right)^2 \right] \\
&s.t. \\
&Model\ A\ (Lumped\ heat\ exchanger\ model) \\
&Fouling\ model \\
&Pressure\ drop\ calculations
\end{aligned} \tag{4.2}$$

The decision variables of the parameter estimation problems referred to as v are the parameters of the fouling model. In the problem defined by Eq. (4.1) these parameters are estimated for a single exchanger, while in that defined by Eq. (4.2) they are estimated for all exchangers in a network simultaneously. The solution of these problems corresponds to step 1 and 4 in Figure 4.1. The only parameters estimated are the deposition constant, α, and the removal constant, γ, while the fouling activation energy is fixed a priori because it is highly correlated with the other parameters (Diaz-Bejarano, Coletti, and Macchietto 2017). In addition, the deposit roughness of each exchanger, ϵ, is estimated for the lumped model (A). The deposit roughness affects the friction factor, the tube side pressure drop, and the shear stress, the later modifies the fouling removal rate. In many cases, the fouling removal rate is very small compared to the fouling deposition rate (Wilson, Ishiyama, and Polley 2017; Diaz-Bejarano, Coletti, and Macchietto 2017) and changes of the shear stress due to changes of the roughness of the deposit may not have a significant effect in the thermal performance of the exchangers. However, it was found better to consider the thermal effects and the hydraulic effects simultaneously and determine all the parameters of the model at the same level using a weighted multi-objective formulation for the parameter estimation problem.

The parameter estimation problem defined for the lumped model is an NLP, whose complexity arises from the many data points, the time varying effects, and few degrees of freedom. The time horizon is discretized using a discrete time approach.

In a more general way, when actual plant dynamic data is available, there are two possible routes to estimate the parameters of the lumped model (A) developed in Chapter 3 for optimizing HEN under fouling. Figure 4.2 summarizes these two routes, and comments

on their considerations and assumptions. The first one is a direct route that uses the measured data as observations in the parameter estimation problem – path 1,2,5,6,7 – and the second one is an indirect route in which the parameters of the distributed model (B) are estimated first, and then the fitted model is used to simulate the system and generate a new data set for the estimation problem of the lumped model – path 1,2,3,4,5,6,7. While in the direct route the data available is limited, and information about pressure drops and intermediate temperature measurements may be lacking, the indirect route makes those features available to estimate the parameters of the lumped model. Both approaches use primary measurements to estimate the fouling parameters of the model, and do not rely on the calculation of the fouling resistance from plant measurements as previous approaches have reported in the literature to simplify the parameter estimation problem. Calculating the fouling resistance based on the observed data amplifies the noise and error of the measurements, hinder the prediction capabilities of the model, and ignore the interactions among the units in a network (Díaz-Bejarano, Coletti, and Macchietto 2015; Tavares et al. 2013)

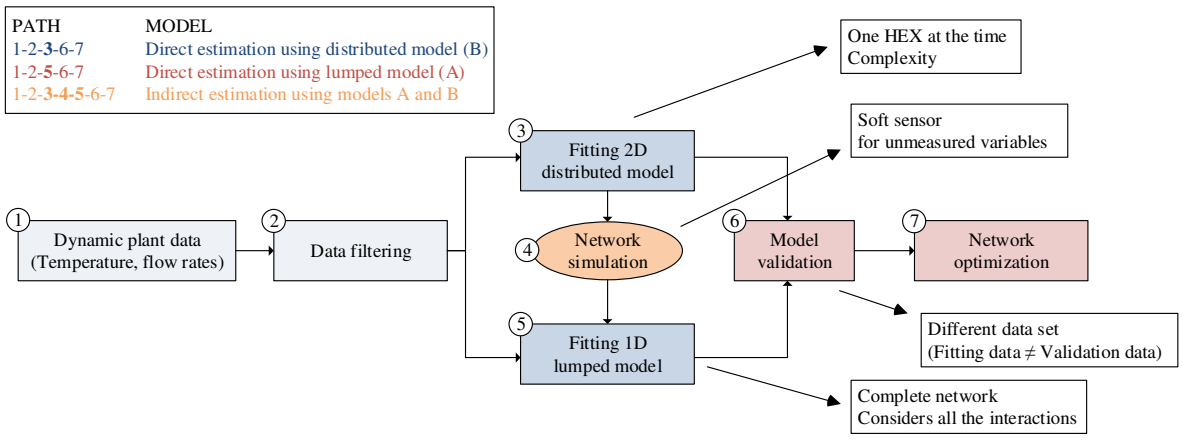

Figure 4.2. Model fitting and validation approaches when plant measurements are available.

In Figure 4.2 the possibility of using the validated distributed model (B) to optimize the network operation is also considered, although this is subject to efficient algorithms to cope with the complexity and large scale of the distributed model. However, model B can still be used at this stage to improve the operation of the system using simulations to evaluate many scenarios under different conditions or alternative fouling mitigation strategies.

4.4. Prediction errors and model validity

A total of eight case studies are used to validate the model developed in Chapter 3, lumped model A, by comparing it with the fully distributed model B (Appendix B).

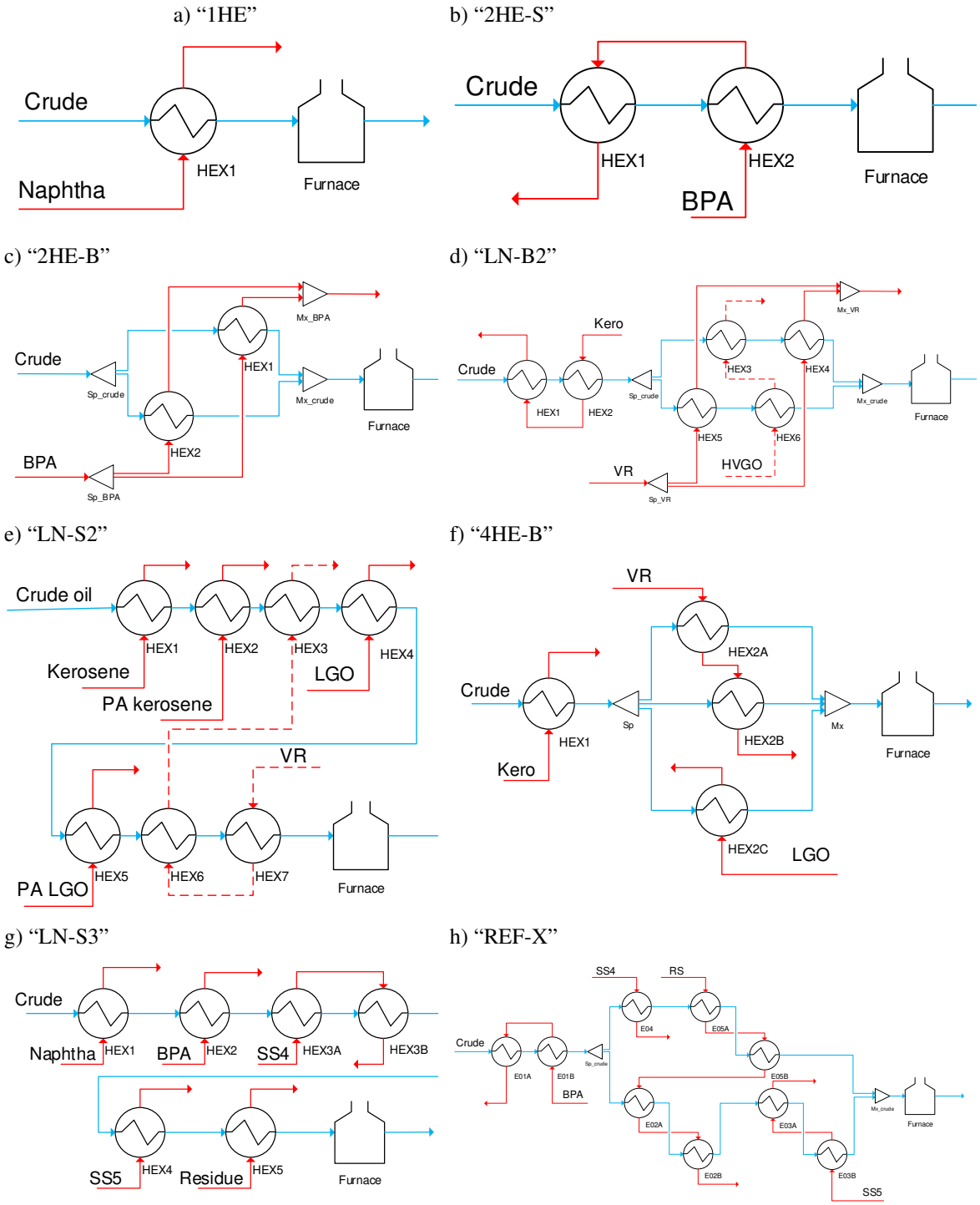

Figure 4.3. Network structure for all cases considered in the model validation

The network structure of the case studies is presented in Figure 4.3, and all the details about their operation and specifications are presented in Appendix A. The model comparison and validation are done for every exchanger of each network, for a total of 37 units analysed. The networks considered cover a wide range of operating conditions (e.g. flow rates, streams temperature) and specifications of shell and tube heat exchangers (e.g. number of tubes, number of passes, baffles) reflecting those normally found in refinery operations, especially in the hot end of preheat trains. Also, the network configurations are all different and include a wide range of features such as interactions on the shell side of various exchangers, multiple parallel branches, and flow split on the shell side.

The case studies range from small to large networks with one to nine heat exchangers, and multiple configurations. These cases are adapted from the open literature, and case "REF-X" is based on a preheat train of an actual refinery. For all case studies the operation is simulated for one year with the distributed model (B), and then those results are used as measurements to estimate the parameters of the lumped model (A).

There is an inherent difference between the two models that cannot be eliminated by fitting the fouling parameters, and will show up both in clean and fouled dynamic conditions. A clean conditions error analysis is done first, followed by a dynamic error analysis.

4.4.1. Validation under clean conditions

Under clean conditions or constant fouling values, the two models may differ as their fundamental equations and assumptions are different, and there are no parameters to tune to make the predictions of the lumped model closer to those of the distributed model. The error between the lumped model (A) and the distributed model (B) is calculated at the initial time for every exchanger in each case studies. Figure 4.4 shows the error distribution, the average error (μ), and the standard deviation of the error (σ) for the outlet tube side temperature, outlet shell side temperature, tube side pressure drop, and heat duty..

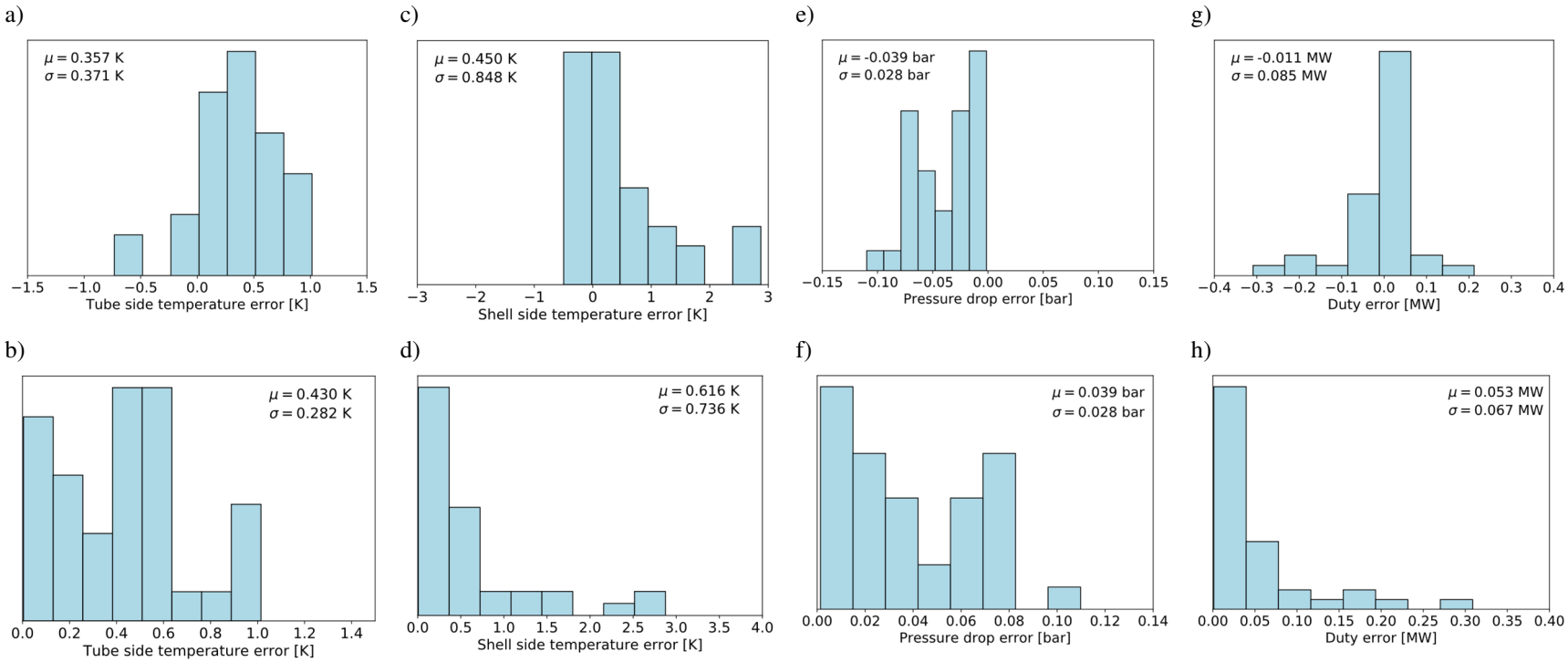

Figure 4.4. Histograms showing the initial error (top) and absolute error (bottom) distributions the key performance variables predicted by model A and B in clean conditions. a, b) tube side temperature, c, d) shell side temperature, e, f) tube side pressure drop, g, h) heat duty.

The distribution of the errors in the tube side temperature and heat duty predictions are approximately normally distributed with mean close to zero and ranges of +/- 1.0 K and +/- 0.3 MW, respectively. These ranges and distributions are acceptable for the order of magnitude of the errors considering that the prediction errors of the distributed model with respect to measure pant data are within or larger than these ranges. On the other hand, the lumped model tends to underestimate the pressure drop, and to overestimate the shell side outlet temperature. The different assumptions about the shell side flow and heat transfer of the two models explains these trends. While the distributed one considers the heat transfer at every axial point for all the passes, the lumped one simplifies it in a single efficiency parameter. Nevertheless, both error distributions are close to zero and the extreme values of the errors are still acceptable given the previous validation of the distributed model against plant data, and that the intended use of the lumped model is in an online and real time optimization routine.

At a network level, the lumped model (A) can also predict with good accuracy the outputs of the distributed model (B). The average error in the CIT predictions of the two models is 0.17 K with a standard deviation of 0.37 K, and the average error of the furnace duty is 0.24 MW with a standard deviation of 0.29 MW. For both network key performance indicators, the average error is below the estimation errors reported for the distributed model (B), so that that model A is a good representation of realistic HEN. The average error obtained in the CIT prediction is lower than that of the tube side outlet temperature of individual exchanger because of the network interactions. Considering all the units in a network the prediction errors of some exchangers may compensate for those of others. Overestimations and underestimations of local key performance variables may substantially reduce the overall differences between the predictions of the two models at a network level.

For all key performance indicators of individual exchangers, the distribution of the absolute error is within the acceptable ranges of the distributed model (B) and the highest frequency is observed for errors that are close to zero. The absolute error of each variable is used as predicted variable in a partial least square (PLS) model to identify what features of the exchangers drive the differences observed between the models (Burnham, Viveros, and MacGregor 1996; Burnham, MacGregor, and Viveros 1999). Using the absolute error helps to identify the features that causes the lumped model to overestimate the shell side

temperature, and to underestimate the pressure drop. The inputs to the PLS are the inlet conditions of the exchangers including flow rates and temperatures, and all the geometric specifications such as number of tubes, shell diameters, and number of baffles. In total the PLS model has 17 observed variables (inputs) and 4 predicted variables (outputs). The first six principal components of the model can explain 63.6% of the variability of the outputs, which is enough to identify what exchangers are more likely to exhibit a difference between the two models.

Figure 4.5 shows the percentage of the variance explained by the principal components in each of the variables predicted. While the PLS model explains most of the variance of the shell side temperature error, pressure drop error, and heat duty error, it does not capture the variability of the tube side temperature error because there is almost no variability among the exchangers considered - normally distributed variable with mean zero. The principal components one and three (PC1, PC3) explain most of the variance of the shell side error, and the heat duty error, while the principal component two (PC2) explains the tube side pressure drop error. The other principal components have a smaller contribution to the predicted variables.

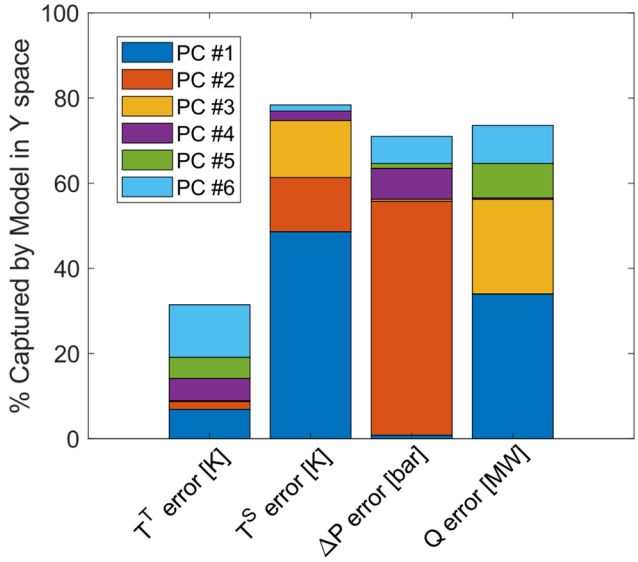

Figure 4.5. Variance capture by the PLS model on the error of each performance indicator variable.

Figure 4.6a shows the loads of the PLS model on the observed variables – w* loads – and Figure 4.6b shows the loads on the predicted variables – q loads of all the principal components. The contribution of the PC1 demonstrates that the baffle spacing, shell diameter, and tube diameter are inversely correlated with the absolute error of the predicted shell side temperature, while the inlet streams temperature are positively correlated with it. The lumped model (A) overestimates the shell side temperature for exchangers with smaller tubes, shell diameter, and baffle spacing – alternatively more baffles – than the average. The same applies for the exchanger duty as it is directly related to the shell side temperature. Similarly, the PC2 indicates that the lumped model (A) underestimates the pressure drop for exchangers with more tubes, more baffles, longer tube lengths, and higher inlet flow rates and temperature than average. The contribution of PC3 has the same tendency as that of PC1, but it includes the baffle cut with an inverse effect on the predicted error. Also, the tube diameter in PC3 is positively correlated with the shell site temperature error being opposite to the effect observed in PC1, although the percentage of the variance explained by PC3 is much smaller than that of PC1. All other principal components have a much lower and disperse distribution over the prediction errors of interest. In summary, this PLS analysis allows to understand the limiting conditions of the lumped model with respect to the distributed one, and to estimate the prediction errors only knowing the exchanger specifications.

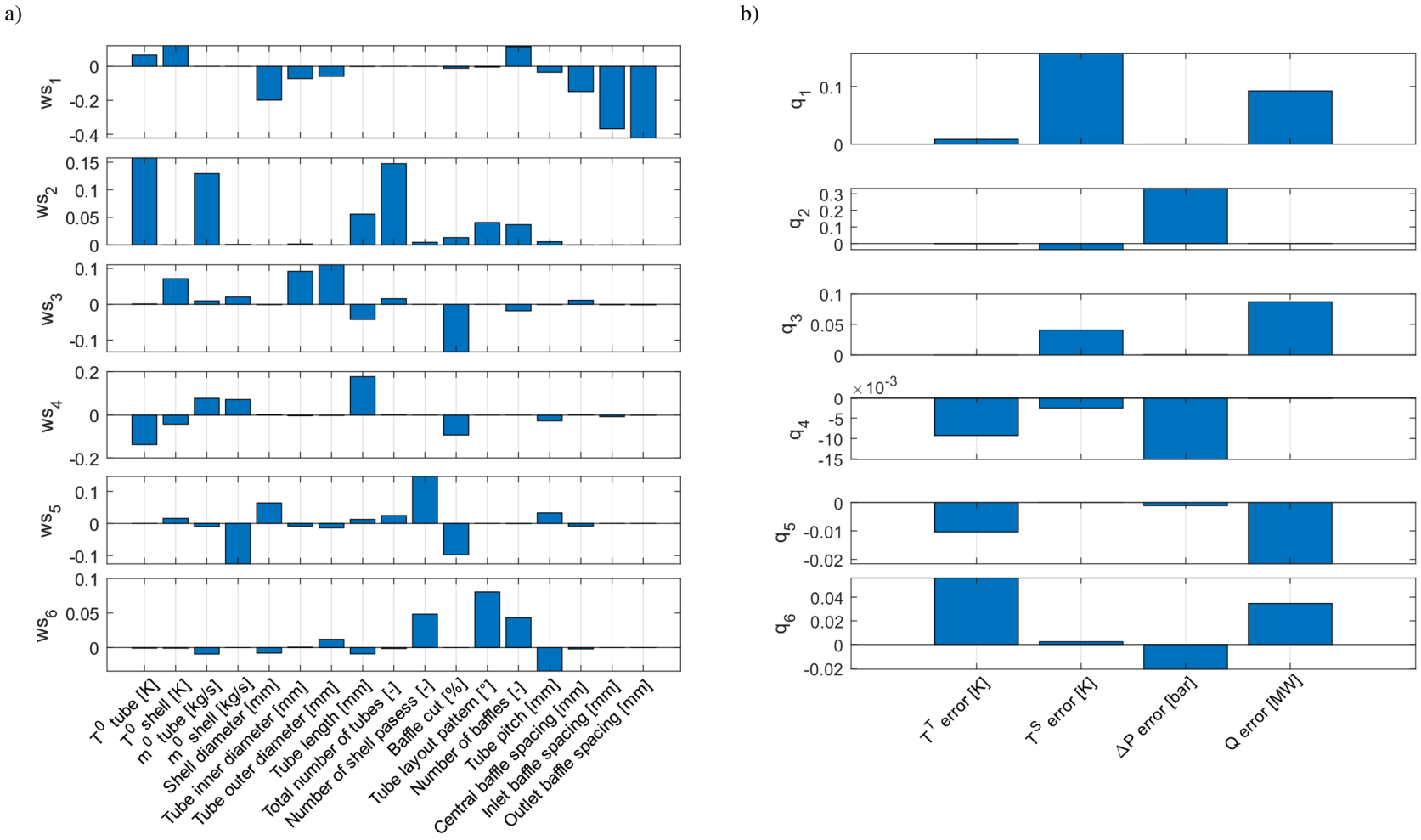

Figure 4.6. PLS model loads on inputs (a) and outputs (b) for the absolute error between the lumped (A) and distributed (B) models

Finally, a cross validation test is performed to evaluate the prediction capabilities of the PLS model developed. The data of the 37 heat exchangers is divided randomly in two. The fist data set with 30 points – 81% of the data – is used to fit a new PLS with six principal components as before. This new instance of the PLS model captures 63.4% of the variance in the outputs, which is not significantly different from that captured by the PLS model developed with the complete data – 63.6% of the variance in the outputs. The principal components and weights of this new PLS model are not significantly different from those of the previous model, and the same trends and effects are observed, so that the two instances of the PLS model are statistically equivalent. The second data set with the remaining data points is used to validate the predictions of the PLS model against the actual observations of the absolute error on the key performance indicators of the heat exchangers.

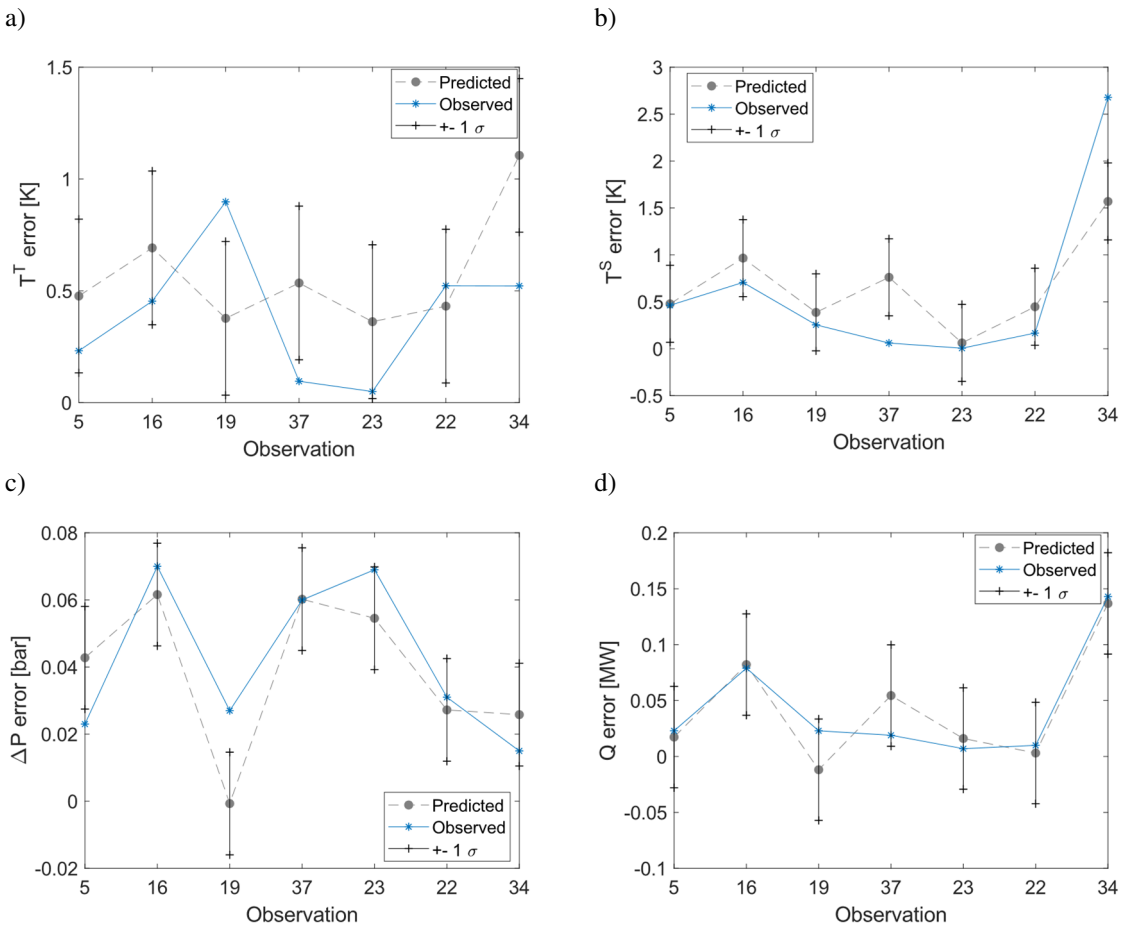

Figure 4.7. Cross validation results of the PLS model for 7 samples. a) Tube side temperature absolute error, b) shell side temperature absolute error, c) tube side pressure drop absolute error, d) heat duty absolute error.

Figure 4.7 compares the predictions obtained with the PLS model and the observations of the tube side outlet temperature, shell side outlet temperature, tube side pressure drop, and heat duty absolute errors. In most of the data points used for validation – 7 different heat exchangers – the difference between the observations and the PLS predictions is within one standard deviation, and the general trend is captured correctly – the effect of the geometric specifications of the exchangers on the key performance indicators error between model A and model B. Hence, the PLS model can be used to estimate beforehand the potential differences between the predictions obtained using the lumped model (A) or the distributed model (B) given the complete specification of an exchanger and its operating conditions. In this way, a decision of whether the lumped model can be adequate to represent a given exchanger can be done without running any simulation of the system or collecting data.

4.4.2. Validation under dynamic fouling operation

For the dynamic validation of the lumped model the data is divided in two sets: one over an estimation horizon for fitting, and another over a prediction horizon for validation. Four estimation horizons are considered: 90 days (24.6%), 180 days (49.3%), 270 days (73.9%), 365 days (100%), where the value in parenthesis is the percentage of data used for fitting. For all the case studies the parameter estimation problem formulated in Section 4.3, Eq. (4.2), is solved to determine the fouling parameters and the deposit roughness of the lumped model. The absolute average error (AAE), Eq. (4.3), between the dynamic profiles predicted by the two models is used as an indicator of the precision of the lumped model. The AAE is calculated for the key performance variables of each exchanger, over the estimation horizon, the prediction horizon, or the overall operating time.

$$AAE = \frac{1}{t_f}\int_0^{t_f}(\tilde{x} - x)dt \tag{4.3}$$

Figure 4.8 shows the AAE results for each key performance variable: the tube side outlet temperature, row 1; the shell side outlet temperature, row 2; the tube side pressure drop, row 3; and the heat duty of the exchanger, row 4. In each of these figures the points represent a single heat exchanger, and the average error is calculated at each estimation horizon. Also, the average trend representing the evolution of the error with respect to the estimation horizon is shown in the figure. The AAE calculated for the estimation horizon – column 1 – indicates the quality of fit of the tuned model, that for the prediction horizon –

column 2 – indicates the prediction error on new observations, and that for the overall operation – column 3 – captures the complete scenario. For all the key performance variables the AAE in the prediction horizon decreases as the estimation horizon increases because more data is included in the estimation problem so that the lumped model (A) represents better the behaviour of the distributed model (B). However, for estimation horizons greater than 180 days no significant improvement on the prediction errors is observed, and on average the lumped model fitted with data up until 180 days of operation is as good as that fitted with the whole data set in predicting the dynamic trends of the distributed model.

While, in the average, the AAE calculated within the prediction horizon decreases with respect to the estimation horizon, the AAE calculated within the estimation horizon remains almost constant. Regardless of the size of the data set used in the parameter estimation problem, the model adapts to the observations and predicts the dynamic behaviour of the distributed model with the same precision, although the variability increases in the case of the tube and shell side temperature. For some specific exchangers, the AAE observed for the overall operation is large. For instance, for HEX2A and HEX2B of case study "4HE-B" with an estimation horizon of 90 days, the AAE of the tube and shell side temperatures is greater than 5 K. These are isolated cases observed on exchangers where the shell side flow rate is 1.5 times higher than that of the tube side, but this error decreases when more data is included in the estimation problem.

The evolution of the optimal parameters of the lumped model is analysed to demonstrate the differences between the two models considered, and how the lumped parameter model adapts to the "observations" of the distributed one. Figure 4.9 shows the fouling parameters and deposit roughness of the two models. The parameters estimated for the lumped model more closely approach those of the distributed model as the estimation horizon increases. In cases of a short estimation horizon, the model parameters, specifically the deposition constant and the deposit roughness, reach their upper bound, hence the predictions obtained with those models exhibit a large error, as observed in Figure 4.8. The estimation horizon and the data available must be sufficient to capture the fouling dynamics and the main interactions of the system for the prediction error to be acceptable.

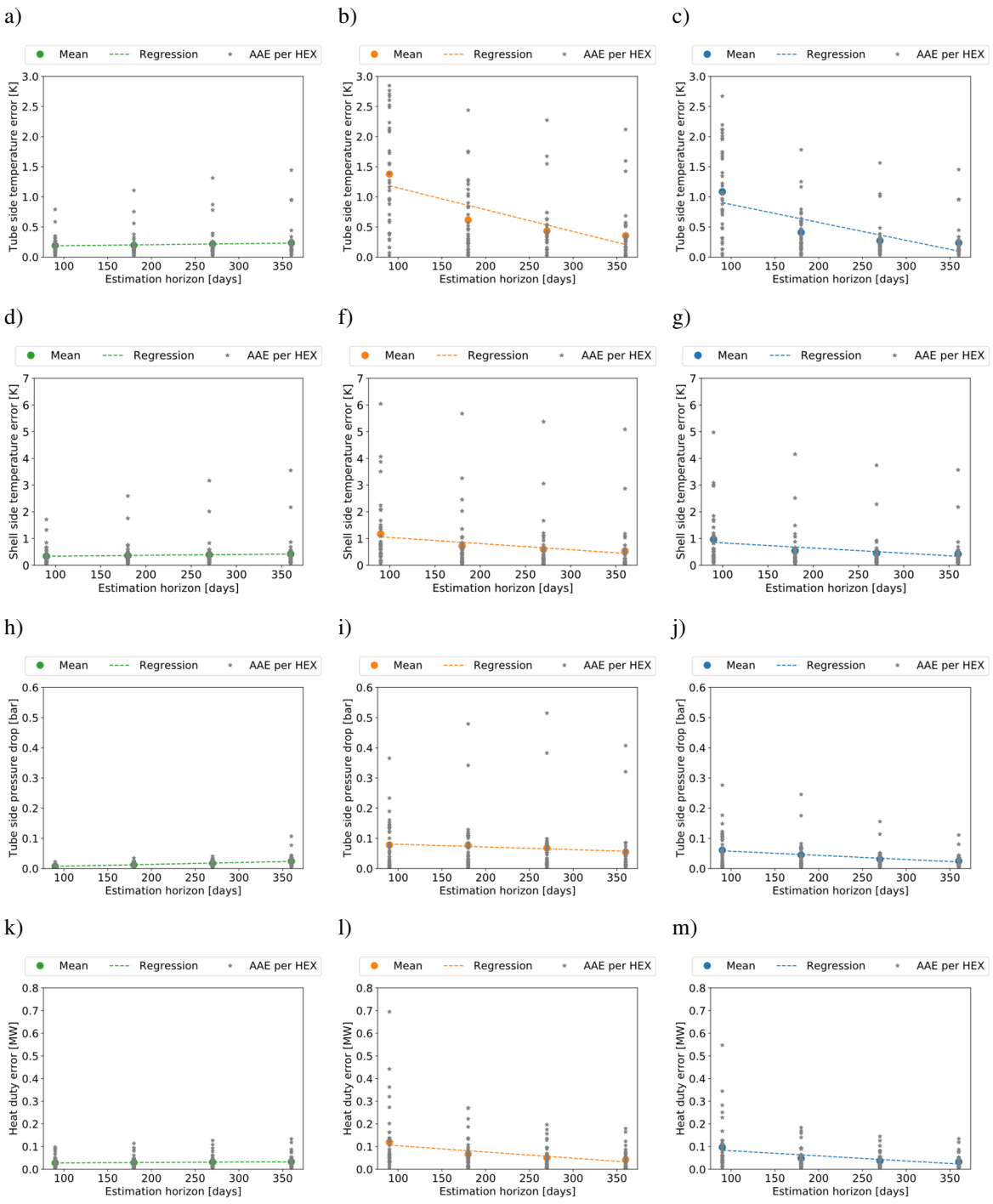

Figure 4.8. AAE evaluated within the estimation horizon (column 1), the prediction horizon (column 2), and the overall operation (column 3) as a function of the estimation horizon for the tube side temperature (row 1), the shell side temperature (row 2), the pressure drop (row 3), and the heat duty (row 4).

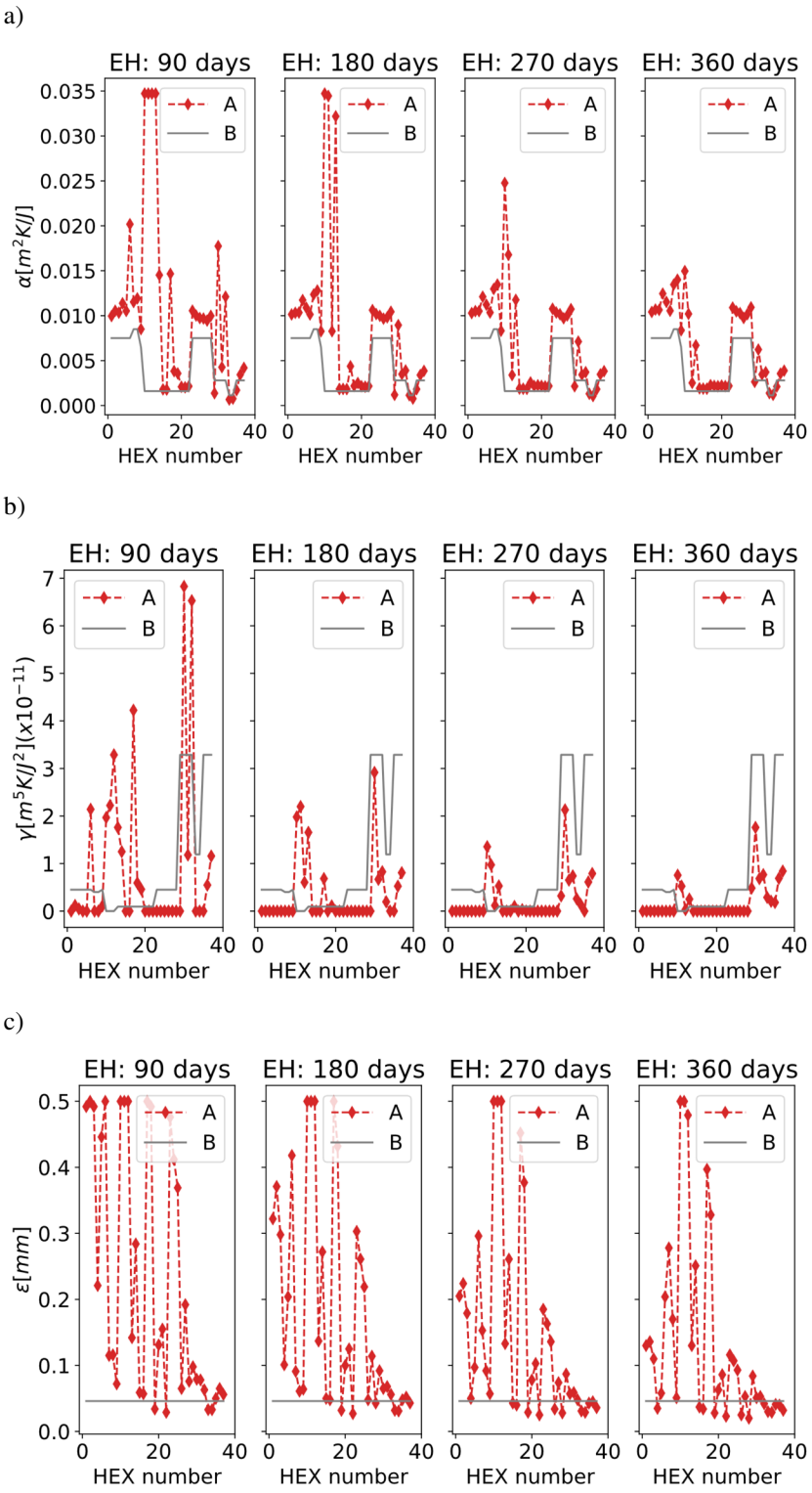

Figure 4.9. Optimal parameters estimated for the lumped model (A) based on the observations of the distributed model (B) as a function of the estimation horizon (EH). a) deposition constant, b) removal constant, c) deposit roughness.

Despite the trend observed, the optimal fouling parameters of the lumped model do not have to be the same as those of the distributed one because the models are based on different assumptions. Given the noted model mismatch, there is no guarantee that, or indeed reason why, the fouling parameters should converge. In addition, the parameters estimated for the lumped model consider all the interactions in a large HEN so that it can predict better the overall effects observed in the system, unlike the estimation procedure of individual exchangers followed for the distributed model. Considering the inherent differences between the models, it is noted that they achieve equivalent prediction accuracy in the key performance of individual heat exchangers and that of the network if their fouling parameter are different. However, the parameters estimated for the lumped model are correlated. The correlation coefficient between the deposition constant and the removal constant is 0.45 considering all exchangers. This hinders to make a distinction between the effect of the two phenomena, deposition and removal, although the same difficulty is observed in the estimation of the distributed model parameters because it is inherent to the structure of the Ebert-Panchal model used to represent the deposition rates.

The cross validation performed varying the estimation horizon to compare the two models – lumped (A) and distributed (B) – demonstrates that they can predict the same performance of individual units and that of network, but their parameters must be different to do so. The cross validation of the lumped model also allows to define the frequency with which the predictive model should be updated if used in an online application that involves continuous sampling to support or automate decision making. Shorter estimation horizons have larger prediction errors, but that can be compensated with more frequent updates of the lumped model.

4.5. Model validation using real plant data

Plant measurements were available for the case study "REF-X" for an operation period of 3.5 years. For each exchanger, not for each shell, the inlet flow rates, and temperature of the tube and shell sides were measured and reported as a daily average value. In total, there are 5 flow indicators and 17 temperature indicators in this network.

The data set is filtered to eliminate abnormal observations, and a time series approach is used to estimate missing measurements. Abnormal operating points are usually observed

during cleaning periods when data is collected but are not meaningful as the unit is not operating. They are easily identified as large unrealistic deviations from nominal conditions. The Hodrick-Prescott filter is used with a smoothing parameter of 1300 (Hodrick and Prescott 1981; Ravn and Uhlig 2002). This approach divides the time series in a trend and a cycle component and allows to estimate the error between the smooth approximation and the actual data. Using this, data that is outside the 95% confidence interval is discarded. As an example, Figure 4.10 shows the application of this approach to identify outliers and estimate missing data for the volumetric flow rate of E01A/B. It shows the actual data, the confidence intervals predicted by the smoothing approach, and the outliers identified. In addition, Figure 4.11 analyses the residuals of the time series estimation proving that they are normally distributed and identifying the points with large errors. This filtering approach is used for all the measured variables in the network.

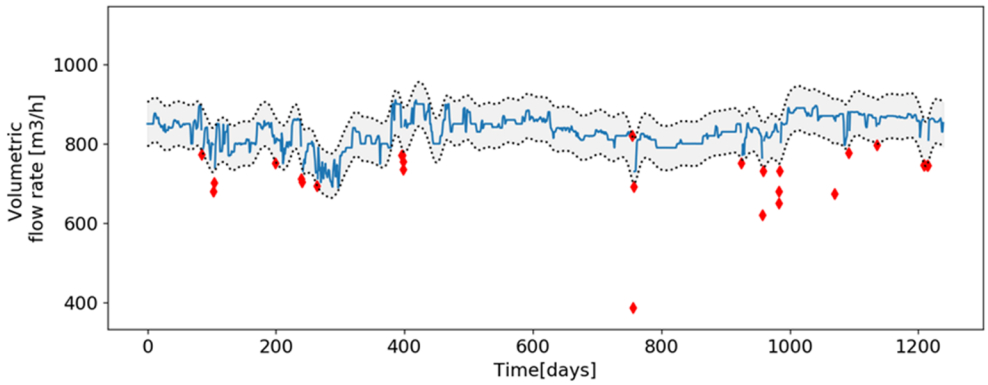

Figure 4.10. Volumetric flow rate measure, time series approximation, and outlier identification for E01 in case “REF-X”. (95% confidence interval: dash line, ♦ outliers).

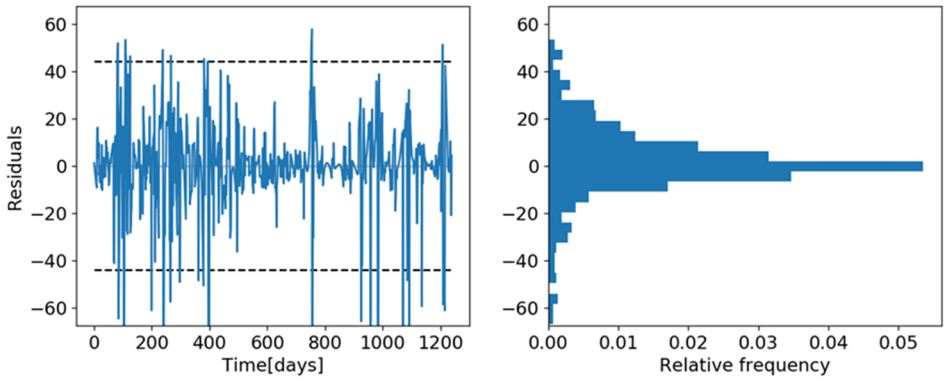

Figure 4.11. Residuals plot (left) and distribution (right) for the volumetric flow rate of E01 in case “REF-X”.

The filtering procedure for the measurements proposed by Coletti (2010) is followed to identify outliers in correlated variables. It is based on calculating the exchanger duty using the tube side, and shell side measurements, then computing their difference and identifying outliers that lay beyond a predefined tolerance ($0 \leq |Q^S - Q^T| \leq \varepsilon^{UB}$). Figure 4.12 shows the absolute error calculated for the heat duty of exchanger E04 of the case "REF-X" and the tolerance defined to identify outliers. The negative values observed are because of missing data and they are out of the acceptable range. All positive values beyond the tolerance are outliers because of extreme or unrealistic operating conditions observed. Using this method, when an outlier is discarded all the measurements at that time point for that exchanger are discarded. Finally, the difference in the calculated heat duties – the one for the tube side and that for the shell side – is not zero indicating a systematic error that may arise from the physical properties specifications or heat losses that are not considered.

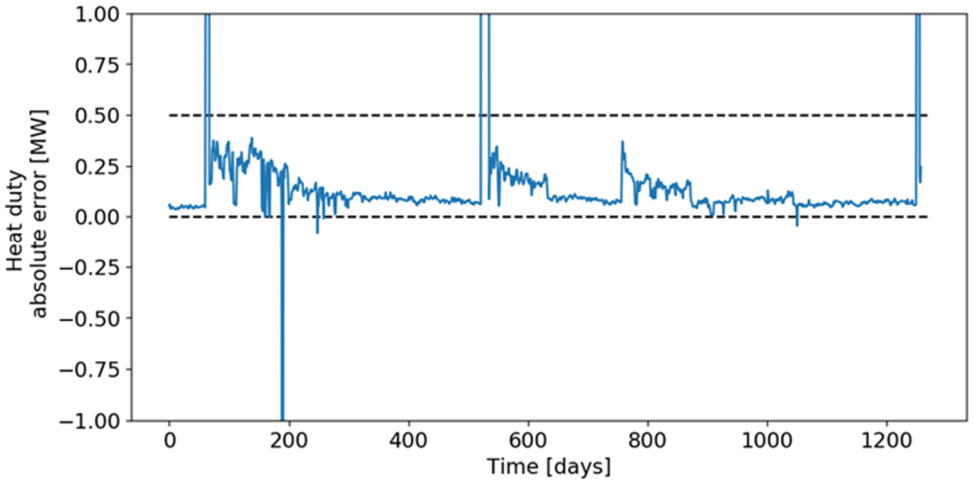

Figure 4.12. Absolute error in the heat duty calculation based on the tube and shell side for exchanger E04 of case "REF-X".

The outliers identified using the Hodrick-Prescott method, and the method based on the duty calculations correspond to 1.64% of the flow measurements of the tube side, 1.46% of the flow measurements of the shell side, 2.14% of the tube side temperatures, and 1.98% of the shell side temperatures. The points discarded are negligible as the total data set has 1240 time measurements, and 22 variables measured (27280 data points).

The parameter estimation problem is solved for the distributed model, and for the lumped model using the direct and indirect approaches described in Section 4.3, Figure 4.2.

The data set in all cases is composed by the measurements between 250 and 450 days of operation when no cleanings were performed. Table 4.2 summarizes the results of the optimal fouling parameters that best fit the measurements for each of the fitting approaches using the different models. While the parameters of the distributed model (B) are estimated individually for each exchanger, those of the lumped model (A) – regardless of the approach – are estimated simultaneous for the whole network. There is good agreement among the models with respect to the order of magnitude and variability of the fouling parameters from one exchanger to another. In the direct estimation approach, an additional constraint is included to make the parameters of all the shells in an exchanger equal because of the lack of intermediate measurements. On the other hand, in the indirect approach, where all the measurements are available from using the distributed model as soft sensor, no additional constraint is needed. The fewer constraints of the indirect approach give it more flexibility and the potential to better explain the variance observed in the data.

Table 4.2. Summary of optimal fouling parameter estimated with each modelling approach for the case "REF-X" based on plant data

	$\alpha[m^2 K/Wday]$			$\gamma[m^4 K/NWday]$		
HEX	**Distributed (B)**	**Lumped (A) - Direct**	**Lumped (A) - Indirect**	**Distributed (B)**	**Lumped (A) - Direct**	**Lumped (A) - Indirect**
E01A	241.66	290.24	227.80	$2.84\text{x}10^{-6}$	$8.07\text{x}10^{-7}$	$4.18\text{x}10^{-7}$
E01B	241.66	290.24	538.23	$2.84\text{x}10^{-6}$	$8.07\text{x}10^{-7}$	$1.52\text{x}10^{-6}$
E02A	241.66	209.15	298.90	$2.84\text{x}10^{-6}$	$4.56\text{x}10^{-7}$	$5.91\text{x}10^{-7}$
E02B	241.66	209.15	320.80	$2.84\text{x}10^{-6}$	$4.56\text{x}10^{-7}$	$6.62\text{x}10^{-7}$
E03A	98.44	60.07	119.58	$1.03\text{x}10^{-6}$	$1.00\text{x}10^{-10}$	$2.49\text{x}10^{-7}$
E03B	98.44	60.07	103.54	$1.03\text{x}10^{-6}$	$1.00\text{x}10^{-10}$	$1.79\text{x}10^{-7}$
E04	241.66	280.75	182.46	$2.84\text{x}10^{-6}$	$1.00\text{x}10^{-10}$	$1.57\text{x}10^{-7}$
E05A	241.66	294.23	306.92	$2.84\text{x}10^{-6}$	$1.05\text{x}10^{-6}$	$5.95\text{x}10^{-7}$
E05B	241.66	294.23	335.33	$2.84\text{x}10^{-6}$	$1.05\text{x}10^{-6}$	$7.27\text{x}10^{-7}$

The prediction capabilities of each model are compared within a time horizon of 90 days of operation immediately following the estimation period. These data were not included in the parameter estimation problem. The initial exchanger conditions – initial deposit thickness – are estimated using the respective model from the previous operating period, and inlet conditions of the network are taken from the measurements available. Figure 4.13 shows the prediction of the outlet temperatures of E05 for each of the modelling approaches and compares them against the actual observations. All models capture the observed trend, the dynamic variability, and the effect of the input variables on the key performance variables.

The tube side temperature is overestimated, and the shell side temperature underestimated by the lumped model using the direct approach, but when the indirect approach is used, the error with respect to the measurement decreases significantly. Using the indirect approach to estimate the fouling parameters of the lumped model, there is no significant difference between its predictions and those of the distributed model, although for both some mismatch is observed with respect to the plant measurements.

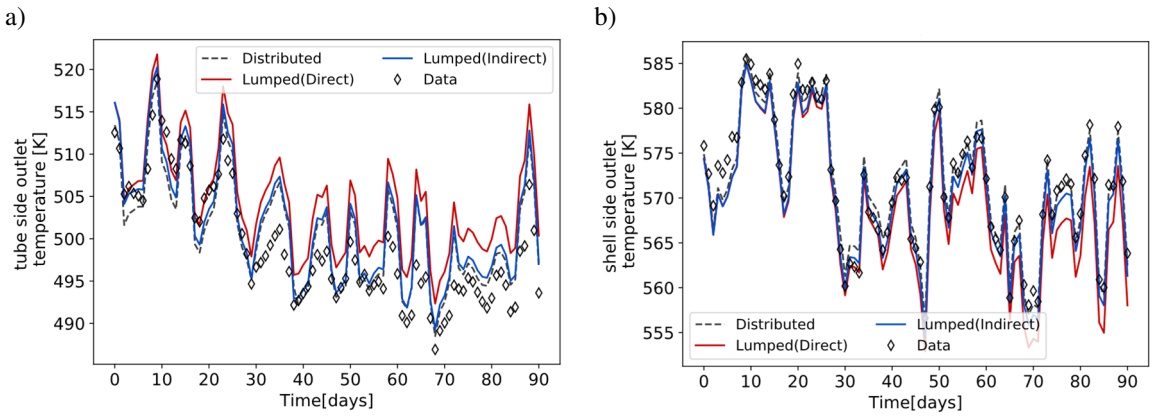

Figure 4.13. "REF-X" case, E05 tube side outlet temperature (a), and shell side outlet temperature (b) predicted with each modelling approach.

The prediction errors on the tube side and shell side outlet temperatures are calculated for all the exchangers in the network and for all the data points – a time horizon of 1240 days. The distributions of these errors are presented in Figure 4.14, the mean and standard deviation are also presented in the figure as the parameters of a normal distribution, $N(\mu, \sigma)$. For all the models the distribution of the errors follows an approximately normal distribution with mean close to zero. The variance of the errors can be large, up to 10 K in some cases, mainly caused by the uncertainty on the initial conditions of the network, and the quality and variability of the data available. Based on these frequency distributions it is not possible to affirm that there is as statistical difference among the prediction accuracy of the thermal performance achieved with the various models. However, there is a significant improvement in the prediction accuracy when the indirect approach is used to determine the fouling parameters of the lumped model with respect to the direct approach. The average prediction error of the tube side temperature achieved with the lumped model is reduced from 3.2 K to 0.8 K using the indirect approach. The shell side temperature average prediction error is also reduced from 1.5 K to 1.3 K, although the variance increases for this variable. These

improvements in the prediction of the thermal performance demonstrate the advantages of using the distributed model as a soft sensor to estimate missing measurements, and then use those in the parameter estimation problem of the lumped model to have a better understanding of the system. Among the three modelling approaches, the distributed model is the one that in average predicts better the outlet streams temperature of the exchangers – average error closer to zero.

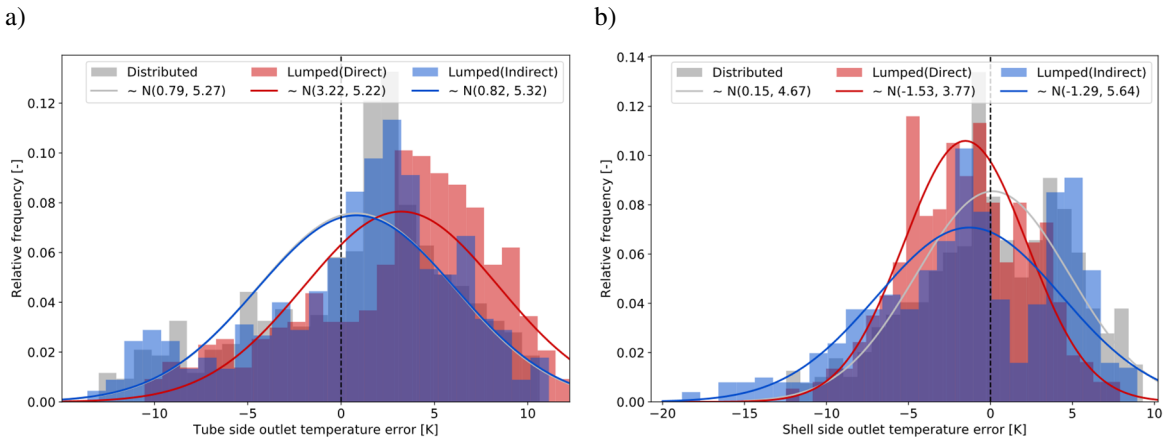

Figure 4.14. Distribution of the prediction error for the tube side outlet temperature (a) and the shell side temperature (b) using three modelling approaches for the case "REF-X".

Finally, the hydraulic performance predicted by the lumped model (A) is validated against of that predicted by the distributed model (B). It is not possible to perform a direct validation against plant data because pressure measurements were not available. Figure 4.15 shows the distribution of the pressure drop errors calculated between the lumped and the distributed models for all heat exchangers in the case study. The parameters of the lumped model have been determined using the direct and indirect approaches – see Figure 4.2. The mean and standard deviation of the errors are presented in the figure as parameters of a normal distribution. It is observed that the predictions of the lumped model improve significantly when the indirect estimation approach is used instead of the direct one – the variability in the distribution of the errors decreases while the average error is close to zero in both cases. In the indirect approach, the deposit roughness, and all other fouling parameters of the exchangers, are estimated using the soft measured pressure drop and intermediate temperatures predicted by the distributed model (B). This allows to achieve better predictions with the lumped model (A). On the other hand, in the direct approach there are no pressure

measurements available to estimate the deposit roughness, and this parameter is assumed to be fixed and constant for all exchangers at the same value used in the distributed model. These results also show that the parameters used locally in the distributed model do not necessary match those of the lumped model that can best explain the variability in the data. Therefore, the lumped model can accurate predict the dynamic performance of HEN under fouling when this estimation procedure is followed.

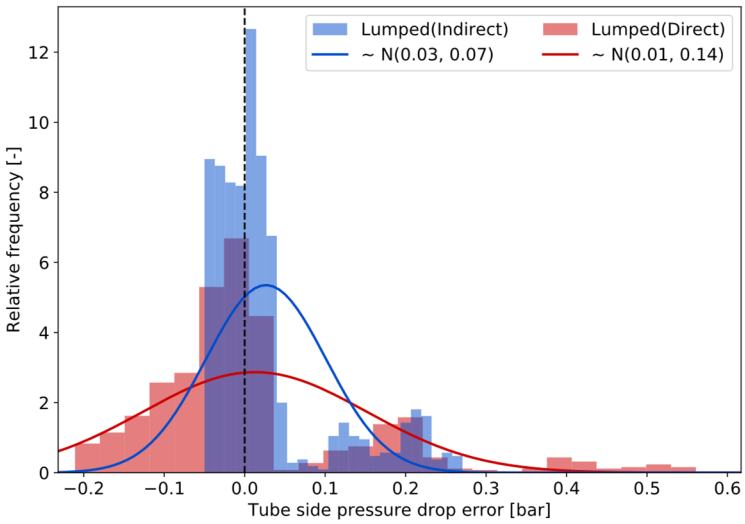

Figure 4.15. Distribution of the prediction error for the tube side pressure drop using two estimation approaches for the lumped model parameters for the case “REF-X”.

4.6. Concluding remarks

The axially lumped, radially distributed model for HEN under fouling developed in Chapter 3 was demonstrated to be valid in a wide range of scenarios, and operating conditions. The model has been validated in two ways. The first, by comparing its prediction capabilities against those of a benchmark previously validated model – a 2D axially and radially distributed model for the heat exchangers. The second, by the ability of the model to predict actual field data observed in a preheat train. Under both circumstances, the model developed has been proven sufficiently accurate and reliable to explain the system dynamics, fouling behaviour, and the effect of the operating variables on the performance of individual heat exchangers and of the whole network.

A parameter estimation approach was used to determine the optimal fouling parameters of the lumped model based on the prediction of the distributed model. This procedure allowed

to achieve comparable prediction accuracy of the key performance variables between the two models, hence the models are interchangeable. However, at clean conditions the lumped model underestimates the tube side pressure drop and overestimates the outlet shell side temperature, and those errors cannot be corrected by a better estimation of the fouling parameters. A PLS analysis is performed and the baffle spacing, baffle cut, and shell diameter are identified as the main features that explain the base error on the shell side temperature. The number of tubes and tube length are identified as the features that explain the pressure drop error. Hence, the PLS model developed can be used to estimate the prediction errors and differences between the lumped and distributed models a-priori – without performing any simulation – using only the heat exchanger specifications and operating conditions. This procedure helps to identify which model is best suitable to accurately describe the performance of a given unit.

A methodology has been developed to estimate the fouling parameters of the lumped model. It exploits the advantages of the two modelling approaches considered here – lumped and distributed models for heat exchangers – using the fitted benchmark model as a soft sensor to estimate missing or unmeasured data. This indirect estimation procedure reduces the average prediction error on tube side temperature from 3.2 K to 0.8 K, and that on shell side temperature from 1.5 K to 1.3 K. It also improves the predictions of the hydraulic performance of the network by narrowing the variability of the errors.

Additional measurements can be helpful to further validate the model developed under different realistic operating conditions, and pressure measurements are valuable to improve the prediction capabilities of any of the models. The validated lumped model for HEN under fouling has the potential to be used within optimization algorithms to determine operation policies, cleaning schedules, and retrofit alternatives without the burden of a huge computational load. In addition, the model parameters can be updated in real time for online applications that support decision making in the operation and maintenance of large HEN.

Chapter 5

Optimizing preheat trains under fouling: solution strategy for large problems

The application of the formulation for optimizing HEN under fouling presented in Chapter 3 is limited by the complexity of the problem and the computational load required to find a solution. In this chapter, an efficient reformulation and solution strategy based on complementarity constraints is presented. It relaxes the integer variables transforming the MINLP problem into an NLP, but it introduces additional constraints so that the relaxed problem converges to the solution of the original formulation. It is demonstrated that the proposed strategy solves the cases presented in Chapter 3 much faster, reducing the computational time by 99%. This allows to address industrial-size problems with many more units and long operating periods in feasible computational times. Finally, the optimal cleaning scheduling and dynamic flow distribution solution achieved with this strategy are validated by implementing them in *Hexxcell Studio*^{TM} for an industrial preheat train. The optimal solution reduces significantly the operating cost ($ 4.3 MM savings) compared to the actual operation of the refinery despite the differences between the models used for optimization and validation.

5.1. Introduction

Solving the simultaneous optimal cleaning scheduling and flow distribution problem for HEN under fouling is a challenging problem. This problem is formulated as a large scale MINLP after discretizing the differential equations – the model developed in Chapter 3 of this thesis. Its main complicating factors are: the nonlinearities and nonconvexities of the expressions, the various time scales involved, and its combinatorial nature because of many discrete decision variables. Nevertheless, the model developed was proven and validated –

Chapter 4 – to be accurate and predictive for the dynamic behaviour of HEN and their main key performance variables.

The integrated optimal cleaning scheduling and flow distribution problem was solved for small case studies involving all important features of large networks, but these cases are still not representative for real industrial applications. In some of the cases analysed in Chapter 3, increasing the number of periods in the time horizon increased the number of feasible schedule combinations such that the problem could not be solved to optimality in a reasonable time. Efficient algorithms for solving this problem are required.

In this chapter, an efficient solution algorithm is presented for the optimization problem formulated in Chapter 3. The first part of the chapter introduces a reformulation of the optimal cleaning scheduling and control problem, and then it presents the mathematical background and assumptions of the solution algorithm. The computational advantages and capabilities of the new solution strategy are demonstrated solving previous case studies and new challenging real industrial problems.

5.2. Problem reformulation with complementarity constraints

The optimal cleaning scheduling and control problem of HEN under fouling is formulated as a MINLP in Eq. (3.54) and in a more general way in can be defined as in Eq. (5.1), where x are the continuous variables, and y the binary variables of the problem. This formulation assumes that the differential equations characterizing the dynamic behaviour of the system have been discretized using an appropriate approach, and that the time horizon is represented by a continuous time discretization. Usually, solution algorithms for MINLP problems treat continuous and discrete variables at different levels. For example, by relaxing and branching on the binary variables, or decomposition strategies segregating the variables in two different optimization subproblems solved iteratively. In those approaches relaxed optimization problems are solved sequentially, and the number of those problems increases with the number of permutations of the binary variables making the computational time prohibitively large rapidly. Avoiding consecutive solutions of subproblems to solve the original MINLP formulation and handling all variables at the same level will be advantageous to reduce the computational time.

$$\begin{aligned}
&\min_{x,y} F(x,y) \\
&s.t. \\
&h(x,y) = 0 \\
&g(x,y) \leq 0 \\
&x \in X \subseteq \mathbb{R}^n \\
&y \in Y = \{0,1\}^q
\end{aligned} \tag{5.1}$$

Complementarity constraints are nonlinear constraints that offer an alternative to model switches, discrete decisions, and any other exclusive 'OR' relationship between two variables. Hence, these constraints can model discrete decisions in an optimization problem that is formulated as an NLP, and that formulation is referred as mathematical problem with complementarity constraints, MPCC (Biegler 2010).

A complementarity constraint can be defined between two bounded variables, and it is represented in Eq. (5.2) assuming one of their bounds is zero. This constraint indicates that either one the inequalities is active at the optimal solution, so that one of the variables is at its bound while the other is free.

$$x_1 = 0, x_2 > 0 \; 'OR' \; x_1 > 0, x_2 = 0 \Rightarrow 0 \leq x_1 \perp x_2 \geq 0 \tag{5.2}$$

Complementarity constraints can be used to model binary decisions. The binary variables are relaxed and bounded within a [0,1] interval, and slack variables are introduced to the formulation. Two slack variables are required per binary variable, one to use as a complement for the true (1) value of the variables, and the other as a complement for the false (0) value of the variable. To ease convergence of the problem, those two slack variables are bounded and must be exclusive between each other. As the binary decisions can only take one of two states at the optimal solution, the slack variables associated follow the same principle (Powell et al. 2016; Ramos, Gómez, and Reneaume 2014). Eq. (5.3) presents the set of constraints necessary to model binary decisions. This set of constraints efficiently replace the binary variable $y \in \{0,1\}$, for its continuous relaxation $y \in [0,1]$ without losing its ability to model discrete events and true/false decisions.

$$\begin{aligned}
&0 \leq y \perp s^1 \geq 0 \\
&0 \leq (1-y) \perp s^0 \geq 0 \\
&0 \leq s^1, s^0 \leq 1 \\
&s^1 + s^0 = 1
\end{aligned} \tag{5.3}$$

The original MINLP problem, Eq. (3.54) or in short notation Eq. (5.1), is reformulated as an MPCC relaxing the binary variables and introducing complementarity constraints, Eq.

(5.4). At the optimal solution the MPCC reformulation satisfies all the constraints of the original problem and their solutions are equivalent. In this way, the principal complicating factors of solving the MINLP problem – mainly its combinatorial nature – are avoided, but new nonlinearities and nonconvexities are introduced in the resulting formulation.

A key difference between the two solution approaches is that standard MINLP solution strategies provide a lower and upper bound for the optimal solution at every major iteration allowing an early termination with a feasible solution, while the MPCC strategy does not and it solves the problem to a local optimum directly. In addition, MPCC problems are not well posed as they do not satisfy constraint qualification conditions for optimality. For instance, they do not satisfy the linear independency of the gradients of the active constraints at the optimal point – linear independency constraint qualification, LICQ – hence some of the constraints multipliers may be unbounded at the optimal solution (Biegler 2010).

$$
\begin{aligned}
&\min_{x,y} F(x,y) \\
&s.t. \\
&h(x,y) = 0 \\
&g(x,y) \leq 0 \\
&0 \leq y_i \perp s_i^1 \geq 0, \qquad i = 1,2,\dots,q \\
&0 \leq (1-y_i) \perp s_i^0 \geq 0, \qquad i = 1,2,\dots,q \\
&s_i^1 + s_i^0 = 1, \qquad i = 1,2,\dots,q \\
&x \in X \subseteq \mathbb{R}^n \\
&s^1, s^0 \in Y = [0,1]^q \\
&y \in Y = [0,1]^q
\end{aligned}
\tag{5.4}
$$

MPCC reformulations have been successfully used for solving dynamic optimization problems involving binary decisions such as the start-up of a batch distillation column (Raghunathan, Soledad Diaz, and Biegler 2004), the operation of a cryogenic distillation unit (Raghunathan, Soledad Diaz, and Biegler 2004), and the relief valve operation for safety considerations in a CSTR operation (Raghunathan and Biegler 2003). This motivates using the MPCC reformulation to solve the optimal cleaning scheduling and flow control problem of HEN for real time applications.

Under the MPCC reformulation, the way operational disjunctions, Eq. (3.30), are considered in the model can be different than using BigM constraints. Although BigM constraints were proven to work well for optimizing small networks, they introduce additional constraints and slack variables and may define a loose relaxation of the problem. While they were advantageous solving the optimal cleaning scheduling MINLP problem

because they only introduce linear constraints, in the MPCC reformulation this is not a significant advantage as important nonlinearities arise from the complementarity constraints. Hence, to reduce the size of the problem and to tighten its integer relaxation – important features when solving a MPCC formulation to avoid local minima or infeasible solutions – the operational disjunctions are formulated as the product of a binary variable and a nonlinear expression. The BigM constraints associated with the heat transfer of each exchanger under either idle or operating states are replaced by the nonlinear expression of Eq. (5.5). This nonlinear expression defines the two possible states of each unit regarding the heat transfer. In addition, the disjunctions associated with the differential equations, those describing fouling and ageing, are redefined as Eq. (5.6) assuming a continuous time representation, and Eq. (5.7) represents the continuity constraints for the variables between two periods. If a unit is idle for a given period, then the derivative of the variable is zero, and the initial condition of the next period is the clean state defined for the unit. All other disjunctions derived previously for the model are not modified, and the BigM formulation is used. Those are the bypass flow around the exchanger and the tube side pressure drop when the units are idle or operating.

$$U_{i,t} = \left(1 - y_{i,t}\right)\left[\frac{1}{h_{i,t}^{S}} + \frac{d_i}{2\lambda_i^{W}} Ln\left(\frac{d_i}{d_{I,i}}\right) + \frac{d_i}{d_{i,t}^{F}}\frac{1}{h_{i,t}^{T}} + R_{f,i,t}\right]^{-1}, \qquad \forall i \in HEX, t \in T \tag{5.5}$$

$$\frac{dx}{d\bar{t}}_{(i,p,t)} = \left(1 - y_{i,p}\right)\mathrm{T}_p\left(RHS_{(i,p,t)}\right), \qquad \forall i \in HEX, (p,t) \in \{(1,2), \dots, (N_p, N_c)\} | t > 1 \tag{5.6}$$

$$x_{i,p,1} = \left(1 - y_{i,t}\right)x_{i,p-1,N_c} + y_{i,p}x_{cl}, \qquad \forall i \in HEX, p \in \{1, \dots, N_p)\} | p > 1 \tag{5.7}$$

A new formulation for the optimal cleaning scheduling and flow distribution problem is obtained using the MPCC strategy and redefining the operating disjunctions. Solving the MPCC reformulation of the problem requires an explicit definition of the complementarity constraints, and a way to handle optimization problems that do not satisfy LICQ. These issues are discussed and addressed in the next section.

5.3. Solution strategy using MPCC

The complementarity between two variables can be defined by their product ($\varphi = x_1 x_2$), by the Fischer-Burmeister function $\left(\varphi = x_1 + x_2 - \sqrt{x_1^2 + x_2^2}\right)$, or by the Natural residual function $\left(2\varphi = x_1 + x_2 - \sqrt{(x_1 - x_2)^2}\right)$ (Herty and Steffensen 2012). First

and second derivatives exist for all these functions, although for the last two the first derivative is not defined when both variables are at their bound. The formulation as a bilinear product of variables is preferred because of its simplicity.

Introducing complementary constraints as equality constraints in the problem formulation, $\varphi = 0$, causes numerical issues for most of NLP solvers as it does not satisfy LICQ. Hence, these constraints are relaxed as inequality constraints by a parameter, ϵ, such that $\varphi \leq \epsilon$. This is a regularized reformulation of the MPCC problem and it is solved sequentially as $\epsilon \to 0$ (Biegler 2010; Fletcher and Leyffer Sven 2004). Note that this approach to handle complementarity constraints is similar to the strategy used in interior point optimization algorithms. Those algorithms use a barrier parameter to solve for the inequality constraints and their multipliers. The barrier parameter can be compared to the ϵ term used in the relaxation of the complementarities, or it can even substitute it and update it within the interior point solution algorithm. These features of the MPCC problem formulation make interior point algorithms, such as IPOPT (Wächter and Biegler 2006), perform well for solving large scale problems efficiently.

The complementarity constraints arising during the reformulation of the optimization problem of interest, Eq. (3.54), are defined as inequalities using the regularized ϵ strategy. The resulting MPCC problem is solved as a series of NLPs as ϵ is decreased from 1.0 to $1x10^{-6}$ using a logarithm sequence. Hence, to obtain the optimal solution, seven NLPs are solved sequentially, and the solution of the final one corresponds to the optimal solution of the original MINLP. For ease of convergence the optimal solution of each relaxed problem is used as initialization of the following one which has a tighter value of ϵ, so that the initial point is close to feasibility. However, for the initial instance of the sequence, $\epsilon = 1.0$, the initialization is defined accordingly to the procedure described in Appendix A for all case studies. Also, because of the initialization of the first NLP problem of the sequence is significantly different to the others, it is expected that this instance requires a longer computational time than the other

5.4. Applications of MPCC reformulation and advantages

A set of HEN, ranging from small ones to those of importance for industrial applications, are considered here to demonstrate the capabilities and advantages of the MPCC

reformulation strategy. First, the case studies used in Chapter 3 to demonstrate the capabilities of the model developed are revised and solved using the new solution strategy. Then, larger problems of industrial relevance, that cannot be solved with standard MINLP algorithms, are addressed to demonstrate the advantages of the proposed solution strategy and the benefits of integrating scheduling and control decisions for fouling mitigation. Finally, the optimal solution obtained for a real preheat train is validated with a more detailed model following a similar validation approach as that presented in Chapter 4.

5.4.1. Comparison with standard solution strategies

Three case studies used in Chapter 3 to demonstrate the capabilities of the model and the advantages of optimal fouling mitigation strategies are revised here. The cases are: 1HE, 2HE-S, and 2HE-B, whose networks are shown in Figure 5.1, and all their specifications and operation conditions are detailed in Appendix A. All cases are modelled under the same conditions as Chapter 3 using a continuous time representation. The optimal cleaning scheduling and flow distribution problem is solved with the MPCC reformulation for each, and the solution is compared against that obtained in Chapter 3. Both solution approaches use the same problem initialization – constant time profiles for all the variables – so that the local optimum found, and the computational effort can be directly compared.

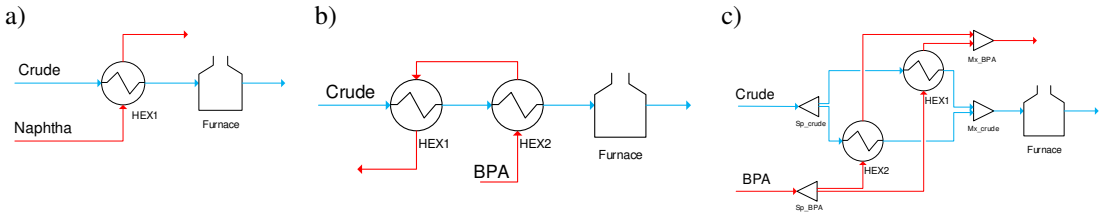

Figure 5.1. HEN representation of the case studies of this chapter. a) Case 1HE, b) Case 2HE-S, c) Case 2HE-B.

Table 5.1. Comparison of optimal solution for small case studies using two solution strategies: branch and bound, and problem reformulation with complementarity constraints.

Case	**1HE**		**2HE-S**				**2HE-B**			
Solution strategy*	**BB-CT**	**MPCC**	**BB-CT**	**BB-CT**	**MPCC**	**MPCC**	**BB-CT**	**BB-CT**	**MPCC**	**MPCC**
n_T [+]	10	10	9	13	9	13	9	13	9	13
Continuous variables	1407	1307	2362	3414	2182	3154	2794	4038	2614	3778
Binary variables	20	0	27	39	0	0	27	39	0	0
Equality constraints	1130	1100	1962	2834	1908	2756	2322	3354	2268	3276
Inequality constraints	2819	2599	4517	6525	4121	5953	5669	8189	5273	7617
CPU time [min] [**]	32.86	0.11	548.64	3000.00	0.29	0.55	374.38	3000.00	0.27	0.38
Total energy [MW-h]	$4.077x10^5$	$4.077x10^5$	$3.800x10^5$	$3.801x10^5$	$3.802x10^5$	$3.801x10^5$	$3.910x10^5$	$3.910x10^5$	$3.910x10^5$	$3.910x10^5$
Production profit [$]	$6.617x10^8$	$6.617x10^8$	$6.617x10^8$	$6.617x10^8$	$6.617x10^8$	$6.617x10^8$	$6.617x10^8$	$6.617x10^8$	$6.617x10^8$	$6.617x10^8$
Fuel cost [$]	$1.101x10^7$	$1.101x10^7$	$1.026x10^7$	$1.026x10^7$	$1.026x10^7$	$1.026x10^7$	$1.056x10^7$	$1.056x10^7$	$1.056x10^7$	$1.056x10^7$
Carbon cost [$]	$1.859x10^6$	$1.859x10^6$	$1.733x10^5$	$1.733x10^5$	$1.734x10^5$	$1.733x10^5$	$1.783x10^5$	$1.783x10^5$	$1.783x10^5$	$1.783x10^5$
Cleaning cost [$]	30000	30000	90000	90000	90000	90000	90000	90000	90000	90000
Total cost [$]	$1.290x10^7$	$1.290x10^7$	$1.052x10^7$	$1.052x10^7$	$1.052x10^7$	$1.052x10^7$	$1.083x10^7$	$1.083x10^7$	$1.083x10^7$	$1.083x10^7$
Cleaning schedule (HEX#, time [days]) [x]	(1, 180)	(1, 180)	(2, 115) (1, 182) (2, 250)	(2, 114) (1, 182) (2, 250)	(2, 82) (1, 174) (2, 237)	(2, 114) (1, 181) (2, 248)	(1, 88) (2, 180) (1, 278)	(1, 80) (2, 172) (1, 261)	(1, 80) (2, 172) (1, 263)	(1, 80) (2, 172) (1, 262)
Lower bound (cost)	$1.122x10^7$	-	$1.052x10^7$	$1.039x10^7$	-	-	$1.083x10^7$	$1.074x10^7$	-	-
Upper bound (cost)	$1.122x10^7$	-	$1.052x10^7$	$1.052x10^7$	-	-	$1.083x10^7$	$1.083x10^7$	-	-
Optimality gap [%]	0.00	-	0.00	1.29	-	-	0.00	0.83	-	-

* BB-CT: branch and bound algorithm using a continuous time formulation, MPCC: reformulation with complementarity constraints

** For the MPCC approach, it represents the total computational time of all sequential solutions of the problem as $\epsilon \to 0$

[+] Number periods used to discretize time with a continues time representation

[x] Cleaning time rounded to the closest integer value for the continues time approach

Table 5.1 presents a detailed comparison of the problem size, computational load, optimal operating cost, and optimal cleaning schedule for each case study using two solution strategies: branch and bound for the MINLP formulation of the problem, and sequential regularized ϵ approach for the MPCC reformulation. There are differences between the two formulations in terms of problem size and nature of the variables involved, the local optimum found, and the computational load necessary to solve it. From an overall perspective, the MPCC reformulation and solution strategy performs better than or as well as the MINLP approach.

In terms of problem size, the MPCC reformulation has fewer variables and constraints than the MINLP formulation using the same number of periods in the time horizon. The reformulation reduces the number of variables and constraints by ~7% which is an improvement, but, given the large scale of the problem, this is not a main advantage in reducing computational time. The main advantage of the MPCC reformulation is that it does not use binary variables to model the states of the units. For all the problems solved to optimality – optimality gap of 0% – the computational time required to find an optimal solution decreases by 99% using the MPCC reformulation instead of the MINLP formulation. The computational time reported for the MPCC is the total time required to solve the sequence of NLP problems, which in this case corresponds to seven instances decreasing the value ofϵ. It was observed that the solution time of the first instance in the sequence of NLPs may represent up to 40% of the total time of the MPCC reformulation because of the initialization – all other instances uses a better initialization which the optimal solution of the previous one. The reduction in the computational time, enables to solve much larger and challenging problems in reasonable times. For instance, the previous formulation of the optimal cleaning scheduling problem of cases 2HE-S and 2HE-B with 13 periods in the time horizon could not be solved to optimality using the branch and bound algorithm in 3000 min of computation, but with the proposed reformulation they are solved in less than 1 min. In this sense, solving the optimal cleaning scheduling and flow distribution problem for large HEN operating over long horizon is feasible using the proposed MPCC reformulation.

The optimal solutions found using the MINLP and MPCC formulations are equivalent. Both solutions achieved the same economic benefits, as the difference in operating costs is not significant, although the optimal cleaning schedule may be different. For the cases with

two exchangers in the network, the optimal cleaning schedule changes with respect to the number of periods used in the time horizon, and with respect to the formulation of the problem, though only the starting time of the cleanings changes while the allocation of the cleanings is the same. These differences can be attributed to: i) the accuracy of the integration that changes with the number of periods, ii) the different representation of the operation disjunctions used in the MINLP and MPCC formulations, and iii) the existence of multiple local optima with the same or similar objective function values. The latter indicates that the timing of the cleaning is not as important as their allocation and sequence. If the cleaning time changes for a given cleaning schedule and within reasonable bounds – for instance, case 2HE-S solved with the MPCC formulation for two time discretization – its effect on the overall cost of the operation can be negligible. In addition, the existence of multiple optimal solutions to the problem, and the low sensitivity of the objective function to the cleaning times hinders closing the optimality gap when standard MINLP solution approaches are used.

The MPCC reformulation has proven to be efficient and precise. The capabilities and advantages of this approach are evaluated with realistic case studies in the following section.

5.4.2. Solving industrial size case studies

The optimal cleaning scheduling and control problem is solved for the following case studies: LN-S1, LN-B1, and REF-X. The structure of the networks is shown in Figure 5.2, and all the operating conditions and specifications of exchangers are presented in Appendix A. All networks correspond to the hot end of preheat trains, so they operate at high temperatures and fouling rates are the highest in the system. The first network has all units in a series configuration and some of them interact through a hot stream in a counter flow configuration. The second network has parallel branches so that control elements – flow split between the branches – are additional degrees of freedom, and the flow distribution in the network can be dynamically adapted with respect to the cleanings. These two cases represent the most common configurations found in refining applications, and all others can be derived from combinations of the two, adding more units or flow splits. The final network is taken from the same real industrial application used in Chapter 4, for which measurements and the fouling mitigation actions taken by the refinery are known. The actual operation of the REF-X case is used to demonstrate the benefits of the optimization approach using a MPCC reformulation with respect to heuristic approaches used in industry.

The large number of units and periods needed to discretize the time horizon – using a continuous time approach – introduce many binary decisions (> 100 for each case). The optimization problems become computationally prohibitive to address with MINLP algorithms, thereby the MPCC reformulation and solution strategy are advantageous.

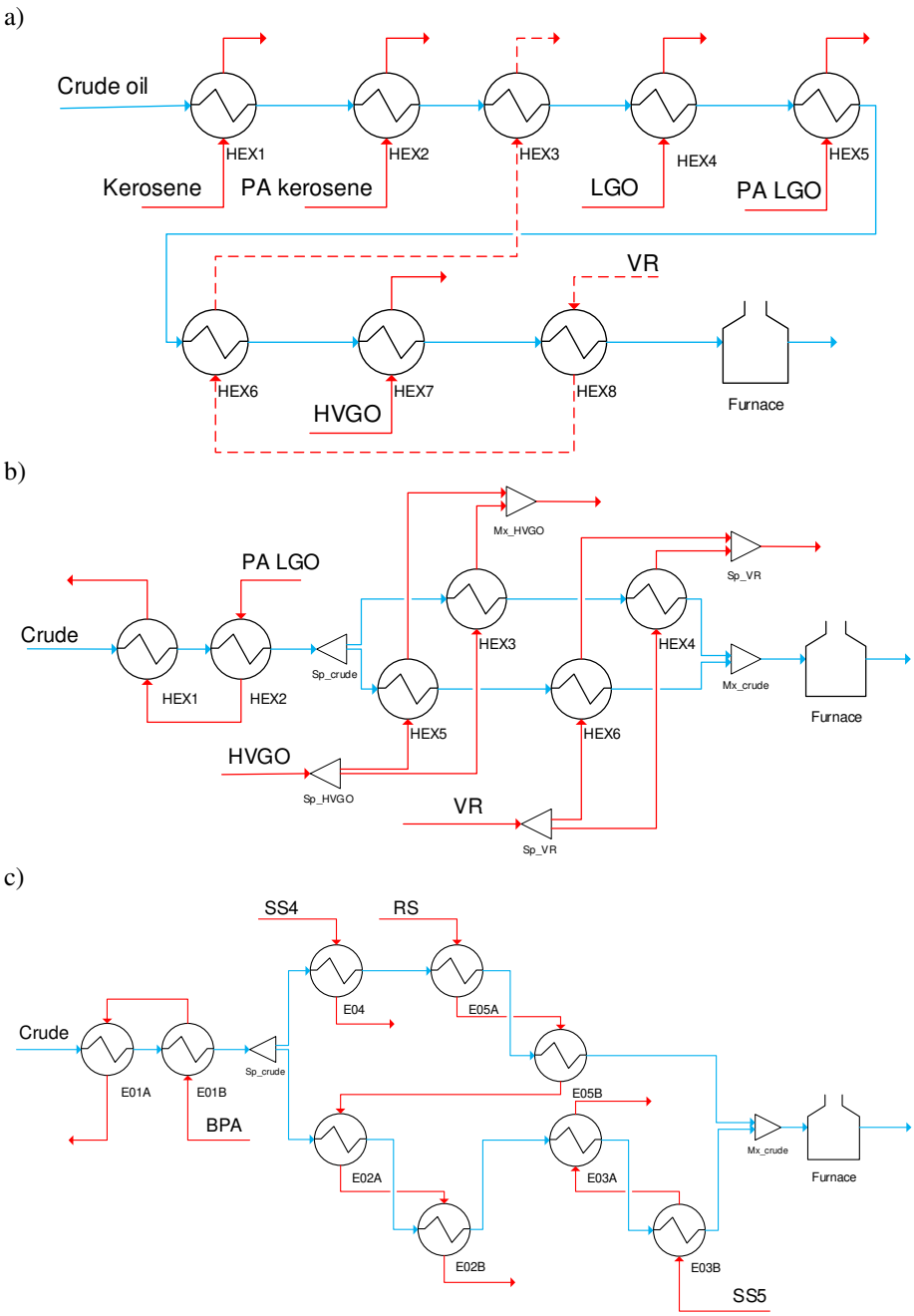

Figure 5.2. HEN representation of the case studies of this chapter. a) Case LN-S1, b) Case LN-B1, c) Case REF-X.

The optimization problem for the case LN-S1 is solved by discretising the time horizon with 20 periods of variable length, and an optimal solution is found in 21.8 min of CPU time using the MPCC reformulation. The optimal cleaning schedule for this case has 10 cleanings over a year of operation, and it is displayed in Figure 5.3a. HEX5 – HEX8 are cleaned twice, HEX3 and HEX4 once, and HEX1 and HEX2 are never cleaned. The optimal solution does not have cleanings at the beginning of the operation nor towards the end because the initial state of the network is clean, and cleanings do not have a positive economic trade off close to the end of the operation. Some exchangers are cleaned simultaneously – there is a constraint of maximum two simultaneous cleanings – which is a good compromise between the operating time with fewer units, hence higher energy consumption, and the heat recovery capacity after cleanings.

Figure 5.3b shows the furnace duty for the case LN-S1. The effect of the cleanings is observed as a peak increase in the duty for the duration of the cleaning, followed by a significant decrease when the unit is back in operation. The energy consumption of the optimal cleaning scheduling solution is lower than that of a no mitigation (NM) strategy, and it is observed in the furnace duty profiles. Despite the temporary increase in furnace duty during cleanings, the overall effect over the operating horizon is a reduction of energy consumption. This energy savings represents a cost reduction of $ 1.28 MM with respect to the alternative of no cleanings.

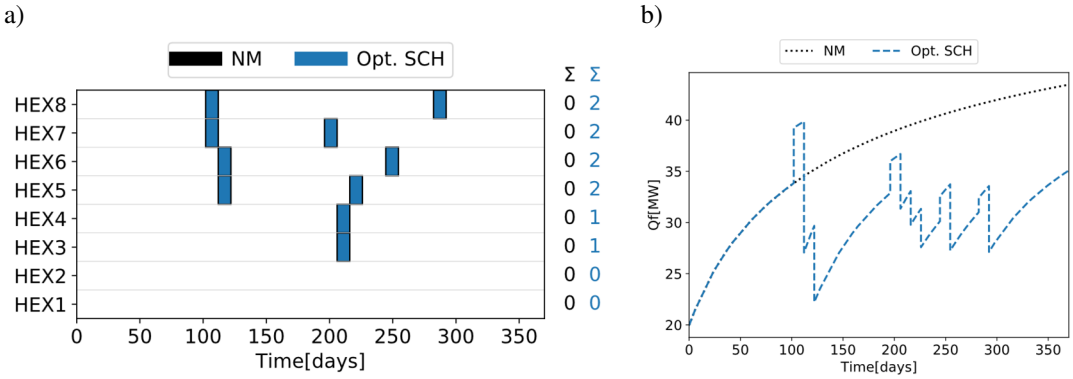

Figure 5.3. Optimal cleaning schedule (a) and furnace duty (b) for case LN-S1.

In the optimal cleaning schedule solution, the exchangers at the end of the network are cleaned more times than those at the beginning because the high temperatures of the crude at those locations promote chemical fouling. Other factors affecting the cleaning sequence are the heat duty of the units at cleaned conditions, and the interaction among the units through

the hot streams. Figure 5.4 shows the fouling resistance and the heat duty for all the exchangers in the LN-S1 network when no cleanings are performed. Those exchangers that are never cleaned – HEX1 and HEX2 – have the lowest fouling resistance, and the lowest heat duty under clean conditions so cleanings are not attractive for those units. On the other hand, units with a large heat duty located at the end of the network loose performance faster than those at the beginning, and cleaning these units is profitable. The importance of the interaction of the units through the hot streams is observed in the heat duty of HEX3 and HEX6 as they reach a maximum, whereas their fouling resistance always increases. While the performance of HEX8 decreases, the outlet temperature of its shell side increases so that the temperature difference in the following exchangers interacting with this stream is larger. Because of this increase in the temperature difference in HEX3 and HEX6 their heat duties increase although their fouling resistances increase.

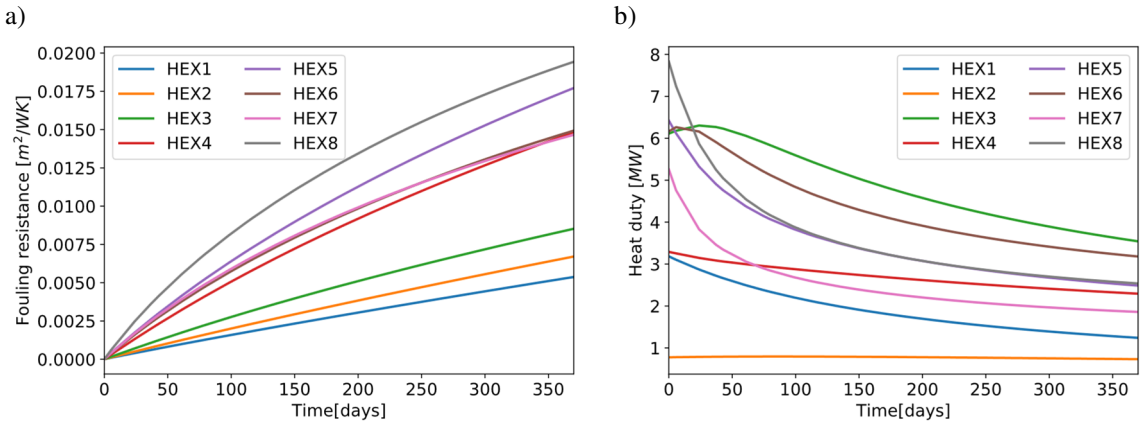

Figure 5.4. Fouling resistance (a) and heat duty (b) for exchangers of case LN-S1 when there are no cleanings.

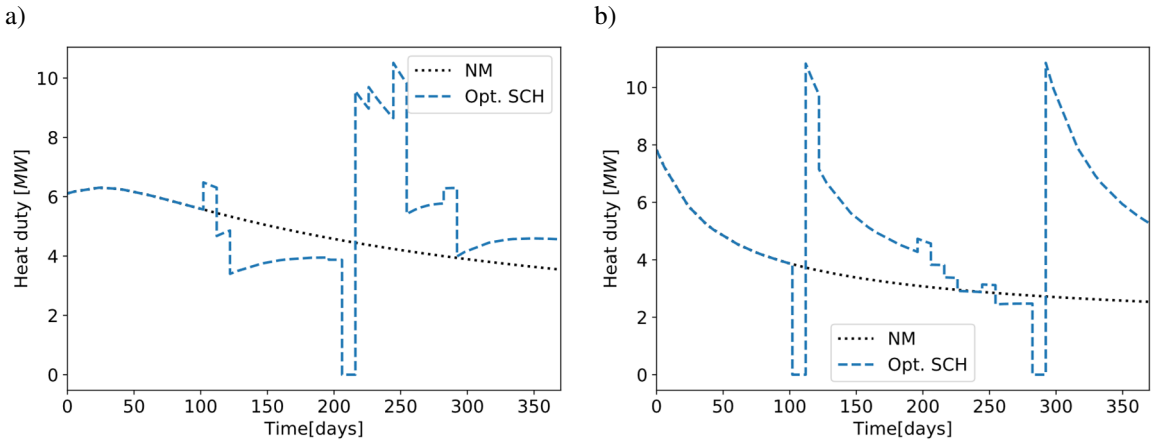

Figure 5.5. Heat duty of heat exchangers HEX3 (a) and HEX8 (b) for case LN-S1

The interaction among the units in a large HEN are still important when the cleanings are optimally defined. Figure 5.5 shows the heat duty of HEX3 and HEX8 of case LN-S1 for the no mitigation and optimal cleaning scheduling scenarios. HEX3 interacts with the hot stream coming from HEX6, and its heat duty exhibits a maximum, while HEX8 does not interact with other hot streams and its heat duty follows the expected decay and recovery behaviour after cleanings. The heat duty of HEX3 is also affected by the cleanings of exchangers that interact with the VR hot stream. For instance, when HEX8 and HEX6 are being cleaned the duty of HEX3 increases – around the first 100 days of operation – because its shell side inlet temperature increases, but after the cleanings of those units, the duty of HEX3 decreases to a value lower than that at which the unit was operating before the cleanings. While cleaning HEX8 or HEX6 allows to recover their thermal efficiency, it decreases that of HEX3, and similar interactions are observed among these three exchangers when another is cleaned. These are complex trade-offs when the units in the network are linked with different streams, but the modelling approach and optimization formulation allow to capture them and make optimal decisions to mitigation fouling and minimize cost.

Two scenarios for the case LN-B1 are considered: one where the tube side flow of the parallel branches is pressure driven (ΔP prefix), and other where it can be freely controlled (no prefix). In both scenarios, the flow distribution of HVGO and VR streams are control degrees of freedom and they can be dynamically modified to minimize the total operating cost. For each of these scenarios four operating modes are analysed – see Table 1.1 for notation and definitions. These are: i) no mitigation (NM), ii) optimal flow control (Sp), iii) optimal cleaning scheduling (SCH), and iv) simultaneous optimal control and scheduling (Sp + SCH). All the split fractions that are degrees of freedom are bounded between 20% and 80%. These operating modes serve to demonstrate the advantages of integrating optimal scheduling and control decisions for relevant industrial applications.

Table 5.2 shows the computational results and the total operating cost of all scenarios of case LN-B1. The pressure flow constrained scenarios require a longer computational time to solve because of the additional nonlinear constraint introduced, although this does not represent a limitation. All optimization problems defined, including those with many binary decisions, are solved in a reasonable computational time – less than 30 min of computation.

Table 5.2. Computational results and optimal solution for various operating modes of LN-B1 case study

Tube side flow*	**ΔP**				**Free**			
Operating mode	**(i) NM**	**(ii) Sp**	**(iii) SCH**	**(iv) Sp + SCH**	**(i) NM**	**(ii) Sp**	**(iii) SCH**	**(iv) Sp + SCH**
n_T [+]	20	20	25	25	20	20	25	25
Continuous variables	15459	15619	15567	15727	15219	15459	15327	15567
Binary variables	0	0	0	0	0	0	0	0
Equality constraints	13840	13840	13840	13840	13760	13760	13760	13760
Inequality constraints	29959	29959	29959	29959	29639	29639	29639	29639
CPU time [min] [**]	18.38	19.17	21.77	30.64	11.32	12.49	18.36	20.57
Total energy [MW-h]	$3.215\text{x}10^5$	$3.214\text{x}10^5$	$2.775\text{x}10^5$	$2.722\text{x}10^5$	$3.166\text{x}10^5$	$3.160\text{x}10^5$	$2.733\text{x}10^5$	$2.633\text{x}10^5$
Production profit [$]	$6.470\text{x}10^8$	$6.470\text{x}10^8$	$6.470\text{x}10^8$	$6.470\text{x}10^8$	$6.470\text{x}10^8$	$6.470\text{x}10^8$	$6.470\text{x}10^8$	$6.470\text{x}10^8$
Fuel cost [$]	$8.681\text{x}10^6$	$8.678\text{x}10^6$	$7.493\text{x}10^6$	$7.349\text{x}10^6$	$8.549\text{x}10^6$	$8.533\text{x}10^6$	$7.378\text{x}10^6$	$7.110\text{x}10^6$
Carbon cost [$]	$1.466\text{x}10^5$	$1.466\text{x}10^5$	$1.266\text{x}10^5$	$1.241\text{x}10^5$	$1.444\text{x}10^5$	$1.441\text{x}10^5$	$1.246\text{x}10^5$	$1.201\text{x}10^5$
Cleaning cost [$]	0	0	270000	300000	0	0	270000	300000
Total cost [$]	$8.827\text{x}10^6$	$8.825\text{x}10^6$	$7.890\text{x}10^6$	$7.773\text{x}10^6$	$8.694\text{x}10^6$	$8.677\text{x}10^6$	$7.773\text{x}10^6$	$7.530\text{x}10^6$

*ΔP: pressure driven tube side flow rate in parallel branches, Free: freely controlled tube side flow rate in parallel branches

** For scheduling problems, the MPCC approach is used, and it represents the total computational time of all sequential solutions

[+] Number periods used to discretize time with a continues time representation

In the LN-B1 case the optimal control strategies marginally reduce the total operating cost, while the optimal cleaning schedule, and the integrated optimal cleaning scheduling and control strategies results in significant savings – all relative to the NM operating mode. The savings achieved with only optimal control strategies are on the order of thousands of dollars, whereas those achieved with any strategy involving cleanings are in the order of millions of dollars. In addition, integrating optimal control and scheduling is the best alternative as the synergies between flow distribution and cleanings are exploited. The alternative of optimizing first the cleaning schedule, and then the flow distribution is not considered at this stage because it ignores important interactions, and it was previously demonstrated in Chapter 3 that it is not as effective as the simultaneous optimization approach. Finally, all the free flow scenarios have a lower operating cost than that of the flow constrained scenarios because of the additional degrees of freedom and the interaction of the flow rates with the cleanings.

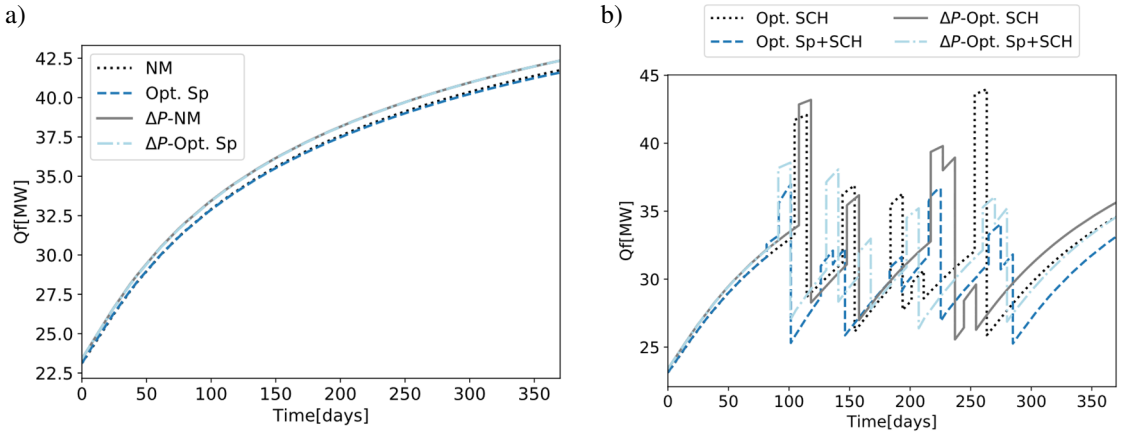

Figure 5.6. Furnace duty of case LN-B1 when the tube side flow is pressure driven or freely controlled. a) No mitigation and optimal control strategies, b) optimal cleaning scheduling and integrated strategies.

The differences between the scenarios where the tube side flow rate is pressure driven and where it can be freely controlled are observed in the furnace duty for each operating mode. Figure 5.6 shows the furnace duty for these two scenarios, and for all the operating modes. Dynamically distributing the tube side flow rate among the branches is advantageous and reduces the energy consumption because the branches in the network are not balanced, the exchangers on each branch have different sizes and operate at different conditions, so their fouling rates are different. For the cases with no cleanings, distributing the flows of the

hot streams – on the shell side – does not have a significant effect and only a marginal reduction in the furnace duty is observed. However, for the simultaneous optimization of the scheduling and control – flow rates of the hot and cold streams – the furnace duty decreases significantly during most of the operating time. Also, the optimal cleaning schedule changes when the flow is pressure driven or when it is freely controlled.

Figure 5.7 displays the optimal cleaning schedule with and without optimal flow distribution for the case LN-B1 when the flow is pressure driven, and when it is free. When the flow through the parallel branches is pressure driven and the hot streams split is fixed, exchangers on opposite branches are cleaned simultaneous so that the pressure of the branches is easily balanced. When the hot streams split is optimized, exchangers of the same branch are cleaned at the same time so that crude flows only through one branch – no need to balance pressure during the cleanings as one branch is completely idle – and all of the hot stream is diverted towards the active units. Also, in this case, cleaning one exchanger of one of the branches is feasible and profitable as the pressure drop of the branches is balanced and the hot stream distribution is adjusted to interact with the changing flow rates of the cold streams. On the other hand, when the tube side flowrate on parallel branches can be freely controlled the economic advantages are higher, and there are more interactions among the cleanings and the system dynamics. In this case, there are no simultaneous cleanings of the exchangers in the parallel branches, as there is no pressure constraint. All the flow rates of the network can respond dynamically in this scenario so that when a unit is idle, they are distributed among the remaining units to maximize the heat recovered.

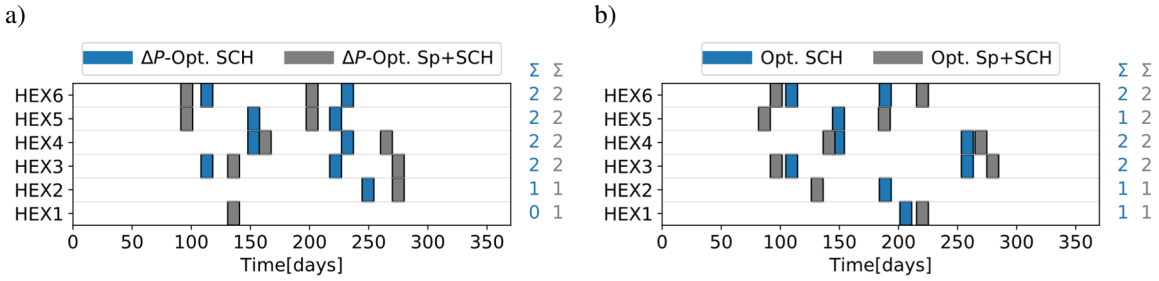

Figure 5.7. Optimal cleaning schedule of case LN-B1 when the tube side flow is pressure driven (a) and when it is freely controlled (b).

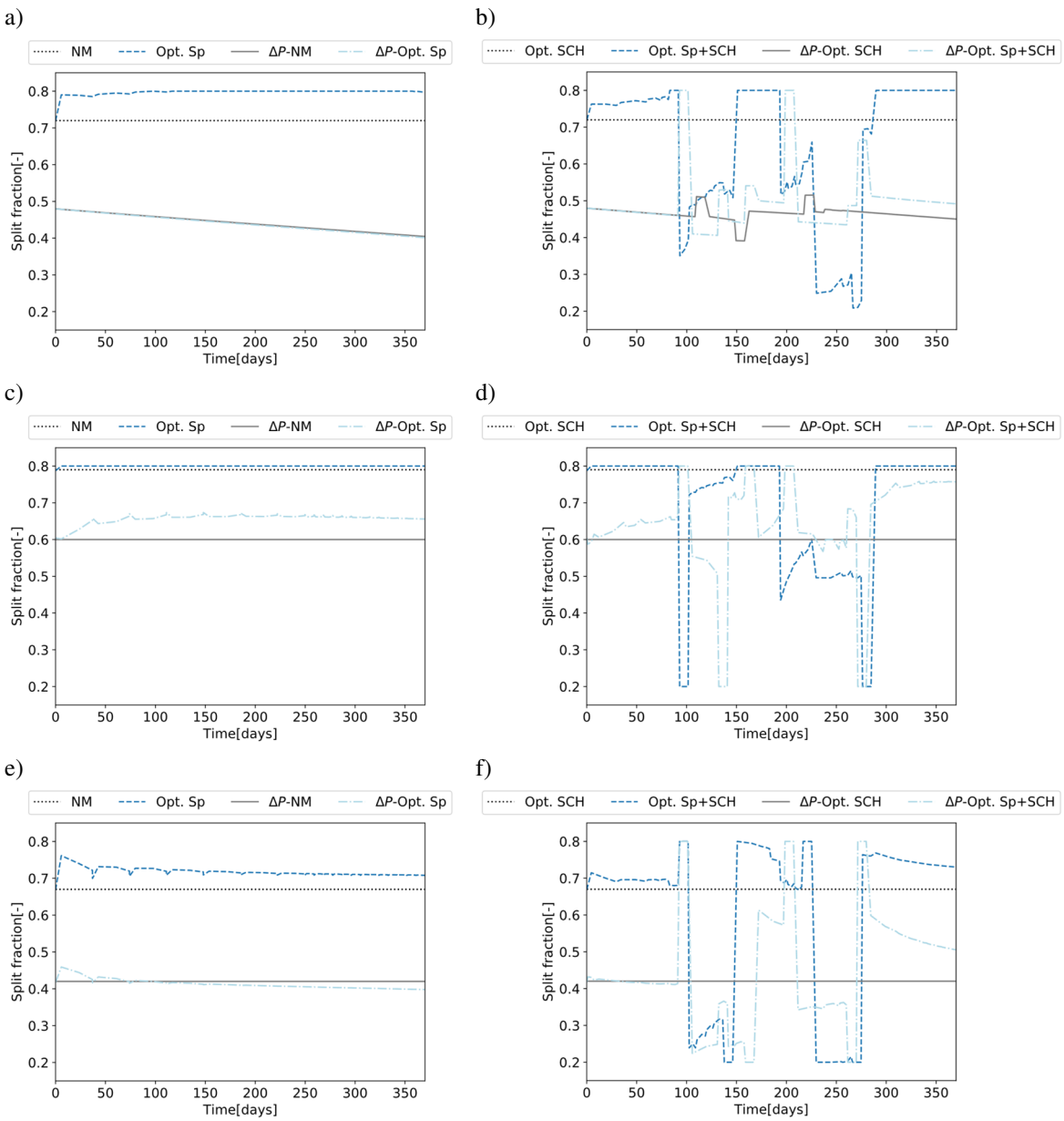

Figure 5.8. Flow split distribution of LN-B1. a, b) Crude split fraction to HEX3 with and without cleanings. c, d) HVGO split fraction to HEX3 with and without cleanings. e, f) VR split fraction to HEX4 with and without cleanings.

Figure 5.8 shows the split fraction of the crude, HVGO, and VR streams of case LN-B1 for all the operating modes. When there are no cleanings and the flow distribution is optimized for all the network, the split fraction of the crude and of the HVGO streams saturates at their upper bound, and that of VR stream exhibits a maximum close to the beginning operating and then it stabilizes at 73%. HEX3 and HEX4 have a higher duty than those on the opposite branch as their configuration has more tubes and passes than the others,

so it is advantageous to divert most of the flow to this branch. Similar trends are observed when the tube side flow is pressure driven, although the split fraction of the hot streams does not react to the same extent. On the other hand, when the cleaning schedule is optimized together with the flow distribution, the heat duties of the branches change dynamically causing the split fractions to change. Even when exchangers of opposite branches are cleaned simultaneously, all split fractions respond dynamically during and after the cleaning. For instance, when HEX3 and HEX6 are cleaned simultaneously at 100 days of operation and the crude split fraction is free, the crude flow is diverted from the HEX3 branch to the HEX5 branch and then it remains split around 50% until the next cleanings scheduled in the network. For the same case, the HVGO flow is diverted to HEX5 during the cleaning, and that of VR to HEX4 which remains operating. Both hot streams react in the same way when the crude flow rate is pressure driven, but less variability in the split fraction of the crude stream is observed, and it only changes significantly when a whole branch is idle.

The LN-B1 case demonstrates the advantages of simultaneously optimizing cleaning scheduling and flow distribution in HEN under fouling, the efficiency of the MPCC reformulation, and how realistic constraints, such as balanced pressure in parallel branches, affect the optimal operation of the system. The final network considered in this section – the REF-X case study – also has parallel branches, and the interactions and advantages discussed are also observed there. It is assumed that the crude flow rate can be freely controlled with split fractions bounded between 20% and 80%.

The model used to characterize the operation of REF-X case is obtained solving a parameter estimation problem. The fouling parameters and deposit roughness of each exchanger are estimated to best predict the plant measurements. The parameter estimation procedure was presented in Chapter 4, and the parameters for this case study are taken from there. Because this model has been successfully validated, the benefits obtained from using it for optimal fouling mitigation can be directly compared with the actual refinery past operation. The cleaning schedule implemented in the refinery for this preheat train during the 1500 days of operation is known and, based on the plant measurements, it is reasonable to assume that the flow distribution of the parallel branches remained constant at 50%.

The optimal cleaning scheduling (SCH), and integrated optimal cleaning scheduling and flow control (Sp + SCH) problems are solved for the case REF-X based on the operating

conditions of the refinery. The effect of the time discretization on the optimal solution is evaluated varying the number of periods in the time horizon. Figure 5.9 shows the effect of the number of periods on the optimal operating cost, and the optimal cleaning cost, and it compares them with the no mitigation alternative (NM), and with the cost of the actual refinery operation. There is an almost constant difference between the optimal total operating cost of the SCH problem, and that of the Sp + SCH problem, although the trend of both is similar. In both cases the total operating cost decreases with the number of periods. However, for a number of periods greater than 30 there is no significant reduction of the total operating cost, though the number of cleanings increases. The cleaning cost increases almost linearly with respect to the number of periods for the case without flow distribution optimization, and it reaches an asymptotical value for the other case. The cleaning cost is proportional to the number of cleanings, and they increase with the number of periods because there are more alternatives available to allocate cleanings as the time horizon grid becomes finer.

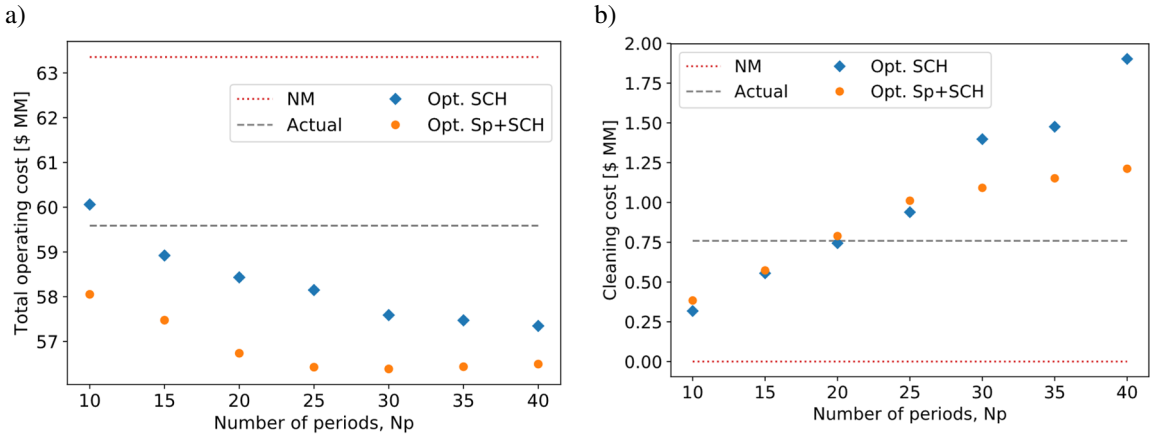

Figure 5.9. Effect of the number of periods in the time horizon on the optimal cleaning schedule of REF-X case. a) Total operating cost, b) Cleaning cost

One clear advantage of the optimal cleaning scheduling approach is that with around the same cleaning budget of the actual operation – $ 0.75MM, solution with 20 periods in Figure 5.9 – the operating cost can be reduced by $ 2.8 MM at most. Hence, the timing and sequence of the cleanings are key for the operation, and not only the total number of cleanings. All optimization alternatives, except that with 10 periods and no flow distribution optimization, perform better than the actual operation of the refinery, and much better than the no mitigation alternative. The optimal operation of the network reduces the total operating cost by $ 0.5 MM - $ 3.0 MM relatively to the actual operation.

The number of units in the REF-X case and its long operating horizon are not a limitation to optimize its cleaning schedule when the MPCC reformulation is used. The computational time required to solve all optimization problems is presented in Figure 5.10, and it increases with the number of periods for the only reason that the problem size is larger. The time reported is the total time required to solve the sequence of NLPs using the regularized ϵ approach. There is no significant difference between the computational effort required to solve the optimal cleaning scheduling problem, and that of the integrated optimal cleaning scheduling and flow control problem. The computational load for solving both problems scales up in the same way – linear trend – for the number of periods explored. Finally, considering that the time horizon is 1500 days and the large size of the problem, the computational load required to find an optimal solution pose no limitations to a recurrent evaluation of the problem, and to frequent monitoring and optimization of the operation of HEN under fouling.

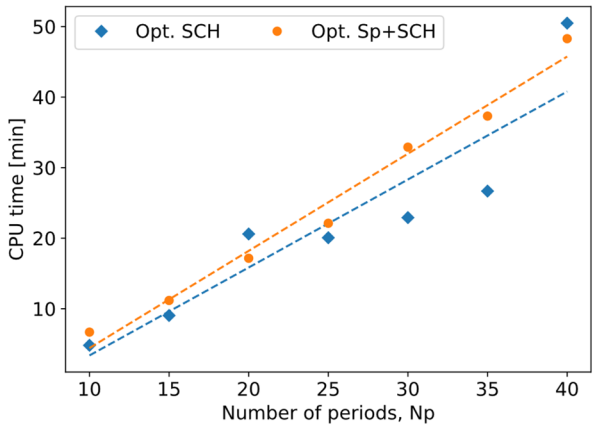

Figure 5.10. Effect of the number of periods in the time horizon on the computational time required to solve the optimal cleaning schedule of REF-X.

The optimal solutions of REF-X case using 30 periods to discretize the time horizon are chosen for a further analysis. Figure 5.11 compares the actual cleaning schedule implemented in the refinery with the optimal ones with and without optimal dynamic flow distribution. The optimal cleaning schedules have more cleanings than the actual operation, and their sequence and timing are different. While the actual operation is conservative with respect to the cleanings, the optimal solutions are more aggressive and have more frequent cleanings of the same units because the overall economic trade-off between energy savings

and cleaning cost is positive. Another difference is that E05A/B is cleaned twice in the actual schedule, but never cleaned in the optimal alternatives. This is the largest heat exchanger with the highest cleaning cost, but not the largest heat duty under clean conditions. Its heat duty in clean conditions (5.2 MW) is comparable to that of E04 which is a single shell exchanger, meaning that the energy savings of cleaning E05A/B are rather low. On the other hand, E01A/B and E04 are cleaned frequently in the optimal solutions, and they were cleaned the most during the actual operation. These two exchangers have the two highest duties of the network and some of the highest fouling rates too, making their cleanings profitable, although they occur at almost regular intervals in the optimal cleaning schedule alternatives.

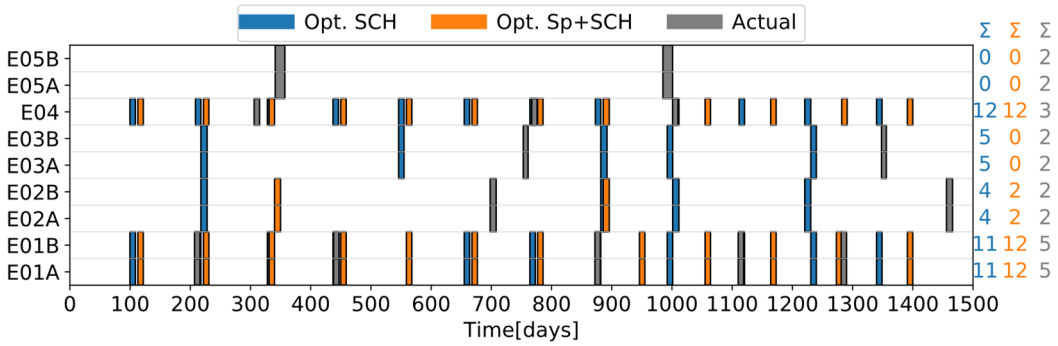

Figure 5.11. Optimal cleaning schedule compare with that of the actual operation for the case REF-X.

The optimal cleaning schedules obtained perform better than the actual operation of the preheat train despite more cleanings. However, the integrated optimal scheduling and flow control alternative has a lower operating cost than that achieved only considering scheduling decisions. The integrated alternative (Sp+SCH) also performs better than sequentially optimizing the cleaning schedule and then the optimal flow distribution of the network. The sequential optimization approach (SCH→Sp) leads to an operation with a cost of $ 56.8 MM, while the simultaneous optimization of the HEN results in a total cost of $ 56.2 MM with fewer cleanings. Figure 5.12 shows the optimal furnace duty for all optimized alternatives, and their optimal flow split. For the sequential approach the furnace duty decreases significantly with respect to that of the optimal scheduling with constant flow distribution (SCH) because the crude stream split fraction reacts dynamically to the cleanings, so that it dynamically diverts the flow towards the branch that recovers more heat over the operating time. Although the sequential and simultaneous approaches considered all

the interactions of the networks and the trade-off between energy recovery and fouling rate – high flow rates in one branch may increase the heat transfer there, at the same time they increase the fouling rate in the opposite branch – the simultaneous approach gives the best operating alternative as it captures the effect of all decision variables at the same level.

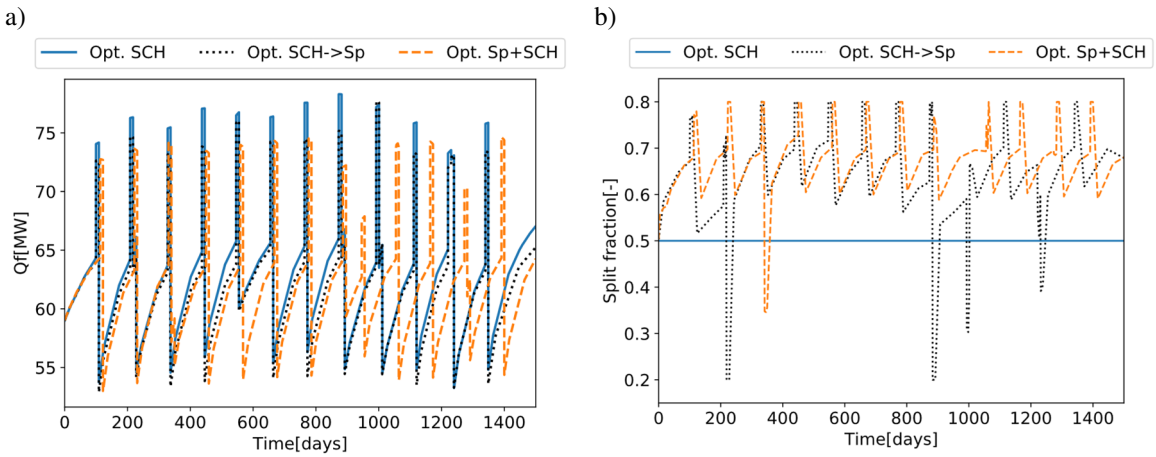

Figure 5.12. Furnace duty (a) and split fraction to E02A/B branch (b) for optimal cleaning scheduling solutions of REF-X case.

The interactions among heat recovery and fouling rate in parallel branches when the flow rates are controlled dynamically can be observed in Figure 5.13. It shows the fouling resistance of E03A/B and E05A/B, which are located in opposite branches of REF-X case, for all the optimization scenarios. The sequential scheduling and then control optimization approach demonstrates how the fouling resistance of the exchangers in one branch decreases, while that of exchangers in the opposite branch increases when the flow split is optimally controlled. In addition, only by controlling the flow rate of certain exchangers their deposit can be partially removed as it is the case of E05A/B in the sequential approach between 800 and 1000 days of operation. The increase in the flow rate going to the branch of exchanger E05A/B during that time increases the shear stress, and hence the removal rate, partially recovering the exchanger performance. Similarly, the fouling resistance of E03A in the simultaneous optimization case remains close to zero during most of the operation because the flow rates are controlled in a way that the deposit generated can be quickly removed by increasing the shear stress. The overall effect of those interactions is observed in an increase of the energy recovered in the network over the operating time.

The optimal cleaning schedule and flow distribution obtained with the MPCC reformulation of the problem for the REF-X case study is validated following a similar procedure to that described in Chapter 4. The optimal solution obtained with the lumped model (A) and the MPCC reformulation is implemented and simulated in *Hexxcell Studio*^{TM} which uses the detailed distributed model (B). Initially, the lumped model (A) used in the optimization procedure was tuned based on the predictions of the distributed model (B) which acts as a soft sensor and provide temperature and pressure drop measurements for the parameter estimation problem.

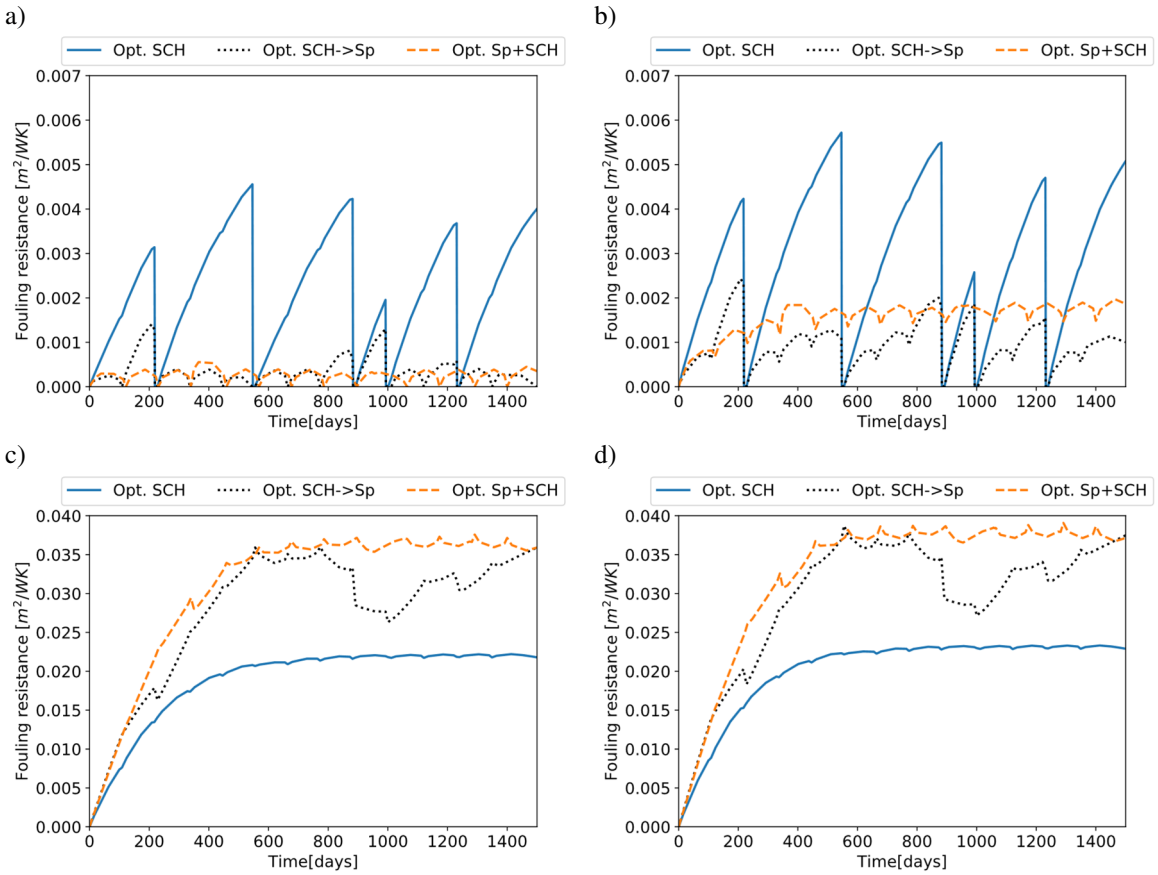

Figure 5.13. Fouling resistance of key heat exchangers of REF-X for optimal cleaning scheduling scenarios. a) E03A, b) E03B, c) E05A, d) E05B.

The two models are used to simulate the following scenarios: no fouling mitigation, actual operation of the preheat train, and optimal cleaning schedule and flow distribution obtained with the MPCC reformulation. Figure 5.14 shows the furnace duty predicted by the two models for each of these scenarios. Both models predict the same trends in the furnace duty, meaning that they capture in the same way the effect and interactions of all variables in

the network, including the decision variables of the optimization problem solved. However, there is a small mismatch between the models, and the lumped one underestimates the furnace duty in all cases, although the bias only becomes significant after long periods without cleanings. The average absolute error in the furnace duty between the two models is 0.38 MW, considering all scenarios, but that same error for the optimal solution is lower, 0.17 MW, because there are no long operating periods without cleanings. These differences in the furnace duty predictions have an effect on the total operating cost of the network. On average this error is $ 0.52 MM over a time horizon of 1500 days, which is negligible with respect to the total operating cost – it corresponds to a 0.87% of the average total operating cost. Also, there are other sources of uncertainty that introduce errors to the total cost estimated such as the varying flow rates, crude blends processed, and market factors, making the mismatch observed in the implementation of the optimal solution acceptable.

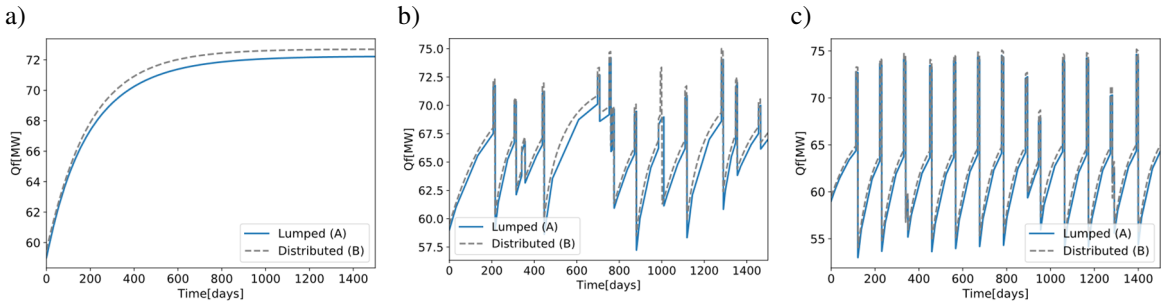

Figure 5.14. Validation of the furnace duty of REF-X case using a distributed model. a) No mitigation, b) Actual operation, c) Optimal cleaning scheduling and flow distribution

The optimal cleaning schedule and flow distribution solution of REF-X is also validated for the individual key performance variables of three exchangers of the networks. Exchangers E01A, E02A, and E03A are selected for this purpose as they have different locations in the network, hence they are exposed to different operating conditions, the effect of which should be predicted by the model used in the optimization. Figure 5.15 to Figure 5.17 show the validation of the heat duty, the fouling resistance, and the tube side pressure drop, respectively, for the three exchangers considered. Good agreement between the models is observed in all the variables when the optimal solution obtained with the lumped model (A) is validated using the distributed model (B). Both models predict the same effect of the decision variables – cleaning actions and dynamic flow distribution – on the performance of the exchangers, so that decisions made based on the lumped model are confirmed by the

distributed model, and thereby deemed valid for the actual operation of the system. The prediction mismatch in these variables is minimal, and the overall error observed in the furnace duty arise from the cumulative effect of the individual errors as they propagate through the network.

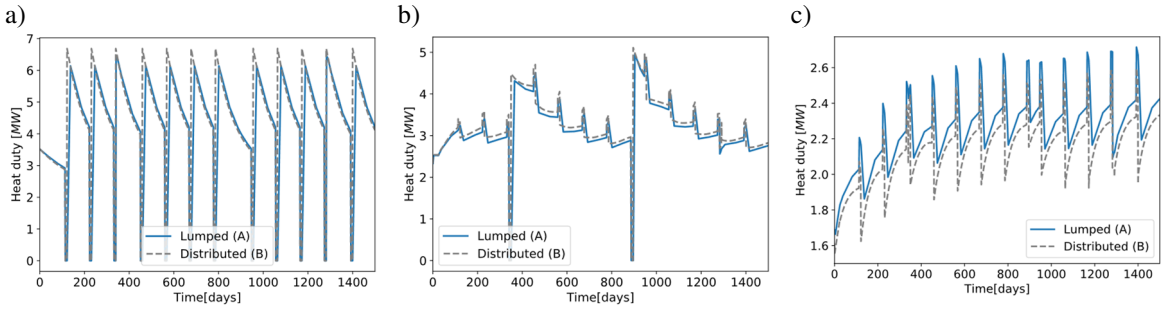

Figure 5.15. Validation of the heat duty of exchangers: a) E01A, b) E02A, c) E03A of REF-X case using a distributed model at the optimal cleaning scheduling conditions.

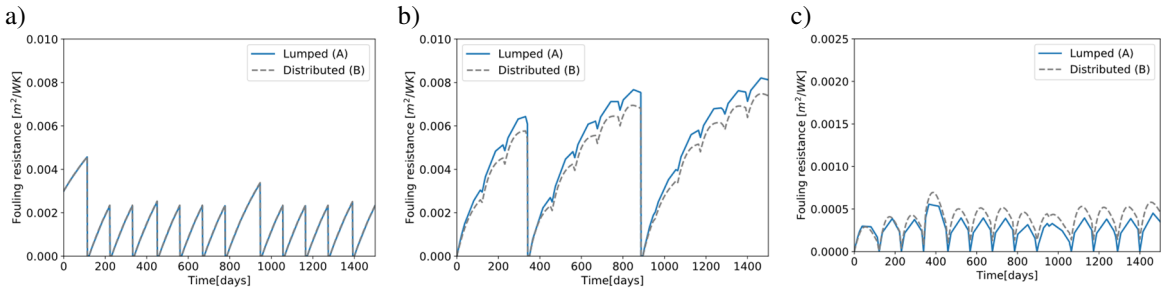

Figure 5.16. Validation of the average fouling resistance of exchangers: a) E01A, b) E02A, c) E03A of REF-X case using a distributed model at the optimal cleaning scheduling conditions.

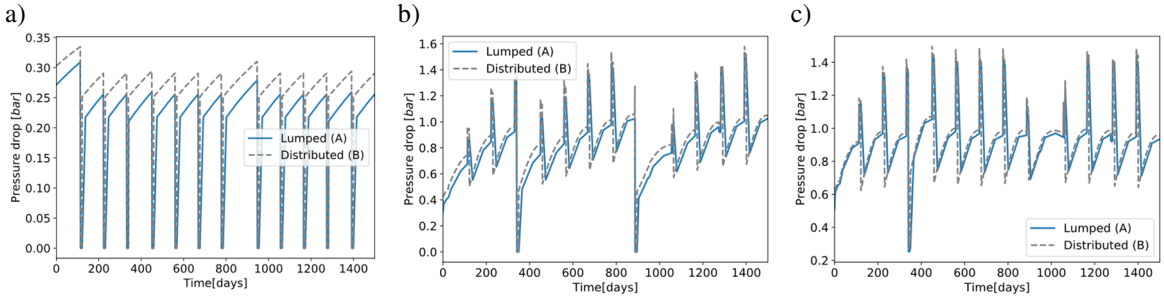

Figure 5.17. Validation of the tube side pressure drop of exchangers: a) E01A, b) E02A, c) E03A of REF-X case using a distributed model at the optimal cleaning scheduling conditions.

Some variables of the heat exchangers differ in nature between the lumped model used for optimization and the distributed one used for validation. While the fouling resistance and

the tube side pressure drop are considered as distributions along the length of the heat exchanger in the distributed model, they are defined as a single value in the lumped model. Because of this difference in the modelling approach, it is not expected for the fouling resistance of the lumped model to match the average fouling resistance estimated with the distributed model. On the contrary, the tube side pressure drop is defined as an overall measurement of the hydraulic performance of the units, and it is predicted correctly by the lumped model.

5.5. Concluding remarks

The simultaneous optimal cleaning scheduling and flow distribution problem of HEN under fouling is solved for industrially relevant cases. The solution strategy applied reformulates the MINLP problem into a MPCC problem by relaxing the binary variables as continuous bounded variables and introducing complementarity constraints. A sequential solution approach that uses a regularization of the complementarity constraints and an interior point algorithm is implemented to cope with the difficulties of MPCC problems.

This solution strategy is proven to be more efficient in solving the optimal cleaning scheduling problems for the case studies presented in Chapter 3, reducing the computational time by 99% compared to standard branch and bound algorithms for MINLP problems.

The significant reduction in computational time allows to tackle larger and more complex problems, and three case studies of large networks (6 – 9 heat exchanges) are analysed using this strategy. The cases cover the most common network configurations found in industry – series and parallel arrangement – and their optimal cleaning schedule is obtained using the MPCC reformulation in a short computational time – less than 30 min of computation. This solution strategy has the potential to be used for real time applications, and the computational time require to find a solution scales up almost linearly with the problem size. For industrial size cases involving parallel branches and control degrees of freedom, it is demonstrated that the simultaneous optimization of the cleaning scheduling and dynamic flow distribution is better than any individual fouling mitigation alternative or a sequential optimization approach.

Finally, the optimal cleaning schedule and dynamic flow distribution of a real preheat train (REF-X) obtained with the MPCC reformulation strategy is validated with a more

detailed, and previously tested model. Implementing the optimal solution in the validation model lead to the same conclusions, and both models predict the same effects of the decision variables. The prediction errors between the two models on the key performance variables of the network are negligible for the optimal cleaning scheduling and flow distribution solution.

With an efficient solution approach to the optimal cleaning scheduling and flow distribution problem of HEN under fouling a constant monitoring and optimization of the system is possible in real time. Additional decision variables could be included in the optimization problem to mitigation fouling such as retrofit alternatives, and a portfolio of cleaning alternatives with different cost and efficiencies.

Chapter 6

Optimal retrofit, cleaning scheduling, and control of preheat trains under fouling

In this chapter the mathematical formulation used to optimize the operation and cleaning schedule of HEN under fouling – Chapter 3 – is expanded to include retrofit decisions. The retrofit decisions include adding new exchangers to an existing network, removing exchangers from an existing network, changing the piping and connections among new and existing units, and modifying the heat transfer area of all exchangers. The HEN is defined as a superstructure to include all possible modifications. Integer variables are introduced defining the existence or not of a subset of exchangers, while all other retrofit decisions – connections and area retrofit – are modelled using continuous variables. Because of the similarities of the cleaning scheduling problem and the network retrofit problem, the solution strategy presented in Chapter 4 is applied here with the nonexistence of exchangers modelled as a unit being continuously cleaned (idle). This modelling approach optimally integrates design, scheduling, and control decisions for HENs under fouling, which has not been done before. Two realistic cases are used to demonstrate the ability of the formulation to handle complex retrofit problems, and the advantages and benefits of integrating all decisions at the same level.

6.1. Introduction

HEN retrofits are common in energy recovery operations to satisfy a production target, reduce energy consumption, debottleneck the operation of the system, or even to reduce fouling. Retrofit alternatives aim to increase the heat transfer area and/or the heat transfer coefficient so that more energy is recovered in a given unit or in the network. The optimal definition of some retrofit alternatives has been widely studied, and those dealing with

network modifications are closely related to the HEN synthesis problem, but the long-term dynamic effects of fouling, and potential fouling mitigation have been ignored.

This chapter addresses the problem of optimal retrofit of HEN under fouling. The retrofit alternatives considered are limited to adding or removing units, modifying the heat transfer area of the exchangers, and changing the connections among the units in a network. Heat transfer enhancement technologies are not considered here because of the lack of understanding of fouling phenomena under those conditions. Retrofit decisions are integrated with optimal operation and fouling mitigation decisions for HEN so that, in a single instance of the problem, all the relevant factors and interactions affecting the performance of the system are considered simultaneously. The following section presents the model developed for optimal retrofit, flow control, and cleaning scheduling of HEN under fouling, which is derived from the formulation presented in Chapter 3. Then, that formulation is applied to two relevant case studies to demonstrate the importance of considering retrofit decisions simultaneously with fouling dynamics and fouling mitigation actions.

6.2. Including retrofit decisions in the optimization problem

The retrofit decisions considered here are: adding new exchangers to an existing network, removing existing exchangers, change the connections among new and existing units, and modifying the heat transfer area. The first three correspond to network level retrofit options, while the last one is related to individual units.

To model the retrofit decisions a superstructure is used to represent the HEN, and an example is presented in Figure 6.1. The exchangers that can be added to or removed from the network are represented with a hashed pattern, and additional mixers and splitters are introduced to define a set of possible new connections among the units. The superstructure example shows two instances of network retrofit. In the first one, unit E2 can be added to a section of the network in a series configuration with respect to E1 before or after it, or in a parallel configuration. In the second one, three existing units can be rearranged so that the sequence of E4 and E5 can be swapped or they can be arranged in parallel. These retrofit alternatives are valid for the cold and hot streams. Although this example only shows the option of adding a new exchanger at three locations and modifying the connections of two

exchangers, the superstructure can be easily modified to consider multiple locations for new units and other new connections in the network.

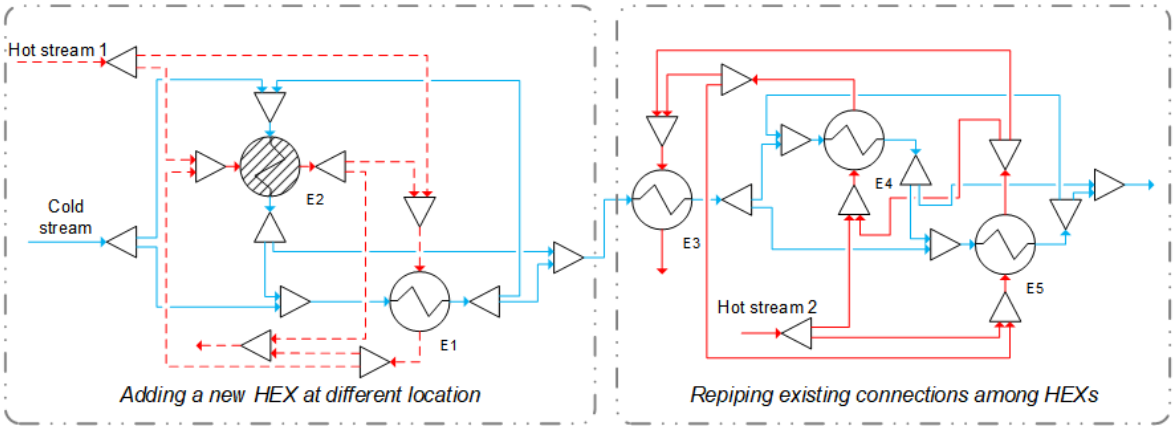

Figure 6.1. Example of HEN superstructure including network retrofit alternatives.

This superstructure is based on the optimal retrofit formulation proposed by Ciric and Floudas (1989); and Floudas, Ciric, and Grossmann (1986). It allows to generate connections between new and existing units, or repiping streams among existing units. Note that when a heat exchanger is not included in the network, the streams around it can still exist as bypasses around the unit are included in the network representation – not shown in Figure 6.1– similarly to the formulation and modelling approach of Chapter 3. Unlike the optimal HEN synthesis problem, where the superstructure defines all possible connections among the heat exchangers, in this retrofit problem not all connections are defined. Only new streams that are identified a priori to be relevant and give potential benefits to the operation are included – for example, using engineering knowledge or a pinch analysis. The more connections and streams splits in the superstructure, the higher the complexity and size of the problem.

Binary variables, $y_{r,i} \in \{0,1\} \forall i \in HEX_r \wedge y_{r_i} = 1 \forall i \in HEX - HEX_r$, are used to model the existence ($y_r = 1$) or not ($y_r = 0$) of a unit in the network, and they are defined over the set $HEX_r \subset HEX$. When a heat exchanger is not part of the network, its operation is modelled as being idle all time, which is the same as if the exchanger was being cleaned during the whole operating time. Therefore, the variables used to define the existence of the units are related to those used to define their cleanings $y_{i,t}, \forall i \in HEX, t \in T$. This analogy between the operating mode of heat exchangers during cleanings and not being part of the network is useful to formulate the optimal retrofit problem based on the optimal cleaning

scheduling problem, and to consider fouling at the same time. Hence, the model developed in Chapter 3 employing a continuous time discretization is used here, and new constraints and variables are introduced to model correctly the retrofit decisions, and the cost associated with them.

Two instances are considered regarding the integration of the scheduling problem and the retrofit problem. In the first one, Eq. (6.1) is a new retrofit constraint included in the model to indicate the implication that if an exchanger does not exist in the network it is idle or being cleaned during all the operating time, but if it does exist it can be cleaned any number of times. In the second one, Eq. (6.2) indicates that if the exchanger is added to the network it is never cleaned during the operating time, and if it does not exist it is idle all the time. If the cleaning scheduling problem is solved simultaneous with the retrofit problem, only Eq. (6.1) must be included in the formulation to allow cleanings of all existing and new exchangers.

$$1 - y_{r,i} \leq y_{i,p}, \qquad \forall i \in HEX, p \in \{1,2,\dots,N_p\} \tag{6.1}$$

$$y_{i,p} = 1 - y_{r,i}, \qquad \forall i \in HEX, p \in \{1,2,\dots,N_p\} \tag{6.2}$$

Additional constraints that have to be modified to ensure feasibility of the optimal retrofit problem using the optimal cleaning scheduling formulation are: the definition of sequential cleanings, Eq. (6.3); the lower and upper bounds of the z variable – the variable that indicates the state of the periods relative to whether one or more units are idle – Eq. (6.4) - (6.5); the maximum number of cleanings per period or simultaneous cleanings, Eq. (6.6); and the maximum number of cleanings per unit, Eq. (6.7). All these constraints are influenced by the binary variables that define the existence of the units.

$$y_{i,p+1} \leq 1 - y_{i,p} + 1 - y_{r,i}, \qquad \forall i \in HEX, p \in \{1,2,\dots,N_p - 1\} \tag{6.3}$$

$$y_{i,p} - (1 - y_{r,i}) \leq z_p, \qquad \forall i \in HEX, p \in \{1,2,\dots,N_p\} \tag{6.4}$$

$$z_p \leq \sum_{i \in HEX} \left(y_{i,p} - (1 - y_{r,i})\right), \qquad \forall p \in \{1,2,\dots,N_p\} \tag{6.5}$$

$$\sum_{i \in HEX} \left(y_{i,p} - (1 - y_{r,i})\right) \leq z_p N_T, \qquad \forall p \in \{1,2,\dots,N_p\} \tag{6.6}$$

$$\sum_{p=1}^{N_p} y_{i,p} \leq N_{HEX}(y_{r,i}) + N_p(1 - y_{r,i}), \qquad \forall i \in HEX \tag{6.7}$$

In the superstructure representing the HEN, the retrofit alternatives are defined by the existence of the exchangers, and by the flow rates in and out of the many new splitters and mixers. Because fouling is a dynamic phenomenon, the flow distribution of all splitters in the network, even those used to define the superstructure, are degrees of freedom and they vary over time. Hence, the optimal retrofit formulation assumes dynamic optimal flow control on the bypasses and parallel branches of the network. However, for comparison purposes alternatives with constant flow rates in each arc of the network are considered, Eq. (6.8).

$$m_{i,j,k,t} = m_{i,j,k,0}, \qquad \forall (i,j,k) \in A, t \in T \mid j \in Sp \tag{6.8}$$

Besides network retrofit alternatives, the individual retrofit of each exchanger by modifying its heat transfer area is also included in the optimal retrofit problem formulation. A continuous variable $0.5 \leq x_{r,i} \leq 1.5, \forall i \in HEX$ is introduced to define the fractional change in the heat transfer area of all exchangers, so that the new retrofitted area is given by Eq. (6.9). It is assumed that only the number of tubes in the exchanger is modified, as modifying the length of the exchanger requires changing the shell and modifying the number of tube passes involve integer variables making the problem more complex. Retrofitting the number of tubes modifies its heat transfer area and the tube side mass flux, hence the tube side velocity and sheer rate decrease when the number of tubes increases. Under those conditions – higher heat transfer area and lower velocity – the fouling rate and the heat transfer rate increase, but they have opposite effects on the performance of the unit. The proposed formulation considers these important interactions explicitly.

$$HTA_i = \pi d_i L_i \left(N_{T,i}\right) x_{r,i}, \qquad \forall i \in HEX \tag{6.9}$$

Any retrofit alternative has a capital cost associated, either from purchasing a new unit or a new tube bundle to modify the heat transfer area. The cost of a new exchanger is calculated using Eq. (6.10) which correlates the cost with the heat transfer area (Gerrard 2000). This cost is then annualized and integrated over the operating time assuming that it is shorter than the payback period of the unit. Correction factors are used to account for the material, operating pressure, and price change to date. It is assumed that the piping cost, usually much lower than the cost of a new unit, is included in this capital cost calculation. The cost of repiping – new connections among existing exchangers – is not considered here as it is function of the actual layout of the units in the plant and it cannot be estimated without

having that precise information. The cost of area retrofit is defined as a function of the extra number of tubes in the new configuration, Eq. (6.11). It is assumed that only increasing the heat transfer area of an exchanger has a cost as it requires purchasing and installing new tubes, and in the case the area is reduced, it is assumed not to have a cost. The maximum function used to characterize the area retrofit cost is modelled using the continuous approximation of Eq. (6.12) which is numerically zero for $x_r < 1$, and $(x_r - 1)$ otherwise.

$$P_{cap,i} = F_M F_P F_{CEPCI} \exp[11.147 - 0.9186 \ln(HTA_i[ft^2]) + 0.0979(\ln(HTA_i[ft^2]))^2], \quad \forall i \in HEX \tag{6.10}$$

$$P_{x-HTA,i} = \max\{0, (x_{r,i} - 1)\}(N_{T,i} P_{tube}), \qquad \forall i \in HEX \tag{6.11}$$

$$\max\{0, (x_{r,i} - 1)\} \cong \frac{1}{2}(x_{r,i} - 1)\left[1 + \frac{(x_{r,i} - 1)}{\sqrt{(x_{r,i} - 1)^2 + 1x10^{-7}}}\right], \qquad \forall i \in HEX \tag{6.12}$$

The retrofit costs are considered together with all other operating cost of the HEN, so that the objective function of the optimal retrofit problem considering fouling, dynamic flow distribution, and fouling mitigation is Eq. (6.13). This objective function includes the fuel cost, carbon cost, cleaning cost, loss of production, annualized capital cost due to new units, and area retrofit cost. The cleaning cost is modified with respect to that of the optimal cleaning scheduling problem because it is necessary to ignore it when a unit is not added or is removed from the network.

$$J = \min\left(P_f \int_0^{t_f} Q_f dt + P_{CO} K_{CO} \int_0^{t_f} Q_f dt + \sum_{i \in HEX} \sum_{t \in T} P_{cl,i}(y_{i,t} - 1 + y_{r,i}) - P_m \int_0^{t_f} m_f dt + \sum_{i \in HEX_r} P_{cap,i} y_{r,i} + \sum_{i \in HEX} P_{x-HTA,i}\right) \tag{6.13}$$

The simultaneous optimal retrofit, dynamic distribution, and cleaning scheduling of HEN under fouling is summarized in Eq. (6.14). This is a large scale MINLP problem that includes the dynamic elements arising from fouling, all the interactions of existing and new units in the network, fouling mitigation strategies, and dynamic control of the flow distribution in the network. Variations of this problem are possible, for example ignoring cleanings of some or all heat exchangers by adding Eq. (3.32) over all periods, assuming constant split fractions for some or all splitters in the network by adding Eq. (6.8), ignoring the area retrofit for some or all units by fixing x_r to 1, and combinations of them.

The solution strategy presented in Chapter 5 to solve the optimal cleaning scheduling problem is used to solve this large scale and complex MINLP problem. The optimal retrofit problem is built from the optimal cleaning scheduling problem, so they share the same characteristics. The solution strategy used before is effective here because the new constraints and variables in the retrofit problem are few and most of them are linear. The MINLP optimal retrofit formulation is reformulated as a MPCC problem in which the binary variables associated with the existence of the units and those with cleanings of the units are relaxed and used to define complementary constraints with respect to slack variables.

$$\min_{y_{r,i},x_{r,i},y_{i,t},m_{a,t}} \; Total\ cost\ (retrofit + operation) - Eq.\ (6.13)$$

$$\begin{aligned} &s.t. \\ &Network\ representation\ using\ superstructure - Section\ 3.2.1 \\ &Heat\ exchanger\ model - Section\ 3.2.2 \\ &Fouling\ model - Section\ 3.2.3 \\ &Operating\ mode\ disjunctions - Section\ 3.2.4 \\ &Operational\ constraints - Section\ 3.2.5 \\ &Continuous\ time\ representation\ and\ time\ related\ constraints - Section\ 3.3.2 \\ &Retrofit\ implications\ with\ respect\ to\ cleanings - Eq.(3.32), Eq.(6.3) - (6.7) \\ &Area\ retrofit - Eq.(6.9) \end{aligned} \quad (6.14)$$

6.3. Practical optimal retrofit of HEN under fouling

The optimal retrofit problem for HEN under fouling is solved for two case studies. Both cases are taken from the literature, and they are studies of HEN retrofit that have considered fouling only after the retrofit decisions. They first proposed network retrofit alternatives, and then tested them in simulations to analyse the fouling effects and the overall cost of the operation. Hence, these cases are good references to test the optimization methodology proposed here, and to demonstrate that better alternatives exist. In addition, the integration of optimal cleaning scheduling, flow distribution, network retrofit, and area retrofit is evaluated for both cases.

6.3.1. Case study NR-S: single retrofit alternative

This case study is adapted from that of Coletti, Macchietto, and Polley (2011), and the superstructure of the network that includes the retrofit alternative is presented in Figure 6.2. All the specifications can be found in Appendix A. The original network – base case – had seven exchangers, HEX1 – HEX7, arranged in series, a desalter, a furnace, and the residue

stream connected HEX7 and HEX3 counter current. The first three exchangers in the network do not exhibit fouling as their operating temperatures are low and the velocities high enough to prevent any deposition from happening. The desalter has a constant temperature drop of 4.5°C, and all units downstream the desalter exhibit significant levels of fouling. The retrofit alternatives considered by Coletti, Macchietto, and Polley (2011) – the network structure of each is presented in Appendix A – aim to find the best location for an additional exchanger, HEX7x, and they are:

- C1: the base case of the network without HEX7x
- C2: HEX7x is added at the end of the network and matched with the hottest part of the residue stream.
- C3: HEX7x is added between HEX5 and HEX6 and matched with the hottest part of the residue stream.
- C4: HEX7x is added between HEX5 and HEX6 and matched with the residue stream after it leaves HEX7.

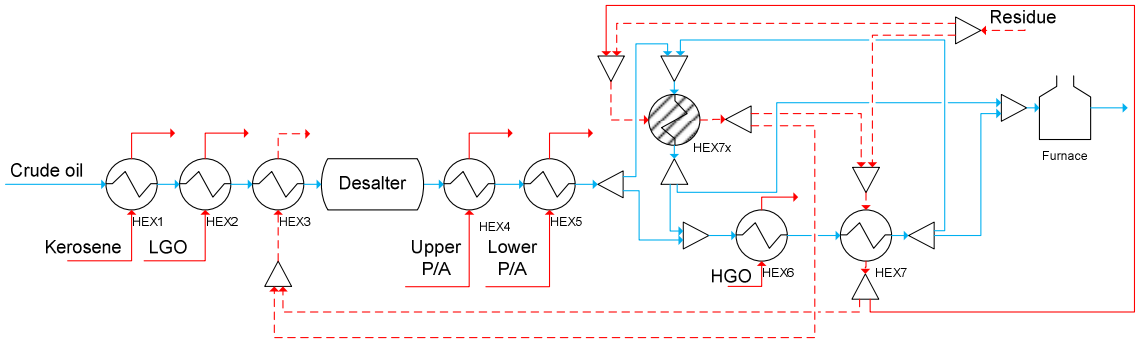

Figure 6.2. Network super structure of case study 1 (NR-S).

The retrofit superstructure defined for this case study captures all above four alternatives and others. For instance, an arrangement of HEX7x in parallel with HEX6 and HEX7 is also feasible using this representation, and the optimization procedure will determine if that is a better retrofit alternative than the others or not.

The optimal network retrofit problem is solved for this case study assuming that there are no cleanings and no area retrofit. These assumptions are used to compare and validate the optimal solution of the problem with the alternatives explored before. The time horizon is 600 days and it is discretized with 20 periods of variable length. The problem has a total of 181 binary variables, although there are many linear constraints among them reducing the

size of the search space. The optimal retrofit problem has only one more binary variable than the optimal cleaning scheduling problem for the same network, but a larger number of linear constraints. The retrofit problem is solved to optimality in 7.39 min of computational time using the MPCC reformulation and sequential solution.

The optimal retrofit solution of this case study corresponds to alternative C4, the same reported by Coletti, Macchietto, and Polley (2011) as having the best performance when the dynamics effects of fouling are considered. Figure 6.3 summarizes the cost of each alternative considered, and the optimal solution. All alternatives that include HEX7x in the network have the same capital cost, but alternative C4 – optimal – has the lowest operating cost. The splitters and mixers defined in the superstructure allow to consider many more alternatives than those mentioned, and the optimal solution indicates that none of them – for example adding HEX7x in a parallel branch – could have performed better than alternative C4. Adding HEX7x at an intermediate position in the network and matching it with the residue stream coming out from HEX7 does not produce a high energy recovery at clean conditions as that of alternative C2, but it is more resilient to fouling. In the optimal retrofit alternative HEX7x is placed at a location such that the wall temperature is not as a high as that at the end of the network, and it can still recover a significant amount of energy.

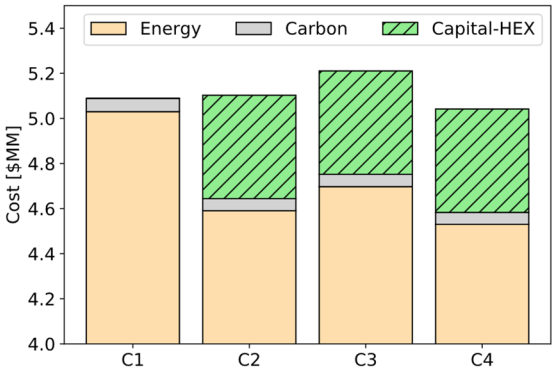

Figure 6.3. Operating cost and capital cost of each alternative explored for case study NR-S

The optimal network retrofit problem is then solved simultaneously including optimal heat transfer area retrofit, optimal cleaning scheduling, and possible combinations among them – see Table 1.1 for abbreviations and descriptions. Figure 6.4 shows the total cost of each optimal solution, and the contributions of retrofit alternatives and fouling mitigation actions. All optimal alternatives reduce the total cost of the operation with respect to that of

the base case, even when the capital cost is included. Also, they reduce significantly the operating cost of the network. The energy cost can be reduced from $ 0.5 MM up to $ 1.0 MM, with the maximum reduction is achieved by optimizing simultaneously retrofit and cleaning scheduling. The operating cost decreases when area retrofit and network retrofit decisions are considered together, although the capital cost is higher because of the additional heat transfer area. Finally, optimizing all decisions simultaneous generates the lowest total cost, although the operating cost is higher than those of other optimal alternatives. Whether the best alternative is to retrofit the network – adding new exchangers with high capital cost – or simply increase the HTA of certain units and perform cleanings optimally is related to the capital cost, the fouling rates, and the operating time of the preheat train. The optimization formulation proposed can handle all these features simultaneously, and for this case it is best to optimally schedule cleanings than to include a new unit in the network.

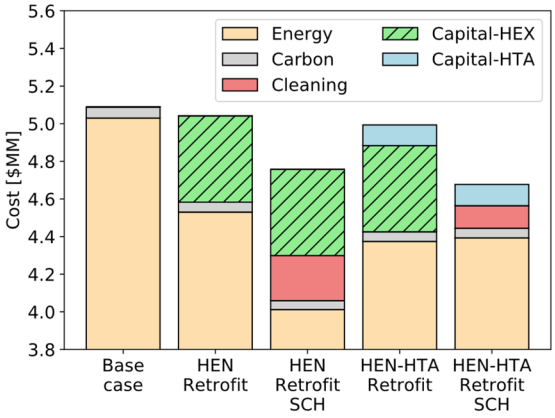

Figure 6.4. Operating cost and capital cost of optimal retrofit alternative with and without fouling mitigation for case study NR-S.

The optimal network structure changes based on the features included in the optimal retrofit problem. Considering only network retrofit optimization (HEN Retrofit), the optimal network structure is alternative C4, and when heat transfer area retrofit is included (HEN-HTA Retrofit) the optimal structure is alternative C2. The network structure C2 is also the optimal solution for the combined network retrofit and cleaning scheduling problem (HEN Retrofit SCH). Finally, for the optimal integration problem – network retrofit, area retrofit, and cleaning scheduling (HEN-HTA Retrofit SCH) – the optimal structure is C1 which does not add HEX7x to the network.

Figure 6.5 shows the furnace duty of the optimal retrofit alternatives with and without cleanings. The optimal retrofit alternatives – network and/or heat transfer area – reduce the duty with respect to that of the base case because of the extra area available for heat transfer. When the optimal cleaning scheduling problem is considered simultaneously with the retrofit decisions, the overall duty decreases further. However, the integrated network retrofit, area retrofit, and cleaning scheduling optimal solution (HEN-HTA Retrofit SCH) that does not include HEX7x has a higher duty than that of the optimal alternative that ignore area retrofit.

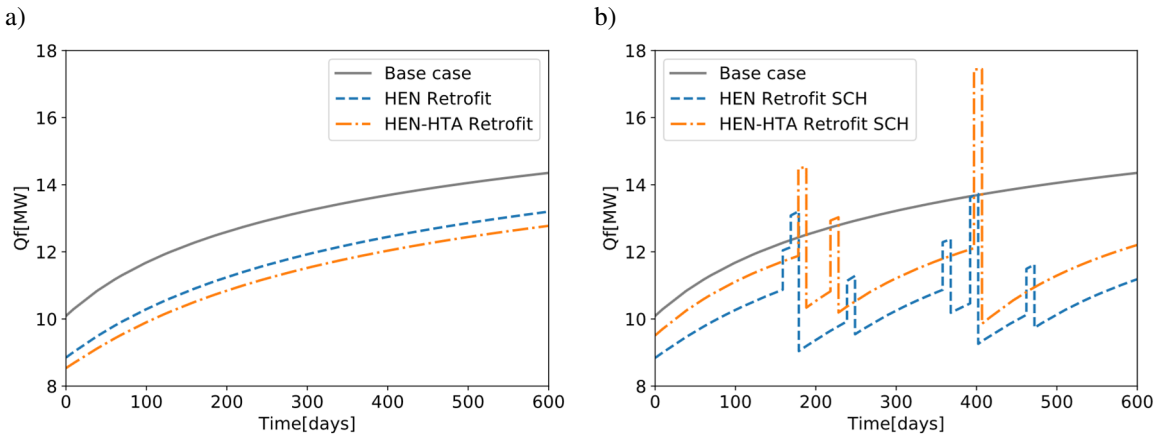

Figure 6.5. Furnace duty of optimal retrofit alternative with and without fouling mitigation for case study NR-S.

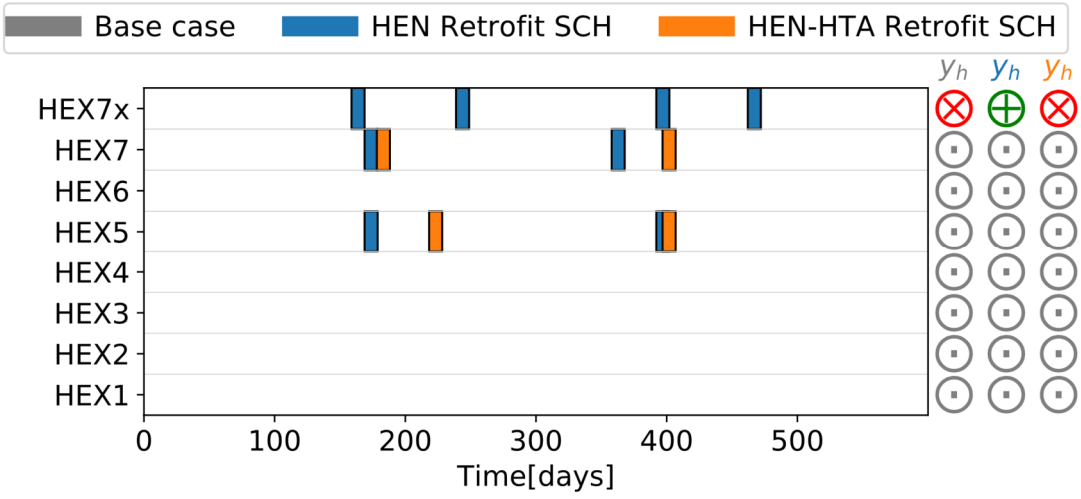

Figure 6.6. Optimal cleaning schedule of case study NR-S considering network and area retrofit (X: exchanger removed, +: exchanger added, ▪ exchanger fixed).

Figure 6.6 presents the optimal cleaning schedule for all optimization scenarios. It shows that when the new unit is included, it is cleaned often, and the starting cleaning time

of existing units is postponed when their HTA is optimally retrofitted. Also, when HEX7x is added to the network, the furnace duty decreases but the cleaning cost increases as this unit has high fouling rates and is cleaned four times during the operation. In this case the interactions among capital cost, energy recovery, and cleaning cost become important to decide on retrofit alternatives. On the other hand, increasing the HTA of existing units without adding HEX7x to the network has a much lower cleaning cost

The retrofit decisions also influence the fouling rates and the heat duty of the units. Figure 6.7 and Figure 6.8 show the fouling resistance and the heat duty of key exchangers in the network for retrofit alternatives without cleanings. For the case of only optimal network retrofit, the duty of all existing exchangers is lower, and their fouling resistance is higher than those of the base case, but the extra unit increases the overall heat recovery. On the other hand, integrating optimal network and HTA retrofit increases the duty of some existing units, but their fouling resistances are similar to those of the base case. The network structure defining the interaction among the units influences fouling and the dynamic performance of the system. It defines whether there is a constant decay on the heat duty or if the decay is damped because of a temporary increase in the temperature difference. In the two optimal alternatives displayed in Figure 6.7 and Figure 6.8, the second exchanger following the residue streams, either HEX7 or HEX7x, exhibits a maximum in its heat duty because of the temporary larger temperature difference between the streams, but later fouling effects dominate and its performance decays.

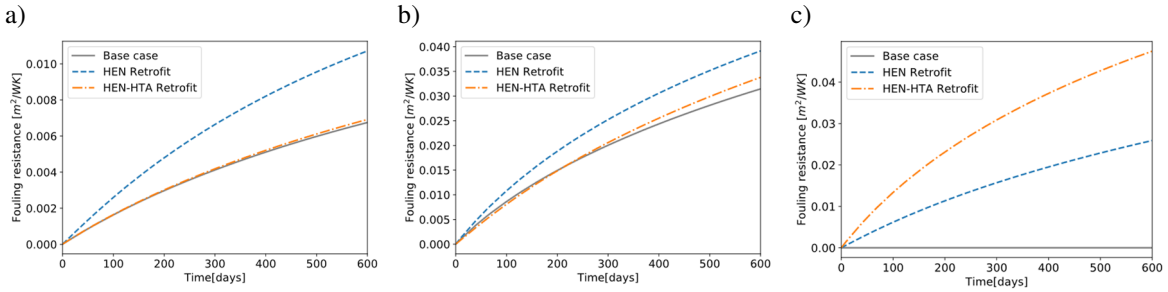

Figure 6.7. Fouling resistance of exchangers HEX6 (a), HEX7 (b), and HEX7x (c) for the optimal network and area retrofit alternatives of case study NR-S.

Finally, Figure 6.9 shows the increase in the HTA of all units for the optimization scenarios that include this decision – optimal retrofit with and without cleaning scheduling. In both cases, the area of HEX3 is increased by the maximum allowed percentage, indicating

that there is a large amount of energy that can still be recovered from the residue stream. In the case without optimal cleanings, the HTAs of HEX7 and HEX7x – new unit – are increased in 28% and 29% respectively. These two exchangers are used to recover energy from the residue stream which has the highest flow rate and highest temperature among all hot streams. On the other hand, when optimal cleanings are introduced, HEX7x is not added to the network and instead the areas of HEX3 and HEX7 are increased to their maximum to recover most of the energy of the residue stream. Also, in this case the area of HEX5 is increased by 9% which is advantageous for the operation without a large capital cost.

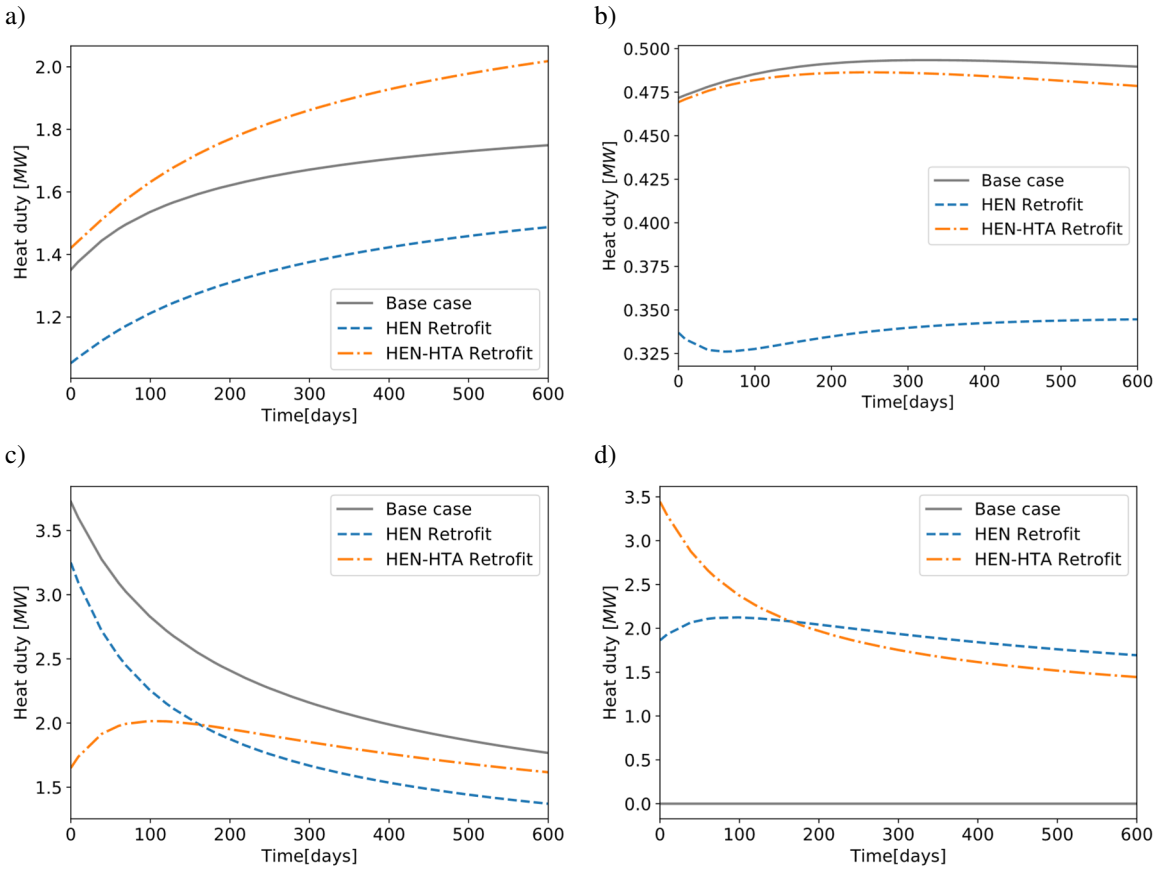

Figure 6.8. Heat duty of exchangers HEX3 (a), HEX6 (b), HEX7 (c), and HEX7x (d) for the optimal network and area retrofit alternatives of case study NR-S.

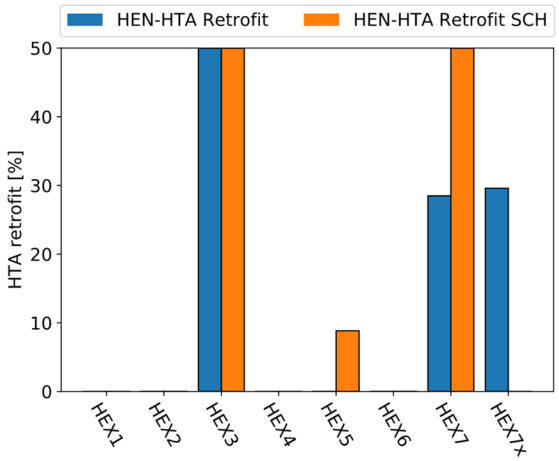

Figure 6.9. Optimal HTA retrofit of all exchangers with and without fouling mitigation for case NR-S.

6.3.2. Case study NR-B: multiple retrofit alternatives and dynamic flow distribution

This second case study is adapted from that of Yeap et al. (2005), and the superstructure of the network that includes the retrofit alternatives is presented in Figure 6.10. The superstructure shows all possible connections for the exchangers, and the streams that can be redistributed are colour coded for clarity, so that the crude oil stream (blue), the VR stream (yellow), and the OR stream (dashed red) can be differentiated. The same colour scheme is used throughout the section to show the optimal network derived from the superstructure for different instances. All the specifications can be found in Appendix A. In the original work two retrofit alternatives are considered, one based on pinch analysis (I), and another aiming to mitigate fouling while increasing heat recovery (II). Between these two alternatives and the base case, five different exchangers, E1a, E5a, E5b, E6a, E6b, can be added to the network in different locations with a capital cost that is function of their HTA. Also, one exchanger, E2, can be removed from the original network with no capital cost. The network structure of these alternatives is presented in Appendix A.

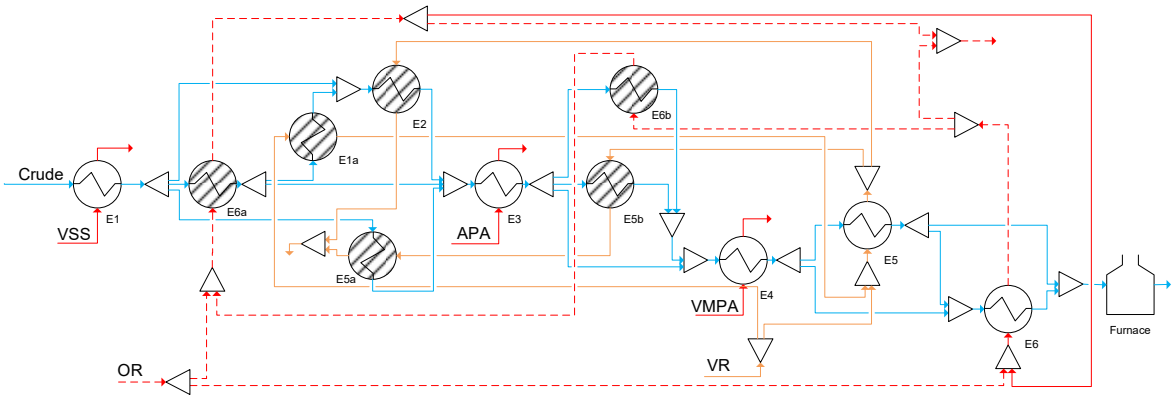

Figure 6.10. Network superstructure of case study 2 (NR-B).

In the original reference, the following networks are considered, and their performance over two years of operation analysed:

- Base case: original network structure where the crude flows in series from E1 to E6, the VR stream flows in counter current from E5 to E2. All other exchangers have a unique hot stream.
- Alternative I: network retrofit alternative proposed based on pinch technology. E2 is removed from the network, and the crude flow is split at three locations: after E1, E3, and E4. New exchangers are added in the new parallel branches. The VR and OR streams are the hot streams of the new exchangers.
- Alternative II: network retrofit alternative proposed to mitigate fouling. E2 is removed from the network, and E1a and E6a are added after E1. The crude flows sequentially though all exchangers and there are no parallel branches. The VR stream connects E1a and E5 in a co-current arrangement, while OR does the same for E6a and E6.

The superstructure for this case study was developed from these three alternatives, but, because of its generality, other network configurations arise. First, the three alternatives of Yeap et al. (2005) are simulated to validate the current implementation and to have a point of reference for future improvements. In addition, for alternative I the dynamic flow distribution is optimized (I + Opt. Sp). Then, the more general optimal retrofit problem for the full superstructure is solved for various retrofit choices – integration of HTA retrofit decisions and optimal cleaning scheduling – and the performance of the network structures obtained is compared against the base case and alternatives I and II.

6.3.2.1. Base case analysis for retrofit and dynamic flow distribution

Figure 6.11 shows the furnace duty for the base case and alternatives I and II, and the flow optimization of alternative I. Retrofit alternatives I and II reduce the furnace duty, so the operating cost is smaller than that of the base case, although the capital cost was not considered by the authors in the original work when designing those network modifications. Including the capital cost in the total cost calculation, none of these alternatives is better than the base case. The retrofit capital cost is higher than the actual reduction in the operating cost. Alternatives I and II are $ 0.46 M and $ 0.26 M more expensive than the base case operation when all the costs are considered over a two years horizon, respectively. On the other hand, optimizing the dynamic flow distribution of alternative I reduces significantly the operating cost and, even considering the capital cost of new units, the total cost of the operation is reduced by $ 0.15 M with respect to the base case.

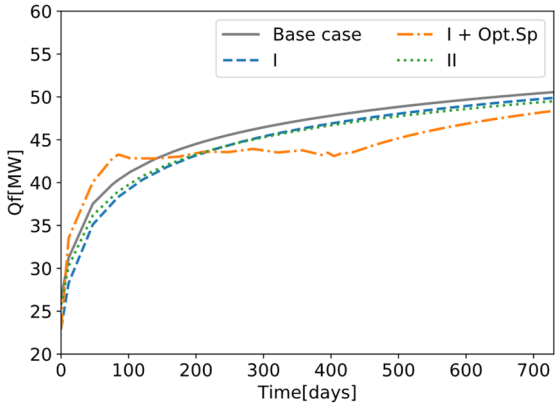

Figure 6.11. Furnace duty for network retrofit alternatives of case NR-B without considering cleanings proposed by Yeap et al. (2005)

The furnace duty of alternative I + Sp exhibits a plateau during a long operating time – see Figure 6.11. This is because the superstructure representation of the network enables dynamic flow control in parallel branches and bypasses. Figure 6.12 shows the bypasses that are active in alternative I and that optimize the flow distribution, while Figure 6.13 shows the time profiles of the split fractions for this alternative (HEN retrofit - dynamic) and compares them with the optimal constant flow distribution of the same network retrofit (HEN retrofit - constant). Three different periods of operation are observed: 1) until 100 days of operation, when all the flow of the OR and VR streams is diverted from exchangers E5a-b and E6a-b, 2) between 100 and 450 days of operation, when the bypass of the hot streams is

dynamically reduced, and the crude split to each branch changes dynamically, and 3) after 450 days of operation, when there is no bypass of the hot streams OR and VR, all the flow goes to the exchangers, and the split fraction of the crude to each branch is constant. During period 1, the furnace duty is higher than in the base case, but in period 2 the duty is almost constant, and then in period 3 it starts increasing again. The additional control degrees of freedom introduced in this retrofit alternative have significant implications for the operation, and the retrofit optimization exploits these interactions over long operating periods.

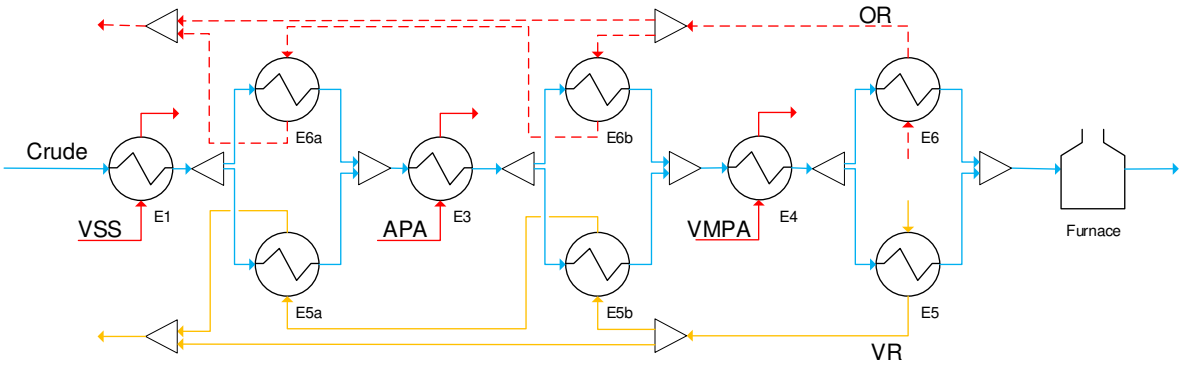

Figure 6.12. New bypasses for alternative I retrofit of case NR-B considering optimal dynamic flow distribution.

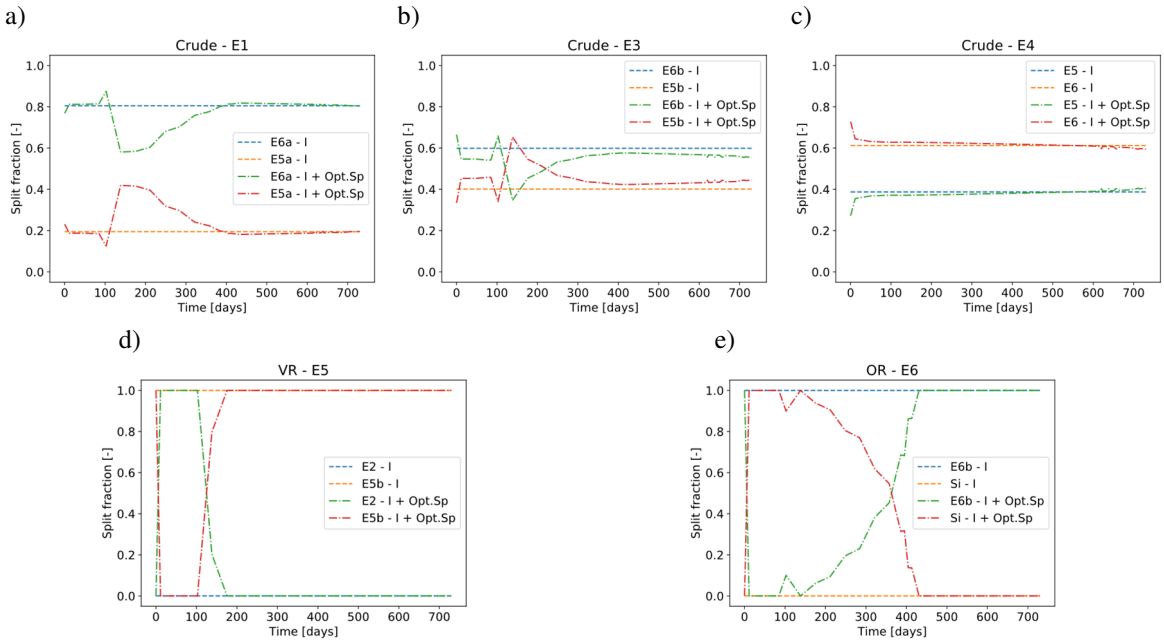

Figure 6.13. Optimal and constant flow distribution of retrofit alternative I of case NR-B. a) crude branch 1, b) crude branch 2, c) crude branch 3, d) VR bypass, e) OR bypass.

The effects of the dynamic flow optimization of retrofit alternative I are observed in the heat duty and fouling resistance of each exchanger, Figure 6.14 and Figure 6.15, respectively. First, the fouling resistance is always lower when the flows are dynamically distributed than when they are constant. Lower fouling resistances are achieved because of the modifications of the wall temperature and of the shear rate that promote lower fouling rates and deposit removal. Second, during the first 100 days of operation almost no fouling is observed in exchangers E5a-b and E6a-b as they are idle for any practical purpose – no hot stream. Third, the duty of the exchangers at the end of the network is always higher when the flow distribution is optimized. Lower fouling resistances and higher temperature difference between the hot and cold streams facilitate heat recovery. Fourth, during the period where the flow split and bypasses change dynamically – between 100 and 450 days of operation – the heat duty of E5a-b and E6a-b starts increasing and reaches a maximum, then it stabilizes at a value higher than that in the network retrofit with constant flow rates. Finally, the optimal flow distribution obtained for retrofit alternative I is equivalent to having some exchangers idle at the beginning of the operation, and then becoming active with varying inlet streams, so there is still an open question of whether those exchangers are beneficial for the overall operation of the network considering their capital cost.

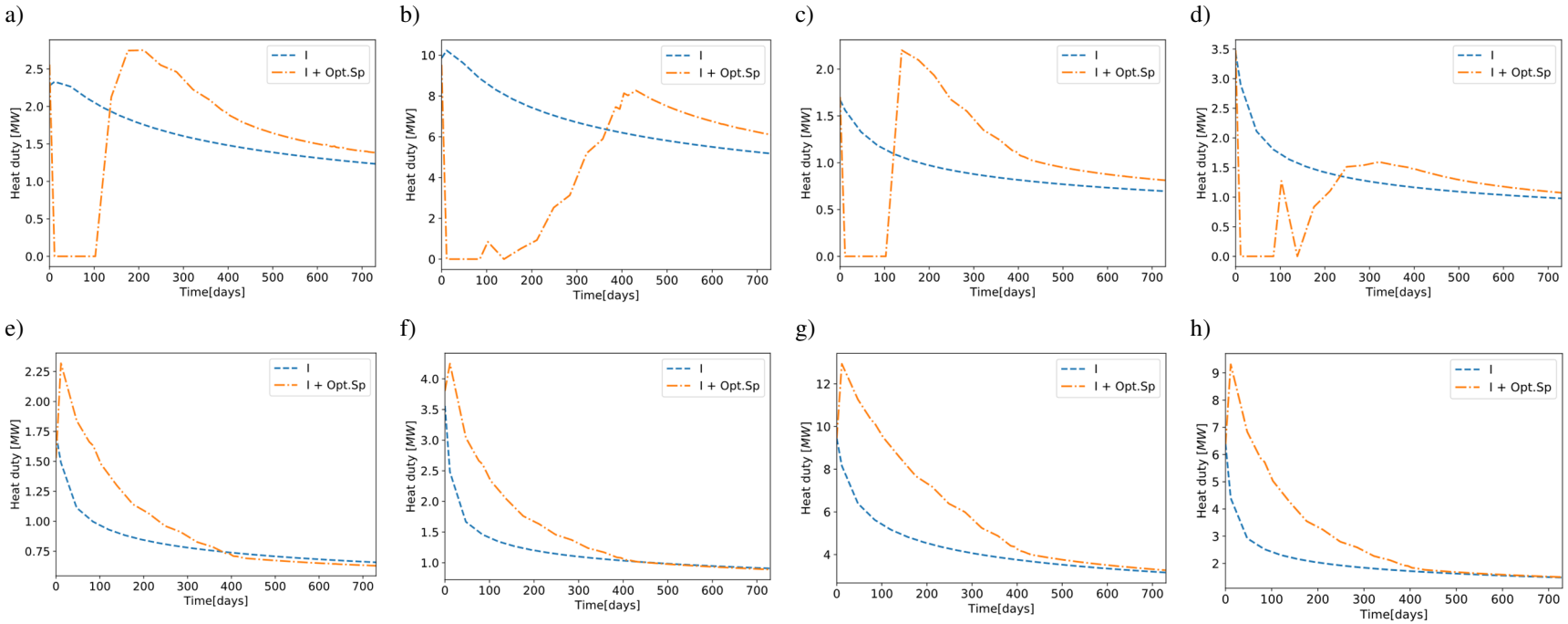

Figure 6.14. Exchanger heat duty of retrofit alternative I of case NR-B optimizing the flow distribution. a) E5a, b) E6a, c) E5b, d) E6b, e) E5, f) E6, g) E3, h) E4.

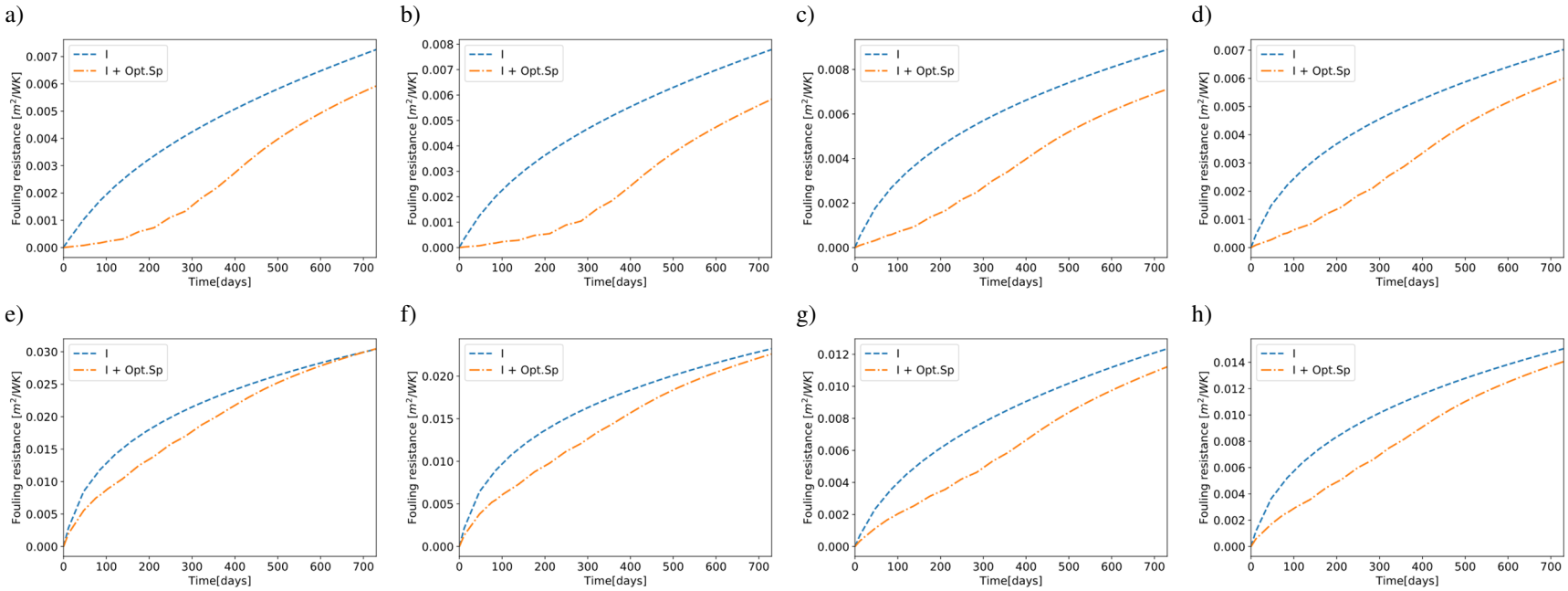

Figure 6.15. Exchanger fouling resistance of retrofit alternative I of case NR-B optimizing the flow distribution. a) E5a, b) E6a, c) E5b, d) E6b, e) E5, f) E6, g) E3, h) E4.

6.3.2.2. Optimal retrofit and flow distribution without cleanings

The previous analysis aimed to highlight the complex interactions among network retrofit, dynamic flow distribution and fouling, now the full optimal network and HTA retrofit problems are solved without cleanings. Figure 6.16 presents the optimal furnace duty of the retrofit schemes: network retrofit with constant flow distribution (HEN retrofit – constant), network retrofit with dynamic flow distribution (HEN retrofit – dynamic), and network and HTA retrofit with dynamic flow distribution (HEN-HTA retrofit). All schemes reduce significantly the operating cost of the network and perform better than the base case, and than the retrofit alternatives I and II. Even considering the capital cost of new units and modification of heat transfer area in the total cost of the operation, these optimal retrofit alternatives produce savings of $ 0.5 M to $ 1.5 M where the highest is that of HEN-HTA retrofit.

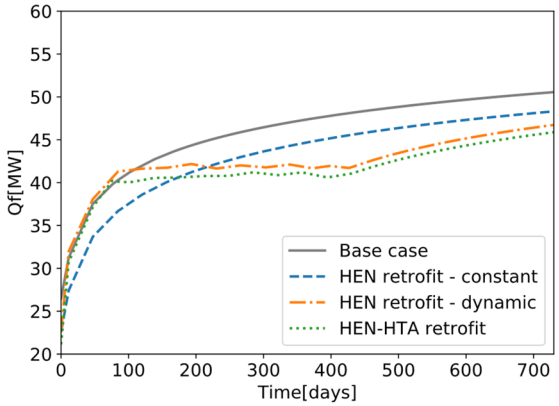

Figure 6.16. Furnace duty for optimal network retrofit alternatives of case NR-B without considering cleanings.

The optimal network retrofit structure obtained for the three retrofit schemes considered is presented in Figure 6.17. None of the optimal network configurations correspond to alternatives I or II proposed by Yeap et al. (2005), instead they are combinations of those alternatives and new configurations arising from the use of the superstructure to represent the problem. For instance, in the optimal network obtained for the scheme HEN retrofit – constant (Figure 6.17a), the VR stream is split in two parallel branches going to E2 and E5b after leaving E5, which introduces additional bypasses that were never considered in retrofit alternatives I and II. Additionally, the optimal solution of the scheme HEN retrofit – dynamic (Figure 6.17b) adds a bypass to the OR stream diverting the flow

from E6b, while the rest of the network remains the same as the optimal one for the scheme HEN retrofit – constant.

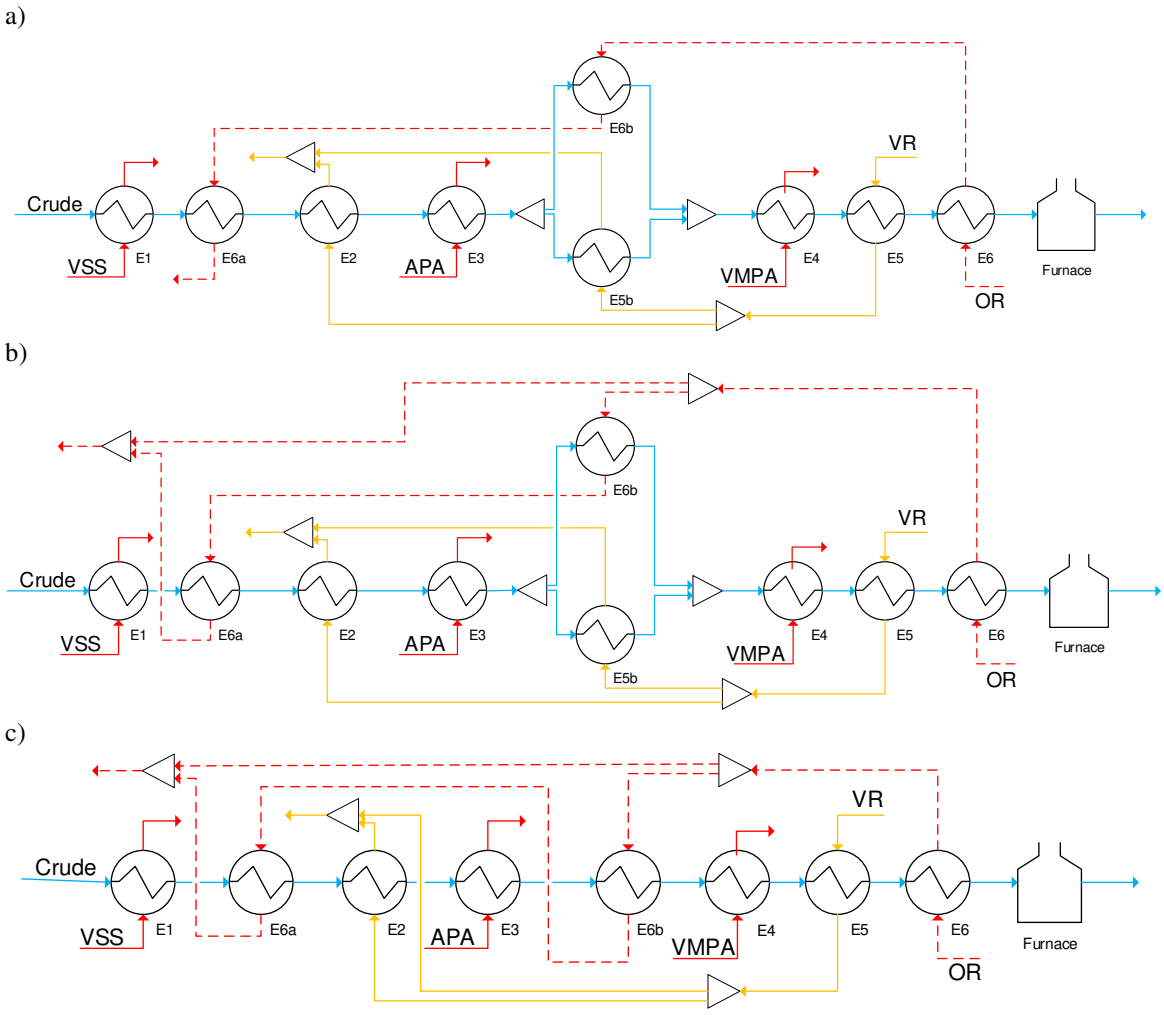

Figure 6.17. Optimal network retrofit without considering cleanings for case NR-B. a) optimal retrofit with constant flows (HEN retrofit – constant), b) optimal retrofit with dynamic flow distribution (HEN retrofit – constant), c) optimal network and HTA retrofit with dynamic flow distribution (HEN-HTA retrofit).

Including HTA retrofit decisions in the optimization problem modifies the optimal structure of the network, and E5b is removed from it (Figure 6.17c). The rest of the network is the same as the optimal one of the scheme HEN retrofit - dynamic. The area of all active exchangers, except E1, is increased by 50% which increases the heat recovery and reduces the furnace duty. The extra area of all exchangers, and the capital cost associated with it, make adding E5b to the network unnecessary and detrimental for the network performance

and cost. Dynamic flow distribution is also considered here, and the trends observed in the furnace duty are similar to those obtained with the scheme HEN retrofit – dynamic (Figure 6.16), but it is always lower for this case. In the case of HEN-HTA retrofit scheme, the bypasses of the hot streams are used to make E2 and E6a-b idle at the beginning of the operation, reducing their overall fouling rate and increasing the heat duty of the exchangers at the end of the network. These exchangers only become active after 100 days of operation when the flow rate of the hot streams increases dynamically.

The interactions between the network retrofit decisions and the dynamic flow control are important and should not be neglected. The split fraction of each of the splitters in the optimal retrofit structures, without HTA retrofit, are presented in Figure 6.18. These are the retrofit schemes HEN retrofit – constant, and HEN retrofit – dynamic. The crude flow rate through the parallel branches react dynamically to the changes on the hot stream. The VR stream is diverted completely to E5b during the first 200 days of operation causing E2 to be idle, but then the flow is distributed between the two exchangers. A similar behaviour is observed for the OR stream that completely bypasses E6b during the first 100 days of operation, then it changes dynamically to reduce fouling rates in the exchangers, and finally all the flow is diverted to E6b. The dynamic flow distribution of the optimal network retrofit has similar effects as those of the retrofit alternative I (I + Opt. Sp). The duty of exchangers located at the end of the network is always higher under dynamic flow distribution than under constant flow. Some exchangers are idle at the beginning of the operation, increasing the furnace duty and reducing the fouling rates, and then the flows are distributed such that heat recovery is maximized over long operating periods while the fouling resistance of each unit is always kept lower than that observed for constant flow rates.

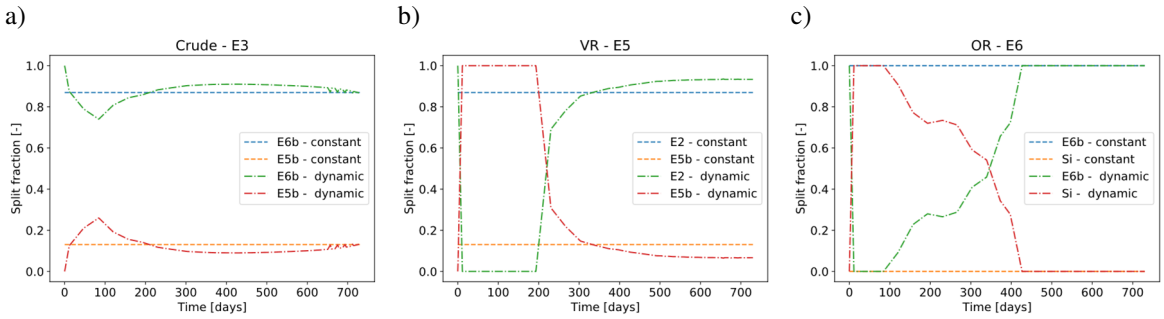

Figure 6.18. Flow distribution, constant or dynamic, of the optimal network retrofit of case study NR-B. a) crude branch, b) VR bypass, c) OR bypass.

6.3.2.3. Optimal retrofit, flow distribution and cleaning scheduling

Optimal cleanings are included in the optimal retrofit schemes. This problem is more complex than those addressed before because it has more binary variables. The two years time horizon is discretized using 20 periods of variable length. The MINLP problem has a total of 245 binary variables, 30720 continuous variables, 25493 equality constraints, and 62661 inequality constraints. Nevertheless, it is solved in 343 min of computational time using the MPCC reformulation approach. Including HTA retrofit decisions in this optimization problem is not a challenge as they are modelled as bounded continuous variables and the computational time does not change significantly.

Figure 6.19 presents the optimal network structure obtained when solving the network retrofit and cleaning scheduling problem. This optimal structure does not change when optimal HTA retrofit decisions are included. The optimal retrofit structure only includes E6a-b in the network, and all the units are arranged in series. There are no parallel branches or bypasses in this optimal structure, so there are no control degrees of freedom to modify the flow distribution of the network dynamically, although this possibility was explicitly considered in the problem superstructure. This network structure was not considered in retrofit alternatives I or II, although it is similar to alternative II, but the flow direction of the OR and VR streams is different and different units are added to the network.

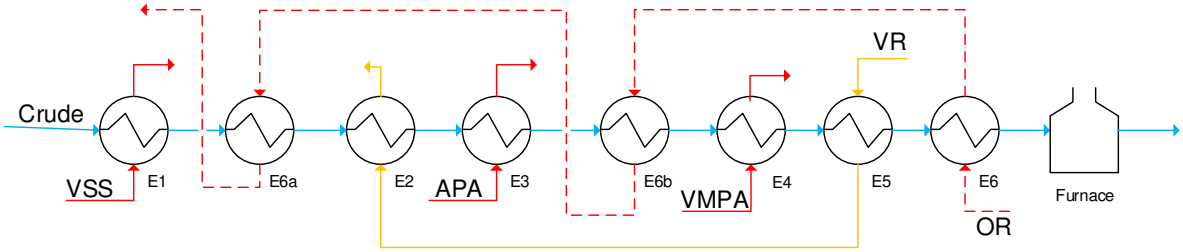

Figure 6.19. Optimal network retrofit for case NR-B considering simultaneous optimization of the cleaning schedule (with and without HTA retrofit).

Figure 6.20 shows the furnace duty of the optimal retrofit scenarios including cleanings and flow distribution in the problem formulation. They are: 'HEN retrofit' that considers network retrofit, cleaning scheduling, and flow distribution; and 'HEN-HTA retrofit' that beyond those decisions also considers area retrofit. The optimal retrofit networks perform better than the base case despite the temporarily increase of the furnace duty when units are idle during cleanings. In the optimal network structure, the HTA of all active exchangers is

increased, except that of E1, increasing the overall energy recovery. Figure 6.21 compares the HTA retrofit for the optimal structure obtained with cleanings (suffix SCH, Figure 6.19), and without cleanings (which structure is shown in Figure 6.17c). Both optimal network structures have the same exchangers and they only differ in the bypasses of the VR and OR streams. When the cleaning schedule is optimized simultaneously with the network structure, the HTA does not increase as much as when cleanings are not considered – see for instance E2 and E6a in Figure 6.21. This indicates that periodic cleanings reduce the need of additional area as the exchangers do not operate at high fouling conditions during long periods.

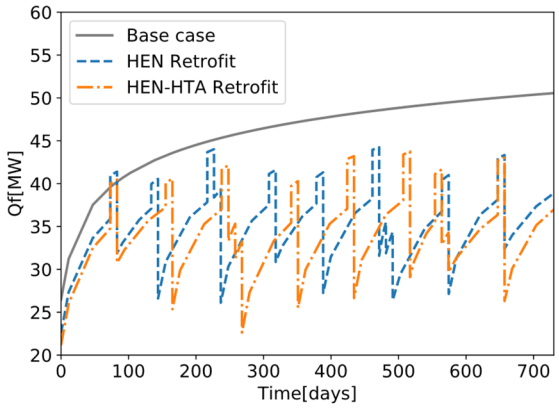

Figure 6.20. Furnace duty for optimal network retrofit alternatives of case NR-B including optimal cleaning scheduling.

Figure 6.21. Optimal HTA retrofit for each exchanger with and without fouling mitigation for case NR-B.

There is an important trade off among the cleaning cost, the capital cost of extra area, and the future savings in energy cost that arise from the interaction of retrofit and cleaning

decisions, and that is implicitly considered in the formulation of the optimization problem. The interaction of cleanings and retrofit options is observed in the optimal cleaning schedule, Figure 6.22, obtained simultaneously with the optimal network structure. This figure shows the optimal cleaning schedule for the optimal networks with and without HTA retrofit, and the exchangers that are added or removed from the network. Exchangers added to the network, E6a-b, are cleaned twice during the operation. Although the network structures of 'HEN retrofit' and 'HEN-HTA retrofit' are the same, increasing the HTA of key exchangers affects the optimal cleaning schedule of the network. Cleanings of exchangers with extra HTA usually starts later during the operation, or the number of cleanings of those exchangers increases. For instance, E3 is cleaned two more times and E2 is cleaned one more time when their HTA is increased. Comparing the optimal HTA retrofit with and without cleanings (Figure 6.21), the area of E2 is increased by 18% instead of by 50%, and it is cleaned once during the operation. In this case, it indicates that the cost of a single cleaning and the energy savings associated with it compensates for the reduction of the HTA.

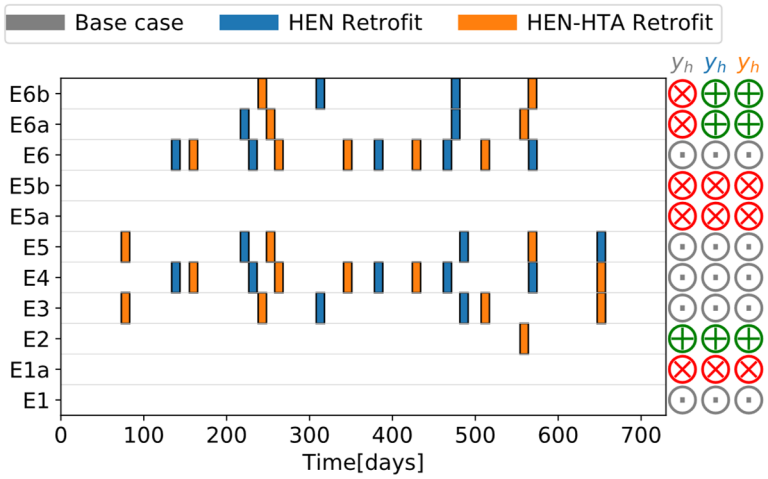

Figure 6.22. Optimal cleaning schedule of case study NR-B considering network retrofit (HEN retrofit) and network and area retrofit (HEN-HTA retrofit). (X: exchanger removed, +: exchanger added, ▪ exchanger fixed).

The total cost of operating the network NR-B is calculated and compared for each retrofit alternative evaluated so far. The total operating cost, and capital cost of each alternative are presented in Figure 6.23. The total cost of all optimal retrofit alternatives is lower than that of the retrofit alternatives I or II, and a significant reduction is observed when

the retrofit decisions are optimized and integrated with fouling mitigation decisions. While the retrofit alternatives I and II only reduce the operating cost, either by increasing heat recovery or reducing fouling rates, they ignore the capital cost and the interaction between design retrofits of the network and its operation. On the other hand, the optimal retrofit approach presented provides a holistic view of the problem considering all interactions of the variables. Compared to the base case, the optimal network and HTA retrofit with cleanings has potential savings of $ 4.2 M over the two years operation, while the case without cleanings has savings of $ 1.5 M – the reduction in operating cost alone for this case is $ 2.3 M. Also, dynamic control of the flow distribution, when possible, reduces the operating cost of the network even further, although when considering simultaneously with the optimal retrofit problem it does not alter the structure of the network and it only defines new bypass streams for certain units.

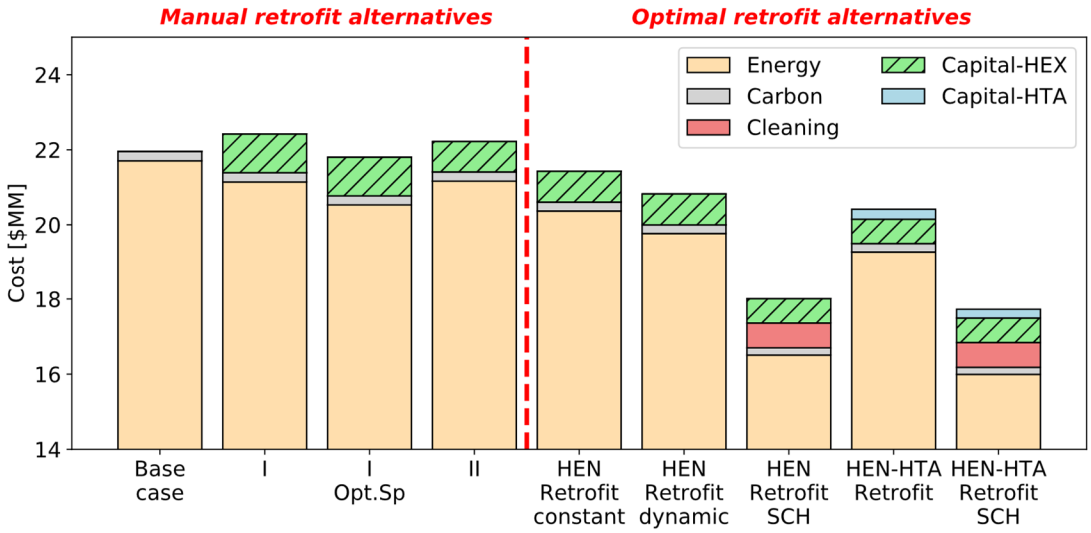

Figure 6.23. Total cost of all retrofit alternatives, manual and optimal, of case NR-B.

6.4. Concluding remarks

A novel mathematical formulation has been introduced for the optimal and simultaneous retrofit and fouling mitigation of HEN. This formulation is an extension of the optimal cleaning scheduling problem achieved by associating the binary variables of the cleanings with those used in the definition of the existence of new units in the network. New connections among the units of the network are modelled using a superstructure that defines

multiple alternatives with additional mixers and splitters. The superstructure representation also allows the dynamic optimization of the flow distribution in the network, and its integration with optimal retrofit and cleaning scheduling decisions. For the first time, optimal retrofit, scheduling, and control decisions are integrated at the same level, exploiting their interactions to mitigate fouling and to maximize the energy recovery in the network.

Despite the complexity and large scale of the MINLP problem associated with the optimal retrofit, cleaning schedule, and control of HEN, it is solved efficiently because the problem formulation is inherited from the optimal cleaning scheduling problem. It was demonstrated in Chapter5 that the optimal cleaning scheduling problem could be solved in reasonable time using a MPCC reformulation.

Two cases studies taken from the literature that address the problem of network retrofit under fouling are revisited here. It is demonstrated that the optimization of the network retrofit and its integration with optimal fouling mitigation actions improves the overall performance compared to those of other alternatives including retrofit options based on pinch technology, expert knowledge, or heuristics aiming to mitigate fouling. The first case study, NR-S, analyses the placing of a single unit in a network, and proves that the optimal solution is not to include it in the network, because it incurs higher cleaning cost during operation compared to the capital cost of increasing the overall heat transfer area. The second case study, NR-B, involved five units for retrofit and the possibility to split some streams in parallel branches and bypasses. This case proves that if the dynamic flow distribution is considered at the level of the retrofit decisions, the effects of fouling over long periods can be mitigated, improving the performance of the network.

Other retrofit options not considered here, like the use of heat transfer enhancement technology, can be included in the optimization problem if an accurate mathematical representation of their effects on the flow patterns and heat transfer rates are available.

The optimal retrofit and fouling mitigation problem is solved for nominal operating conditions, although it is well known that the operation of preheat trains is highly variable and dynamic. Future work should consider the uncertainty on the operation of preheat trains, their effect on optimal retrofit decision to guarantee a profitable operation over long periods, while minimising the capital investment associated with new units or extra area.

Chapter 7

Online optimization of preheat trains: integration of flow control and cleaning scheduling

The operation of refinery preheat trains is subject to large variability and uncertainty arising from their operating conditions, the crude blend processed and its properties. This variability has a significant impact on fouling and on the performance of preheat trains, but it has been usually ignored when deciding on fouling mitigation alternatives. For the first time an online optimization-based fouling mitigation approach is developed and validated here. It uses a multi-loop advanced control strategy to optimally define the cleaning actions and the dynamic flow distribution in the network, based on the predictions of an accurate model that is updated at regular intervals accordingly to the data available. The proposed online fouling mitigation approach is tested on a real case study and its performance compared with the actual operation of the preheat train. It is demonstrated that the online approach can cope with the large variability of the process and that it reduces significantly the operating cost. Finally, the methodology is applied to a series of scenarios with large disturbances, extreme cases of model-plant mismatch, and tested with different settings of the feedback loops to show its applicability, advantages, and the effect of the main variables and parameters.

7.1. Introduction

The mathematical formulation of the optimal cleaning scheduling and dynamic flow distribution of HEN under fouling presented in Chapter 3 was validated and used to solve problems relevant to industrial applications in Chapter 5. However, one of the main

assumptions so far is that the inputs of the system – flow rates, streams temperature, and properties of the crude oil – are constant over time, which is not accurate in refineries. In refining operations, the flow rate of crude, and hence those of all other streams in the process, changes frequently depending on the production targets and the market (Mozdianfard and Behranvand 2013; Nategh, Malayeri, and Mahdiyar 2017). Moreover, refineries can store crude from different geographical locations and then blend them accordingly to meet their requirements. Crude from different sources has different physical properties, sulphur content, yields, and fouling propensity – usually associated with the content of asphaltenes (Ho 2016b; Bennett 2012). Ignoring all these sources of variability when deciding on fouling mitigation operations can have severe consequences. For instance, if the cleaning frequency is defined based on high flow rates – low cleaning frequency as fouling may not be too severe – then when the flow rates decrease and the cleaning frequency is not modified, the fouling rate increases and the operation may become unfeasible, reaching pressure or thermal limits. Hence, the variability and uncertainty of the operation must be considered when deciding on operation alternatives or fouling mitigation actions.

Predictive models for HEN under fouling are usually defined for a small range of operating conditions and their validity is limited to the data used for their estimation (Costa et al. 2013). In the context of varying operating conditions, and processing crudes with unknown fouling characteristics, a single model may not be accurate enough for all ranges of operation. Operating or maintenance decision based on a predictive model determined for a specific data set may rapidly become invalid as the operating point of the system changes. Because of this variability, it is not possible to know with certainty the potential benefits of fouling mitigating actions, or the future state of the system. The complexity of the crude oil fouling phenomenon makes it challenging for a single model to capture accurately all interactions in all possible operating conditions, so there is need of models that can be adapted online based on the behaviour of the system, and on the measurements available.

Heuristic approaches that have been used to define the cleaning schedule of heat exchanger networks can, in principle, be used online to response to changing operating conditions. Although these heuristics are available, they ignored process variability and have only been used to define cleaning actions under nominal conditions once and offline for long horizons (Ishiyama et al. 2010; Ishiyama, Paterson, and Wilson 2009). Alternatively,

optimization based approaches have been used online, in a receding horizon scheme, to define the operation of evaporation systems – heat exchanger networks. In those cases, the optimization of the system and the cleaning time have been decoupled and solved sequentially, first defining the operating conditions and then the cleaning cycle of each unit individually, while using plant data to update the models – a state space representation of the operation and an empirical model for fouling (Pitarch Pérez, Gomez Palacin, and Prada Moraga 2017; Pitarch et al. 2017). Optimization approaches like this one consider process variability explicitly in a feedback loop, but oversimplified the representation of the problem and ignore the network effects and interactions when defining the cleaning actions.

Considering process variability within an integrated optimal control and scheduling application to mitigate fouling should, in principle, bring significant benefits to the operation. In this chapter, a multi-loop feedback control approach is presented to optimally control the flow rates and define the cleaning schedule of HEN under fouling. The repeated sampling allows to update the predictive models based on the information available, and the feedback approach corrects the optimal decisions accordingly to the variability and disturbances.

7.2. Multi-loop MHE/NMPC for fouling mitigation

The online optimization approach of the cleaning schedule and dynamic flow distribution of HEN under fouling is based on advanced control strategies. It defines two feedback control loops, one for the fast dynamics of the process associated with flow distribution, and another for the slow dynamics associated with fouling and cleaning. A single feedback loop cannot cope properly with the two time scales without sacrificing the accuracy and validity of the decisions. Figure 7.1 shows a block diagram of the control loops, their components and interactions. This implementation follows dual control principles in which each feedback loop deals with a specific time scale of the process, although here the outer loop correspond to an integrated scheduling and control problem. Each of the loops has two components: a nonlinear model predictive controller (NMPC) to optimize the operation of the network, and a moving horizon estimator (MHE) to update the model parameters based on the latest data. The NMPC controllers of each layer are economic oriented aiming to minimize the operating cost of the process, and it is expected for a time varying operation to

perform better than steady state solutions because the high variability of the process (Ellis, Liu, and Christofides 2017).

In each of the stages of the block diagram presented in Figure 7.1 an optimization problem is solved using an accurate model of the system based on the mathematical formulation developed in Chapter 3. Variations of this formulation where certain variables are fixed, or the objective function is modified, are extensively used in the proposed online framework. There are also disturbances that affect the whole system, and their effect is considered explicitly in the control scheme proposed. Using two feedback loops that interact with each other allows to capture all the time scales of the process, and to optimally react to the different levels of variability and uncertainty that exists in the operation.

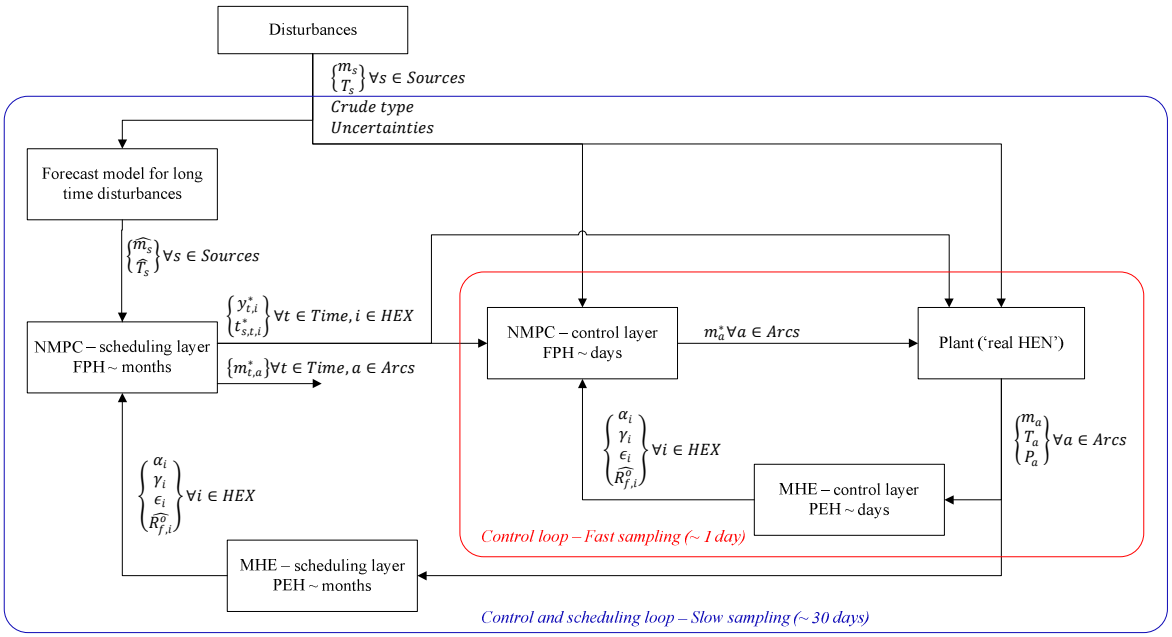

Figure 7.1. Representation of the online, integrated optimal cleaning scheduling and control of HEN subject to fouling and disturbances.

At the core of each feedback loop there is a NMPC controller and an MHE estimator. Figure 7.2 shows how they operate on a moving horizon, and how they constantly update the model parameters, and the actions taken on the process. At each sampling time, t^*, first, the MHE problem is solved over a past estimation horizon (PEH) to determine the model parameters that best describe the plant measurements observed and to estimate the current conditions of the system; and then the NMPC problem is solved over a future prediction horizon (FPH) to minimize the operating cost and determine the future actions – flow

distribution and/or cleanings – to take. The solution of the NMPC problem includes all future realization of the manipulated variables, but only the first one is implemented and all other are discarded because the predictions may change given the disturbances and uncertainties. At the next sampling time ($t = t^* + \Delta t$) the procedure is repeated, a new MHE and a new NMPC are solved based on the current states of the system. This rolling horizon approach improves the estimation obtained with the MHE, as new and more recent information is included in the problem every time. It also improves the predictions and actions determined with the NMPC controller because it is updated accordingly to the current state of the system (Zavala and Biegler 2009; Allgöwer et al. 1999; Meadows and Rawlings 1997; Robertson, Lee, and Rawlings 1996; Bemporad 2009).

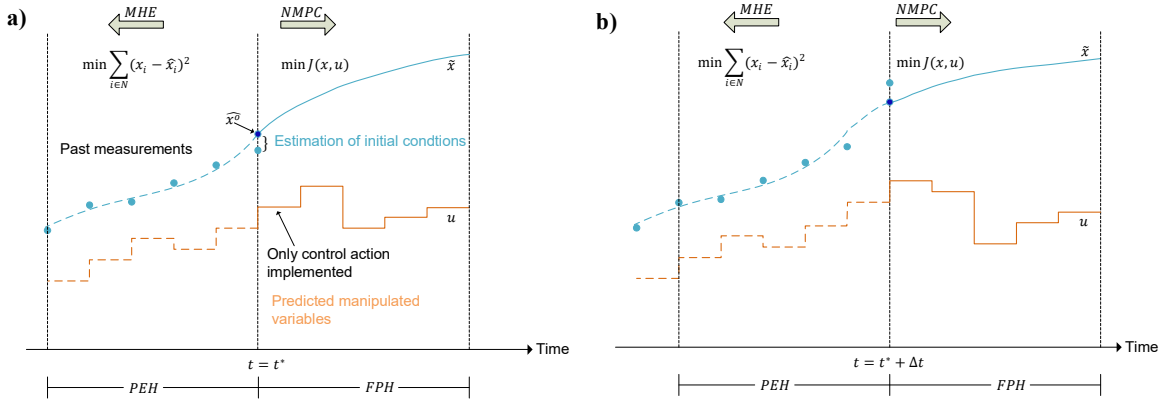

Figure 7.2. Schematic representation of a moving horizon for NMPC and MHE. Past measurements and predictions at $t = t^*$ (a), and at $t = t^* + \Delta t$ (b).

Each feedback loop of the online methodology follows the same principles, using an MHE for parameter estimation, and a NMPC for optimization, but their assumptions, inputs, and outputs are different. The specific optimization problems, their assumptions, and the flow of information of each of the control loops of the online fouling mitigation methodology are described next.

7.2.1. Flow distribution feedback loop

The flow distribution feedback loop is that within the red box in Figure 7.1. It deals with the fast dynamics of the process and the sampling time of this loop is of the order of days or shorter. The main objective of this loop is to reject the disturbances of the system by

optimally modifying the flow distribution in the network. The elements of this feedback loop are identified with the subscript C.

The MHE_C problem solved in this feedback control is defined in Eq. (7.1). The objective function is the same as that used in Chapter 4 for parameter estimation and model validation, and the weights in the errors are the same as those used before. It minimizes the quadratic error between the main measurements of the network – tube side outlet temperature, shell side outlet temperature, and tube side pressure drop for each heat exchanger– subject to the model of the HEN and fouling considering all operating constraints. The past estimation horizon, PEH_C, is represented using a discrete time approach because it is assumed that all past measurements are recorded at regular intervals. This optimization problem is an NLP, and discontinuities observed arising from previous cleanings or disturbances are considered explicitly in the model as changes in the operating mode. These transitions can be easily modelled using the formulation presented in Chapter 3 and fixing the realization of the binary variables associated with the state of each heat exchanger in the network. Finally, the solution of the MHE_C defines for each exchanger in the network the parameters of the fouling model – deposition and removal constants – , the surface roughness, and an estimation of the fouling resistance at the current time.

$$\min_{\alpha,\gamma,\epsilon,R_{f0}} \sum_{i=1}^{N_{HEX}} \sum_{j=1}^{PEH_C} \left[w_{T^T} \left(\widetilde{T^T}_{i,j} - T^T_{i,j} \right)^2 + w_{T^S} \left(\widetilde{T^S}_{i,j} - T^S_{i,j} \right)^2 + w_P \left(\widetilde{\Delta P}_{i,j} - \Delta P_{i,j} \right)^2 \right]$$

$$s.t.$$

$$\begin{aligned} &Network\ representation - Section\ 3.2.1 \\ &Heat\ exchanger\ model - Section\ 3.2.2 \\ &Fouling\ model - Section\ 3.2.3 \\ &Operating\ mode\ disjunctions - Section\ 3.2.4 \\ &Operational\ constraints - Section\ 3.2.5 \\ &Discrete\ time\ representation\ and\ time\ related\ constraints - Section\ 3.3.1 \end{aligned} \tag{7.1}$$

The model parameters thus estimated are used in the $NMPC_C$ formulation to optimize the operation of the network over the FPH_C. The optimization problem solved here is summarized in Eq. (7.2), and is a large scale NLP. The objective function is an economic objective function, so that the NMPC is defined as an economic-oriented controller instead of using the usual set point tracking definition. A set point tracking formulation is not suitable for this application because the aim here is to maximize the temperature at the end of the network – equivalent to maximize energy recovery – instead of controlling it at a specific value. The objective function only includes the elements associated with energy cost, carbon

cost, and production profit, and it ignores the cleanings cost because at this level – fast dynamics and frequent updates – the time scale is too short for cleanings to have a significant effect. They are therefore assumed to be known in the FPH_C. The definition of the cleanings is done by fixing the binary variables of the original formulation so that they become parameters in this problem. The solution of the $NMPC_C$ problem defines the optimal flow distribution of the network, which includes the optimal flow split of parallel branches, bypasses, and the optimal inlet flow rate of hot streams that can be controlled.

$$\begin{aligned}
&\min_{m_a}\left(P_f\int_0^{FPH_c}Q_f\,dt+P_{CO}K_{CO}\int_0^{FPH_c}Q_f\,dt-P_m\int_0^{FPH_c}m_f\,dt\right)\\
&s.t.\\
&Network\ representation-Section\ 3.2.1\\
&Heat\ exchanger\ model-Section\ 3.2.2\\
&Fouling\ model-Section\ 3.2.3\\
&Operating\ mode\ disjunctions-Section\ 3.2.4\\
&Operational\ constraints-Section\ 3.2.5\\
&Discrete\ time\ representation\ and\ time\ related\ constraints-Section\ 3.3.1
\end{aligned}\tag{7.2}$$

The two optimization problems considered in the fast feedback loop are NLPs, the one associated with the MHE_C defines the model parameters used in the $NMPC_C$ to optimize the dynamic flow distribution in the network. There are no decisions associated with the cleanings of units in this feedback loop as they are optimally defined by the outer loop and become set parameters for the inner loop. The main factors affection the scheduling and cleaning decisions are associated with the slow dynamics of fouling, and the cumulative effect of the operating variables over long periods, features that are not capture in the FPH_C.

7.2.2. Cleaning scheduling feedback loop

The cleaning scheduling feedback loop is that within the blue box in Figure 1.1. It deals with the slow dynamics of the process, the interactions between control and scheduling decisions, and it uses a longer sampling time than that of the flow control feedback loop. The main objective of this loop is to define the optimal cleaning schedule of the network over long operating periods, while considering the variability of the system and the interactions between scheduling and control. The elements of this feedback loop are identified with the subscript S.

The MHE_S problem solved in this feedback loop, Eq. (7.3), is similar to the previous one, and it uses the same weights in the objective function as those defined in Chapter 4.

Both formulations use the same objective function and set of constraints, but the main difference is that the PEH_S is much larger than the PEH_C. The data set use for estimation in the scheduling layer is much larger and has much more variability over long operating periods than that of the flow control layer. This difference is necessary because the parameters estimated at each layer are used in models that serve different purposes. While the flow control layer models optimize the current operation of the network, and deals with fast disturbances, the scheduling layer model defines the future cleaning actions over longer operating periods and must consider the overall variability observed in the system, not just the current disturbances. The MHE_S is an NLP that defines the fouling parameters, and estimates the current fouling resistance for the predictive model used in the optimal cleaning scheduling problem.

$$\begin{aligned}
&\min_{\alpha,\gamma,\epsilon,R_{f0}} \sum_{i=1}^{N_{HEX}} \sum_{j=1}^{PEH_S} \left[w_{T^T} \left(\widetilde{T^T}_{i,j} - T^T_{i,j} \right)^2 + w_{T^S} \left(\widetilde{T^S}_{i,j} - T^S_{i,j} \right)^2 + w_P \left(\widetilde{\Delta P}_{i,j} - \Delta P_{i,j} \right)^2 \right] \\
&s.t. \\
&Network\ representation - Section\ 3.2.1 \\
&Heat\ exchanger\ model - Section\ 3.2.2 \\
&Fouling\ model - Section\ 3.2.3 \\
&Operating\ mode\ disjunctions - Section\ 3.2.4 \\
&Operational\ constraints - Section\ 3.2.5 \\
&Discrete\ time\ representation\ and\ time\ related\ constraints - Section\ 3.3.1
\end{aligned} \tag{7.3}$$

$$\begin{aligned}
&\min_{y,m_a} \left(P_f \int_0^{FPH_S} Q_f dt + P_{CO} K_{CO} \int_0^{FPH_S} Q_f dt + \sum_{i \in HEX} P_{cl,i} \sum_{t \in T} y_{i,t} - P_m \int_0^{FPH_S} m_f dt \right) \\
&s.t. \\
&Network\ representation - Section\ 3.2.1 \\
&Heat\ exchanger\ model - Section\ 3.2.2 \\
&Fouling\ model - Section\ 3.2.3 \\
&Operating\ mode\ disjunctions - Section\ 3.2.4 \\
&Operational\ constraints - Section\ 3.2.5 \\
&Continuous\ time\ representation\ and\ time\ related\ constraints - Section\ 3.3.2
\end{aligned} \tag{7.4}$$

The $NMPC_S$ problem solved is summarized in Eq. (7.4). It is a large scale MINLP that minimizes the total operating cost by defining the optimal cleaning schedule and the optimal flow control over the FPH_S. The objective function includes the cleaning cost, and all the operating costs because this problem considers explicitly the cleaning decisions. Contrary to the NMPC problem of the flow control layer, this one is much more challenging to solve because of the large number of binary variables and feasible cleaning schedules with similar performance. Nevertheless, it can be solved efficiently and in real time using the solution strategy of Chapter 5.

The solution of the $NMPC_S$ problem gives the optimal cleaning schedule over the FPH_S, but only that section of the schedule defined between the current time and the next sampling time is passed on, as fixed values, to the flow control layer, and implemented in the actual plant. This makes the methodology reactive to the uncertainty and future variability of the operation. Another important output the $NMPC_S$ solution is the dynamic profiles of the flow rate distribution, which is determined simultaneously with the optimal cleaning schedule, although this part of the solution is discarded and not implemented in the plant. That flow distribution obtained at the scheduling layer is based on average predictions of the operating conditions over long periods, but those conditions can rapidly deviate from their predictions, and the flow control layer can respond faster and in an optimal way to those changes. In summary, the scheduling layer optimizes simultaneously the cleaning schedule and flow distribution considering their interactions, but the actual optimization of the flow distribution based on the variability of the system is done at the flow control layer.

7.2.3. Overall methodology for online fouling mitigation

The flow control layer and the scheduling layer have strong interactions. The inputs to the flow control layer $NMPC_C$ are: the model parameters and initial conditions estimated in the MHE_C, the process disturbances, and the cleaning actions and starting cleaning times defined by the scheduling layer. The inputs to the $NMPC_S$ are similar: the model parameters and initial conditions estimated in the MHE_S, and a forecast of the future inputs and disturbances of the process. In both layers, the MHE uses plant measurements which reflect the past states and past actions including control and scheduling decisions.

For each of the feedback control loops the following parameters must be specified:

- Future prediction horizon (FPH): future time for which a prediction model is solved to determine the optimal operating conditions. Since all the feedback loops have economic objective functions, the control horizon is equal to the FPH. In standard MPC formulations, the control horizon – the time where the manipulated variables vary – is shorter than the prediction horizon to ensure stability, and to reduce the variability in the inputs (Qin and Badgwell 2003).

- Past estimation horizon (PEH): the period from which plant measurements are taken for solving the parameter estimation problem, MHE. The PEH varies for each feedback loop capturing different dynamics.
- Disturbance forecast model: the most common disturbances in preheat trains are observed in the temperature and flow rates of the inlet streams, and in the composition of the crude which affects its fouling propensity. The formers are measured, the latter typically not. All have significant effects on the operation, and on the solution of related optimization problems. Hence, an accurate forecast of these disturbances improves the quality of the solution of the optimization problems. For the flow control layer, a constant forecast of the disturbances is used so that they are fixed at their current value over the FPH_C, while for the scheduling layer a moving average forecast is used to estimate the disturbances based on the measurements of the previous month. Other forecast models could be used, for example those based on time series, but this is beyond the scope of this thesis.
- Time discretization: it refers to the number of periods used in the continuous time representation of the FPH of the scheduling layer. The number of periods defines the scale of the problem as it is associated with the number of binary variables used to model the cleanings of exchangers over time. Also, the number of periods should be representative for the length of the FPH, so that if a long prediction horizon is used, more periods are required to model the cleaning decisions correctly. This parameter only applies to the $NMPC$ problem of the scheduling layer. The flow control layer, and all the MHE problems use a discrete time approach with a time step equal to the sampling time of the inner loop feedback loop.

These parameters affect the overall performance of the online fouling mitigation methodology, the computational complexity of the associated optimization problems, and the ability of the framework to cope with process variability and large disturbances.

7.2.4. End of operation considerations

The online methodology presented assumes a continuous operation on a rolling basis, so that constant feedback helps the system to react to variability and disturbances. However, there are instances when the end time (t_{end}) of the operation is known. For example, a

planned turnaround of the refinery or a shutdown may be known in advanced so that any mitigation action such as cleanings close to this time will be counterproductive. To consider this sort of scenarios a shrinking horizon approach is implemented for each of the feedback loops (Gupta and Maravelias 2016). In this approach, each FPH is defined as $min\{FPH, t_{end} - t^*\}$ so that it is progressively shrank as the rolling horizon approaches the end time of the operation. Figure 7.3 compares two cleaning schedules for an illustrative example with two exchangers. In Figure 7.3a the schedule is defined with an open-end horizon approach, while in Figure 7.3b the shrinking horizon method is used to account for the end time of the operation. It also illustrates how the final cleaning schedule is constructed from the optimal solution of a series of optimization problems in a rolling horizon scheme: it shows which part of the schedule are implemented, and which part are discarded.

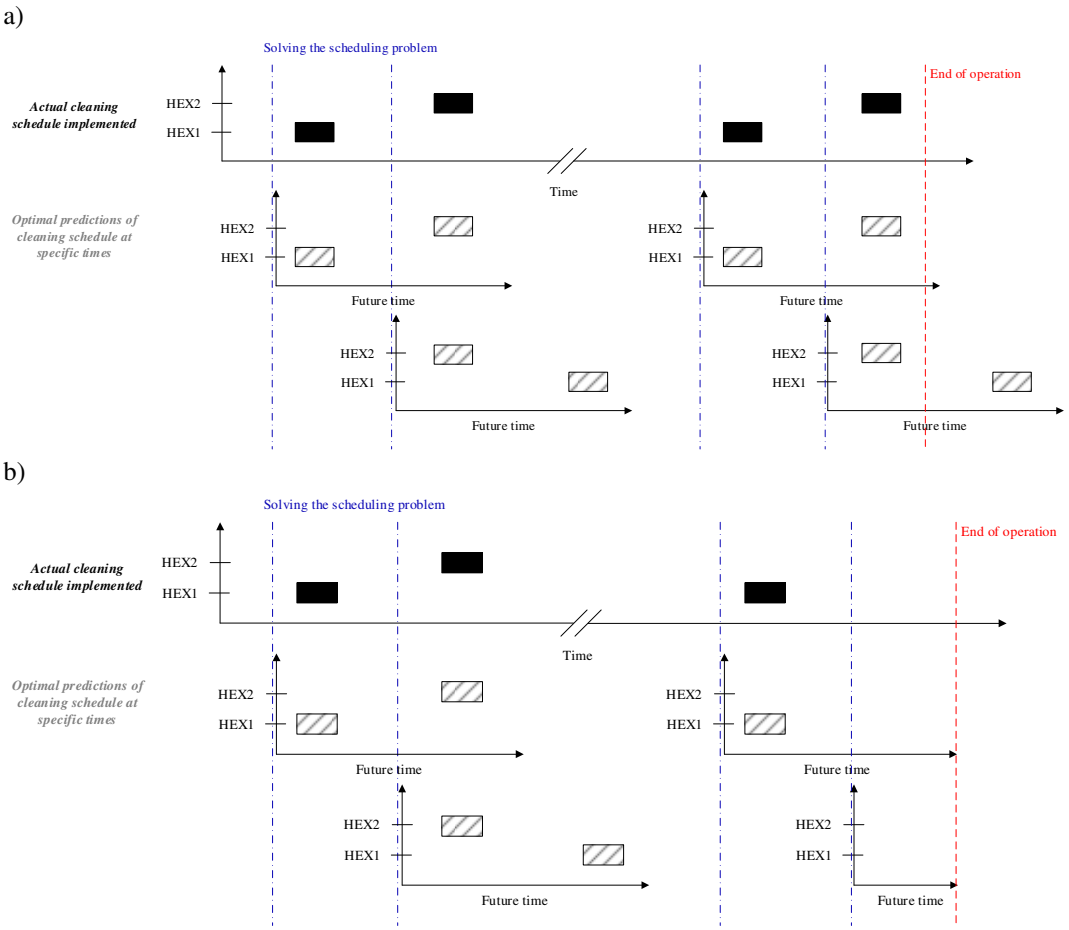

Figure 7.3. Representation of scheduling construction in rolling horizon scheme. a) assuming an open-end operation, b) shrinking horizon to account for the end of operation.

7.3. Online optimization of an industrial preheat train

The REF-X case study is used to demonstrate the benefits of the online fouling mitigation methodology proposed. The complete description of the case study can be found in Appendix A, and the network representation is presented again in Figure 7.4 for ease of reference. The network has five exchangers, of which four are double shell, and the crude oil flow is split in two parallel branches that are unbalanced. The split fraction in each branch is constrained to be between 30% and 70%.

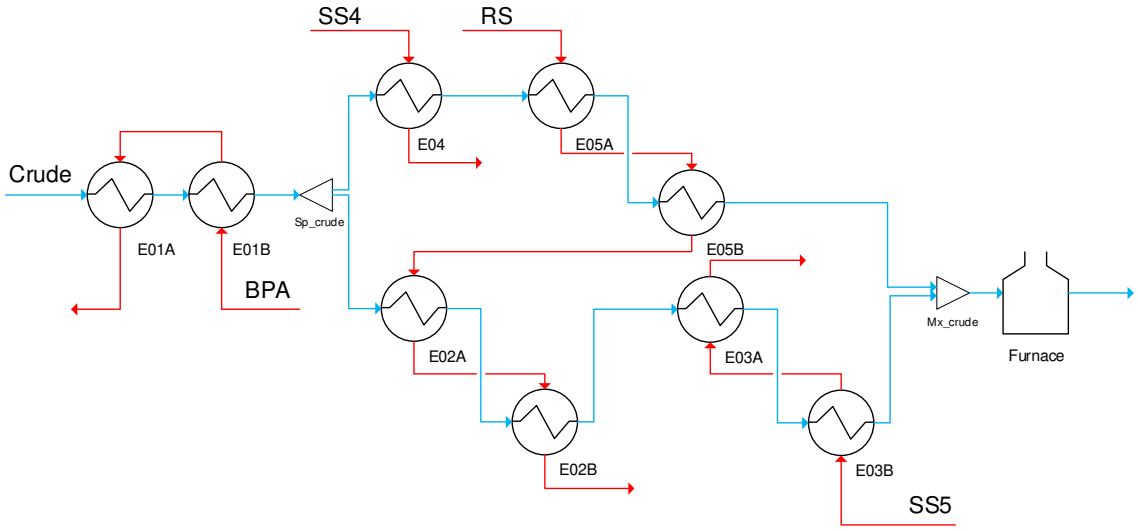

Figure 7.4. Network representation of REF-X case study used in the application of the online fouling mitigation methodology.

This case study is taken from an actual preheat train and measurements are available, as well as the actual cleaning actions implemented in the refinery. A data set of 3.4 years of operation is used in this application. It includes flow rates and inlet streams temperature measurements, which are used to characterize process variability and to define the disturbances. Figure 7.5 presents the actual inputs to the network. A large variability is observed in the flow rates, especially that of the crude stream. Also, the input variables are highly correlated. The flow rates of all hot streams are products of the CDU, hence they are correlated to the inlet flow rate of crude oil. For the same reason hot streams temperature are correlated among themselves.

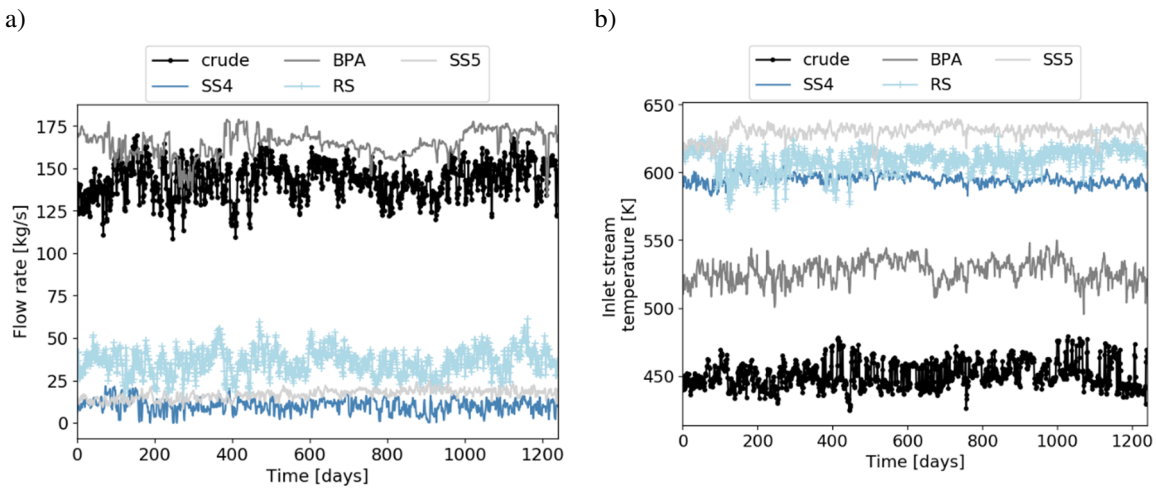

Figure 7.5. Actual measurements of the inlet stream flow rates (a), and temperature (b) for the case study of REF-X.

The data set available has measurements of the outlet streams temperature which were used for model validation in Chapter 4, although they are not used in the online fouling mitigation approach. Because, it is expected that the online optimization approach will define alternative operating modes – a different cleaning schedule and flow distribution – than that of the actual operation, so the outputs of the system are not comparable. For this same reason an alternative representation of the actual system is needed. The same model developed in Chapter 3, and used as predictive model within the NMPC problems, is used here to simulate the actual operation of the system (plant). The parameters of this model are first estimated offline based on the results presented in Chapter 4, and later they may be modified to simulate a degree of mismatch between the predictive models of the feedback loops and the actual operation of the plant. Using the same model to represent the actual plant operation, and to make prediction in the NMPC problems enables exploring two scenarios. The first one is where the plant model and the predictive model are exactly the same, so there is no need to solve an estimation problem (MHE) and the function of the feedback loops is to react to disturbances. The second is where there is a mismatch between the plant and the model – as it is expected in reality – so that the estimation problem aims to characterize the plant performance, and the feedback loops to react to disturbances.

7.3.1. Online optimization assuming perfect model

The first approach to evaluate the performance of the proposed online optimization approach is to assume perfect knowledge of the system. The model used to simulate the real operation of the preheat train, is also used as the predictive model in the NMPC problems of the feedback loops. Furthermore, it is assumed the type of crude oil never changes, hence the model fouling parameters are constant and known so there is no need to solve the MHE problems. The model represents perfectly the system dynamics and there is no mismatch.

By simplifying the problem in this way , this section aims to specifically evaluate the effects of the input variability observed, and to compare the following alternatives: i) the actual operation of the preheat train with the cleaning schedule performed during the operation of the network (Actual), ii) the optimal online flow distribution control with the actual cleaning schedule which is assumed fixed (Opt. C), iii) the optimal online cleaning schedule, with a fixed flow distribution, split fraction set at 50% (Opt. S), and iv) the simultaneous online optimization of the flow distribution and cleaning scheduling (Opt. S + C). Although there is no mismatch between the predictive models and the actual preheat train, there are disturbances in all the inputs to the network.

As daily data are available, the sampling time is 1 day. Although the operating conditions of the preheat train may change more often, their daily average value is a representative measurement considering the long-time scales involved. In this case, the update frequency of the flow control layer is selected to be the same as the measurements sampling time because it aims to reject the effect of disturbances. That of the scheduling layer is set as 180 days, although this is a rather long time between consecutive solutions, it is long enough to capture the slow dynamic of fouling and to avoid unstable operating modes that may arise if the cleaning decisions change frequently based on the disturbances. The future prediction horizon of the control layer is set at 10 days, while that of the scheduling layer is set at 500 days. The FPH is always longer than the sampling time in each layer, giving more importance to the current events and changes than to the future ones that are uncertain. Finally, the FPH is discretized using 10 points for the control layer, and 20 periods of variable length for the scheduling layer.

The actual operation of the refinery under varying conditions is compared against all online optimization scenarios. In addition, a heuristic approach, which is described in detail

in Appendix C, is also used to determine and update a cleaning schedule under varying operating conditions. This heuristic algorithm defines the cleanings on a rolling horizon using a quadratic model to predict the heat duty decay of each exchanger, and an economic threshold criterion to determine potential beneficial cleanings. It can be coupled with a steady state optimization of the flow distribution to determine the flow split at every time instance. Table 7.1 shows the operating cost and extra energy at the furnace for each of the alternatives considered. The heuristic approach on its own, using the actual flow distribution of the refinery, leads to a cleaning schedule worse than that used in the actual operation. Erroneous and ineffective cleaning decisions are suggested by the heuristic algorithm, as it ignores the effect of varying operating conditions, such as flow rates and inlet temperature, on the performance prediction of the units. However, when a steady state optimization of the flow distribution is performed at every sampling time simultaneously with the heuristic algorithm for cleaning scheduling, the operating cost is reduced by $ 1.50 M compared to that of the actual operation of the refinery. This highlights the importance of considering the interaction between control and scheduling decisions to mitigate fouling.

Table 7.1. Total operating cost for online fouling mitigation and the actual refinery operation.

	Total energy [MWh]	**Energy cost [$ M]**	**Cleaning cost [$ M]**	**Total cost [$ M]**
Actual operation (Actual)	1.59×10^6	39.888	0.705	40.585
Heuristic – Quadratic model	1.61×10^6	40.331	0.729	41.061
Heuristic – Quadratic model + flow control	1.53×10^6	38.360	0.729	39.090
Online optimal flow control (Opt. C)	1.55×10^6	38.884	0.705	39.553
Online optimal cleaning scheduling (Opt. S)	1.44×10^6	36.001	2.487	38.497
Online integrated optimal flow control and cleaning scheduling (Opt. C+S)	1.43×10^6	35.960	1.638	37.543

All online optimization alternatives provide a better operation than the actual operation of the refinery. They all reduce the operating cost by decreasing the extra energy requirements of the furnace. These optimization alternatives consider the varying operating conditions explicitly using a moving horizon for predicting the performance of the system, and a feedback loop to update the operating conditions based on the disturbances. The maximum reduction in operating cost, $ 3.04 M, is achieved when the control and scheduling

decisions are integrated online using two feedback loops, although using individual feedback loops is also advantageous for the operation. The optimal integration of flow control and cleaning scheduling performs better than the integration based on heuristics to define the cleanings. Using only the scheduling feedback loop for online optimization leads to higher cleaning cost than those of all other alternatives – too many cleanings – which may introduce many unacceptable disruptions in the operation, but there are fewer cleanings when the two feedback loops are used to integrate control and scheduling decisions.

Figure 7.6 compares the actual cleaning schedule of the preheat train with those obtained online using heuristics and the online optimization alternatives. The number on the right-hand side of this figure represent the total cleanings per exchanger. While the heuristic approach only defines cleanings for E01A/B and E04, the units with the highest fouling rate, the online optimization approaches define cleanings for all exchangers. The cleaning sequence and starting time of the online optimal schedules are significantly different from those of the actual operation, or the heuristic algorithm. These optimal schedules respond to the variability of the inputs of the system, exploit the interactions in the network, and minimize the total operating cost. The total number of cleanings decreases when control and scheduling decisions are considered simultaneously, relative to those when only scheduling decisions are optimized. Fewer cleanings are ideal from a practical perspective as they reduce disruptions and the risk arising from cleaning interventions.

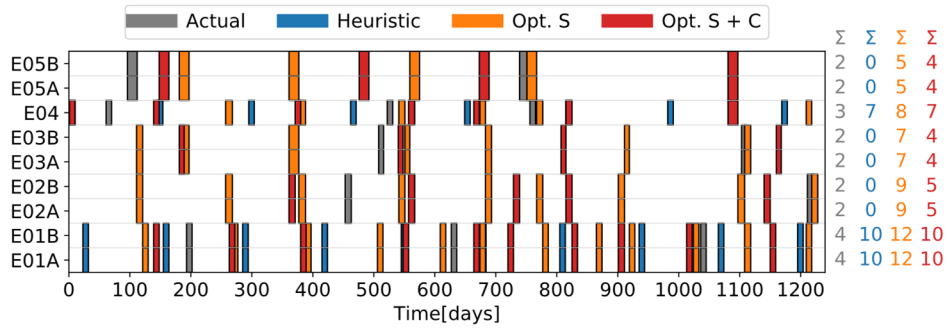

Figure 7.6. Comparison of cleaning schedules for all online scenarios considered of the case study REF-X.

The importance of the interactions between flow distribution and cleaning scheduling decisions through the two feedback loops is observed in Figure 7.7. It shows the split fraction between the parallel branches in the network for the actual operation, for the online

optimization of the flow distribution with fixed schedule (Opt. C), for the integration of scheduling decisions using heuristics (Heuristic + Opt C), and for the multi-loop strategy (Opt. S+C). The actual operation could be significantly improved by just modifying the split fraction to react dynamically to disturbances as the flow control feedback loop defines the split fraction considering the trade-off between fouling rate and energy recovery in the two branches. For instance, when E05A/B is cleaned in the actual operation – at 100 and 750 days of operation – the flow optimization indicates that most of the flow is diverted towards that branch, and the split fraction is a function of the disturbances. When the two feedback loops are used to integrate online control and scheduling decisions, the reduction in operating cost is even larger. There are interactions between the flow distribution and the allocation of cleanings, and it is more evident when a large unit – E02A/B or E05A/B – on one of the branches is cleaned. The heuristic algorithm used to define the cleanings do not capture these important interactions as it ignores the effects of flow rates and temperature – the main disturbances – on the decay rate of the exchanger performances. Integrating optimal steady state control with the heuristic algorithm saturates the split fraction at its upper bound for most of the time, which shows that the definition of the cleanings in this way ignores the dynamic effect of the flow distribution.

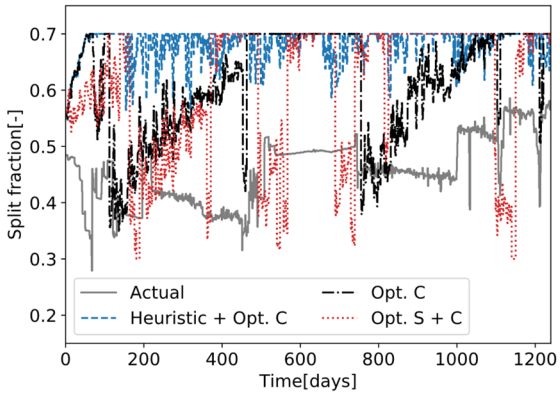

Figure 7.7. Flow split fraction towards E02A/B for all online scenarios of REF-X case.

Figure 7.8 shows that the fouling resistance of E02A is always lower when the flow distribution is optimized online (Opt. C) than during the actual operation. Hence the heat duty of the exchanger is always higher, and it can recover more energy. This only shows the effect of flow distribution in one exchanger in one of the branches. On the other branch, the opposite effects are observed, which are: higher fouling resistance and lower heat duty

because of the lower flow rate. The feedback optimization of the control layer considers these trade offs and disturbances to give the best possible flow distribution in the system.

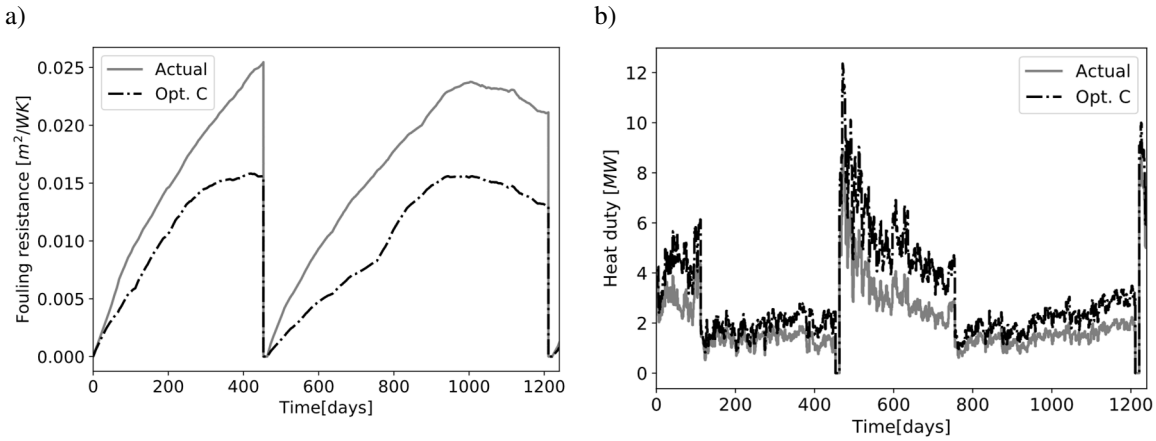

Figure 7.8. Effects of optimal flow distribution for online fouling mitigation, case of E02A. a) Fouling resistance, b) heat duty

It has been demonstrated that the best alternative is to integrate flow distribution and cleaning scheduling using the multi-loop feedback strategy proposed – Opt. S+C. The analysis presented next is relative to that alternative.

Despite assuming a perfect model for the NMPC loops, the optimal predictions at every sampling time change because the effect of disturbances. The effect of disturbances on the NMPC predictions of the control layer is observed in Figure 7.9. It shows the CIT observed (black line) and predicted (red line) at the control layer for three consecutive time instances, at three different times. The dark area of the figure represents the FPH of the control layer. A good agreement is observed between the predicted behaviour of the system over the FPH_C and the actual response of the plant. The predictions of the control layer also capture the effect of the cleanings, as observed in the evolution of the first and last FPH on Figure 7.9 – dark area from top to bottom. The cleanings defined at the scheduling later – outer feedback loop – are shared with the control layer and introduce discontinuities in the operation, but the control layer considers these discontinuities in its own predictions of the system performance. The NMPC of the control layer is solved at the same frequency at which the disturbances occur, so its predictions and optimal actions are constantly adapting to reflect those effects.

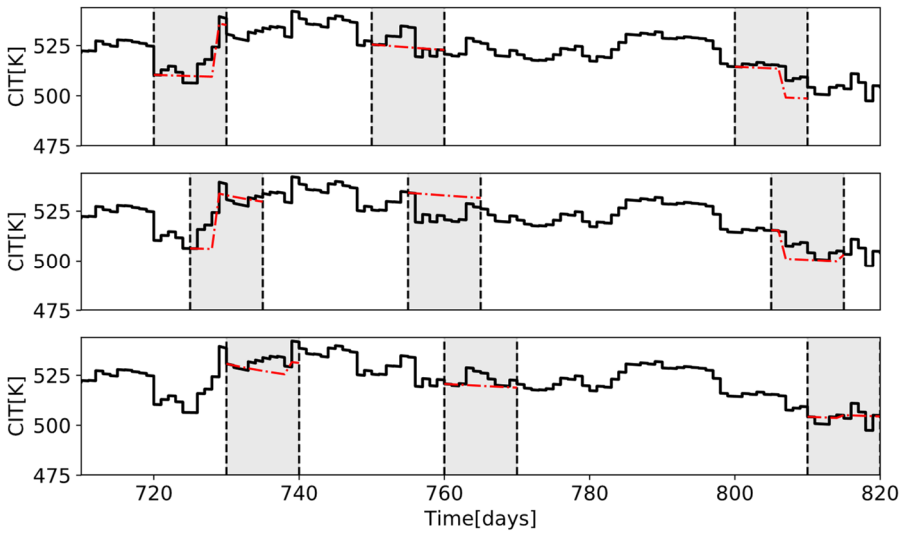

Figure 7.9. CIT observed (continuous line) and predicted (dash line) at the control layer for the scenario Opt. S+C of REF-X at three consecutive time instances – time evolution from top to bottom.

The predicted performance of the system can also be tracked at the scheduling layer. The evolution of the CIT and its prediction at different times are shown in Figure 7.10, while the executed and predicted cleaning schedules are presented in Figure 7.11. The dark areas correspond to the FPH_S and include the predicted variables (red), while the black lines or boxes are the plant responses or the execution of the cleaning actions. The time evolution is observed from top to bottom in these figures. The scheduling feedback control loop captures the effects of cleanings, cleaning times, and flow distribution on the performance of the network. Also, the accuracy of the predicted CIT trend is good in the first half of the moving window, but deteriorates in the second half – that closer to the end of the FPH – because of the cumulative effect of all the disturbances on the fouling rate, deposit thickness, and general performance of the units. After long prediction times, the values used to forecast the behaviour of the disturbances, a moving average in this case, becomes less representative of the actual operation. Similar discrepancies between the execution and prediction of the cleaning schedule are observed for the same reasons. Hence, a constant revision and update of the fouling mitigation is paramount for a good operation.

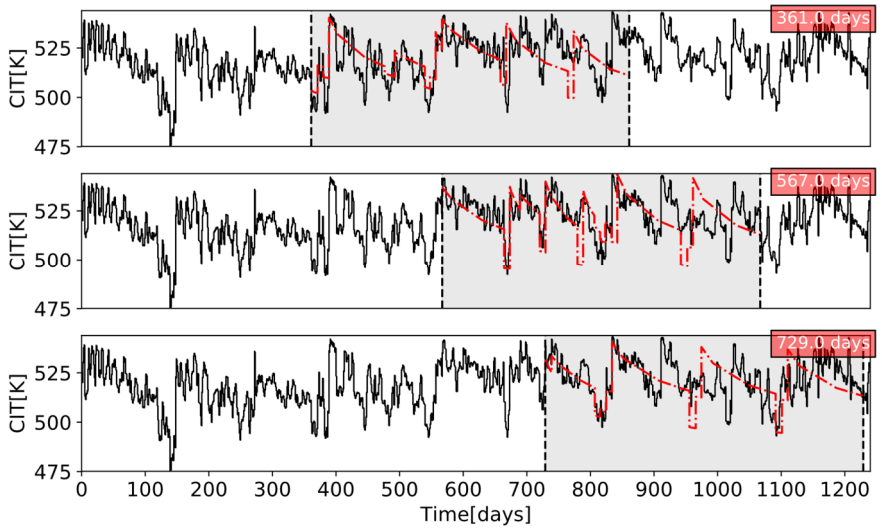

Figure 7.10. CIT observed (continuous line) and predicted (dash line) at the scheduling layer for the scenario Opt. S+C of REF-X at three consecutive time instances – current time of the prediction on the upper right corner.

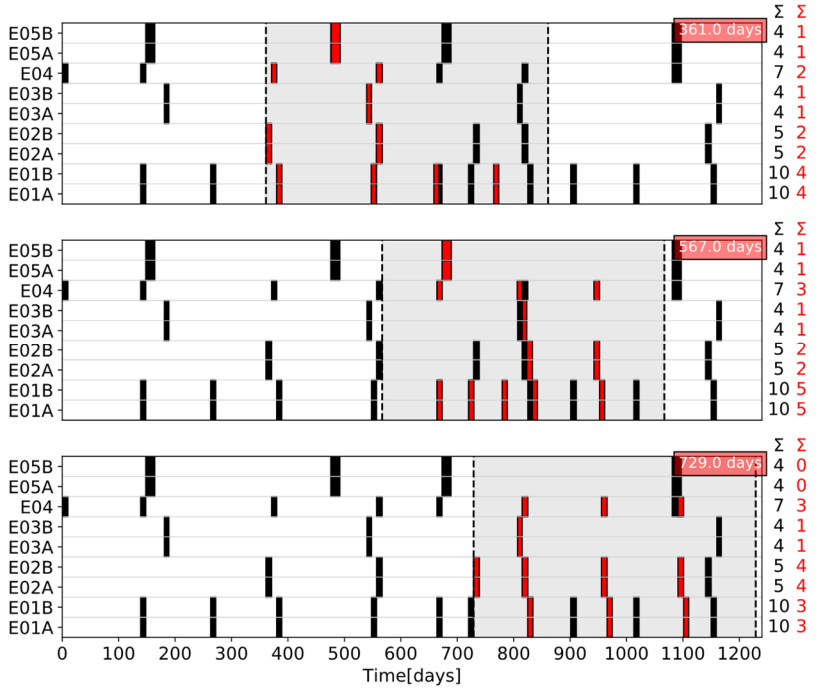

Figure 7.11. Cleaning schedule executed (black) and predicted (red) at the scheduling layer for the scenario Opt. S+C of REF-X at three consecutive time instances – current time of the prediction on the upper right corner.

The dynamic flow distribution and its interaction with the cleanings is also considered at the scheduling layer of the online optimization. Figure 7.12 shows the split fraction predicted by the solution of the NMPC of the scheduling layer at 361 days and compares it with the actual execution of this manipulated variable. The optimal flow distribution predicted responds to the cleanings predicted for the FPH_S, although it ignores the variability introduce by the disturbances at a smaller time scale. The control layer deals with the short term effect of the disturbances, and optimally defines the split fraction at every time instance while considering the inputs from the outer feedback loop. In addition, there is a good agreement between the flow distribution predicted at the scheduling layer, where the effect of disturbances is averaged, and that executed by the flow control layer to reject disturbances and minimize operating cost at a faster frequency.

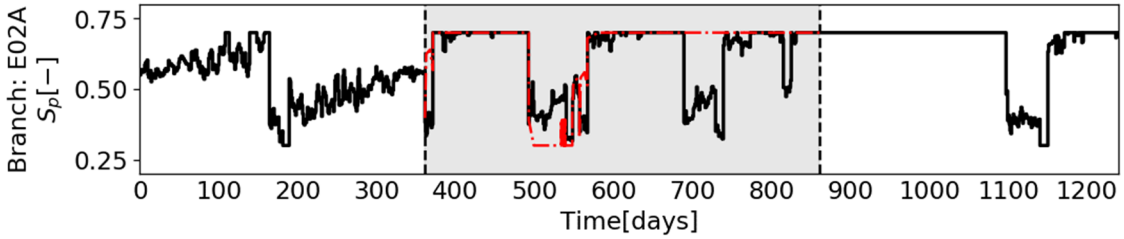

Figure 7.12. Optimal split fraction implemented (continuous line) and predicted (dash line) at the scheduling layer for the scenario Opt. S+C of REF-X. Prediction at 361 days.

The final scenario considered for the online optimization of the REF-X case study under the perfect model assumption is when the end time of the operation is known, assumed to be 1240 days. The optimal cleaning scheduling and control problem – Opt. S+C – is solved online using the proposed method under a shrinking horizon mode for the prediction of the NMPC on both feedback loops. Figure 7.13 shows the cleaning schedule executed based on the moving horizon optimization assuming a continuous open-ended operation, and one with a finite horizon. Differences are only observed at the end of the operation when the shrinking of the FPH_S and of the FPH_C has an effect on the optimal solution and on the feedback actions. When the end of the operation is explicitly considered, some of the cleanings are executed earlier, and there are additional cleanings. The operation executed with a shirking horizon has a total operating cost of $ 37.46 M, while that for a continuous operation is $ 37.54 M.

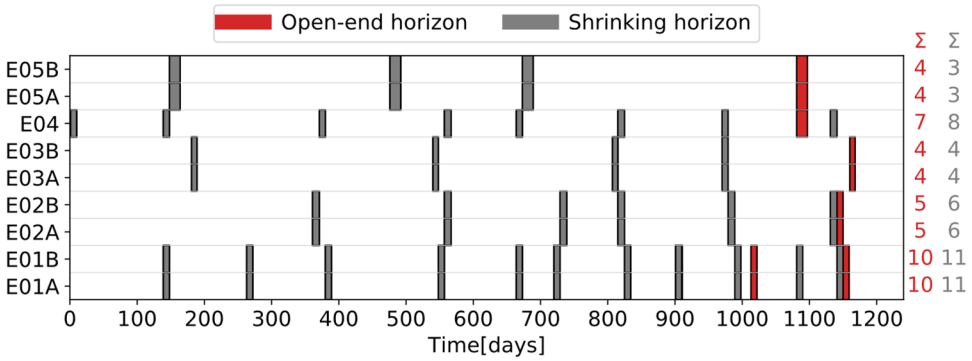

Figure 7.13. Comparison of the optimal cleaning schedule determined online assuming the end time is known and using a shrinking horizon approach for the NMPC.

The differences observed in the operating cost are explained because of their different predictions towards the end of the operation, and the different actions feedback to the plant. The last three predictions before the end of the operation of the CIT and of the cleaning schedule at the scheduling layer are presented in Figure 7.14 and Figure 7.15, respectively. These figures compare the FPH of the scheduling layer and the predictions obtained within this horizon towards the final time of the operation assuming a continuous open-ended operation (a), and an end time using shrinking horizon (b). The FPH in (a) goes beyond the end of the operation, and the NMPC solution predicts the system performance during that period and mitigation actions that are not necessary and are never implemented. On the other hand, the FPH in (b) is variable and decreases as the end of the operation approaches so that it never exceeds the final time. By doing so, it ensures that the prediction of the system performance and all mitigation actions always falls within the actual operating time. In this case, there are no cleanings predicted beyond the end of the operation, and it guarantees that all the cleanings performed before the operating finishes are beneficial from an economic perspective.

a)

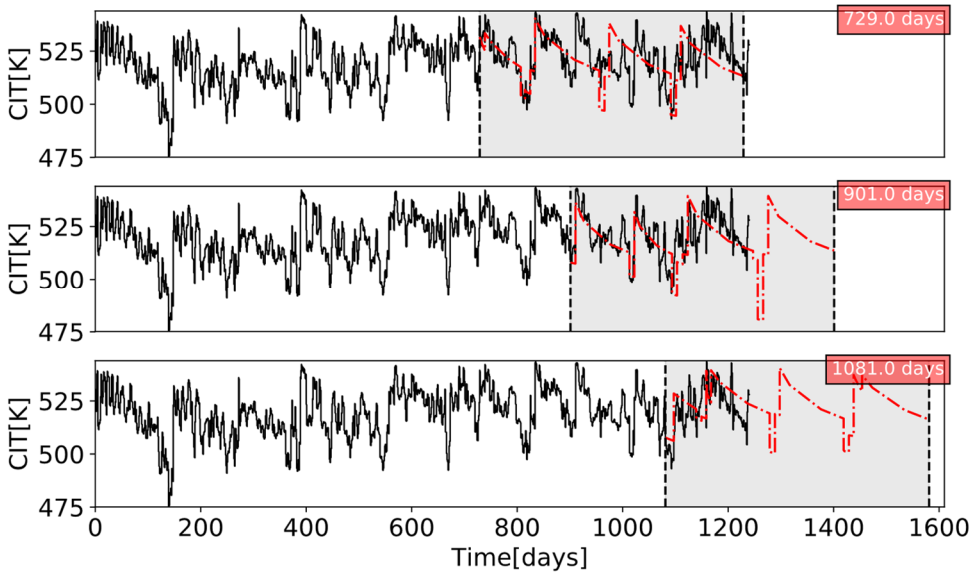

b)

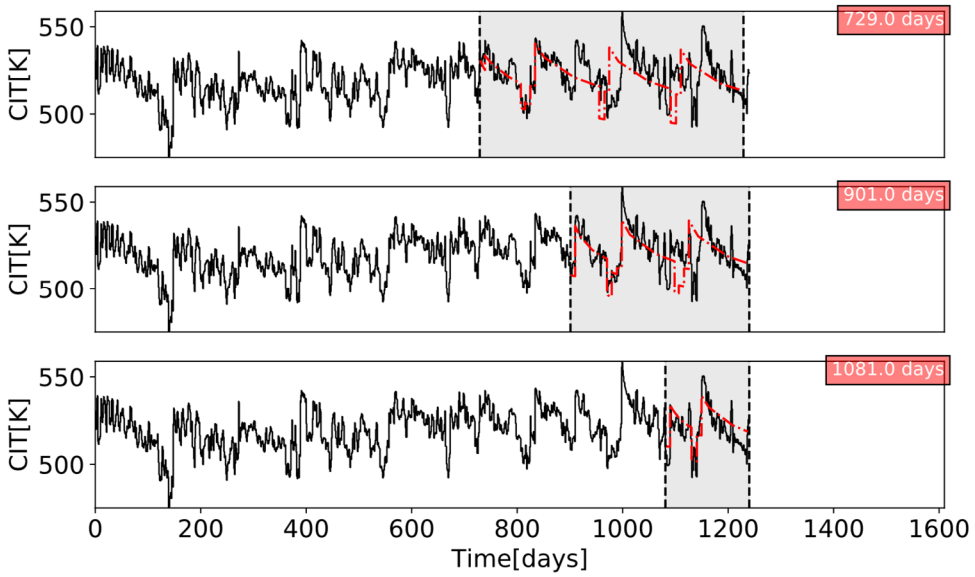

Figure 7.14. CIT observed (continuous line) and predicted (dash line) at the scheduling layer towards the end of the operation. a) open-ended online optimization, b) shrinking horizon optimization.

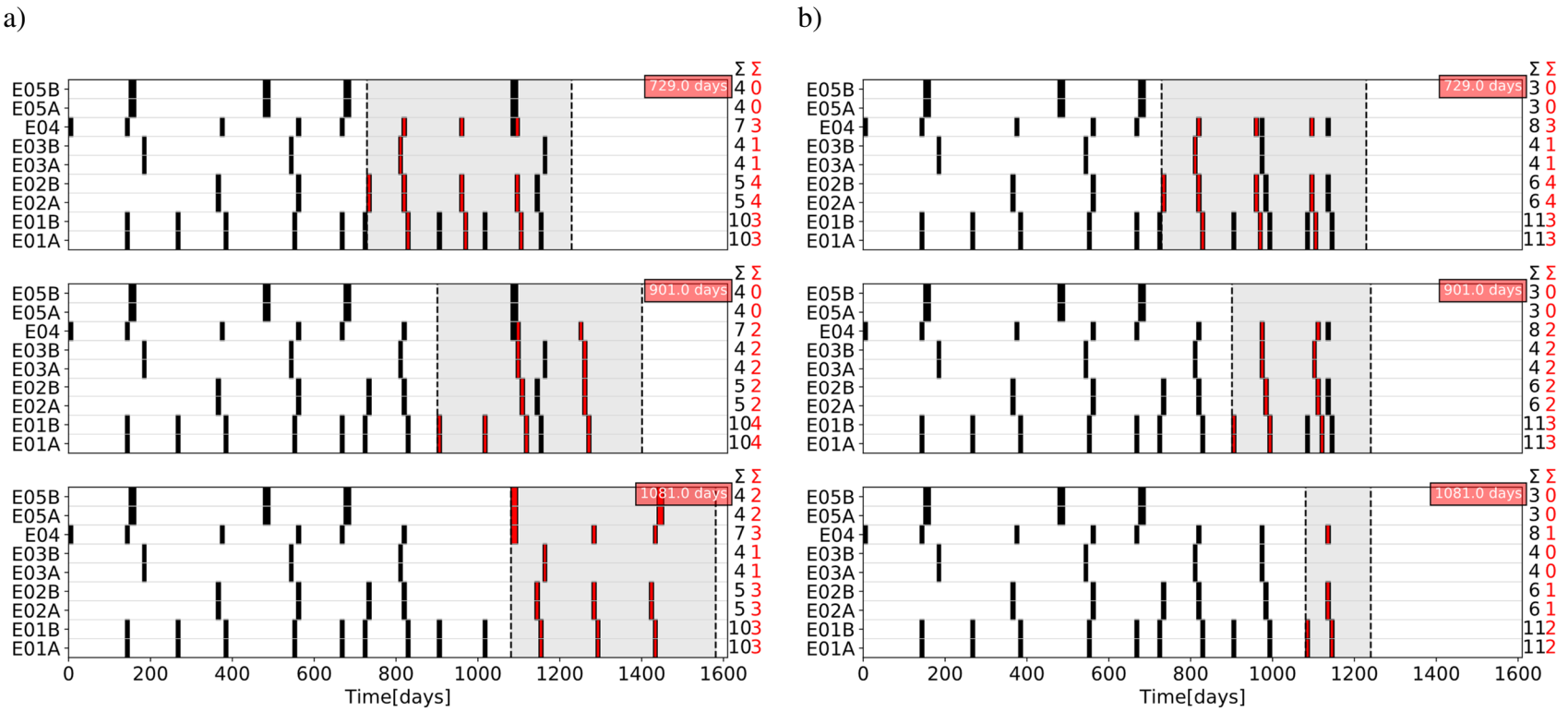

Figure 7.15. Comparison of the cleaning schedule executed (black) and predicted (red) at the scheduling layer towards the end of the operation. a) open-end online optimization, b) shrinking horizon optimization.

7.3.2. Online optimization under plant mismatch

Introducing model plant mismatch in the online optimization of preheat trains under fouling represents a more realistic scenario. In this case, the parameters of the model used to simulate the plant operation are unknown to the predictive models in the NMPCs, and the MHE problem of each layer must be solved to estimate them based on past observations.

Model plant mismatch is introduced by modifying the fouling deposition constant of each exchanger in the plant model. This aims to mimic the effect of processing different crudes or crude blends in the preheat train, as they can have different fouling propensity, which is captured in the fouling model parameters. The deposition constants change over time, but their actual value is unknown to all predictive models used in the online optimization approach. The variability of the actual deposition constants in each exchanger is model as a pseudo random process around their average values. Because all exchangers process the same crude at a given time their deposition constants are not independent, and their correlation is captured when their variability is defined as a random process. Figure 7.16a presents an example of how the deposition constant in two exchangers vary with time randomly around their mean, and Figure 7.16b presents the variability of the deposition constant for each exchanger in the network. The average deposition constant, and its variability are different for each exchanger in the network. For instance, the coefficient of variance ranges from 12% to 31%, and the minimum and maximum values deviate by up to 79% with respect to their average.

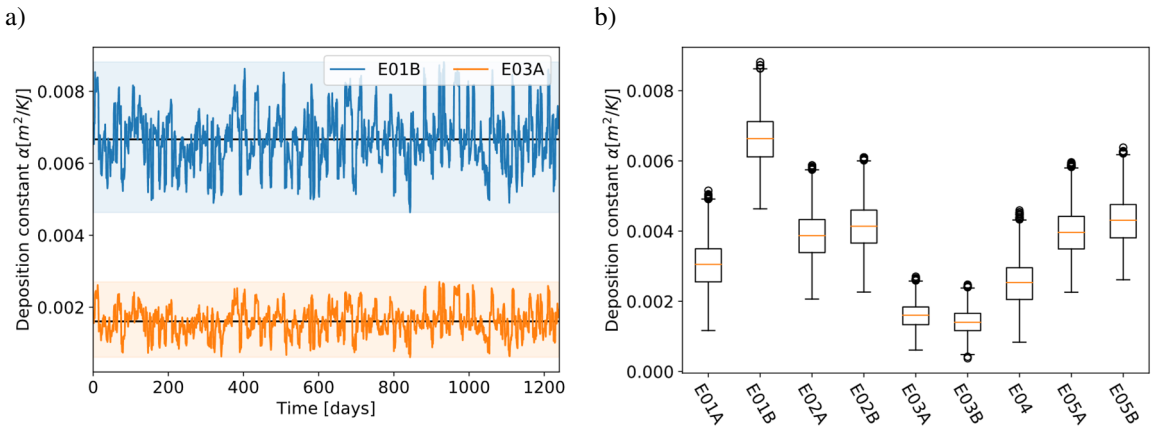

Figure 7.16. Model plant mismatch defined varying the deposition constant of each exchanger of the plant. a) example of time variability for two exchangers, b) box plot representing the variability in the deposition constant for each exchanger in the network.

The integrated and online flow distribution and cleaning scheduling problem is solved for the REF-X case with a model-plant mismatch as defined above. The specifications defining the NMPC of each layer are the same used in Section 7.3.1. To account for the mismatch, the MHE problems are solved at the same frequency as the NMPC of the respective layer. For the control layer a PEH_C of 20 days is used, while the PEH_S of the scheduling layer is 180 days. The PEH_C is chosen twice as long as its FPH_C to capture the short term dynamics and variability of the plant, and to account for the effect of cleanings, which in this case study last between 9 and 16 days depending on the exchanger. The PEH_S of the scheduling layer is much longer than PEH_C because it aims to capture the long term variability of the plant and the slow fouling dynamics. In this case, the PEH_S is chosen to be equal to the interval at which the $NMPC_S$ is solved (180 days), so that all the new information collected between sampling times is included in the estimation problem.

Figure 7.17 shows the cleaning schedule executed when the Opt. S+C operation is optimized online using the proposed approach and compares it with the actual cleaning schedule executed by the refinery. For a fair comparison the actual schedule of the preheat train is simulated for the model plant mismatch scenario where the deposition constant of the plant varies dynamically. The optimal cleaning schedule has many more cleanings than the actual one, all exchangers are cleaned more often, and the benefit of these actions is a cost reduction of $ 2.54 M. Exchangers E01A/B and E04 are cleaned more often because they have the highest fouling rates and largest heat duty, and the solution of the MHE problems estimates correctly this behaviour. The largest contribution to the economic savings observed is from the integration of flow distribution and cleaning scheduling decisions. Figure 7.18 compares the optimal furnace duty and flow distribution for the actual and the online Opt. S+C operations. Despite the variability caused by the changing inputs and the varying deposition constants, the furnace duty of the optimized alternative is lower than in the actual operating during most of the time. The split fraction reacts to the cleanings to recover the maximum amount of energy in the network depending on the disturbances and on the state of the exchanges. All the benefits of integrated scheduling and control decisions are obtained regardless of the existence of model mismatch, and the need of estimating the model parameters online.

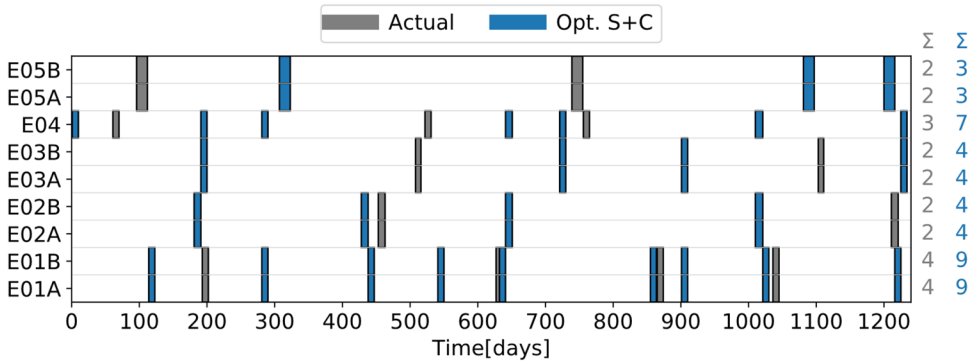

Figure 7.17. Cleaning schedule executed in the actual operation and with the online optimization approach considering model plant mismatch.

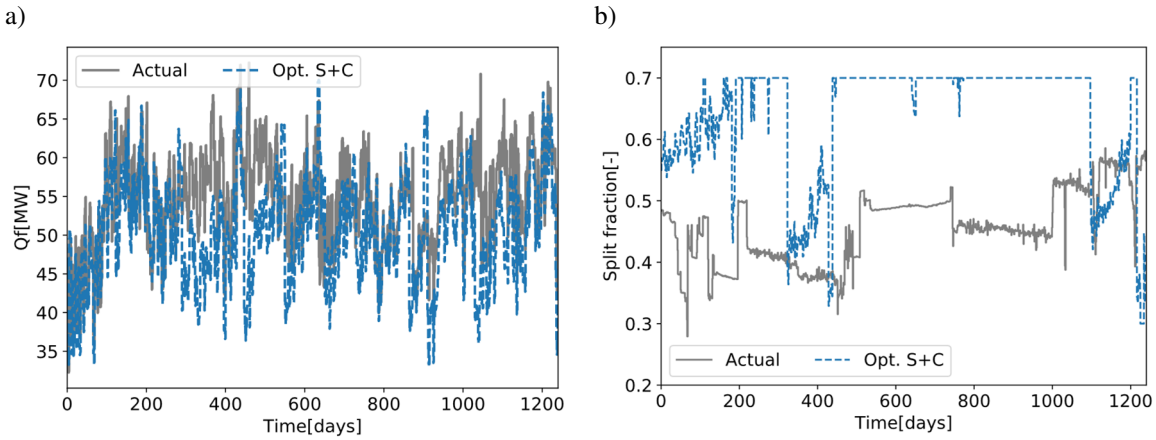

Figure 7.18. Furnace duty (a) and split fractions towards E02A/B (b) for the actual operation and the online optimization considering model plant mismatch.

The efficient implementation of the online optimization approach proposed depends on the solution of the MHE and $NMPC$ optimization problems in each control loop. The size and the average solution time of each problem are summarized in Table 7.2. In each layer, the limiting step is the solution of the MHE problem as it requires a higher computational time than the $NMPC$ problem, although the solution time is much shorter than the actual sampling time of the respective control loop. The sampling time of 1 day for the flow control loop is greater than the total computational time for solving the two optimization problems, and the same is true for the scheduling layer, with a much longer sampling time. The difference in computational load required to solve the MHE and $NMPC$ problems comes from their difference in size – the MHE of each layer is almost twice as large as its corresponding NMP –, the large data set used in the parameter estimation problem that makes

the evaluation of the objective function complex, and the high correlation of the model parameters estimated at this stage. On the other hand, the $NMPC$ problems are solved relatively easily. That of the control layer is an NLP, and that of the scheduling layer an MINLP which, despite having binary decision variables, is solved efficiently and fast using the complementarity constraints reformulation. Considering this good computational performance, it would be possible to reduce the sampling time to the order of hours or minutes for the flow control feedback loop, and to the order of days or hours for the scheduling feedback loop. This will improve the ability to handle fast dynamics and disturbances, and to execute better control actions reacting to the operational changes.

Table 7.2. Model size and solution time summary of the optimization problems involved in the proposed online approach considering model-plant mismatch.

	Control layer		**Scheduling layer**	
	MHE_C	$NMPC_C$	MHE_S	$NMPC_S$
Variables	5158	2552	42278	20050
Binary variables	0	0	0	200
Equality constraints	4713	2343	38793	18920
Inequality constraints	10692	5412	49332	37679
Average CPU time [min]	0.91	0.08	169.2	23.95
Standard deviation of CPU time [min]	0.38	0.03	37.11	4.75
Instances solved	1230	1240	6	6

The online optimization of the preheat train under model-plant mismatch relies on an accurate estimation of the model parameters and of the current state of the system at every sampling time. The estimation of model parameters has to be precise in order to result in appropriate fouling mitigation actions. Figure 7.19 shows the CIT of the network, observed (continuous line), predicted in the FPH_C (dash line – light grey area), and estimated in the PEH_C (dotted line – light blue area) for three consecutive time instances of the control feedback loop and two time windows starting at 80 and 200 days of operation. The estimation of the network performance and the model parameters of the control layer are obtained solving the corresponding MHE problem at every sampling time, and a good agreement is observed between the observed and predicted values. The absolute error between the predicted values of the CIT at the control layer, and the observed ones is, on average, less than 1.0 K. In addition, the fitted model is used at every sampling time to predict the system

performance and the optimal actions to execute in the plant. The predictions follow the trend observed in the actual operation including the effect of cleanings.

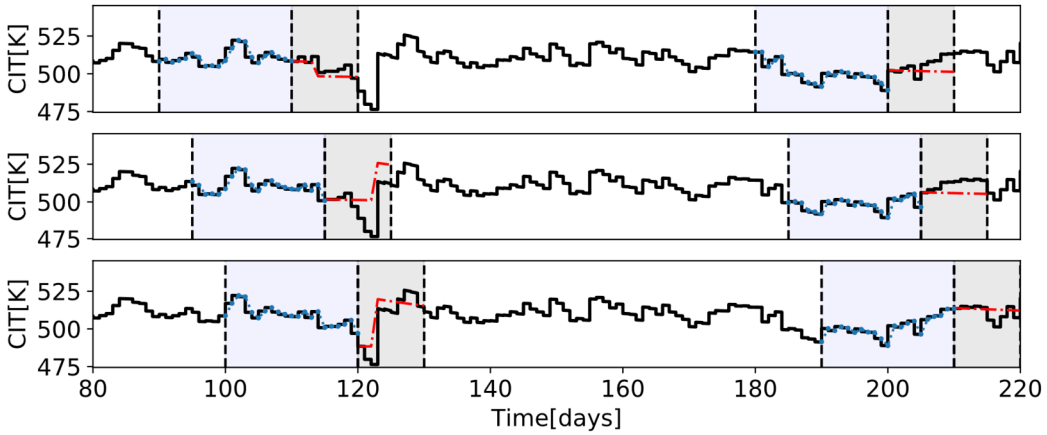

Figure 7.19. CIT observed (continuous line), predicted (dashed line), and estimated (dotted line) at the control layer for the scenario Opt. S+C of REF-X at three consecutive time instances under model plant mismatch. Time evolution is from top to bottom.

In the scheduling layer the MHE_S problem is solved to estimate the model fouling parameters and the current state of the preheat train. The main difference is that the PEH_S and the FPH_S are much longer than the PEH_C and the FPH_C, respectively. The observed plant measurements used in MHE_S cover a longer operating time, possibly with many cleanings, to ensure that the parameters estimated reflect the slow dynamics of fouling and the effects of variable operating conditions on the network performance. Figure 7.20 shows the CIT observed during the whole operation (continuous line), and the CIT estimated (dotted line) and predicted (dashed line) at three consecutive solutions of the scheduling feedback loop. The current time when the scheduling layer is solved is shown in the upper right corner of each figure. A higher variability is observed in this feedback loop compared to the flow control loop, but the MHE_S copes with it and provides accurate estimations of the system performance despite the large data set, variability, and cleanings. The parameters estimated solving the MHE_S problem are used in the $NMPC_S$, and its predictions are accurate with respect to the later observations. However, the quality and accuracy of those prediction decreases over the FPH_S – the cumulative effect of the disturbances becomes significant, and the parameters estimated at the MEH_S become less representative of the plant operation.

Frequent updates of the MEH_S and $NMPC_S$ problems ensure an excellent overall performance of the online integrated scheduling and control approach.

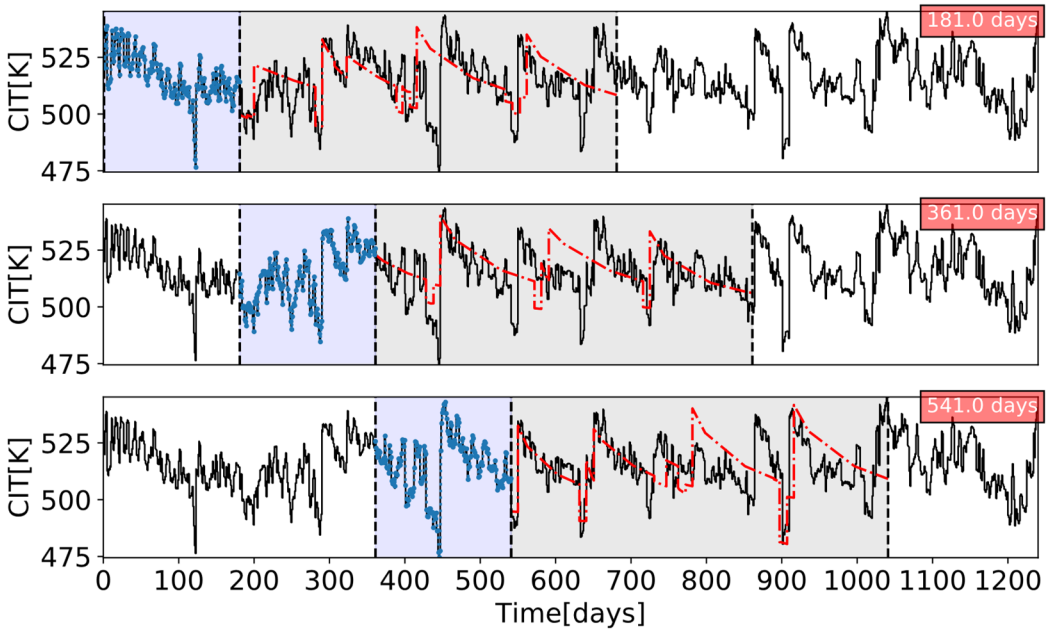

Figure 7.20. CIT observed (continuous line), predicted (dashed line), and estimated (dotted line) at the scheduling layer for the scenario Opt. S+C of REF-X at three consecutive time instances under model plant mismatch – time evolution from top to bottom.

The way model-plant mismatch is considered in this scenario, a simulation of the actual plant with varying deposition constants at every sampling time, allows to compare the estimated parameters at each feedback loop with the 'real' ones. Figure 7.21 and Figure 7.22 show the actual deposition constants used in the plant and those estimated by solving the MHE problem at the control and scheduling layer, respectively. At the control layer, the estimated parameters exhibit a seemingly chaotic behaviour, although their general trend follows that of the actual plant. In addition, the box plot of Figure 7.21b compares the mean values and variability ranges of the actual deposition constant and the predicted one for each heat exchanger in the network. There is not significant difference between the average values of the deposition constants estimated and those used in the actual plant, but the variability of the estimated parameters is larger. At the scheduling layer, similar features are observed for the estimation of the deposition constant of the exchangers, although the MHE_S is solved only six times during the operation. The fewer solutions of the MHE_S problem relative to those of the MHE_C problem reduce the variability observed on the estimations – step changes

in Figure 7.22b. However, the box plot shows that there is no significant difference between the average of the constants estimated and those of the actual plant.

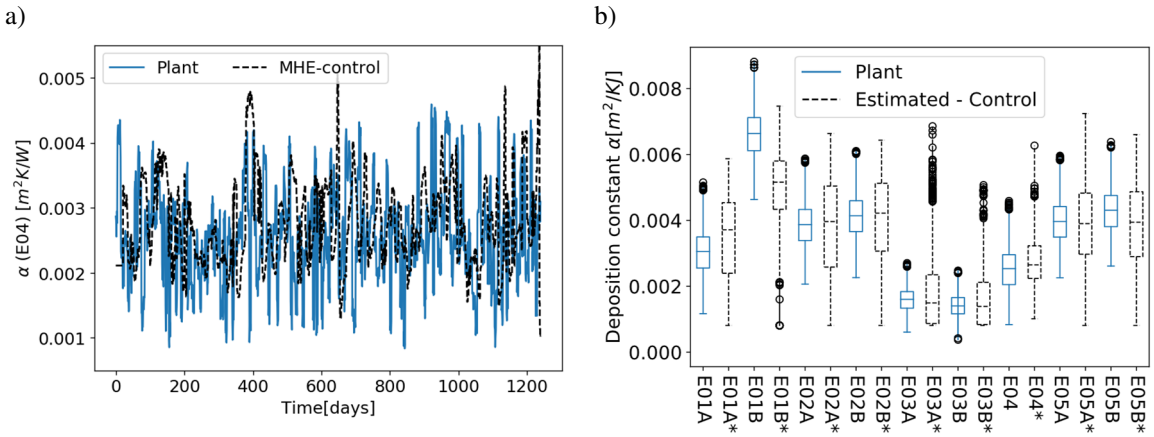

Figure 7.21. Comparison of the actual deposition constant and that estimated at the control layer for REF-X case. a) time series example for E04, b) box plot comparing every exchanger in the network.

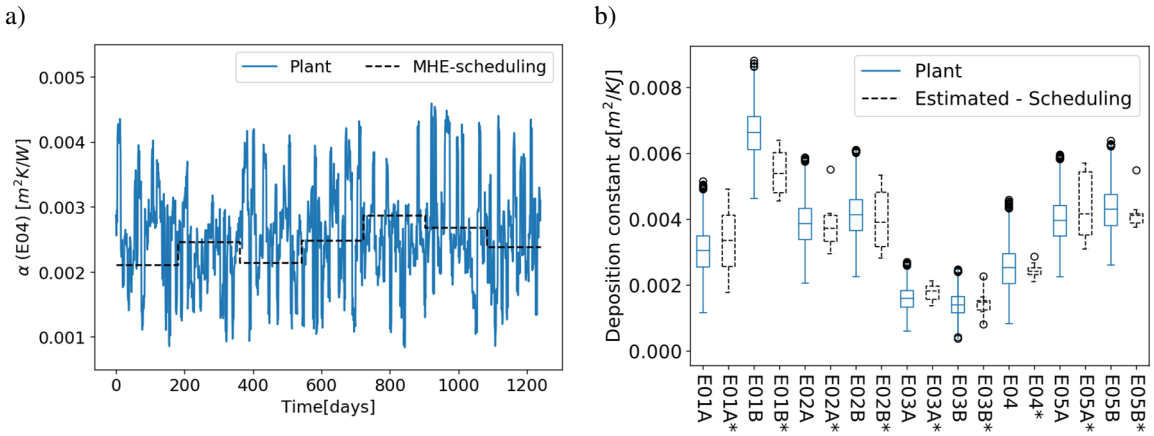

Figure 7.22. Comparison of the actual deposition constant and that estimated at the scheduling layer for REF-X case. a) time series example for E04, b) box plot comparing every exchanger in the network.

It is not expected that the parameters estimated by the *MHE* of each control loop match exactly those of the real plant. First, the MHE solution is a single set of parameters that represent the past observations of the plant, while in the actual operation they are changing dynamically. For example, at the scheduling layer a single set of parameters aims to estimate the plant behaviour correctly over the past 180 days of operation when many changes occurred in the plant, including different deposition rates. Second, the fouling parameters of

the Ebert-Panchal model are highly correlated, so that different combinations of deposition (α) and removal (γ) constants may predict the same or similar behaviour observed in the plant. Third, the MHE solution determines simultaneously all the fouling parameters of every exchanger in the network and it considers all the interactions, hence a single parameter for one exchanger is not representative of the overall performance of the network, and correlations among the parameters are important.

7.3.3. Effect of multi-loop MHE/NMPC parameters

The MHE/NMPC loop settings (update frequency, estimation horizon, and prediction horizon) have a significant effect on the closed-loop performance. To evaluate these effects the update frequency and the future prediction horizon of the scheduling layer are varied under the model-plant mismatch conditions defined in Section 7.3.2, while those of the flow control loop are set constant at the values used in that same section. Because the control layer is solved as frequent as measurements are collected and there is no limitation to solve it faster, it is not worth exploring other update frequencies. In addition, longer FPH_C and PEH_C are not expected to have a significant effect on the overall closed-loop performance as the disturbances and process variability are fast and not captured in the $NMCP_C$ predictions. Also, it has been demonstrated in Section 7.3.1 that most of the economic savings generated come from the execution of the scheduling layer.

Two update intervals of the scheduling layer are explored here, 30 and 90 days, while the FPH_S is varied from 90 days to 720 days, with five points evaluated in this range. Besides this interaction between the FPH_S and the update frequency, there are more interactions involving the FPH_S and other settings of the multi-loop control strategy. The number of periods of variable length used to discretize the prediction horizon, and the length of the PEH_S are correlated with the FPH_S. The longer the FPH_S the more periods needed to discretize it appropriately, and the longer PEH_S needed to capture correctly the plant dynamics. To simplify this, the number of periods is defined as an explicit function of the FPH_S according to Eq. (7.5), and the past estimation horizon as a function of the update interval, Eq. (7.6). Eq. (7.5) assumes a linear relation so that the number of periods increases by a factor of 1/30 of the FPH_S, while the PEH_S is always 30 days longer than the update interval of the scheduling layer, T_S^*, to ensure that all new information is included in the

parameter estimation problem at the next sampling instance. Assuming these relations are appropriate, only the effect of the update intervals and the FPH_S are evaluated independently.

$$N_p = \frac{FPH_S}{30} + 6 \tag{7.5}$$

$$PEH_S = \mathrm{T}_S^* + 30 \tag{7.6}$$

The closed loop performance, in terms of operating cost, for each of the combination of parameters explored is shown in Figure 7.23. More frequent scheduling layer updates lead to lower energy cost, and higher cleaning cost. The cleaning decision predicted in the FPH_S are affected by the realisation of the disturbances in the past and the current state of the system. If these conditions are evaluated often and they are changing, new cleanings may become profitable closer to the current time, hence they are executed. On the other hand, increasing the FPH_S reduces the energy cost, and increases the cleaning cost. As the prediction horizon is longer there are more periods to allocate cleanings, so that more effective and profitable cleanings may fall between updates of the scheduling layer. There is a clear effect on the energy and cleaning cost by varying these parameters of the multi-loop optimization, although the changes in the total operating cost are rather small. For all the combinations of parameters considered the total operating cost only varies within a range of $ 0.24 M, which is small for an operation of 3.4 years. Therefore, other performance indicators such as the total number of cleanings – directly related to the cleaning cost – that indicates the number of disruptions and risk of the operation should be used to decide the best settings of the multi-loop strategy.

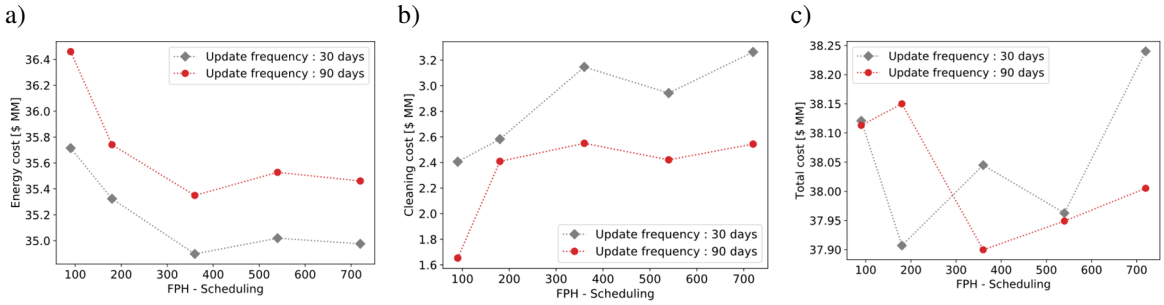

Figure 7.23. Effect of the FPH_S and T_s^* of the scheduling layer on the closed-loop performance for case REF-X. a) energy cost, b) cleaning cost, c) total operating cost.

The multi-loop settings used in Section 7.3.2 – update frequency of 180 days, and FPH_S of 500 days – are not covered in the sensitivity analysis presented here. The update frequency used in that case was rather long and allowed many operational changes to happen between

consecutive solutions of the scheduling layer, which may cause problems in the operation of an actual preheat train. Hence, faster updates of the scheduling layer should be considered. In addition, all the combinations of parameters evaluated here result in a lower operating cost – Figure 7.23 – than in the previous section case, $ 38.89 M, indicating that faster updates of the scheduling layer improve the closed-loop performance of the system.

7.3.4. Effect of inlet flow rate disturbances in the system

The effect of large disturbances in the closed-loop operation of the system is evaluated here. All the previous cases simulated the plant operation using the actual time-varying inputs of the refinery, although there are no extreme operational changes. It is common in refinery operations to have sudden changes to cope with market changes or internal requirements of the whole refinery. The online optimization approach proposed can deal with these large disturbances.

Sustained step changes of +/- 30% with respect to the average are introduced in the input flow rates of the network. This disturbance is modelled in the same way for all the streams as all the flow rates are correlated with the crude flow rate. Figure 7.24 shows the step disturbances introduced to the system. The red area highlighted shows the positive step, while the blue one the negative step. This colour convention to differentiate the disturbances is used though all the analysis of this section.

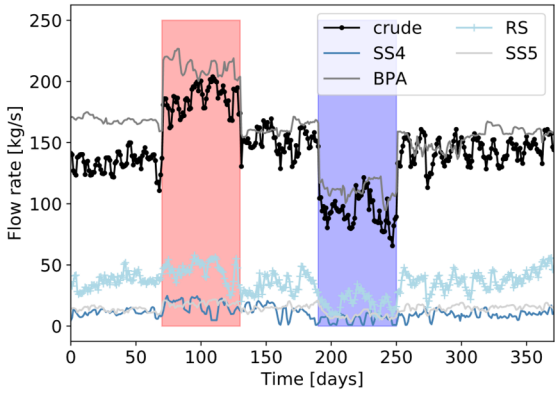

Figure 7.24. Step disturbances in the inlet flow rates of case REF-X over one year of operation.

The online optimization of the flow distribution and cleaning scheduling (Opt. S+C) is done for one year of operation considering the above large disturbances in the inlet flow rates,

and assuming an opened-ended horizon. Model plant mismatch is considered in the same way as in Section 7.3.2, the settings of the control layer are also taken from there, and the scheduling layer is solved on demand with a FPH_S of 90 days and a PEH_S of 60 days. At the beginning of the operation the scheduling layer is solved every 15 days, but it is also solved every time a large disturbance occurs so that the overall multi-loop strategy can react to drastic operational changes. Later, after 250 days of operation the update frequency is changed to 30 days. This variable update frequency aims to demonstrate the versatility and robustness of the online optimization approach.

Figure 7.25a shows the cleaning schedule executed by the multi-loop optimization approach and compares it against the actual one. The optimal cleaning schedule reduces the total operating cost by $ 0.51 M, although there are cleanings defined towards the end of the horizon from which the savings are not realized. In the optimal online solution, the number of cleanings is higher during the period of high input flow rates because the furnace duty and the energy cost are higher – Figure 7.25b – hence frequent cleanings become profitable, although high flow rates reduce the fouling rate of certain units in the network. The opposite effect is observed during the period of low input flow rates when the number of cleanings is reduced compared to all other operating periods and the furnace duty decreases.

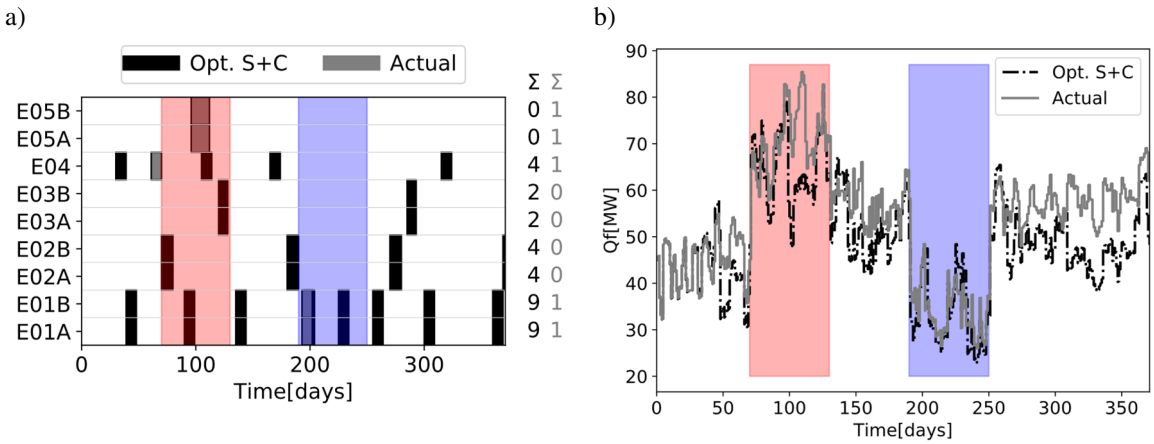

Figure 7.25. Cleaning schedule executed (a) and furnace duty (b) for REF-X case when step disturbances in the input flow rates are introduced.

The effect of the step disturbances in the input flow rates is clearly observed in the furnace duty, Figure 7.25b. The online (Opt. S+C) optimization approach keeps it lower than for the actual operation during the period of highest energy requirements – red area. Also,

after the period of low energy requirements – blue area – optimal cleanings are executed because the input flow rates increase, so the potential energy savings of cleanings increase.

The effect of disturbances and how they affect the manipulated variables can be visualized on the individual performance of the units. Figure 7.26 shows an example for exchanger E01B. The change of frequency in the cleanings during periods of high and low input flow rates is observed as well as the changes in the fouling rate. High flow rates increase the shear stress, hence the removal rate of the deposit increases, while at lower input flow rates the fouling rate increases because the shear stress decreases, and the crude is exposed to higher wall temperatures for longer times. This figure also compares the actual operation against the online optimal operation, and it shows that in the actual operation E01B has high levels of fouling during most of the time so that the step changes in the flow rates have almost no effect on its performance – it has reach the asymptotical fouling level which completely compromise the energy recovery of the unit. On the other hand, the online optimization approach reacts efficiently to the large disturbances, exploits their effects, and increases the energy recovery of the units when possible.

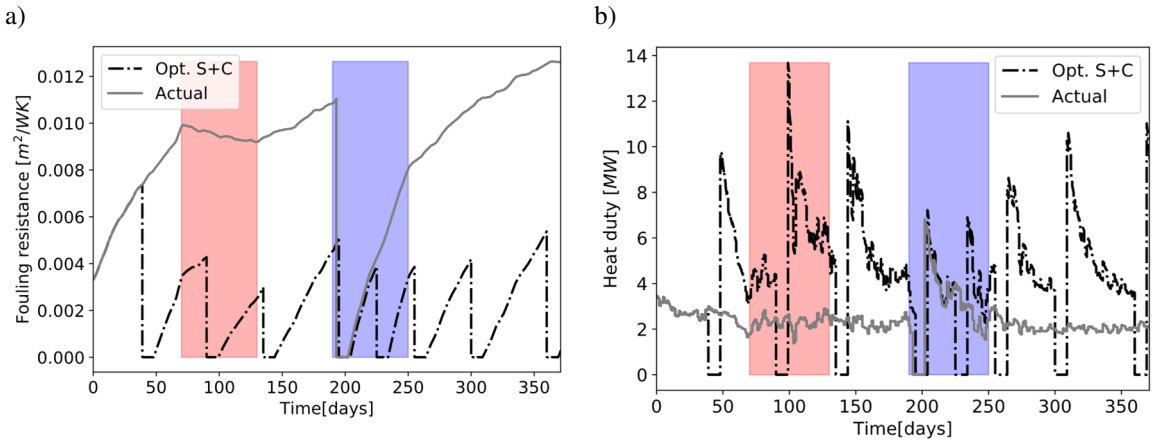

Figure 7.26. Fouling resistance (a) and heat duty (b) of exchanger E01B of REF-X case when step disturbances in the input flow rates are introduced.

The presence of large disturbances in the system represents a challenge for estimating accurate and representative parameters for the models used in the online approach, and for forecasting the behaviour of the disturbances over the FPH_S. Figure 7.27 shows the evolution of the predicted (red) fouling resistance of E02B at the scheduling layer $NMPC$, the observed value (black), and the estimated (blue) one solving the MHE_S problem. From top to bottom

it shows four consecutive evaluations of the scheduling layer – the execution time is shown on the top right corner – where the first two are before the step change from nominal to low flow rates, and the last two after the disturbance. The prediction quality is compromised for the first two instances as higher flow rates than the actual ones are used in the solution of the $NMPC$ problem, but after that, and using an on demand update frequency, the prediction improves and becomes more accurate using a better forecast for the input disturbances.

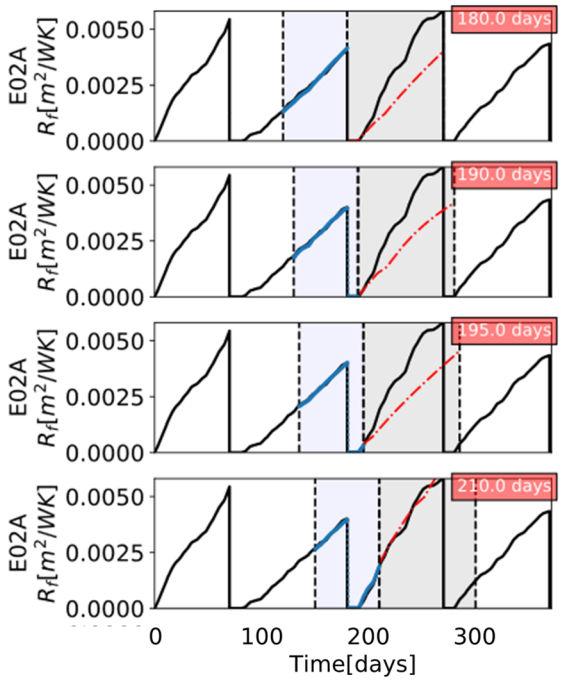

Figure 7.27. Evolution of the predicted fouling resistance of E02A for REF-X case at four consecutive solutions of the scheduling layer of the online optimization approach.

7.3.5. Effect of crude blend disturbances in the system

This section presents the case of large model plant mismatch, which is modelled as sustained step disturbances in the 'real' deposition constants used to simulate the actual plant. While Section 7.3.4 analysed the effect of input flow rate disturbances and how the optimal solution of the $NMPC_S$ adapts to them, this one focuses on how the MHE_S copes with large discrepancies between the actual plant and the predictive models.

The 'real' deposition constant of each exchanger in the REF-X case study is subject to large changes. The mismatch approached used in Section 7.3.2 is inherited here, but three sustained step changes are introduced. Figure 7.28 shows the time series for the deposition constant of two exchangers, and three consecutive step changes. The same relative step

change is applied to the deposition constant of all units in the network because it is assumed that they are all correlated. The intensity of the grey areas represents the deviation from the average values of the deposition constant during those periods, which are: -80%, +150%, +60%, and +200, in that order. This visual representation of the disturbances is used throughout the analysis presented in this section. The last step change has the largest deviation from the average operation, and it also introduces a larger variability than that of all other operating periods. This last period represents a more challenging scenario for testing the multi-loop online optimization approach, its ability to adapt the predictive models and to optimize the preheat train operation.

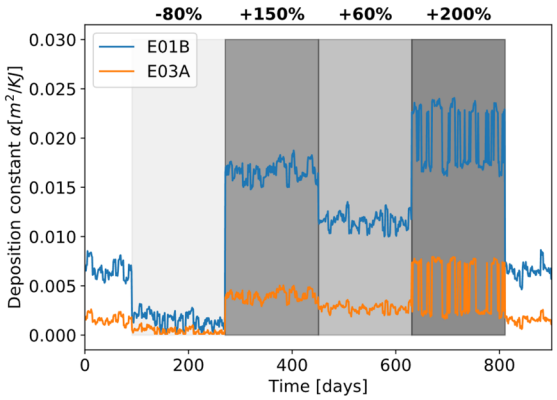

Figure 7.28. Example of the step change in the 'real' deposition constant of case REF-X.

The online optimization approach is applied to the REF-X case under this large mismatch in the deposition constants for the first 900 days of operation, and varying input conditions. The configuration of the control layer is the same used in Section 7.3.2, while the scheduling layer uses an update frequency of 30 days, a FPH_S of 90 days, and a PEH_S of 60 days. The closed-loop optimal solution (Opt-Closed loop) obtained with these settings is compared against the actual operation of the refinery (Actual) and against the open loop optimization (Opt-Open loop) of the preheat train. The open loop optimization is the solution of the problem formulated in Chapter 5 assuming constant input flow rates, stream temperatures and deposition constants, estimated from previous data. The constant operating conditions used are defined as the average values of the variables during the operating time, and the deposition constants are those used in Chapter 5. The open loop optimization ignores the effect of the disturbances and operational changes, so that it is not known a priori that the

crude processed in the future will have a higher or lower fouling propensity than that processed before, based on which the fouling parameters of the model were estimated.

Figure 7.29 compares the cleaning schedule obtained with these different approaches. It is observed that the online approach reacts as expected to the changes in deposition rates. There are almost no cleanings during the period of lowest deposition rate (-80%), when great part of the deposit can be removed by modifying the flow rates through the exchangers, while there are many more in the periods with the highest rates (+150% and +200%). These changes are completely ignored in an open loop optimization and ineffective cleanings are allocated during low deposition rate periods. The Actual cost of the 900 days operation is $ 30.96 M, savings of $ 0.55 M are achieved with the Opt-Open loop alternative, while savings of $ 2.43 M with the Opt-Closed loop approach. The latter leads to the lowest operating cost as it considers the actual variability of the process, although it has the highest cleaning cost – $ 1.90 M vs $ 0.76 M for the open loop optimization. The timing and allocation of those cleanings is optimized considering all disturbances and correcting for the mismatch between the predictive models and the actual plant.

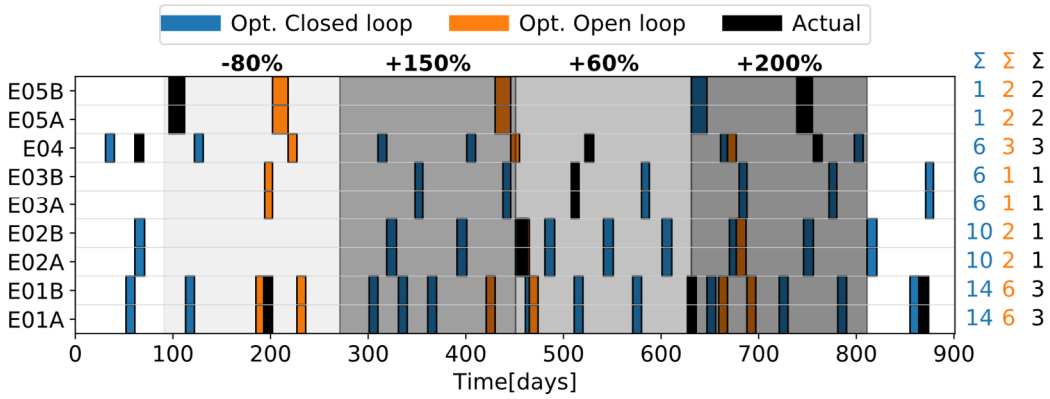

Figure 7.29. Cleaning schedule of REF-X operating under large mismatch in the deposition constants. Comparison of closed-loop optimization, open-loop optimization, and actual operation.

The effect of the large changes in deposition constant – crude blends processed – and fouling mitigation actions are observed in the furnace duty, Figure 7.30. For instance, during the period of low deposition rate even the furnace duty of the actual operation decreases – there are almost no cleanings during this period – because the removal rate is higher than the deposition rate. Also, the furnace duty achieved with the online optimization approach is

lower than that of the other approaches during most of the operation being the only one able to react to the dynamic changes.

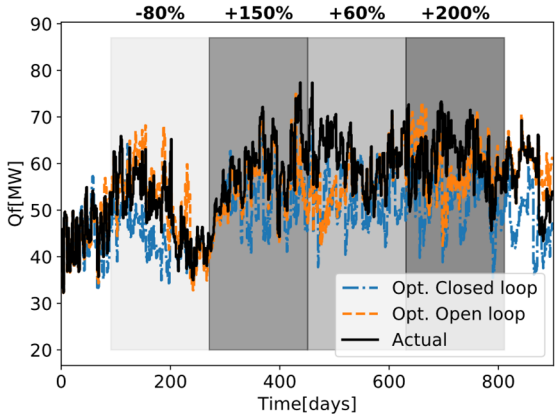

Figure 7.30. Furnace duty of REF-X operating under large mismatch in the deposition constants. Comparison of closed-loop optimization, open-loop optimization, and actual operation.

An example of the interactions between the varying operating conditions, changing deposition rates, and individual exchanger performance is presented in Figure 7.31. It shows the fouling resistance and the heat duty of E03A for alternatives analysed previously. It is observed that the fouling resistance changes dramatically between the periods defined by the step changes in the deposition constant. During the low deposition period, the fouling rate is supressed for the actual operation, while for both optimal approaches the removal rate is higher than the deposition rate, and the deposit is almost completely removed by the end of this period. An improved heat duty of the exchanger is also observed in that period, and it is more noticeable for the open loop optimization case where this exchanger is cleaned at 200 days of operation. That cleaning is ineffective, although optimal under the open loop assumptions, because the actual deposit of the exchanger was almost inexistent at that time. In the following periods – all with a positive deviation from the average deposition rates – the fouling resistance of the exchanger increases much faster, but the optimal approaches can mitigate this effect by cleaning this unit or varying the flow distribution of the network to increase the shear stress of certain exchangers. These actions achieve a higher heat duty, lower fouling resistance, or reduce the fouling rate. Finally, in all cases the transition from a high deposition rate period to a low deposition rate period – transitions before the -80% step,

and after the 200% step – promotes the removal of the deposit, so this combined with a flow distribution optimization significantly improve the performance of the network.

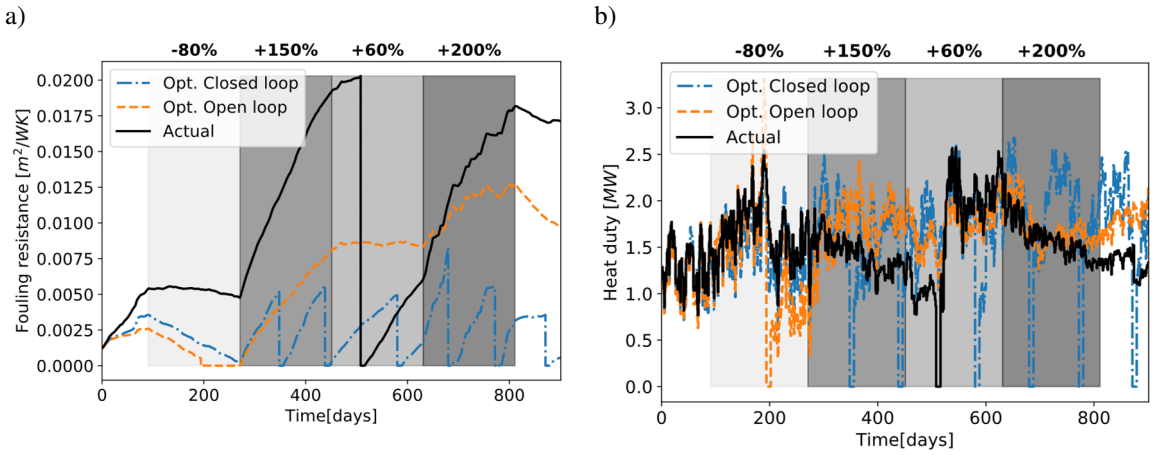

Figure 7.31. Fouling resistance (a) and heat duty (b) of exchanger E03A of REF-X operating under large mismatch in the deposition constants.

The significant improvements on the preheat train operation achieved by the closed loop optimization approach are due to an efficient and accurate estimation of the model parameters at very sampling time, and for every feedback loop. As an example, Figure 7.32 shows the time series evolution of the 'real' deposition constant and the one estimated at the control and scheduling layers of the online approach for E04. The estimated values at both layers show a good agreement with the actual ones used to simulate the plant, despite the large step changes and high variability. The estimated parameters for the prediction models at the MHE of each layer follow the same trend as the actual ones. However, a delay of one sampling time is observed in the results of both control and scheduling layer after the large step changes in the deposition constants occur. This delay is clearly observed at the transition from the first step change to the second. It is caused by the nature of the MHE where only the past measurements within the PEH are used to estimate the model parameters. Therefore, immediately after a large change in the system the models still reflect the old information until the next sampling time, when those changes are incorporated in the estimation problem. Figure 7.33 shows how the predictive models adapt in the presence of large mismatch. The predictions before the largest step changes – -80% step change (a) and +200% step change (b) – are erroneous, but they are immediately corrected at the next sampling time, when new information containing the effect of the changes is available.

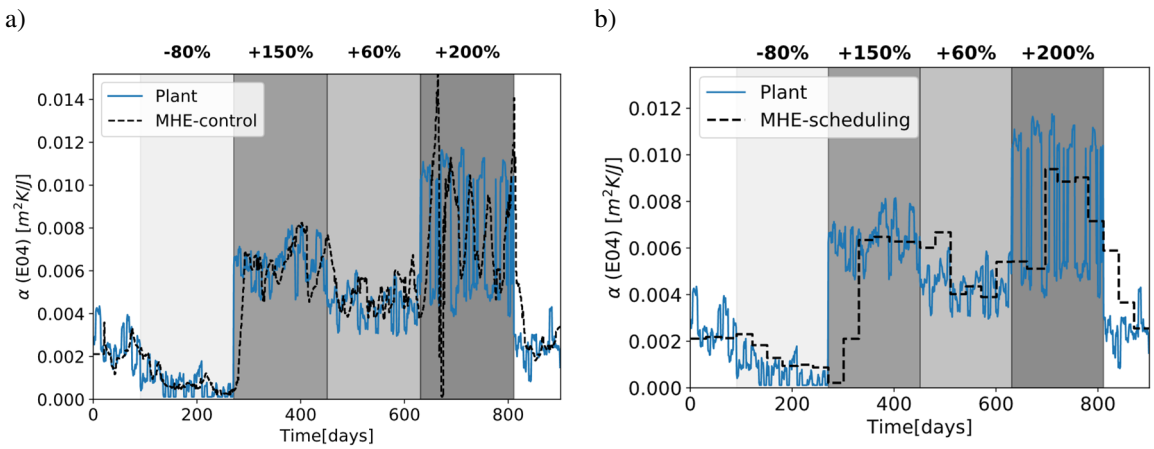

Figure 7.32. Comparison of the 'real' deposition constant and the estimated one at the control layer (a) and at the scheduling layer (b) for E04 of REF-X case operating under large mismatch

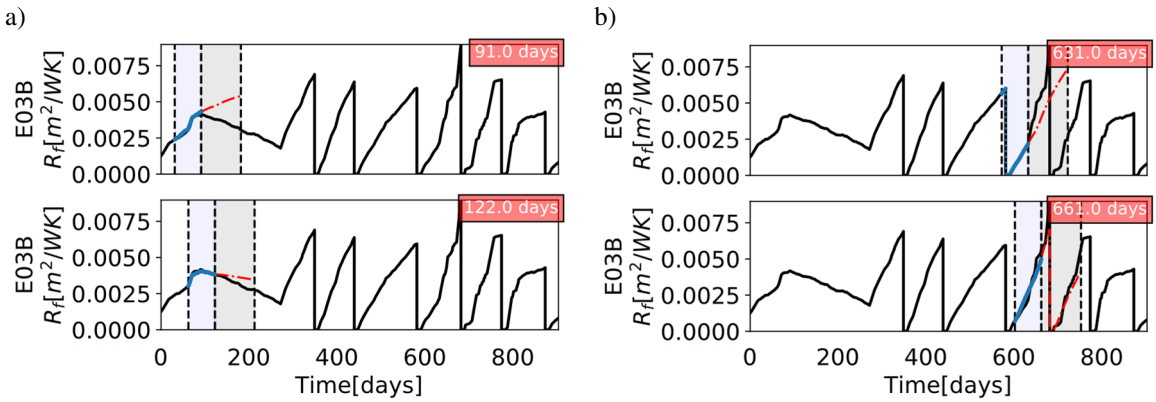

Figure 7.33. Moving horizon prediction and estimation of the fouling resistance before the -80% step change (a), and the +200% step change (b) of the deposition constant for E03B of REF-X case.

The rapid reaction of the control layer to adapt to the changes and disturbances of the system as seen in Figure 7.32a allows to exploit all the benefits of integrating scheduling and control decisions. In the case where the control model parameters are not updated by solving the MHE_C problem at every instance, but are defined accordingly to those of the scheduling layer, the performance of the system worsen. For this specific example, the total operating cost increases by $ 50.000 and the number of cleanings by 2. Although that configuration of the multi-loop optimization approach can be seen beneficial to reduce computational time and to avoid large changes in the control actions, it is only worth pursing when large disturbances are not expected – only oscillations around an average operating point as those

considered in Section 7.3.2. Given the nature of the problem, high variability is expected in the operation of the preheat trains because of the constant changes of the crude blends and their properties, which justifies a constant update of the control layer parameters.

7.4. Concluding remarks

A novel approach for online fouling mitigation and optimization of preheat trains operation was presented. The online optimization approach uses two feedback control loops, each containing an MHE, to estimate the current state of the system and the parameters of predictive models, and an economic oriented $NMPC$, to determine the optimal control actions in the operation. The inner feedback loop optimizes the flow distribution of the network on a short time scale, while the outer feedback loop optimizes simultaneous the cleaning schedule and flow distribution on a longer time scale. These two loops interact strongly to reject disturbances, and optimize the operation over all time scales. For the first time, a comprehensive online optimization approach considers the dynamics of the system, the variability of the operating conditions, disturbances, and model-plant mismatch.

The application of the online optimization approach proposed was extensively tested using a case study based on a real preheat train and its actual variable operating conditions. The main advantages and findings are:

1. The outer loop integrates cleaning scheduling and control decisions over long horizons, while at a lower level only control decisions reject disturbances and minimize operating cost on short horizons. It was demonstrated that this approach leads to better performance of the network than that achieved by the actual operation policy of the refinery or by heuristic algorithms that can be applied online.
2. The predictive models are updated online based on the most recent observations of the plant, so that regardless of mismatch or variable conditions, the MHE solutions at each layer are found to be accurate, and the parameters to be representative of the current operation of the preheat train.
3. The decisions based on the predictive models updated online – $NMPC$ solutions – achieve an improvement of the performance (cost reduction).
4. The FPH_S and the update frequency of the scheduling layer have a significant effect on the closed-loop performance, and the total operating cost can be reduced

modifying those parameters. For the case study analysed it was shown that longer FPH_S (> 300 days) and shorter solution intervals provide better results.

5. The online optimization approach copes efficiently with large and extreme disturbances – large changes in inlet flow rates, and the processing of different crudes – because of the frequent updating of model parameters and predictions in the feedback loops. It was shown that the closed-loop optimization reduces much more the operating cost than an open-loop optimization considering average operating conditions.

All optimization problems involved are solved efficiently and in a much faster time than the sampling time of the feedback loop. Hence, frequent sampling can be selected to achieve a fast response to disturbances and operational changes. However, updating the control decisions too frequently may cause instabilities in the system when the actions involve binary decisions. It can also be unpractical to modify a planned cleaning schedule too often. Evaluating the stability of the closed-loop performance is key to ensure that the control and fouling mitigation actions planned are feasible as well as beneficial from an economic point of view. The issues about closed-loop stability are addressed in Chapter 8.

Finally, the online approach presented is general and not restricted to HEN under fouling. The principle of defining multiple feedback loops, each appropriate for a representative time scale – which create a good balance between planning ahead decisions and reactive immediate decisions – and linking them correctly can be applied to other system where the integration of control and scheduling decisions is advantageous or necessary. Examples of this are batch plants for specialized products, energy systems, and dynamic systems involving switches or on/off decision.

Chapter 8

Online optimization of preheat trains: closed loop schedules stability

It has been shown in other fields that the repeated online optimization of schedules can be unstable. From a practical perspective, a stable cleaning schedule of preheat trains under fouling is desired – one that does not change (erratically, too much, or unnecessarily) over time – but still accounts for the process variability and optimizes the operation. The goal of this chapter is to evaluate the trade-off between closed loop economic performance, and schedule stability for the online optimization of preheat trains. A general approach to improve schedule stability is proposed. First, it defines quantitative measurements of instability – task timing instability, task allocation instability, and overall schedule instability – which are developed as practical metrics of the performance. Then, options to improve closed-loop scheduling stability based on MPC and re-scheduling concepts are developed and tested. A realistic refinery preheat train, including the actual input variability and mismatch in the predictive models, is used to demonstrate the key aspects of closed-loop scheduling stability and the options proposed for improving it.

8.1. Introduction

Closed-loop stability of any control system or online application that directly manipulates the actions on a system is paramount for a reliable and practical operation. This issue becomes important in the operation of preheat trains under fouling when the cleaning schedule is optimized in a feedback loop using a moving horizon as proposed in Chapter 7. The changes in the optimal cleaning schedule predicted at every evaluation aim to minimize the operating cost based on the current state of the system, the disturbances of the process, and other operational changes that have occurred or may take place within the prediction

horizon. However, the cleanings allocation and their starting time may change between consecutive evaluations of the optimal schedule in the feedback loop, which may introduce instabilities and make planning of long term activities in the refinery a difficult task. Improving scheduling stability is desired from a practical perspective – the cleanings are not automated and required manual intervention – but it may compromise the ability of the feedback loop to adapt the optimal actions according to the changes of the system. The aim of this chapter is to quantify and mitigate the effect of scheduling instability in the online optimization of preheat trains under fouling without compromising the closed loop performance and the potential economic benefits.

For the purpose of this chapter, schedule stability is understood as a property of an online schedule application where the executed actions do not exhibit unexpected changes with respect to those predicted between consecutive evaluations.

The problem of schedule stability is not unique to the online optimal cleaning scheduling of HEN under fouling. It has been a topic of interest for operations research, where a schedule is revised at certain time intervals, when new unexpected orders arrived, after large changes of demand or prices, after long delays of a certain task, if a unit breaks down, or when new key information is available (Graves 1981). In operations research, this is referred to as re-scheduling or reactive scheduling, while the concept of schedule instability is referred to as schedule nervousness, and a stable or robust schedule refers to one insensitive to variability and uncertainty (Li and Ierapetritou 2008). Although in practical applications the schedule is revised multiple times during its execution and it may be partially modified (Cott and Macchietto 1989), it is rarely defined completely online and automated in a feedback loop to constantly account for the effect of disturbances and operational changes. On the other hand, in process control applications it is common, if not universal, to use feedback loops that constantly update and modify the control actions reacting to disturbances and operational changes, and it happens automatically in real time. However, there is a big difference in time scales and ease of implementing new actions in the process between scheduling and control. While control actions are executed by fast elements – opening of valves, power of engines – that enable a rapid response of the process, scheduling actions require long term planning, use of resources, and human intervention for their execution. In

principle they can both be automated in a feedback loop as it was proposed in Chapter 7 for preheat trains, but schedule stability must be guaranteed for its application.

In online scheduling, instability may occur even when there are no uncertainties or changes in the process. For instance, in Risbeck, Maravelias, and Rawlings (2019) a production schedule of two products in a single unit was analysed and defined using an receding horizon optimization approach. It was shown that the production schedule predicted at every instance, although optimal, was never executed and the unit remained idle. In nominal cases with no uncertainties or disturbances the length of the prediction horizon has a direct effect on schedule stability (Risbeck, Maravelias, and Rawlings 2019). At every evaluation, new information is available for the scheduling problem that was not considered in the previous solution, and this may change the trade-offs among different decisions.

This chapter builds on the online optimization approach presented in Chapter 7, and it takes it further to analyse the closed loop stability of the scheduling feedback loop, to ensure it is suitable for practical applications. The flow control feedback loop does not exhibit stability issues as it is assumed to be automated and it responds much faster to operational changes. The following section presents novel definitions of schedule instability that are general for any scheduling application and aim to quantify the variability between consecutive evaluations of a schedule. Then, a combination of strategies developed from MPC and re-scheduling concepts are presented to reduce the closed-loop instability of the online cleaning scheduling of HEN. Finally, those strategies are tested in a realistic case study, and the trade-off between stability and economic performance is discussed.

8.2. Measuring closed loop scheduling instability

Closed-loop schedule instability must be quantified to determine efficient strategies to reduce it, but no single metric is adequate. In production scheduling, it has been quantified as the difference in the overall quantity of a given product produced between two consecutive evaluations of the schedule at a given time (Sridharan, Berry, and Udayabhanu 1988). Other attempts have quantified the changes in starting time of the same task between two consecutive solutions (Pujawan 2004), or the changes in task allocations among the units available (Pujawan 2004; van Donselaar, van den Nieuwenhof, and Visschers 2000). The problem of interest here is a type of maintenance scheduling for which there is no production

of a given product, hence it is impossible to measure instability as the change of production between two instances. On the other hand, the differences in the starting time of tasks – starting time of the cleanings – and in the task allocations – number of cleanings per exchanger – can be used to quantify schedule instability. Figure 8.1 shows two consecutive evaluations of a cleaning schedule and a representation of the main sources of instability including changes in task allocations (which units are cleaned) and the starting time of the tasks (when cleanings start). The schedule instability is only defined for those actions within the overlapping time in the future prediction horizon of two consecutive schedule evaluations ($OT - FPH_k$ defined between t_k and t_{k-1}), where an evaluation of the schedule corresponds to solving the MHE and the $NMPC$ problems of the scheduling feedback loop. Four metrics of schedule instability are defined based on these considerations: 1) task time instability, 2) task allocation instability, 3) overall instability, and 4) overall weighted instability. The first two metrics are developed as modifications from some previously reported in the literature, while the others are new contributions of this work.

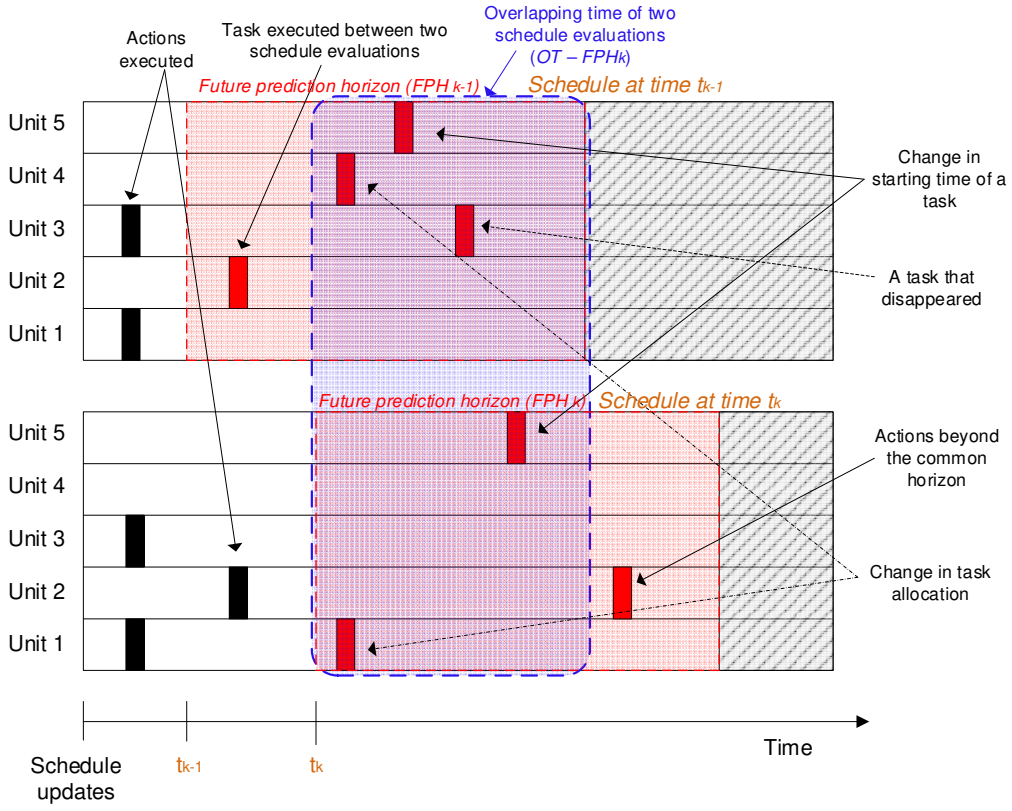

Figure 8.1. Representation of sources of scheduling instability and the elements used to quantify it.

Each of these definitions of schedule instability is explained next. It is assumed that a continuous time representation is employed at each schedule evaluation (Chapter 3, Section 3.3.2), so that the predicted schedule is defined for a set of units, tasks, and periods of variable length. Although a discrete time representation is common for scheduling problems, using a continuous does not limit the generality of the following developments. Throughout this thesis a continuous time representation has been used to optimize preheat trains under fouling, so the formulation and definitions used so far are directly compatible with the following concepts.

All the metrics of schedule instability are defined between consecutive schedule evaluations. In this way, instability metrics are generated every time a schedule is evaluated, and their time evolution can be tracked in the same way as the solutions of the scheduling problem are tracked on an online application based on a rolling horizon.

The following definitions, sets and indexes are used to define the instability metrics for the online scheduling problem:

- $Units = \{1,2,\dots,N_U\}$. Set of units.
- $Tasks = \{1,2,\dots,N_{TS}\}$. Set of tasks that can be allocated to the units.
- $T = \{1,2,\dots,n_T\}$. Set representing time in the FPH as defined in Chapter 3.
- $SE = \{1,2,\dots,n_{SCH}\}$. Set of schedule evaluations performed over time.
- $y_{I,i,j,t,k} \in \{0,1\} \forall i \in Units, j \in Tasks, t \in T, k \in SE$. Binary variable indicating the allocation of a task j to a unit i starting at a time t in a schedule evaluation k.
- $t'_k \forall k \in SE$. Time of the operation at which schedule k is evaluated.
- $\mathrm{T}^*_{S,k} = t'_k - t'_{k-1} \forall k \in SE \backslash \{1\}$. Time elapsed between two consecutive schedule evaluations.
- $\tau'_{i,j,k} = \left\{t'_k + t | y_{I,i,j,t,k} = 1 \wedge 0 \leq t \leq FPH_{k-1} - \mathrm{T}^*_{S,k} \forall t \in T\right\} \forall i \in Units, j \in Tasks, k \in SE \backslash \{1\}$. Set of the starting times of all tasks j allocated to unit i in a schedule evaluation k and within the operating time $OT - FPH_k$.
- $\tau^0_{i,j,k} = \left\{t'_{k-1} + t | y_{I,i,j,t,k-1} = 1 \wedge \mathrm{T}^*_{S,k} \leq t \leq FPH_{k-1} \forall t \in T\right\} \forall i \in Units, j \in Tasks, k \in SE \backslash \{1\}$. Set of the starting times of all tasks j allocated to unit i in a schedule evaluation $k-1$ and within the operating time $OT - FPH_k$.

- $\tau^{*}_{i,j,k} = argmin\{|\tau'_{i,j,k}|, |\tau^{0}_{i,j,k}|\} \forall i \in Units, j \in Tasks, k \in SE \backslash \{1\}$. Set assigned to $\tau'_{i,j,k}$ or $\tau^{0}_{i,j,k}$ based on which has the minimum number of elements.
- $\tau^{*C}_{i,j,k} = \{\tau'_{i,j,k}, \tau^{0}_{i,j,k}\} - \tau^{*}_{i,j,k} \forall i \in Units, j \in Tasks, k \in SE \backslash \{1\}$. Set defined as the complement of $\tau^{*}_{i,j,k}$.

Note that for the problem of cleaning scheduling of HEN considering only mechanical cleanings, the set $Units$ is equivalent to the set HEX, which was defined in Chapter 3, and the set $Tasks$ has a single element $\{1\}$ corresponding to one type of mechanical cleaning. The variable y_I defined here, is equivalent to the variable y of the problem formulation presented in Chapter 3. It is still possible to assign multiple mechanical cleanings – multiple instance of the same type of task – to one unit at different times, and this is one of the sources of schedule instability in the problem.

8.2.1. Task timing instability

Task timing instability at the schedule evaluation k, $I_{ts,k}$, is defined as the difference in the starting time of the common predicted executions of task j in unit i during schedule evaluations k and $k-1$ over the $OT - FPH_k$. Its mathematical representation is presented in Eq. (8.1). Note that this difference only exists for those predicted executions of a task j that are defined in both schedule evaluations k and $k-1$. If multiple executions of task j are predicted over the $OT - FPH_k$ in both schedule evaluations, k and $k-1$, the difference in their starting times is only relevant for the minimum number of instances of task j predicted. In addition, if in the schedule evaluation k, or $k-1$, there are no predicted executions of task j in unit i, there is no contribution of this pair of task and unit to the overall task timing instability metric.

$$I_{ts,k} = \frac{1}{FPH_k} \sum_{i \in Units} \sum_{j \in Tasks} \left[\sum_{t \in \tau^{*}_{i,j,k}} \min\left\{(t - \hat{t})^2, \forall \hat{t} \in \tau^{*C}_{i,j,k}\right\} \right]^{1/2}, \qquad \forall k \in SE \backslash \{1\} \tag{8.1}$$

This instability metric is divided by the future prediction horizon of the scheduling problem at update k, FPH_k, to transform it in a dimensionless quantity. The task timing instability takes a value of zero when there is no difference in the predicted starting time of all the common tasks allocated to the units in two consecutive schedule evaluations, or when there are no task of the same type allocated to the same unit in two consecutive schedules –

all the tasks allocated to a unit disappeared or are shifted to another one. The task timing instability increases when the difference in the starting times of a task allocated to a unit in two successive schedules is large – the maximum difference possible is the FPH_S.

In the case of interest – cleaning scheduling of HEN under fouling – there is a single type of task to allocate to the units, that is, a "cleaning" task. This simplifies the definition of the task timing instability as it is not necessary to keep track of type of tasks allocated to the units and their starting times.

8.2.2. Task allocation instability

Task allocation instability at schedule evaluation k, $I_{T,k}$, is defined as the change on the total number of executions of tasks j allocated to unit i during the $OT - FPH_k$, with respect to the total number of executions of the same task in the same unit in the previous schedule evaluation, $k-1$, over the same time horizon. It is expressed mathematically in Eq. (8.2). This expression assumes that all the tasks have the same relative importance for the stability, and only considers their total number of executions. In the cleaning scheduling problem, this refers to the change in the total number of cleanings of each exchanger within the $OT - FPH_k$, regardless of their starting time.

$$I_{T,k} = \frac{1}{\sum_{i\in Units}\sum_{j\in Tasks} N_{i,j}^{max}} \sum_{i\in Units}\sum_{j\in Tasks}\left[\sum_{t\in T | t\leq FPH_{k-1}-\mathrm{T}_{S,k}^{*}} \left(y_{I,i,j,t,k} - y_{I,i,j,t+\mathrm{T}_{S,k}^{*},k-1}\right)^2\right], \quad \forall k \in SE\backslash\{1\} \tag{8.2}$$

This definition of instability is standardized by dividing it by the summation of the maximum number of executions of task j that are allowed to be executed in unit i, $N_{i,j}^{max}$. This is a parameter of the scheduling problem, and it is specified by the user. For example, in the cleaning scheduling problem of HEN under fouling, it corresponds to the maximum number of cleanings per exchanger that can be executed in the future prediction horizon – it is the parameter N_{HEX} in the problem formulation presented in Chapter 3.

The task allocation instability becomes zero when there are no changes in the number of executions of the tasks – cleanings, in the problem of interest of this thesis – scheduled in each unit regardless of their starting time, or when there are no tasks of a given type scheduled in the future prediction horizon. This instability metric increases when one or more instances

of task are added to or deleted from one or multiple units in the current schedule evaluation with respect to the previous one.

8.2.3. Overall schedule instability

The overall schedule instability at schedule evaluation k, considers all the changes between two schedule evaluations such as changes in the starting time of the tasks, changes in task allocation, addition of new tasks, and disappearance of previous tasks. To compute the overall schedule instability, the $OT - FPH_k$ (overlapping time between consecutive evaluations k and $k-1$) is discretized using a step time that is lower than or equal to the duration of the tasks. In this case the sampling time of the process, 1 day, is used. This time discretization defines a matrix representing the schedule with N_U rows, one per each unit, and N_D columns, each representing a snapshot of the planned execution of the tasks at each time step in $OT - FPH_k$. The only entries of the matrix are either 0, representing no task allocated, and 1, representing a task allocation. This definition assumes there is a single task type to be performed in the schedule (specific to the cleaning scheduling problem of HEN), but it can be extended to a more general formulation with multiple task, with different integer values associated to each task type.

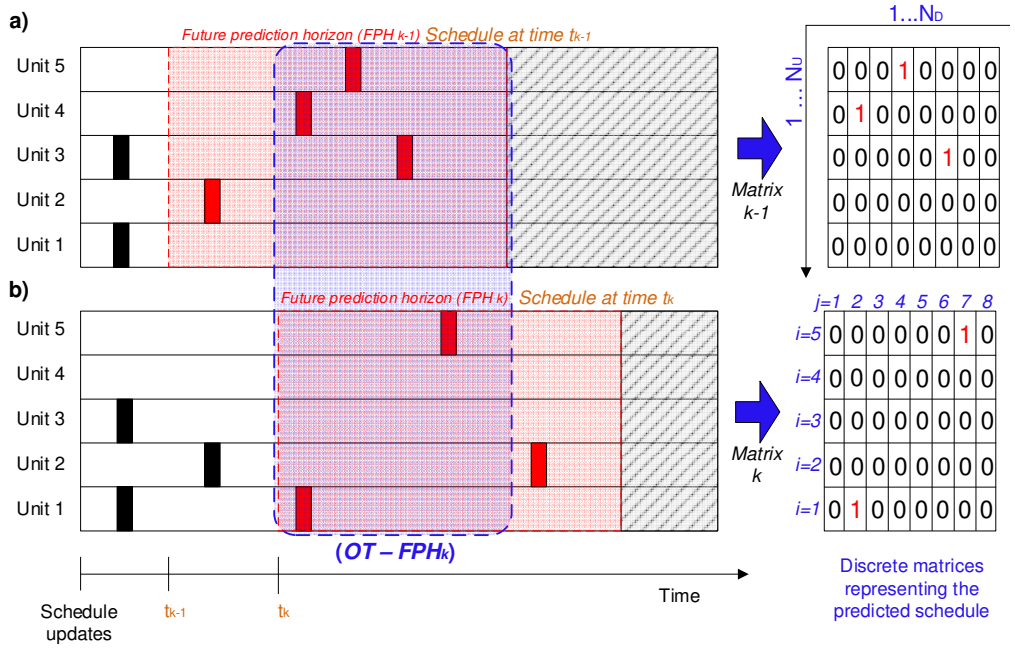

Figure 8.2. Matrix representation of a schedule with a unique task for a simple example. a) Schedule update $k-1$ at time t_{k-1}, b) Schedule update k at time t_k

Figure 8.2 illustrates how to generate a schedule matrix for a simple example with two schedule evaluations at times t_k and t_{k-1}. At every schedule evaluation, k, a schedule matrix is constructed. All matrices generated have the same dimensions because the $OT - FPH$, the sampling time, and the number of units in the system never change between updates. Therefore, it is possible to calculate the difference between two successive schedules based on the difference of each individual element of the schedule matrices. Each element of the schedule matrix is referred to as $x_{i,j,k}$ where i is an index for the units (rows), j an index for the time instances in the $OT - FPH_k$ (columns), and k an index for the schedule evaluations.

A metric of overall schedule instability at schedule evaluation k, $I_{ov,k}$, is defined in Eq. (8.3), where the quadratic difference between two consecutive schedule matrices, k and $k - 1$, is calculated element by element, and all the differences are added up. This difference is only computed for the overlapping period of consecutive schedule predictions ($OT - FPH_k$). Also, this instability metric is standardized by dividing it by the dimension of the schedule matrix ($N_U N_D$). All schedule changes are assumed to have the same effect on the overall schedule instability metric. They affect it by the same magnitude, and it is not possible to differentiate whether the changes in the schedule are due to changes in the starting time of the task, time delays, or changes in task allocation. Because this metric is standardized, it is bounded between zero and one, and it increases with the number of differences between consecutive schedule evaluations.

$$I_{ov,k} = \frac{1}{N_U N_D} \sum_{j=1}^{N_D} \sum_{i=1}^{N_U} \left(x_{i,j,k} - x_{i,j,k-1}\right)^2, \qquad \forall k \in SE \backslash \{1\} \tag{8.3}$$

In the example presented in Figure 8.2, there are five changes in the schedule matrices between schedule evaluations k and $k - 1$ (see columns 2, 4, 6 and 7 of the matrices in the figure). Then, applying the metric defined in Eq. (8.3), the overall schedule instability of that example is 0.125.

8.2.4. Time weighted overall schedule instability

The above overall schedule instability definition ignores when the difference in schedule evaluation occurs – timing effects. For example, the values of the overall schedule instability for two different schedule evaluations can be the same even if the differences and changes in the schedule are observed at the beginning of the FPH_S, which has large

implications on the operation because those are the actions to be executed in the current time step; or at the end of the FPH_S, when they are not very important and the uncertainty is high. In a closed loop or online scheduling implementation, schedule changes closer to the current execution time have a larger impact on the closed loop stability and performance.

Considering the limitations of the overall instability definition, one that accounts for the timing effects on the schedule changes is more informative. A time weighted overall schedule instability metric at schedule evaluation k, $I_{ovw,k}$, is defined in Eq. (8.4), where the weights represent the relative importance of each difference in the schedules with respect to time. This expression uses the same definitions of the overall schedule instability, Eq. (8.3), which are based on a matrix representation of the schedule over the $OT - FPH_k$. In this instability metric, the weights are selected to decrease linearly from one to zero, Eq. (8.5), between the current time of evaluation ($w_j = 1$ for $j = 0$) and the end of the $OT - FPH_k$ ($w_j = 0$ for $j = N_D$). The differences occurring closer to the current time are given a higher relative importance than those that occur later in the prediction horizon.

$$I_{ovw,k} = \frac{1}{N_U \sum_{j=1}^{N_D}(w_j)} \sum_{j=1}^{N_D} \sum_{i=1}^{N_U} w_j \left(x_{i,j,k} - x_{i,j,k-1}\right)^2, \qquad \forall k \in SE \backslash \{1\} \tag{8.4}$$

$$w_j = 1 - \frac{j-1}{N_D - 1}, \qquad \forall j \in \{1,2,\dots,N_D\} \tag{8.5}$$

The concept of using weights to characterize the relative importance of current changes with respect to later changes had been proposed by other authors (Sridharan, Berry, and Udayabhanu 1988; Kadipasaoglu and Sridharan 1997) to calculate schedule instability based on the production quantity of different products, but the task allocation and timing was ignored. Also, they used an exponential decay function to define the weights as a function of time. That definition can also be used here, instead of the linear function proposed, without adding complexity to the problem. The only difference is that the exponential decay function requires the analysts to set a parameter that indicates the rate of decay of the function, which can be translated as a preference to ignore or not schedule modifications occurring after a critical future time.

The time weighted overall schedule instability metric explicitly accounts for the effects of time to indicate that large variability close to the current time is undesirable, and that

occurring later can be tolerable. However, it does not distinguish whether the source of variability is due to changes in the task allocation or starting time of the task.

Applying the metric defined in Eq. (8.4) to the example presented in Figure 8.2, the time weighted overall schedule instability is 0.136 which is higher than the overall schedule instability, 0.125. This happens because most of the differences between consecutive schedule evaluations occurs close to the current time, t_k, which is reflected in a larger number of differences between the schedule matrices in columns with low indexes (see columns 2 and 4 of the matrices in the Figure 8.2). This example shows how the time weighted metric gives more importance to changes in the schedule that occur closer to the current time, and that may require an immediate action.

8.3. Alternatives to reduce closed loop scheduling instability

There are various alternatives to improve the closed-loop stability of online scheduling, but their actual benefits are not clear, nor is their effect on the overall economics of the process. Alternatives taken from MPC theory, and practical implementations of scheduling solutions are evaluated here in the context of cleaning/maintenance schedules. They are: 1) introducing a terminal cost with respect to a steady state in the objective function, 2) freezing a subset of the scheduling decisions in the FPH_S for consecutive evaluations, and 3) penalizing the changes in the scheduling decisions between consecutive evaluations. These alternatives are described next in the context of online cleaning scheduling of preheat trains under fouling.

8.3.1. Terminal cost penalty

In MPC the closed-loop stability properties have been widely studied from practical and theoretical perspectives. One alternative to ensure closed loop stability with a finite prediction horizon is to include a 'terminal cost' in the objective function of the optimization problem solved at every sampling time (Maciejowski 2002). Eq. (8.6) represents a general objective function – where x are continuous variables, y integer variables, and u manipulated variables – solved in an MPC implementation at each sampling time. The function V is the 'running cost' that, in tracking problems, is defined as the quadratic difference of the states with respect to a reference point. On the other hand, the function l is the 'terminal cost' and

it is only a function of the variables at the end of the prediction horizon, t_{FPH}. The parameter ρ_l represents a penalty on the terminal cost and indicates its relative importance with respect to the running cost – higher values ensure stability as every prediction will reach the final state defined. For the terminal cost to ensure stability it must be defined as the norm of the difference with respect to the desired operating point. Under these conditions the objective function J will decrease monotonically with every solution of the optimization problem – assuming global optimality (Maciejowski 2002).

$$\min J_k = \rho_l l\big(x(t_{FPH}), y(t_{FPH})\big) + \int_0^{FPH_S} V(x(t), y(t), u(t))dt\,, \qquad \forall k \in SE\backslash\{1\} \tag{8.6}$$

There are differences with the goals of the general MPC formulation, and the one of the closed loop scheduling that hinder the applicability of adding a 'terminal cost' to improve stability. First, the assumptions to guarantee stability in MPC state that the objective function must decrease with the number instances evaluated, but in the case of closed-loop scheduling the objective is economic which violates this assumption. Second, the maintenance/cleaning scheduling problem does not have a stable reference point to use in a tracking function. The clean state (ideal) is not achievable without infinite cleanings, and the asymptotic operating point where all units have minimum performance is undesirable or infeasible. Third, the scheduling problem includes discrete variables over a long time scale instead of continuous variables over short time scales. Finally, stability for MPC is defined accordingly to whether the system remains in the same operating point (outputs of the plant) regardless small disturbances (Maciejowski 2002), while for closed-loop scheduling stability is defined based on the intensity of the changes of the scheduling variables (inputs to the plant) between consecutive solutions.

For closed-loop maintenance/cleaning scheduling the reference point of the terminal cost is therefore defined as the limited operation point when the performance of the system is minimal – each exchanger has reached its asymptotic or maximum fouling level or an operational constraint has been reached. This limited operation point is determined performing a simulation of the system assuming average operating conditions and no mitigation actions. Alternatively, this operating point can be defined based on engineering judgement of the operation – worst, but realistic possible state expected or observed in the past. Although this reference point represents the worst state of the system, it is usually a

stable point that can be reached from any state. This reference point only applies to the maintenance/cleaning scheduling problems, and other scheduling problems may have cyclic solutions that can be used as references for stability (Risbeck, Maravelias, and Rawlings 2019).

The terminal cost used here in the online optimization of flow distribution and cleaning schedule is defined in Eq. (8.7). It is the quadratic difference between the temperature predicted at the end of the FPH_S of each stream in the network, $T_{a,t=FPH}$, and that of the limited operating mode without cleanings, T_a^{∞}. The set A refers to the set of arcs in the network defined in Chapter 3, whose elements are all the streams connecting all the nodes. Pressure drop predictions are ignored in this terminal cost because the thermal effects generally represent the highest contribution to the total operating cost of the system. In addition, in the cleaning scheduling problem of HEN, the overall integral of the running cost, V, is the total operating cost of the preheat train which is the objective function of the online scheduling problem defined in Eq. (7.4).

$$l = \rho_y \sum_{a \in A} \left(T_{a,t=FPH_S} - T_a^{\infty}\right)^2 \tag{8.7}$$

This alternative has a single parameter, ρ_y, that can be modified to represent the desired trade-off between closed-loop stability and operating cost.

8.3.2. Freezing decision in prediction horizon

Fixing or freezing some of the scheduling decisions within the prediction horizon retaining those of a previous evaluation explicitly reduces scheduling instability (Blackburn, Kropp, and Millen 1986; Jacobs et al. 2005). Every time a scheduling problem is solved, a fraction of the decisions from the previous schedule evaluation is frozen, and the rest are considered free. The fixed actions are defined as equality constraints in the next scheduling problem. The different time intervals for online scheduling, and the nature of the decisions at each evaluation are shown in Figure 8.3 for three successive schedule updates. It shows that the actions executed between sampling times are mixed between those frozen from the previous solution, and those obtained at the current evaluation. The length of the frozen interval and the scheduling decisions included, such as task allocated and starting time of the tasks, gives a trade-off between stability and closed-loop performance. For instance, fixing

all scheduling variables within the frozen periods leads to a more stable solution at the expense of not being able to react to disturbances or any other changes in the operation of the system.

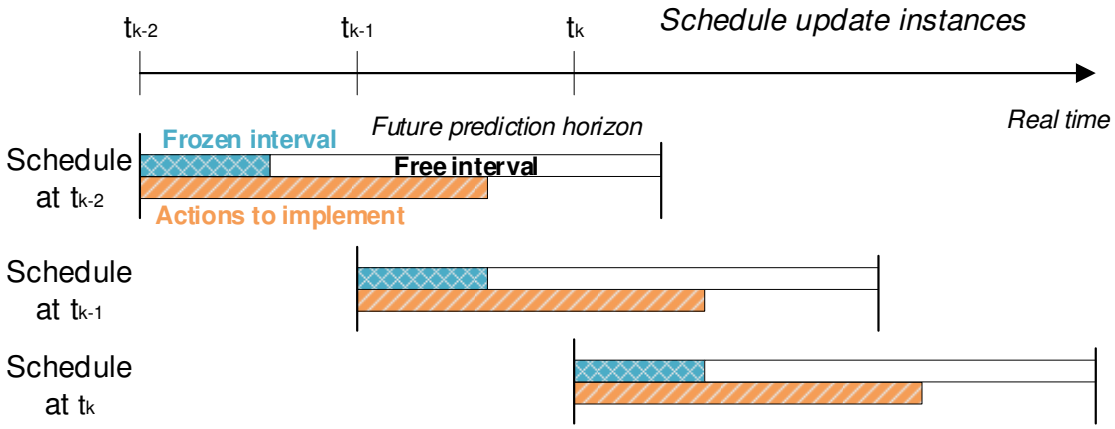

Figure 8.3. Representation of freezing scheduling parameter for improving closed-loop schedule instability.

In the online cleaning scheduling and flow distribution problem of HEN, there are two kind of decisions that can be kept constant between consecutive schedule updates: the assignment of cleanings to periods and units, and the starting time of the cleaning actions. Equality constraints are introduced in the optimization problem formulation to freeze the selected cleaning actions of the current schedule to the values calculated in the previous one. Eq. (8.8) shows this constraint for the binary decisions, where the $*$ symbol denotes the previous optimal solution of the scheduling problem. These equality constraints assign the cleanings to the units and periods, but because the periods have variable length – due to the continuous time representation – the starting time of the cleanings is not fixed. To allow more flexibility, inequality constraints are introduced to restrict the variability of the cleanings starting time with respect to those of the previous optimal schedule. This is shown in Eq. (8.9) which can be transformed into an equality constraint if necessary.

$$y_{i,t(n),k} = y^{*}_{i,\mathrm{T}^{*}_{sch}+t(n),k-1}, \qquad \forall i \in HEX, n \in \{1,\dots,N_z\}, k \in SE\backslash\{1\} \tag{8.8}$$

$$-\Delta\mathrm{T}^{cl} \leq \tau^{cl}_{i,t(n),k} - \tau^{cl*}_{i,\mathrm{T}^{*}_{sch}+t(n),k-1} \leq \Delta\mathrm{T}^{cl}, \qquad \forall\, i \in HEX, n \in \{1,\dots,N_z\}, k \in SE\backslash\{1\} \tag{8.9}$$

The number of periods where decisions should be frozen and the bounds in the starting times of the cleanings are tunable parameters of this approach to balance closed-loop stability and economic performance.

8.3.3. Penalizing variability

Penalizing the change of scheduling decisions between two consecutive scheduling evaluations is another alternative to improve closed-loop schedule stability. Instead of using constraints to reduce the variability between consecutive schedule evaluations, as it is done in the freezing horizon approach, variability is minimised by introducing a penalty in the objective function of the scheduling problem. The variability between two schedule evaluations is only penalized within the period overlapping the future prediction horizons ($OT - FPH_k$). The definition of this period can be observed in Figure 8.1 where the main concepts of schedule stability are described.

The penalty expression accounting for scheduling variability is included in the optimization formulation of the scheduling problem solved online. This penalty is divided in two independent terms: one for the changes in the allocation of tasks, Eq. (8.10), which can be related to the task allocation instability metric; and another for the changes in the starting time of the tasks, Eq. (8.11), which can be related to the task timing instability metric. These penalties are only defined within the time horizon $OT - FPH_k$. Each of these expressions has a penalty parameter ρ that characterizes its importance relative to other and to the economic objective function of the scheduling problem. The final overall objective function for each instance of the scheduling problem is Eq. (8.12), and it shows the compromise between stability and process economics. Also, the integral of the running cost, V, corresponds to the total operating cost of the preheat train which is the objective function of the online scheduling problem defined in Eq. (7.4).

$$l_{y,k} = \rho_y \sum_{i \in Units} \sum_{j \in Tasks} \sum_{t \in T | t \leq FPH_{k-1} - \mathrm{T}^*_{S,k}} \left(y_{I,i,j,t,k} - y^*_{I,i,j,t+\mathrm{T}^*_{sch},k-1} \right)^2, \qquad \forall k \in SE \backslash \{1\} \tag{8.10}$$

$$l_{\tau,k} = \rho_\tau \sum_{i \in Units} \sum_{j \in Tasks} \sum_{t \in T | t \leq FPH_{k-1} - \mathrm{T}^*_{S,k}} \left[t y_{I,i,j,t,k} - (t + \mathrm{T}^*_{sch}) y^*_{I,i,j,t+\mathrm{T}^*_{sch},k-1} \right]^2, \qquad \forall k \in SE \backslash \{1\} \tag{8.11}$$

$$\min J_k = l_{y,k} + l_{\tau,k} + \int_0^{FPH_S} V(x(t), y(t), u(t)) dt, \qquad \forall k \in SE \backslash \{1\} \tag{8.12}$$

A similar approach to minimize closed-loop schedule instability was proposed by Ave et al. (2019) for multipurpose plants. It considers a multi objective function formulated from the penalization of variability, and the maximization of profit. That work highlights the importance of choosing the penalty values for a good trade-off in the scheduling of multipurpose plants, but ignores maintenance or cleaning scheduling stability. The penalty

parameter of each expression must be determined before the closed-loop implementation and should capture a correct balance between the three objectives – two stability penalties and one economic objective – and their different orders of magnitude.

8.4. Cleaning scheduling stability in preheat trains operation

The closed-loop scheduling stability is analysed for the online optimization of preheat trains under fouling using the approach presented in Chapter 7. Two realistic case studies are considered: 4HE-B and REF-X. Figure 8.4 presents their network structure, and all the specifications and operating conditions can be found in Appendix A. The first case study, 4HE-B, is used to evaluate all alternatives proposed in Section 8.3 to improve closed-loop stability, and their effect on the instability metrics of Section 8.2 and on the economic performance of the operation. The second case study, REF-X, is based on an actual refinery preheat train, which exhibits large variability in the inputs and model mismatch, and requires a reactive approach for optimal cleaning scheduling.

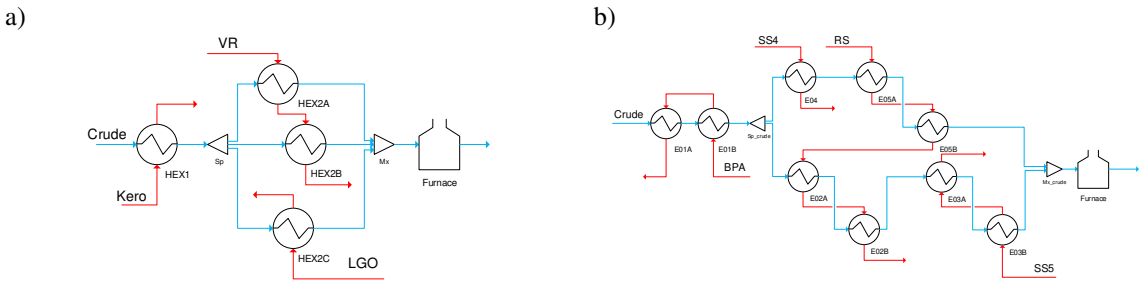

Figure 8.4. Network structure of the cases for closed-loop instability. a) 4HE-B, b) REF-X

The alternatives proposed to mitigate closed-loop schedule instability are directly incorporated in the formulation of the $NMPC_S$ problem solved online at every sampling time of the scheduling feedback loop. The only modifications required are in the objective function of the scheduling problem and adding few constraints to the problem. The $MPCC$ reformulation proposed to solve the problem is still valid and can efficiently cope with the new elements introduced to improve scheduling stability.

8.4.1. Case 4HE-B. Comparing alternatives to improve stability

Here, it is assumed a nominal operation – constant inlet streams flow rates and temperatures – and that there is no model-plant mismatch, so that the predictive models used

in the feedback loops represent perfectly the plant. These assumptions lead to a simpler problem than a real application of the online approach, but allow to make an isolated analysis of the stability of the cleaning schedule executed online. This case also aims to demonstrate that there can be schedule instability even under constant operating conditions and perfect prediction models. In practical terms, this implies that the starting time of predicted cleanings may change, or new cleanings be introduced in successive schedule evaluations.

The online Opt. S+C – see Table 1.1 for definitions – optimization problem is solved with the following settings for the control layer: a FPH_C of 10 days and update intervals of one day, and for the scheduling layer: a FPH_S of 120 days, update intervals of 15 days, and 15 periods of variable length. The MHE problems are not solved in the feedback loops because there is no plant model mismatch. These settings of the closed loop scheme lead to 25 solutions of the optimal cleaning scheduling problem – over one year of operation – which are used to calculate the schedule instability between consecutive solutions.

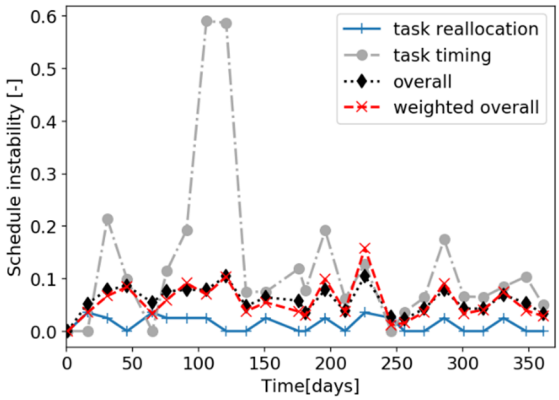

Figure 8.5. Closed-loop scheduling instability time evolution - 4HE-B, base case.

Figure 8.5 shows the schedule instability metrics measured at every cleaning schedule update. For all solution instances there is some variability of the optimal cleaning schedule with respect to the previous one and the instability metrics change along the operation horizon. The peaks of the task timing instability occur when a cleaning is postponed, and the task allocation instability changes when cleanings are included or removed from the predicted schedule. Finally, the overall instability and the time weighted overall instability are good single indicators of the instability of the system as their behaviour is aligned with that of the other metrics.

The variation of the scheduling instability metrics observed in Figure 8.5 can be explained by the evolution of the cleaning schedule. Figure 8.6 presents the cleaning schedule executed (black) and predicted (red) at every sampling time. For instance, the maximum value of task timing instability is observed between 90 and 120 days of the operation because the starting time of the cleanings predicted for HEX2A and HEX2B change significantly, and even their precedence order is reversed. As another example, between the schedule evaluations at 65 days and 76 days there is one additional cleaning introduced, causing the increase in the task allocation instability metric. The final example is about the overall instability and the time weighted overall instability metrics that quantify all the changes in the cleaning schedule. Consider the consecutive schedule solutions at 211 and 226 days, when two new cleanings are predicted and the starting time of the HEX2A cleaning is shifted closer to the current time. The weighted overall instability metric is higher than the overall instability because all the changes occur closer to the execution time.

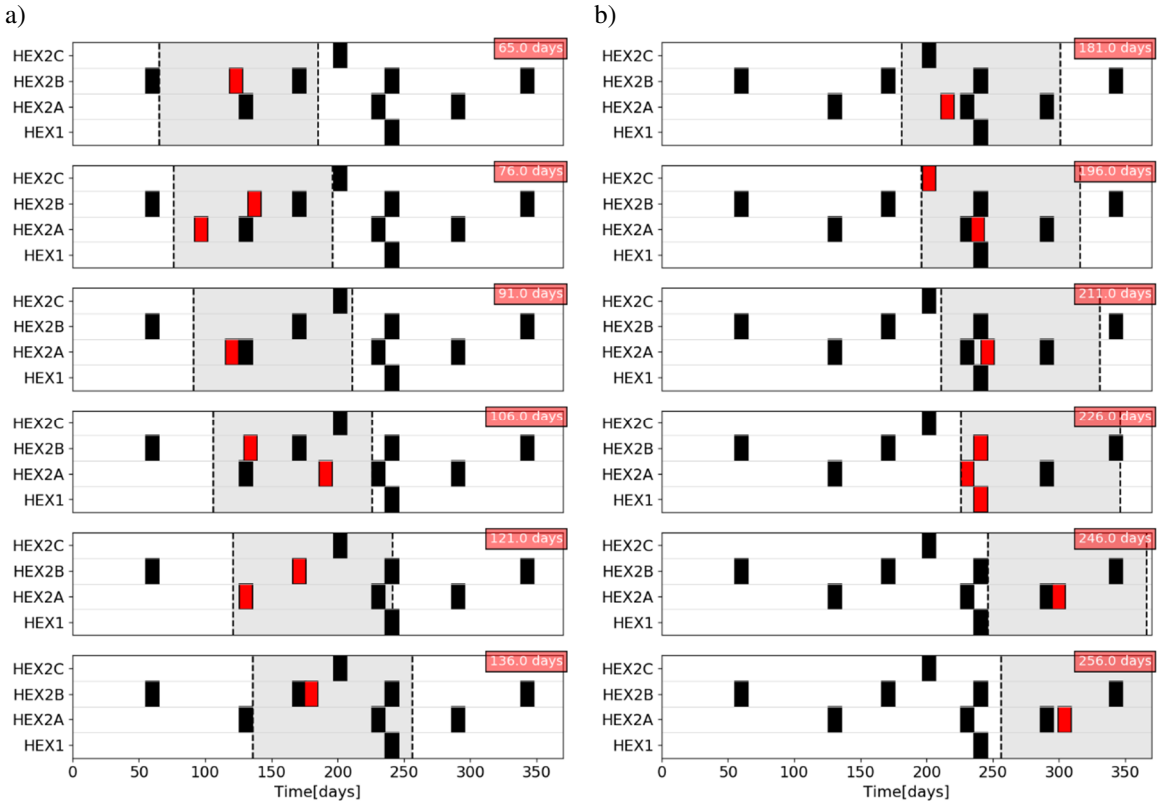

Figure 8.6. Evolution of the cleaning schedule predicted (red) and executed (black) for the base case of 4HE-B at various sampling times (upper right corner). a) from 65 to 136 days, and b) from 181 to 256 days.

There are two factors explaining schedule changes when there are no disturbances or model mismatch: (i) the additional information about the process that becomes available at every sampling interval, and (ii) the accuracy of integration of the differential equations at the scheduling layer. Both can be visualized in the fouling resistance of the heat exchangers, and Figure 8.7 shows two examples. For the factor causing instability (i), Figure 8.7a shows that a cleaning of HEX2B is introduced from one schedule evaluation to the next because in the latest time window considered, the fouling resistance reaches a level such that a cleaning becomes profitable. For the second factor causing instability (ii), Figure 8.7b shows the difference in the integration accuracy of the DAE system between the scheduling layer and the flow control layer.

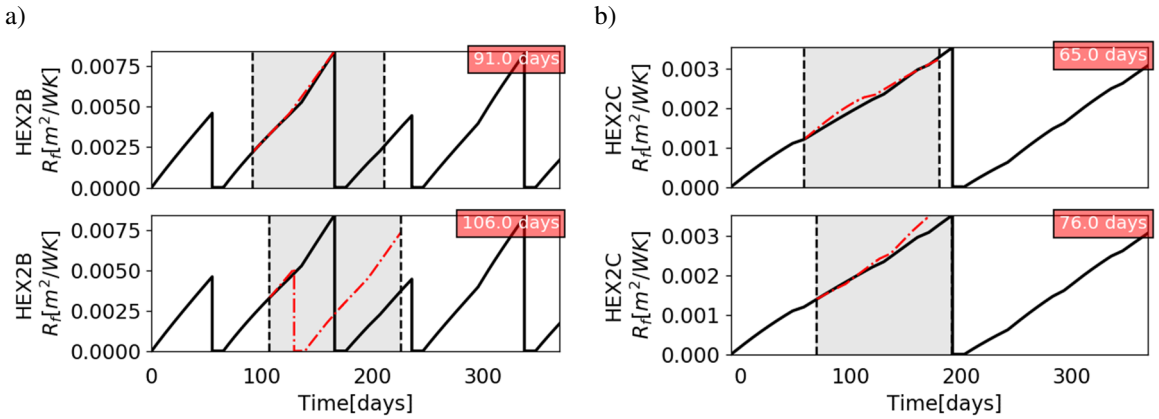

Figure 8.7. Observed (black) and predicted (red) fouling resistance for the base case of the network 4HE-B. a) HEX2B at 91 and 106 days, and b) HEX2C at 65 and 76 days, to show sources of instability.

The three alternatives proposed in Section 8.3 to improve closed-loop scheduling stability are implemented for the case 4HE-B and their parameters are varied as follows:

- The terminal cost penalty, ρ_l, is varied between $1x10^{-1}$ and $1x10^{-9}$ in a logarithm scale.
- In the freezing horizon alternative, the number of periods in which decisions are kept constant, N_z, is varied between 2 and 10; and the maximum allowed variation in the cleaning starting time, ΔT^{cl}, is varied between 1 day and 100 days.
- The penalty parameter of the cleanings allocation variability, ρ_y, is evaluated between $1x10^{-3}$ and $1x10^{2}$, while the penalty parameter of the cleaning starting

time variability, ρ_τ, is varied between $1x10^{-4}$ and $1x10^{0}$. The different ranges are due to the differences in the order of magnitude of the metrics.

Figure 8.8 shows the results for closed loop performance of the case 4HE-B using the terminal cost alternative to reduce instability for various penalty parameters. Increasing the terminal cost penalty improves the schedule stability but increases the operating cost. At the upper limit of the terminal cost penalty, $\rho_l = 1x10^{-1}$, the closed-loop solution corresponds to one with no cleanings scheduled over the entire horizon. This is the most stable solution, but at the same time the least desirable and most costly.

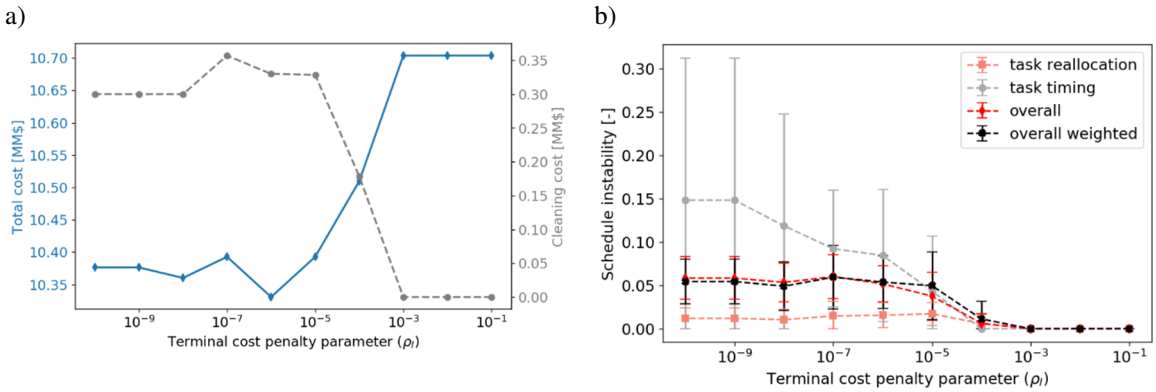

Figure 8.8. Effect of the terminal cost penalty (ρ_l) in the closed loop performance - case 4HE-B. a) Process economics, total cost (left) and cleaning cost (right), b) Average schedule instability and its standard deviation.

On the other side of the spectrum of the terminal cost, low penalties reduce the operating cost as they allow more variability and a higher reactivity in the scheduling actions. For terminal cost penalties lower than $1x10^{-7}$, the total operating cost as well as the average of most instability metrics do not change significantly, but the task timing instability changes. When large variability of the scheduling decisions is allowed (low penalties), the effect of changes in the starting time of the cleanings dominates over that of the assignment of cleanings to units. Figure 8.8b only displays the average schedule instability, and the bars represents the standard deviation of each metric. These statistics may be used as a single indicator of the overall closed-loop schedule stability.

For the alternative of freezing some scheduling decisions beyond the scheduling sampling time, Figure 8.9 presents the effect of various instances on the closed loop performance. It shows the total cost and the average of the overall weighted schedule

instability – for clarity only the average value is shown without indicating the variability around it – as a function of the number of periods frozen and the maximum change allowed in the starting time of cleanings. Only the overall weighted instability is used here as it is the most comprehensive and illustrative one among the schedule instability metrics proposed. The total operating cost increases with the number of periods frozen, while the schedule instability decreases, although no clear trend is observed – the nonlinearities and the combinatorial nature of the problem lead to local optimal solutions and make it difficult to identify clear trends and patterns. The higher the number of periods frozen, the fewer degrees of freedom in the scheduling problem, limiting the opportunity to react optimally. When the range of changes of the cleaning starting time is also restricted, it is observed that for lower values of this bound, the closed loop schedule is more stable than for higher values, and its total operating cost is higher. For a cleaning starting time variability bound greater than 10 days there is no significant changes in the schedule stability, but the operating cost can vary. In those scenarios, the allocation of cleanings and the total number of cleanings have a higher impact in the process economics than their starting time.

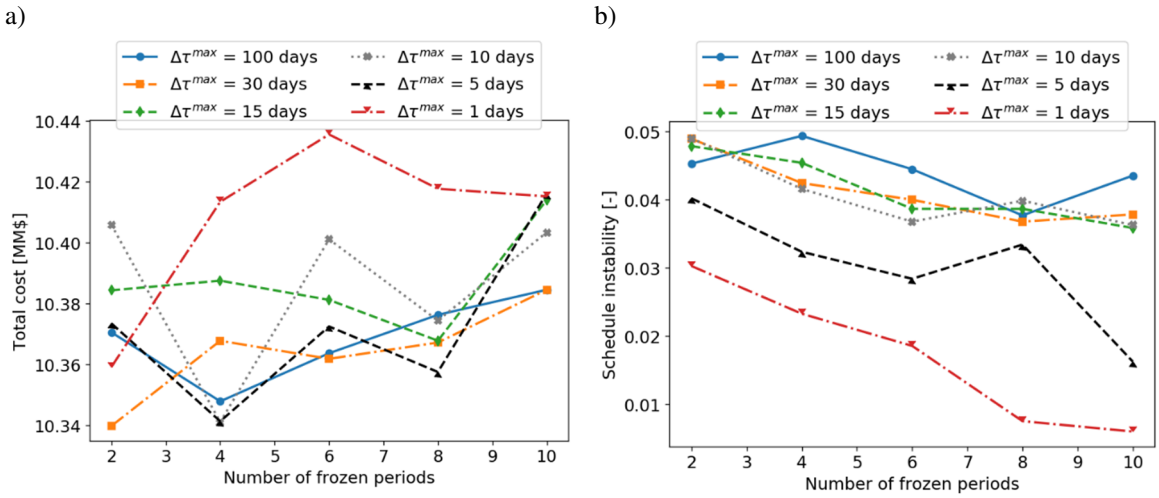

Figure 8.9. Effect of the number of frozen periods (N_z) and the maximum allowed variation in the cleaning starting time (ΔT^{cl}) on the closed loop performance of case 4HE-B. a) Total operating cost, b) Average schedule overall weighted instability.

For the alternative that penalizes the variability between consecutive schedule evaluations, Figure 8.10 presents the effect of its parameters on the closed-loop performance and schedule stability. Once more, only the average overall weighted instability is presented

for clarity. Although no clear trend is observed, the total operating cost increases when the penalties on the variability are higher, while the schedule instability decreases. For values of ρ_τ lower than $1x10^{-3}$ the schedule instability does not change, but the operating cost can still vary indicating that the effect of the starting time of the cleanings is not as significant as that of the allocation of the cleaning actions. Finally, the two penalties of this alternative are correlated, and there are different combinations leading to similar closed loop performances of the overall system.

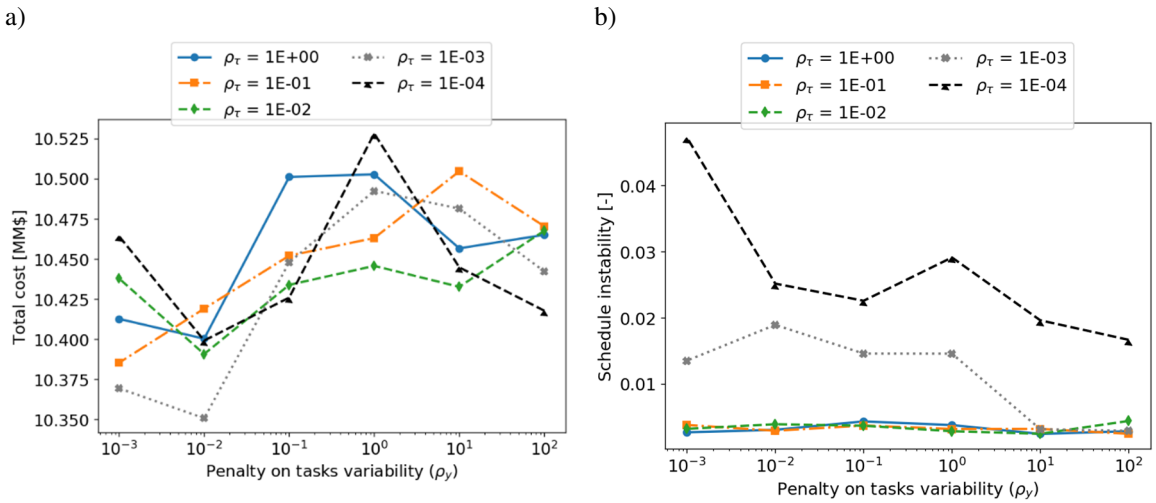

Figure 8.10. Penalty on task variability (ρ_y) and the penalty on cleaning starting time (ρ_τ) on the closed loop performance of case 4HE-B. a) Total operating cost, b) Average overall weighted instability.

All the alternatives presented to improve closed loop schedule stability do so by either penalizing the changes in the scheduling decisions or fixing some of those decisions in the future prediction horizon. In all scenarios considered, improving schedule stability compromises the total operating cost, hence there is a trade-off between how fast the system can react to changes and the long-term predictability of the scheduling decisions. A data envelope analysis (DEA) (Farrell 1957; Charnes, Cooper, and Rhodes 1978) is used to evaluate this trade-off for all the scenarios considered in all the alternatives simultaneously. A point in the DEA analysis represents a solution of the closed loop scheduling problem using any alternative to improve stability and the specifications of its parameters, hence there are 71 points in total – 1 base case, 10 for the terminal cost alternative, 30 for the freezing decisions alterative, and 30 for the penalizing schedule variability alternative. The total

operating cost and the average overall weighted instability of the schedule are considered as 'inputs' to the standard representation of the DEA analysis, while there are no 'outputs', and an efficiency is calculated for each point solving a linear programming problem.

The results of the DEA analysis are presented in Figure 8.11, where the points are classified based on the alternative used to improve stability, and the efficiency frontier corresponds to the approximation constructed from the DEA. The points that lay on the frontier have a 100% efficiency – they represent the best combination of the inputs, and no other data point available can be as good or better – and all other points underperformed with respect to those. All the points corresponding to the terminal cost alternative lay inside the frontier, so they are not as efficient as those defined by the other alternatives or even as the base case, which does not consider stability in the online schedule optimization. This underperformance of the terminal cost alternative is because the reference point used to ensure closed-loop stability corresponds to the worst conditions to operate the preheat train, although it is stable. The other two alternatives improve the closed loop schedule stability but compromise the operational cost. For these data points two clusters are observed: one for the freezing decisions alternative that, on average, reduces the schedule instability without a large cost penalty, and another for the penalizing variability alternative that, on average, achieves a larger improvement in stability with a larger operating cost. Some of the data points of the two clusters overlap representing intermediate solutions.

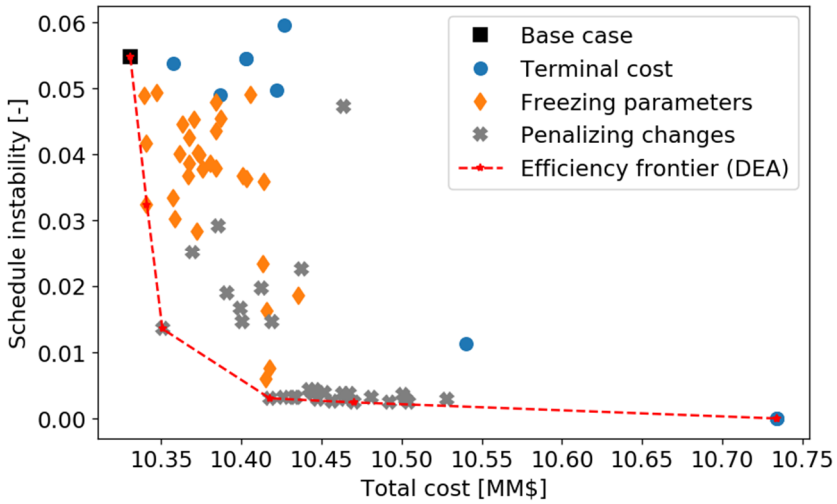

Figure 8.11. DEA analysis for all the closed loop solutions of the scheduling and control problem - case 4HE-B.

A more rigorous DEA could have been performed including all instability measurements as 'inputs', but the outcome would have not change significantly. The overall weighted instability metric quantifies correctly the closed-loop instability, and captures the trends, effects, and interactions of all other instability measurements.

The DEA results suggest that penalizing the variability between consecutive schedules is a better approach to reduce schedule instability, while achieving a good economic performance than the other two alternatives considered. The terminal cost alternative was proven to be least efficient, and fixing scheduling decisions in future instances of the scheduling problem can be too restrictive in the presence of disturbances, so that not all the economic benefits of implementing an online fouling mitigation strategy are achieved.

8.4.2. Case REF-X. Closed loop schedule stability in an industrial preheat train

The REF-X case study is analysed here. Time-varying input streams flow rates and temperatures are considered for the online optimization, as well as model-plant mismatch, which is implemented by modifying the deposition constants of the fouling model used to simulate the 'real' plant. The complete specifications of the problem are the same as those used in Section 7.3.2. The online optimisation solved here is Opt. S+C.

The flow control optimization layer uses a FPH_C of 10 days, an update frequency of 1 day, and a PEH_C of 20 days. For the scheduling layer, a PEH_S of 120 days is used, and the update frequency and FPH_S are varied as it was done in Section 7.3.3 in order to evaluate the effect of these parameters on closed-loop schedule stability. One aim is to tests the claim from MPC theory that larger prediction horizon improves closed-loop stability. Although this claim is specific for set point tracking control loops with continuous variables, the similarities between MPC and online scheduling encourage exploring this question.

Figure 8.12 presents the average closed-loop instability and it standard deviation measured with each metric developed in Section 8.2, as a function of the FPH_S, for two update intervals of the scheduling layer. The closed-loop performance, in terms of operating cost, for the same range of parameters was presented in Figure 7.23. The results show that there are no significant differences in the overall or overall time weighted instability values, as there are no large differences in the closed-loop performance. The total operating cost only varies by $ 0.24 M among all scenarios, although the energy cost decreases, and the cleaning

cost increases as the FPH_S increases. On the other hand, the timing instability – Figure 8.12a – increases with respect to the FPH_S, while it is largely unaffected by the solution frequency of the scheduling layer. It has a wider standard deviation at longer FPH_S, where more cleanings are typically included in the schedule. Drastic changes in the cleaning starting time are due to disturbances, model-plant mismatch, and different operating conditions.

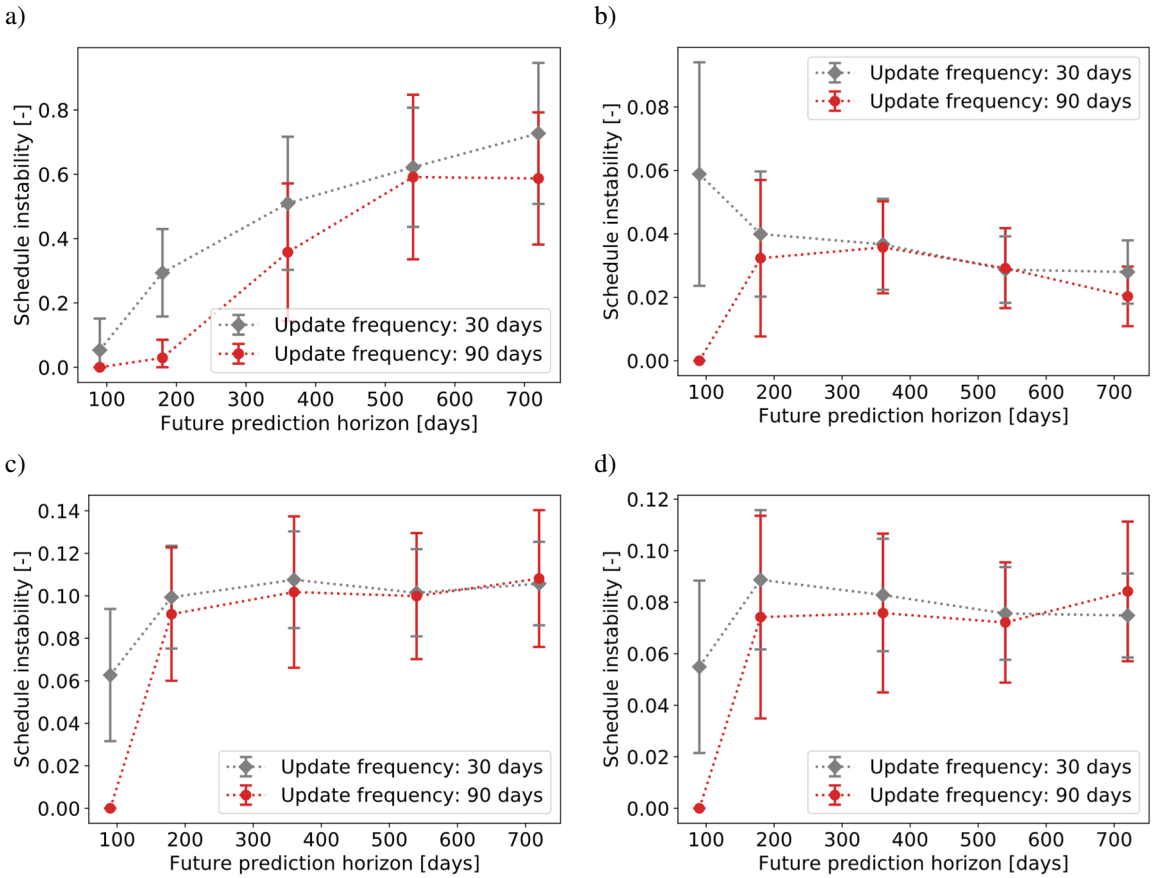

Figure 8.12. Closed-loop schedule instability measured as: (a) task timing instability, (b) task allocation instability, (c) overall instability, and (d) overall weighted instability for case REF-X varying the FPH_S and update frequency of scheduling layer.

The scenario that uses a FPH_S of 90 days and the same update interval for the scheduling layer has a closed-loop instability of zero (0) because all the cleanings predicted at each optimal solution of the scheduling problem are executed. Under these settings, there are no actions predicted beyond the time when the next schedule is evaluated. Hence, there is no previous schedule predicted to calculate the closed-loop instability.

For this case study and for the ranges of the parameters considered, no significant improvement was observed in the closed-loop stability, unlike reported for an MPC application with continuous manipulated variables (Maciejowski 2002). The binary decisions associated with the cleanings cause the closed-loop scheduling problem to behave differently from MPC controllers, so that theory does not seem to apply, at least in this case. Therefore, other alternatives to improve closed-loop stability are necessary.

Next, a FPH_S of 180 days and a sampling frequency of 90 days are used to evaluate the closed-loop stability of the REF-X case. This on-line scenario exhibits a good level of schedule instability, as seen previously, that can potentially be improved using the alternatives proposed in this chapter. The alternative to penalize changes between consecutive schedules, as described in Section 8.3.3, is tested. The two penalty parameters – penalty on task allocation, ρ_y, and penalty on task timing, ρ_τ – are varied, defining different settings for the on-line optimization. Results are compared against the base case – which does not use any instability mitigation – in terms of schedule stability and total operating cost.

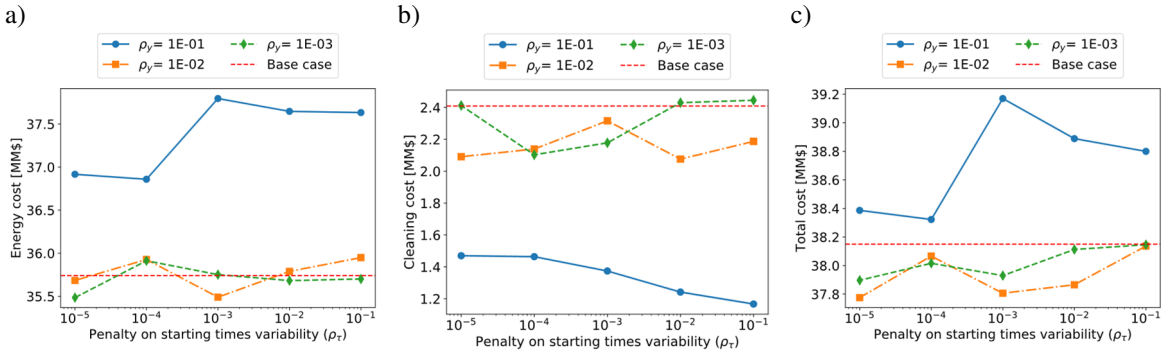

Figure 8.13. Closed loop performance of REF-X when varying the penalty parameters of schedule variability. a) energy cost, b) cleaning cost, c) total cost.

The closed-loop performance of REF-X when the schedule variability is penalized is presented in Figure 8.13. The closed loop overall time weighted instability is presented in Figure 8.14a, and a Pareto plot between the operating cost and schedule instability is presented in Figure 8.14b. Only the scenarios that use a task allocation penalty, ρ_y, of $1x10^{-1}$ have a larger operating cost than the base case, with an increase of $ 1.0 M at most. This cost increase is due to large energy cost and fewer cleanings during the overall online operation. However, those scenarios exhibit the lowest schedule instability. Fewer cleanings are predicted at every schedule update because adding new cleanings to or removing some

cleanings from a previous schedule is heavily penalized. The predicted cleaning schedules therefore have minimal changes between updates. This also inhibits the ability of the scheduling feedback loop to react to disturbances and operational changes to mitigate fouling and minimize the cost of the operation.

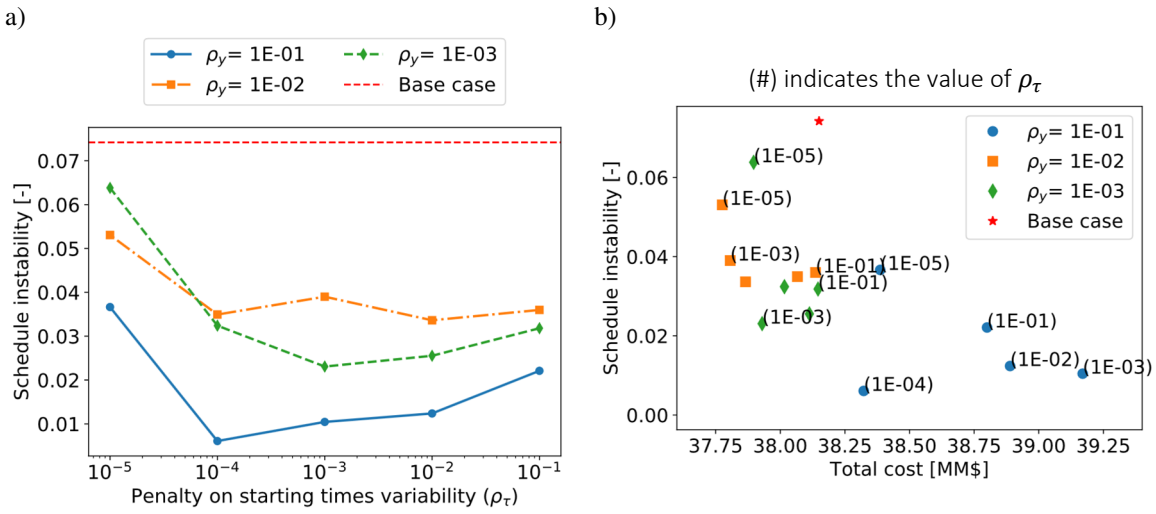

Figure 8.14. Closed loop average overall weighted instability (a) and Pareto plot (b) for the performance of REF-X when varying the penalty parameters of schedule variability.

For task allocation penalty parameters $\rho_y < 1x10^{-1}$, the closed-loop performance is not very different from the base case, and it can be even improved, reducing the total operating cost by $ 0.37 M maximum. In addition, all those scenarios have a lower schedule instability than the base case, meaning that they improve the closed-loop performance and closed-loop stability at the same time. This is better observed in Figure 8.14b that shows a Pareto plot between operating cost and instability. All scenarios with $\rho_y < 1x10^{-1}$ are more efficient than the base case, but they have larger closed-loop instability than those with $\rho_y = 1x10^{-1}$. This observed simultaneous improvement in the two metrics of closed-loop performance contradicts the expectations of multi objective optimization problems, but in this case reflects the effect of uncertainty, disturbances, and variability in the operation. The input flow rates and streams temperature change constantly and that is unknown to the predictive model of the scheduling layer, as only a constant forecast – time moving average – is used at each evaluation.

The effect of the penalty parameter on the task timing instability is not as significant as that of the penalty parameter on the task allocation instability. The operating cost increases

only slightly when the task timing penalty increase from $1x10^{-5}$ to $1x10^{-1}$, but this difference is no more than $ 0.37 M for $\rho_y < 1x10^{-1}$, while for $\rho_y = 1x10^{-1}$ the operating cost ranges from $ 38.4 M to $ 39.2 M, depending on the task timing penalty, ρ_τ. For the overall closed-loop performance, the starting time of the cleanings is not as important as the allocation of cleanings to heat exchangers. Under variable and uncertain operating conditions modifying the cleaning starting time of an already predicted cleaning task for a given unit does not have a big potential to reduce the energy cost. In terms of closed-loop scheduling instability a reduction is observed between $\rho_\tau = 1x10^{-5}$ and $\rho_\tau = 1x10^{-4}$, and then the changes in instability are minimal when ρ_τ.increases further. The lowest penalty, ρ_τ, allows the largest variability in the cleaning starting times between consecutive schedule evaluations. For larger values of ρ_τ the changes in the predicted cleaning time are minimal, and most of the schedule instability comes from changes in the allocation of cleanings to the heat exchanger as new cleanings are predicted.

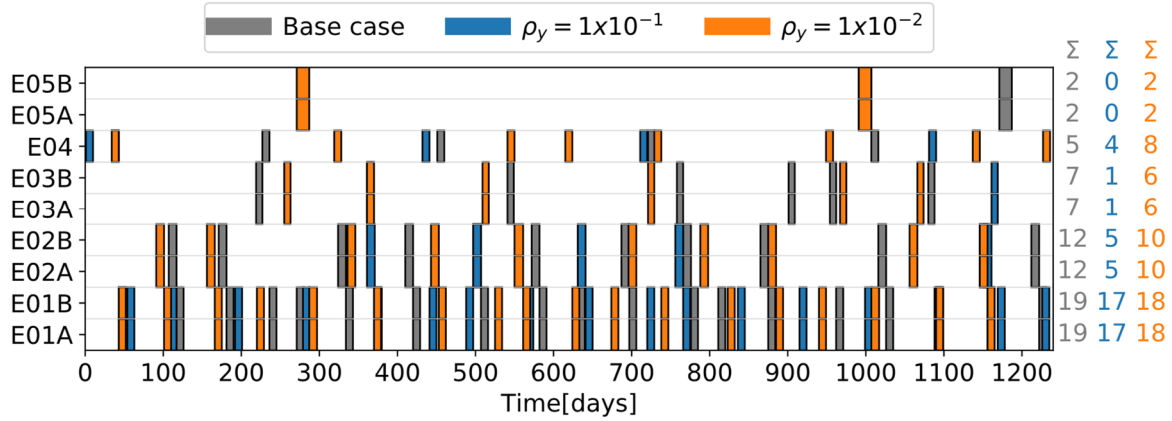

Figure 8.15. Cleaning schedule executed for online optimization of REF-X. Base case with no schedule instability mitigation and schedule instability mitigation with two penalty parameters.

To better illustrate the sources of schedule instability and how the proposed methods reduce it, the executed cleaning schedule, and its updates in a moving horizon are analysed. The base case – no instability penalty – is compared with two on-line optimisation scenarios that penalize schedule instability and that were analysed before. Both use a penalty ρ_τ of $1x10^{-3}$, but two different values of ρ_y: (Pen A) $\rho_y = 1x10^{-1}$ (lowest instability and highest operating cost), and (Pen B) $\rho_y = 1x10^{-2}$ (better stability and operating cost than base case).

Figure 8.15 shows the executed cleaning schedule for these scenarios. The total number of cleanings changes significantly, and the scenario with $\rho_y = 1x10^{-1}$ is conservative with very few cleanings and long operating times between cleanings of the same exchangers, while the other two scenarios have similar cleaning schedules.

Figure 8.16 - Figure 8.18 shows the predicted cleaning schedule and CIT at three updates of the scheduling feedback loop, at 270days, 360 days and 450 days of operation, for the same three scenarios (base case, Pen A, Pen B). First, it is observed that the models estimated at each update show good agreement between observed and estimated values within the PEH_S, and predict the right trends and effects of cleanings in the FPH_S. Second, for the base case the main source of schedule instability results from adding new cleanings to a predicted schedule that must be immediately executed. This is not practical from a planning perspective, as the response to cleaning decisions is not immediate, and resources are needed for their execution. Third, the Pen A case (with $\rho_y = 1x10^{-1}$) exhibits low variability in the schedule evaluations, and new cleanings are added to the schedule only if they are strictly necessary and profitable for the operation. Finally, the Pen B case with ($\rho_y = 1x10^{-2}$) exhibits a larger schedule variability than the previous one, but lower than the base case. The starting time of the cleanings changes within a range of 30 days, and if new cleanings are added to a schedule in theFPH_S, they are allocated far ahead from the current time so that there is enough time for personnel to practically plan their execution.

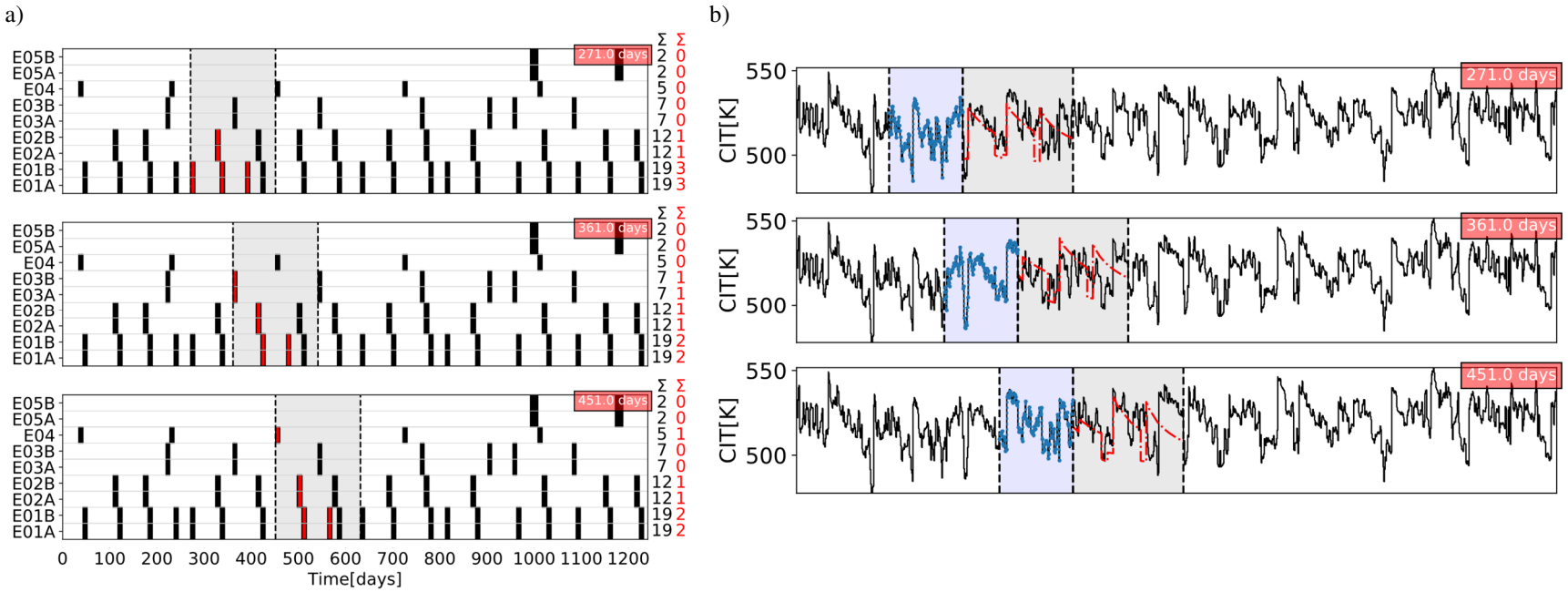

Figure 8.16. Online optimization of REF-X - Base case (no instability reduction). Cleaning schedule as executed (black) and predicted (red) (a), and CIT as observed (black), estimated (blue) and predicted (red).

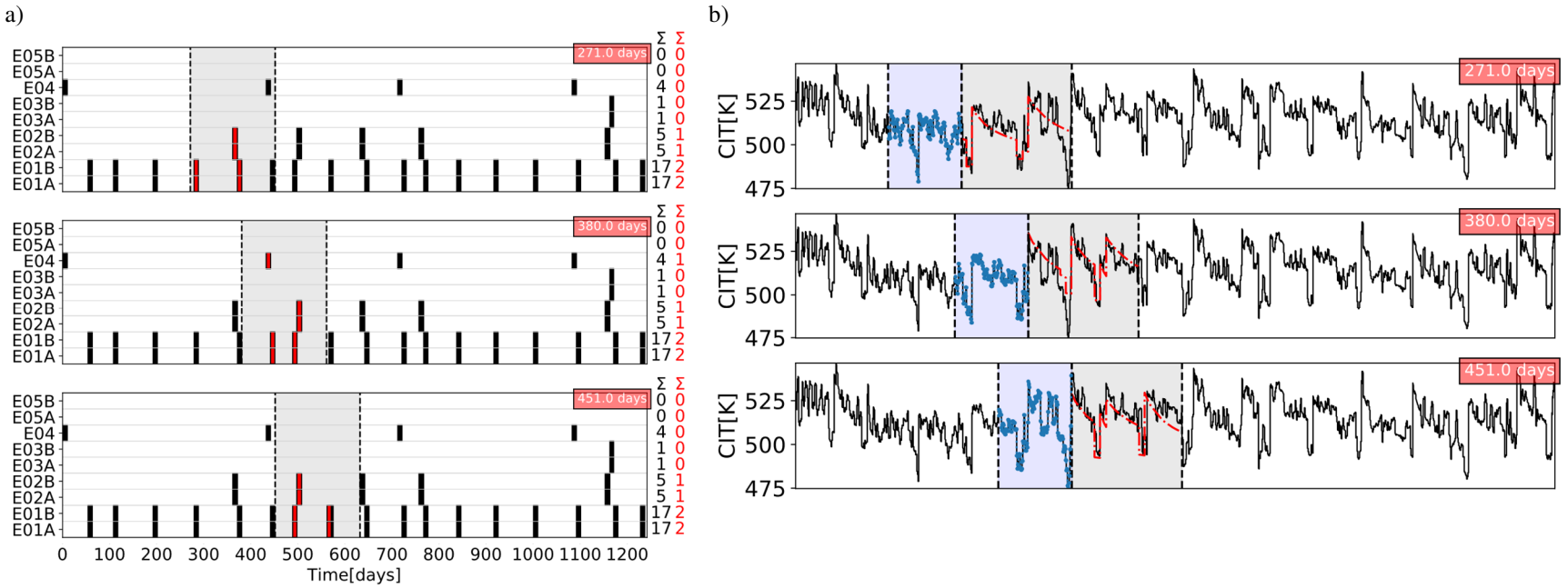

Figure 8.17. Online optimization of REF-X – Pen A case (penalizing schedule variability) with $\rho_\tau = 1x10^{-3}$ and $\rho_y = 1x10^{-1}$. Cleaning schedule as executed (black) and predicted (red) (a), and CIT as observed (black), estimated (blue) and predicted (red).

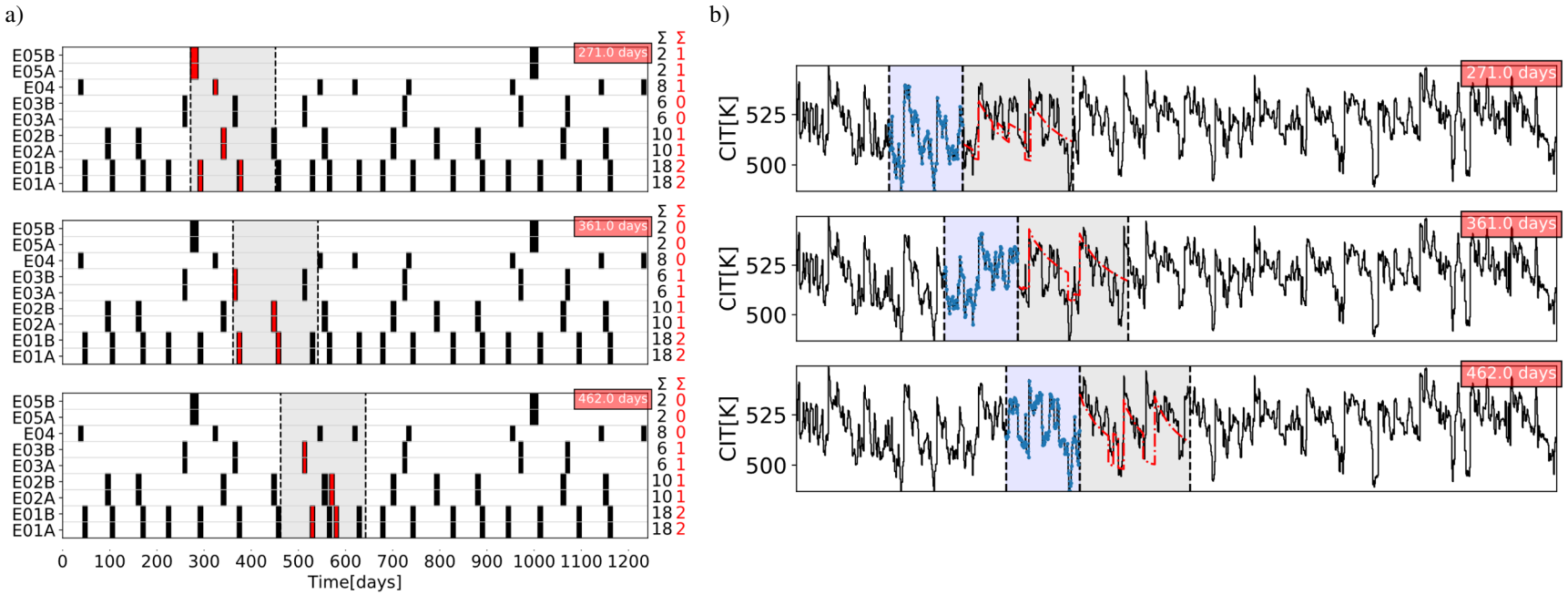

Figure 8.18. Online optimization of REF-X – Pen B case (penalizing schedule variability) with $\rho_\tau = 1x10^{-3}$ and $\rho_y = 1x10^{-2}$. Cleaning schedule as executed (black) and predicted (red) (a), and CIT as observed (black), estimated (blue) and predicted (red).

8.5. Concluding remarks

This chapter revisits the online optimization approach presented in Chapter 7, and analyses the stability of the closed-loop cleaning scheduling defined that way. Cleaning scheduling decisions optimized on a moving horizon may change between consecutive evaluations and the premise is that too many reactive changes in the schedule may hinder its practical application, as long term planning and resources – capital, equipment, and work force – are necessary to execute them.

First, a set of new and general expressions are developed to quantify schedule stability. They are not restricted to the online cleaning scheduling of HEN, and are applicable to other cases such as multi product plants, although minor modifications may be required. Second, alternatives to mitigate schedule instability are developed from a MPC and re-scheduling perspective. Three alternatives are evaluated – adding a terminal cost in the objective function, freezing some scheduling decisions early in the prediction horizon, penalizing schedule variability between evaluations. Although general for online scheduling applications, they are tailored to the online optimal cleaning scheduling of HEN. Finally, those alternatives are tested in practical problems related to fouling in preheat trains, and the stability measurements are used to quantify their impact.

Using a small but representative HEN, it is demonstrated that closed-loop cleaning schedules exhibit instabilities even under constant operating conditions and no model-plant mismatch. The same case is used to evaluate the performance of the instability mitigation alternatives developed, and it is found that the terminal cost alternative is ineffective as the reference point used correspond to a stable but undesired state, while the other two alternatives proved to be effective reducing schedule instability. Improving the closed-loop schedule stability increases the overall operating cost in the cases analysed.

A realistic case study with input variability and plant mismatch is used to demonstrate the expected effect of real closed-loop schedule instability and how the alternatives proposed here can improve it. Penalizing the variability of scheduling decisions between consecutive evaluations improves the closed-loop stability, but compromises the ability of the online optimization approach to react to disturbances and operational changes so that all the economic potential is not achieved. Nevertheless, it was observed in some scenarios that the

schedule instability and the operating cost can be simultaneously reduced. This is an effect of the process variability, model mismatch, and uncertainty.

Quantifying closed-loop schedule instability is still a challenging problem. All factors driving the changes observed in the optimal prediction of the scheduling actions are difficult to capture in a single indicator. A better identification of sources of (in)stability, as well as their relative importance is needed to find ways to mitigate it. It is also necessary to have clear and defined ranges that indicate the level of instability or variability in consecutive evaluations of the schedule that are acceptable for a given application, so that the online optimization approach can be tuned based on those ranges and it will be able to achieve the maximum economic potential.

Chapter 9

Conclusions

This thesis addressed the problem of fouling in crude preheat trains from a process systems engineering approach. The main goal was to develop a sufficiently accurate formulation that could work within an optimization framework to define fouling mitigation strategies – flow distribution, cleaning schedule, network retrofit – under real, variable and uncertain operating conditions. In this chapter, the main conclusions of the research work are drawn, the key contributions highlighted, and future work directions suggested.

This work has highlighted the need of model-based optimization strategies for fouling mitigation in crude preheat trains, and it has demonstrated their potential benefits to minimize operating cost, energy consumption and carbon emissions while ensuring a feasible and profitable operation. The literature review of Chapter 2 revealed that most current approaches used to optimize preheat trains operation and fouling mitigation strategies do not capture adequately the dimension and reality of the problem, nor guarantee an optimal robust solution. The key missing features to be overcome are: the use of simplified and unrepresentative models for fouling and heat transfer to support decision making; ignoring the natural dynamic behaviour of the process, variability and uncertainty in the operation of preheat trains; decoupling the effect of fouling mitigation strategies and assuming they are independent; and using heuristics to define fouling mitigation actions. This thesis overcomes these issues and facilitates online optimal decision making for fouling mitigation in preheat trains. Each chapter of this thesis addresses specific goals to fulfil this general objective.

A novel and general mathematical formulation for optimizing networks of shell and tube heat exchangers under fouling, which was developed in Chapter 3, presents a good trade-off between model accuracy, representation of the system, and mathematical complexity. This MINLP formulation was successfully used for the simultaneous optimization of the cleaning scheduling and flow distribution of various heat exchanger networks. The networks

used here were small but representative of configurations normally found in refinery preheat trains. This formulation includes important features usually find in refining operations such as ageing of the deposit, reduction of the flow diameter, pressure drop limits, furnace duty limits, and cleaning sequence constraints. The MINLP formulation copes with those scenarios, and their solution showed how optimal fouling mitigation actions depends on the conditions and constraints of the system. It was determined that the large number of binary variables hinders the solution of large scale MINLP problems.

A model validation strategy is developed and applied in Chapter 4 to ensure that the heat exchanger and fouling models used within the optimization formulation are sufficiently accurate and representative for real industrial operations. First, the models developed are validated and tuned against a more detailed and previously validated distributed model for heat exchangers. Then, the model parameters are estimated through an indirect validation approach that uses real plant measurements and the distributed model as a soft sensor. Comparison of results for 37 different heat exchangers and for an industrial network, demonstrate that the model developed captures correctly the process dynamics and performance with acceptable prediction errors (average prediction errors lower than 1.5 K in streams temperature, and lower than 0.2 bar in pressure drop).

Chapter 5 introduced a novel solution strategy for the mathematical formulation developed in Chapter 3 so that the optimal cleaning scheduling and flow distribution problem can be solved for problems of industrial scale. The MINLP problem is reformulated as a MPCC by relaxing the binary variables, introducing complementarity constraints, and reformulating some of the disjunctions as nonlinear expressions. A sequential solution approach is proposed for this reformulation. This solution strategy reduces the computational effort by 99% for cleaning scheduling of small networks that can be solved with standard branch and bound algorithms. The optimal cleaning schedule for industrial scale problems can be found in less than 30 min of computational time, which is a significant reduction compared to other solution strategies. In addition, the optimal solution obtained with the MPCC reformulation is validated using the benchmark distributed model of Chapter 4, with errors in the economic benefits obtained lower than 1% for an industrial preheat train.

The fouling mitigation problem is extended in Chapter 6 where retrofit decisions are introduced in the problem formulation. The optimal fouling mitigation problem now

includes: cleaning scheduling, dynamic flow distribution, heat transfer area retrofit of selected exchangers, and network configuration retrofit. The formulation of the cleaning scheduling problem is inherited and expanded so that decisions involving adding or removing exchangers from the network are modelled as cleanings. New constraints and variables are introduced to ensure a correct modelling of these decisions. For the first time an optimization approach to the network retrofit problem for systems under fouling is proposed and efficiently applied. Two case studies demonstrated that the optimal retrofit network under fouling is different from, and performs better than other network configurations obtained from pinch technology or heuristic analysis. For both cases the minimum operating cost, including capital cost of retrofit options, is always achieved when all decisions – fouling mitigation, operation, and retrofit – are considered at the same time.

Chapter 7 focuses on the online optimization of preheat trains under variable and uncertain conditions. It presents a multiloop approach based on control principles to estimate the model parameters and to optimize fouling mitigation decisions online at two different time scales. Two control loops are defined based on an MHE / NMPC scheme, one for the fast dynamics and flow distribution optimization, the other for the slow dynamics and cleaning scheduling optimization. For each loop, the predictive models, estimation strategies and optimization algorithms are based on the developments in earlier chapters. These two loops are designed so that the interactions of flow distribution and cleaning scheduling are still considered, and their synergies exploited to minimize the operating cost of the preheat train. An industrial case study is extensively used to demonstrate the economic benefits of this approach over heuristic and open-loop optimization approaches that either ignore key interactions, the effect of important variables, or the input stream variability to the system. In addition, this online approach copes efficiently with model-plant mismatch, variability in the input streams, and large disturbances.

In Chapter 8 the practical problem of closed-loop schedule stability – avoiding too many schedule changes – is studied. Novel and general measurements are developed to quantify the stability in online scheduling which are not restricted to the cleaning scheduling of HEN. It is demonstrated that schedule changes may occur under constant conditions because, in a moving horizon optimization approach, at each schedule update new information – a new time window in the prediction horizon – becomes available, which

modifies the feasible region of the optimization problem. Three strategies – adding a terminal cost, freezing some scheduling decisions in the prediction horizon, penalizing scheduling variability – are developed for improving schedule stability, based on MPC and re-scheduling principles. They aim to improve schedule stability while retaining a good performance of the system. These strategies can be used to generate a series of alternative that show difference balances between stability and economic performance, so that the operator can choose which to implement. It is shown that the three alternatives evaluated improve the closed-loop schedule stability, but at the same time reduce the closed-loop performance – higher operating cost. The alternative that penalizes schedule variability is investigated further to quantify and mitigate the closed-loop schedule instability in an industrial preheat train, and in some cases simultaneously improving both schedule stability and cost performance.

The mathematical formulation, solution strategy and optimization framework developed offer significant new possibilities to improve the retrofit and operation of crude preheat trains under fouling. It overcomes major difficulties found to date for practical, accurate and realistic solutions. Also, this framework is not limited to crude oil fouling problems and can be extended to other systems involving heat exchanger networks with decaying performance.

9.1. Contributions and achievements

They key contributions of this thesis to the modelling and mathematical formulation of the optimization problem of heat exchanger networks under fouling are:

- The development of a lumped model for shell and tube heat exchangers and fouling that considers explicitly the radial heat transfer distribution and averaged the axial effects. The model captures the main factors affecting the deposition rate and deposit ageing, it predicts the dynamic thermal and hydraulic performance of the units, and overcomes the usual thin layer assumption of the deposit layer. This model is more accurate than other previous lumped models that ignore the radial effects, the composition of the deposit, and the temperature distributions.
- An alternative formulation for the disjunctions defining the state – idle or operating – of the heat exchangers in the network that is coupled with a continuous time discretization using periods of variable length. The continuous time representation

reduces the number of binary variables – complicating variables – needed for representing the problem, while ensuring an accurate integration of the DAE system using a further discretization with orthogonal collocation on finite elements for each period. Also, this time representation allows defining the cleaning times with a better precision than that achieved with a fixed grid time discretization used in previous works. It also allows to optimize pre-set cleaning schedules or only certain variables of the problem such as the cleanings starting time of a cleaning schedule.

- A model tuning and validation procedure that uses a more detailed distributed model for the heat exchangers together with plant data as a soft sensor. This ensures that the lumped model used for optimization purposes represents correctly the performance and dynamics of the system. The fouling parameters of the lumped model thus estimated closely predict the performance of the benchmark distributed model or that observed during the actual operation of a network.

The above models can be used with confidence to optimize the operation of preheat trains under fouling, and to determine optimal fouling mitigation actions. The key contributions of this thesis to the optimization of preheat trains under fouling and the solution of the MINLP problem associated are:

- An efficient formulation of the cleaning scheduling problem using a continuous time discretization that allows to simultaneously optimize the dynamic flow distribution of the network. The formulation allows to exploit the synergies between these two fouling mitigation strategies, so that their simultaneous optimization surpass their individual or sequential optimization.
- A reformulation of the MINLP problem as a MPCC problem where the binary variables are relaxed reducing the complexity of the problem. Instead of solving a combinatorial integer optimization problem, a sequence of NLP problems is solved, converging to the same optimal solution. This reformulation reduces significantly the computational effort, allowing to solve industrial size problems and enabling their online application.
- The optimal network retrofit of HEN under fouling – adding or removing exchangers, changing the connectivity of existing exchangers, and modifying the heat transfer area – using a superstructure representation, which is obtained

extending the formulation of the optimal cleaning scheduling problem. This formulation allows the integration of retrofit, scheduling and control decisions at the same level exploiting the synergies among them.

These developments on the solution of the optimal fouling mitigation problem – cleaning scheduling and control – allows to make optimal decisions online in a closed loop, reacting to input variability and disturbances in the operation of preheat trains. The key contributions of this thesis to the online optimization of preheat trains under fouling are:

- A multi-loop MHE / NMPC scheme that deals with the fast and slow dynamics and disturbances of preheat trains under fouling. The same first principle models at its core are used for parameter estimation, prediction, and optimization based on the current and past states of the network. This multi-loop strategy allows to estimate the current fouling state of each exchanger in the entire network, then to simultaneously optimize the flow distribution and the cleaning scheduling on a receding horizon using an economic objective function.
- A way to deal with uncertainty and variability that are common in the operation of preheat trains – large disturbances in the inlet conditions, uncertainty in the crude properties and on the fouling propensity. The multi-loop online optimization approach updates the predictive models at regular intervals – solving a parameter estimation problem on a moving horizon – so that changes in the crude oil properties are accurately captured, and the optimal fouling mitigation actions are defined using those models – solving an optimization problem over a future horizon.
- Ways to quantify closed-loop schedule instability, and options to mitigate it, by modifying the formulation of the scheduling problem solved online. Closed-loop schedule instability may be a barrier for practical application. Here it is mitigated without a large penalty on the closed-loop economic performance of the system. Although these concepts are applied to preheat trains under fouling, they can be extrapolated to other online scheduling or re-scheduling applications.

This research effort led so far to the publication of 3 articles in peer-reviewed journals, 6 papers in edited conference proceedings, and various presentations at international conferences.

9.2. Future work

Future directions of research and work identified from the development of this thesis are summarized below.

- The model representing the heat exchangers assumes that the axial effects are not representative, and they are only described in terms of an average. It is still an open question to what extent heat transfer and fouling effects should be considered in the axial distribution to predict the overall performance of the units.
- The Ebert-Panchal model for crude oil fouling is extensively used in the optimization problems of this thesis, but there are many modifications of this semi-empirical model that are claimed to provide better representations of fouling rates (Wilson, Ishiyama, and Polley 2017). Other fouling models could be integrated in the optimization formulation for a more accurate representation of the problem, and this may include deposition models based on more fundamental principles that account for the effect of crude composition. Molecular dynamic models or surrogates developed based them or experimental data are also potential candidates.
- The thermal and hydraulic predictions achieved with the model developed has been validated against another benchmark simulation model, and historical plant data. The plant data used to validate this formulation only included temperature measurements so that a hydraulic validation of the model against actual data is still missing.
- The optimal cleaning scheduling problem only considers mechanical cleanings and it assumes that they completely remove the deposit. An extension of this formulation may include chemical cleanings with a fixed cleaning time and known cleaning efficiency, in terms of percentage of the deposit removed.
- The MPCC reformulation of the MINLP cleaning scheduling problem provides an efficient practical solution, but multiple solutions with the same or similar objective function value may exist. Further investigations on dealing with the degeneracy of the problem will improve the efficiency of any solution strategies.

- The optimal network retrofit formulation could be expanded to deal with the HEN synthesis problem, so that the dynamic effects of fouling are considered early in the design stage.
- The online multi-loop fouling mitigation approach developed relies on forecasts of the disturbances. In this thesis those forecasts are based on simple constant models. Improving the quality of the disturbance forecast over the future prediction horizon will have a significant effect on the overall closed-loop performance of the system. Alternatives based on time series analysis or data-analytics are worth exploring.
- The performance of the multiloop optimization approach depends on the tuning parameters of the MHE and NMPC of the control and scheduling layer. Systematic approaches or algorithms for tuning could be explored to improve the overall closed-loop performance of the system.
- The MHE – online estimation – problems in the online optimization approach may present a limitation when the sampling time is reduced to the order of hours. In those cases, and for very large past estimation horizons, more efficient solutions of the estimation problem are needed.
- The uncertainty and variability in the operation of preheat trains under fouling has been addressed in a feedback scheme using two control loops. Large disturbances and high variability may lead to large schedule instability, which hinders a practical implementation. Alternative approaches such as robust or stochastic optimization together with a correct quantification of the uncertainty are attractive to avoid instability issues, although they may compromise the economic benefits.
- Some ways to quantify closed-loop schedule instability are developed in this thesis. To extend their application to more general scheduling problem such as multiproduct multiunit batch plant it is necessary to revise them.
- Practical guidelines about schedule stability are necessary to set the bounds on acceptable levels of variability on the scheduling decisions. Then, this could be imposed as a constraint in the optimal cleaning scheduling problem solved online, or as a design specification of the multi-loop approach.
- The final aim of the online optimization strategy developed in this thesis is to apply it to a real system so that operating and maintenance decisions can be automated, or

at least automated informed and quantitative guidelines may be given to the operators and engineers. Although this remains to be done, a first step towards this goal could be an off-line application to support engineering decisions – cleaning scheduling and network retrofit – on the long term operation of refinery preheat trains considering constraints such as budgets and availability of resources. The optimization strategy should be refined – improving models, feedback loop settings, constraints specifications – during this stage to satisfy the requirements and constraints of the site and those of the operators Then, after empirical verification of the benefits of the proposed optimization strategy when its actions are executed manually, the feedback loop can be closed to automate the process.

- The developments of this thesis can be applied to other systems that in general are defined as network with units exhibiting decaying performance. The heat exchanger and fouling models can be adapted to exchangers other than shell and tube, and other deposition phenomenon, while the network representation, mathematical formulation, and solution strategy developed in this thesis can be directly applied. For example, in solar power generation plants where air-cooled exchangers are used to condensate steam and they are subject to particulate fouling – deposition of dust or sand – which deteriorates their performance and frequent cleanings are required to satisfy the cooling demand. Another industrial application that can benefit from the online cleaning scheduling and control developments of this thesis are evaporation processes. Arrangements of evaporators are commonly used in the food industry for concentration of products, in the production of fabrics and dyes. Fouling in each of these applications is caused by different factors, such as decomposition of the material or the presence of impurities that deposit over the surfaces. An optimal cleaning schedule and operation of the evaporators have the potential to significantly reduce the energy consumption of the process.

Appendix A.

Case studies and networks specifications

This appendix presents the details of all case studies developed in this thesis. It includes the network structures, heat exchanger specifications, physical properties calculations, and streams conditions.

A.1. Physical properties equations

The streams considered in all case studies of this thesis are different blends of crude, or products of crude oil distillation – CDU product streams. Hence the physical properties are calculated based on the stream temperature, API, and boiling point measurements, but to simplify the nature of the equations they are approximated to correlations of temperature. Eq. (A.1) – (A.4) are the correlations used to calculate the physical properties of each stream. The density, specific heat capacity, and thermal conductivity are linear functions of temperature, while the viscosity is an exponential function of the inverse of temperature. The parameters of these correlations are estimated for each stream type (e.g. crude oil, kerosene) of each case study as the specifications of the crude may change from one network to the other.

$$\rho = k_1^{\rho} T + k_0^{\rho} \quad \text{(A.1)}$$

$$Cp = k_1^{Cp} T + k_0^{Cp} \quad \text{(A.2)}$$

$$\lambda = k_1^{\lambda} T + k_0^{\lambda} \quad \text{(A.3)}$$

$$\mu = k_0^{\mu} \exp\left(k_1^{\mu}/T\right) \quad \text{(A.4)}$$

Using these physical properties correlations allows to have a standard framework for different scenarios and case studies when the information collected from different sources. Depending on the case study and the network, the parameters of the physical properties correlations may be estimated from API relationships, data reported in the literature (Riazi

2005), or other correlations reported in specific papers (e.g. quadratic correlations for the specific heat capacity).

A.2. Case studies

In this thesis a total of 13 case studies are considered, and they are networks ranging from a single heat exchanger – for illustration purposes – up to ten heat exchangers which are common in practical applications of heat recovery in refineries. In all cases the cold stream is the crude oil, and it flows through the tube side of all exchangers, while the hot streams, which are side streams, pump arounds, or products of the atmospheric distillation unit, flow thought the shell side. The network structure and the details of each case are presented in detail here.

For any optimization problem of the case studies the following initialization procedure was used: a constant time profile for all the variables, all binary variables are initialized at 0.5, negligible fouling for all exchangers ($R_f = 1x10^{-5}, \delta = 1x10^{-5}, x^f = 1$), in networks with parallel branches the flow split is set at 50%, the mass flow rates and temperature of a stream (e.g. crude, naphtha) in the whole network are set at their inlet conditions, the length of the periods and their starting time are initialized as being evenly distributed – total operating time divided by the number of periods. The equality constraints of the model are used to initialize all other variables.

The optimization solvers used for all case studies are BONMIN, for the MINLP formulation of small networks, and IPOPT, for all other optimization problems. BONMIN is a branch and bound solver which is only used in the optimal cleaning scheduling problem of networks with up to two exchangers with its default options. For solver IPOPT, an NLP interior point solver, the linear solver ma57 is used, and the barrier parameter, the bound push parameter, and the slack bound push parameter are all set at $1x10^{-6}$.

Table A.1 summarizes the main cost parameters and operational constraints for each case study.

Table A.1. Cost parameters and operational constraints of all case studies

Case No.	**1**	**2**	**3**	**4**	**5**	**6**	**7**	**8**	**9**	**10**	**11**	**12**	**13**
Case ID	**1HE**	**2HE-S**	**2HE-B**	**4HE-S**	**4HE-B**	**LN-S1**	**LN-S2**	**LN-S3**	**LN-B1**	**LN-B2**	**REF-X**	**NR-S**	**NR-B**
COT [K]	623.15	623.15	623.15	623.15	623.15	640.0	640.0	613.15	640.0	640.0	623.15	640.0	640.0
Firing limit [MW]	100	100	100	90	90	90	90	100	90	90	90	90	90
Operating time [days]	370	370	370	370	370	370	370	370	370	370	1500	600	600
LB period length [days]	10	10	10	10	10	10	10	10	10	10	10	10	10
UB period length [days]	90	90	90	90	90	90	90	90	90	90	350	150	150
Production cost [$/kg]	0.23	0.23	0.23	0.23	0.23	0.23	0.23	0.23	0.23	0.23	0.23	0.23	0.23
Fuel cost [$/MW-h]	27	27	27	27	27	27	27	27	27	27	25	27	27
Carbon cost [$/ton]	30	30	30	30	30	30	30	30	30	30	0	30	30
Carbon emission factor [ton/MW]	0.015	0.015	0.015	0.015	0.015	0.015	0.015	0.015	0.015	0.015	0	0.015	0.015
Furnace efficiency [%]	90	90	90	90	90	90	90	90	90	90	80	90	90
Max. simultaneous cleanings [-]	2	2	2	2	2	2	2	2	2	2	2	2	2

A.2.1. Case 1: "1HE"

This case study is a single exchanger adapted from one of the units of the network presented in Coletti and Macchietto (2011a, 2011b). Figure A.1 shows the network, Table A.2 presents the configuration of the exchangers, fouling and cleaning parameters, and Table A.3 the streams conditions and physical properties parameters.

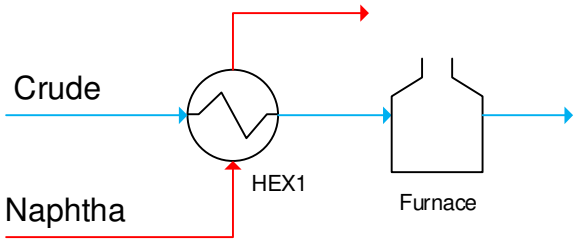

Figure A.1. Network representation of case "1HE".

Table A.2. Heat exchangers specifications for case "1HE"

	HEX1
Shell diameter [mm]	1295
Tube inner diameter [mm]	19.86
Tube outer diameter [mm]	25.40
Tube length [m]	6.1
Number of tubes [-]	800
Number of passes [-]	2
Baffle cut [%]	25
Tube layout [°]	45
Number of baffles [-]	5
Surface roughness	0.046
Deposition constant [$m^2K/Wday$]	648.0
Removal constant [$m^4K/NWday$]	$3.89x10^{-7}$
Fouling activation energy [J/mol]	35000
Ageing frequency factor [1/day]	0
Ageing activation energy [J/mol]	50000
Cleaning time [days]	10
Cleaning cost [$]	30000

Table A.3. Stream specifications and physical properties for case "1HE"

	Crude	**Naphtha**
Flow rate [kg/s]	90.0	37.7
Inlet temperature [K]	463.15	483.15
k_1^{ρ}[kg/m^{3}K]	-0.783	-1.248
k_0^{ρ}[kg/m^3]	1076.9	1145.4
k_1^{λ}[W/mK^2]	-1.25x10^{-4}	-1.09x10^{-4}
k_0^{λ}[W/mK]	0.161	0.141
k_1^{Cp}[J/kgK^2]	3.669	3.298
k_0^{Cp}[J/kgK]	950.0	1201.5
k_1^{μ}[K]	2185.1	2275.1
k_0^{μ}[Pa s]	6.01x10^{-6}	3.52x10^{-6}

A.2.2. Case 2: "2HE-S"

This case study is a small network with two heat exchangers in series adapted from the units of the network presented in Coletti and Macchietto (2011a, 2011b). In this case the hot steam flows counter current through the exchangers with respect to the crude stream. Figure A.2 shows the network structure, Table A.4 presents the configuration of the exchangers, fouling and cleaning parameters, and Table A.5 the streams conditions and physical properties parameters.

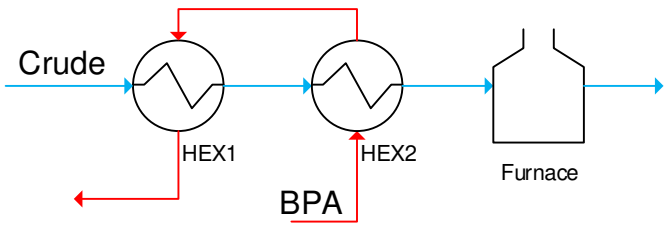

Figure A.2. Network representation of case "2HE-S".

Table A.4. Heat exchangers specifications for case "2HE-S"

	HEX1	**HEX2**
Shell diameter [mm]	1400	1295
Tube inner diameter [mm]	19.86	19.86
Tube outer diameter [mm]	25.40	25.40
Tube length [m]	5800	6100
Number of tubes [-]	840	800
Number of passes [-]	2	2
Baffle cut [%]	25	25
Tube layout [°]	45	45
Number of baffles [-]	6	8
Surface roughness	0.046	0.046
Deposition constant [$m^2K/Wday$]	648.0	648.0
Removal constant [$m^4K/NWday$]	$3.89x10^{-7}$	$3.89x10^{-7}$
Fouling activation energy [J/mol]	35000	35000
Ageing frequency factor [1/day]	0.00	0.00
Ageing activation energy [J/mol]	50000	50000
Cleaning time [days]	10	10
Cleaning cost [$]	30000	30000

Table A.5. Stream specifications and physical properties for case "2HE-S"

	Crude	**BPA**
Flow rate [kg/s]	90.0	33.7
Inlet temperature [K]	463.15	523.15
k_1^{ρ}[kg/m^3K]	-0.789	-0.671
k_0^{ρ}[kg/m^3]	1079.5	1025.0
k_1^{λ}[W/mK^2]	$-1.25x10^{-4}$	$-1.31x10^{-4}$
k_0^{λ}[W/mK]	0.161	0.169
k_1^{Cp}[J/kgK^2]	3.631	3.702
k_0^{Cp}[J/kgK]	967.9	1085.5
k_1^{μ}[K]	2165.1	2397.2
k_0^{μ}[Pa s]	$6.27x10^{-6}$	$5.00x10^{-6}$

A.2.3. Case 3: "2HE-B"

This case study is a small network with two heat exchangers in parallel adapted from the units of the network presented in Coletti and Macchietto (2011a, 2011b). In this case the hot and cold streams are split and distributed to two exchangers. Depending on the operating mode the flow through the parallel branches can be: pressure driven, fixed, or free. This is the first case that introduces control elements using the split fraction of parallel branches. Figure A.3 shows the network structure, Table A.6 presents the configuration of the exchangers, fouling and cleaning parameters, and Table A.7 the streams conditions and physical properties parameters.

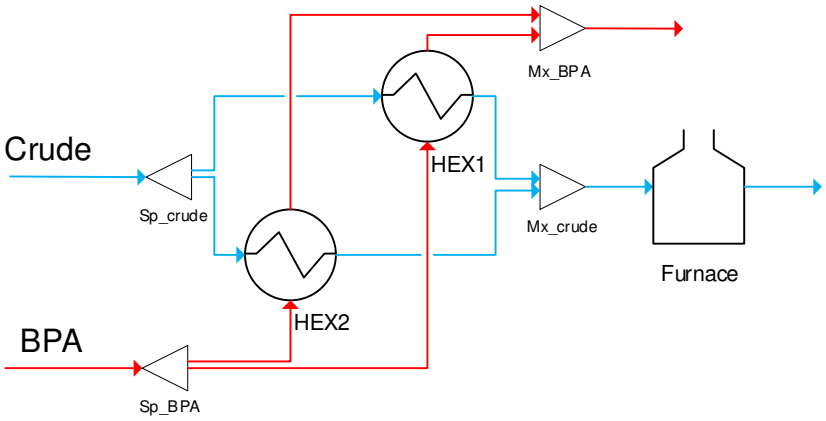

Figure A.3. Network representation of case "2HE-B".

Table A.6. Heat exchangers specifications for case "2HE-B"

	HEX1	**HEX2**
Shell diameter [mm]	1295	1295
Tube inner diameter [mm]	19.86	19.86
Tube outer diameter [mm]	25.40	25.40
Tube length [m]	6100	6100
Number of tubes [-]	800	800
Number of passes [-]	2	2
Baffle cut [%]	25	25
Tube layout [°]	45	45
Number of baffles [-]	8	8
Surface roughness	0.046	0.046
Deposition constant [$m^2K/Wday$]	648.0	648.0
Removal constant [$m^4K/NWday$]	$3.89x10^{-7}$	$3.89x10^{-7}$
Fouling activation energy [J/mol]	35000	35000
Ageing frequency factor [1/day]	0.00	0.00
Ageing activation energy [J/mol]	50000	50000
Cleaning time [days]	10	10
Cleaning cost [$]	30000	30000

Table A.7. Stream specifications and physical properties for case "2HE-B"

	Crude	**BPA**
Flow rate [kg/s]	90.0	28.2
Inlet temperature [K]	463.15	523.15
k_1^{ρ}[kg/m^3K]	-0.786	-0.871
k_0^{ρ}[kg/m^3]	1078.1	1091.6
k_1^{λ}[W/mK^2]	$-1.25x10^{-4}$	$-1.22x10^{-4}$
k_0^{λ}[W/mK]	0.161	0.158
k_1^{Cp}[J/kgK^2]	3.650	3.417
k_0^{Cp}[J/kgK]	958.7	1094.2
k_1^{μ}[K]	2175.0	2409.7
k_0^{μ}[Pa s]	$6.14x10^{-6}$	$4.47x10^{-6}$

A.2.4. Case 4: "4HE-S"

This case study is a network with four heat exchangers in series adapted from the units of the network presented in Coletti and Macchietto (2011a, 2011b). There are three independent hot streams, and one of them flows counter current through exchangers HEX2 and HEX3. This case is used to demonstrate how a continuous time approach can optimize selected features of a cleaning scheduling problem. Figure A.4 shows the network structure, Table A.8 presents the configuration of the exchangers, fouling and cleaning parameters, and Table A.9 the streams conditions and physical properties parameters.

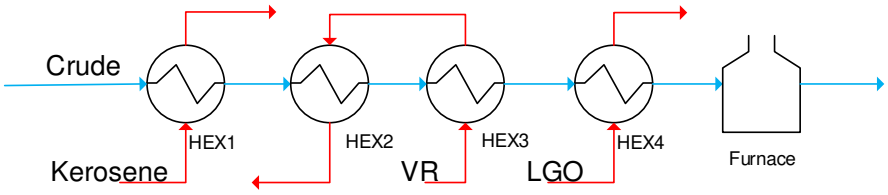

Figure A.4. Network representation of case "4HE-S".

Table A.8. Heat exchangers specifications for case "4HE-S"

	HEX1	**HEX2**	**HEX3**	**HEX4**
Shell diameter [mm]	1295	1295	1295	1295
Tube inner diameter [mm]	19.86	19.86	19.86	19.86
Tube outer diameter [mm]	25.40	25.40	25.40	25.40
Tube length [m]	6100	6100	6100	6100
Number of tubes [-]	800	800	800	800
Number of passes [-]	2	2	2	2
Baffle cut [%]	25	25	25	25
Tube layout [°]	45	45	45	45
Number of baffles [-]	8	8	8	8
Surface roughness	0.046	0.046	0.046	0.046
Deposition constant [$m^2K/Wday$]	872.2	872.2	872.2	872.2
Removal constant [$m^4K/NWday$]	$3.26x10^{-11}$	$3.26x10^{-11}$	$3.26x10^{-11}$	$3.26x10^{-11}$
Fouling activation energy [J/mol]	35000	35000	35000	35000
Ageing frequency factor [1/day]	50.0	50.0	50.0	50.0
Ageing activation energy [J/mol]	50000	50000	50000	50000
Cleaning time [days]	10	10	10	10
Cleaning cost [$]	30000	30000	30000	30000

Table A.9. Stream specifications and physical properties for case "4HE-S"

	Crude	Kerosene	VR	LGO
Flow rate [kg/s]	90.0	40.0	20.0	20.0
Inlet temperature [K]	443.15	473.15	633.15	528.15
k_1^{ρ}[kg/m^{3}K]	-0.784	-0.697	-0.615	-0.673
k_0^{ρ}[kg/m^3]	1076.9	1072.6	1242.0	1096.2
k_1^{λ}[W/mK^2]	-1.25x10^{-4}	-1.30x10^{-4}	-1.41x10^{-4}	-1.34x10^{-4}
k_0^{λ}[W/mK]	0.161	0.167	0.182	0.172
k_1^{Cp}[J/kgK^2]	3.668	3.767	2.977	3.491
k_0^{Cp}[J/kgK]	949.1	907.9	974.2	1028.0
k_1^{μ}[K]	2194.9	1145.2	-310.8	1424.8
k_0^{μ}[Pa s]	5.90x10^{-6}	2.51x10^{-5}	1.06x10^{-4}	2.02x10^{-5}

A.2.5. Case 5: "4HE-B"

This case study is a network with four heat exchangers of which three are distributed in parallel branches. It is adapted from the units of the network presented in Coletti and Macchietto (2011a, 2011b). This case has two control degrees of freedom that corresponds to two of the three flow rates of the parallel branches. Figure A.5 shows the network structure, Table A.10 presents the configuration of the exchangers, fouling and cleaning parameters, and Table A.11 the streams conditions and physical properties parameters.

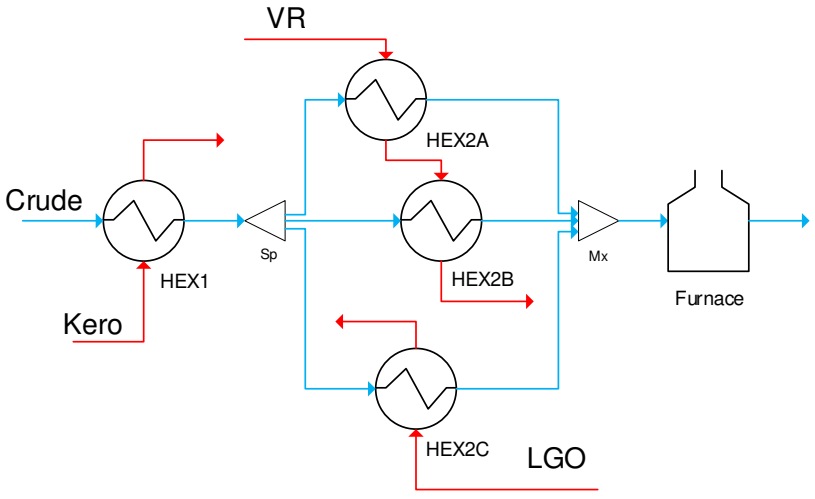

Figure A.5. Network representation of case "4HE-B".

Table A.10. Heat exchangers specifications for case "4HE-B"

	HEX1	HEX2A	HEX2B	HEX2C
Shell diameter [mm]	1295	1400	1400	1400
Tube inner diameter [mm]	19.86	19.86	19.86	19.86
Tube outer diameter [mm]	25.40	25.40	25.40	25.40
Tube length [m]	6100	5800	5800	6100
Number of tubes [-]	800	600	600	600
Number of passes [-]	2	2	2	4
Baffle cut [%]	25	25	25	25
Tube layout [°]	45	45	45	45
Number of baffles [-]	8	6	6	7
Surface roughness	0.046	0.046	0.046	0.046
Deposition constant [$m^2K/Wday$]	648.0	734.4	734.4	561.6
Removal constant [$m^4K/NWday$]	$3.89x10^{-7}$	$3.46x10^{-7}$	$3.46x10^{-7}$	$3.89x10^{-7}$
Fouling activation energy [J/mol]	35000	33000	33000	38000
Ageing frequency factor [1/day]	0.00	0.00	0.00	0.00
Ageing activation energy [J/mol]	50000	50000	50000	50000
Cleaning time [days]	10	10	10	10
Cleaning cost [$]	30000	30000	30000	30000

Table A.11. Stream specifications and physical properties for case "4HE-B"

	Crude	Kero	VR	LGO
Flow rate [kg/s]	90.0	40.0	20.0	20.0
Inlet temperature [K]	443.15	473.15	633.15	528.15
k_1^{ρ}[kg/m^3K]	-0.784	-0.697	-0.615	-0.673
k_0^{ρ}[kg/m^3]	1076.9	1072.6	1242.0	1096.2
k_1^{λ}[W/mK^2]	$-1.25x10^{-4}$	$-1.30x10^{-4}$	$-1.41x10^{-4}$	$-1.34x10^{-4}$
k_0^{λ}[W/mK]	0.161	0.167	0.182	0.172
k_1^{Cp}[J/kgK^2]	3.668	3.767	2.977	3.491
k_0^{Cp}[J/kgK]	949.1	907.9	974.2	1028.0
k_1^{μ}[K]	2194.9	1145.2	-310.8	1424.8
k_0^{μ}[Pa s]	$5.90x10^{-6}$	$2.51x10^{-5}$	$1.06x10^{-4}$	$2.02x10^{-5}$

A.2.6. Case 6: "LN-S1"

This case study is a network with eight heat exchangers in series, where some of them interact though the hot stream. It is adapted from the units of the network and operating conditions presented in Coletti and Macchietto (2011b) and Ishiyama et al. (2015). This is the first case of industrial relevance regarding the number of units in the network. Figure A.6 shows the network structure, Table A.12 presents the configuration of the exchangers, fouling and cleaning parameters, and Table A.13 the streams conditions and physical properties parameters.

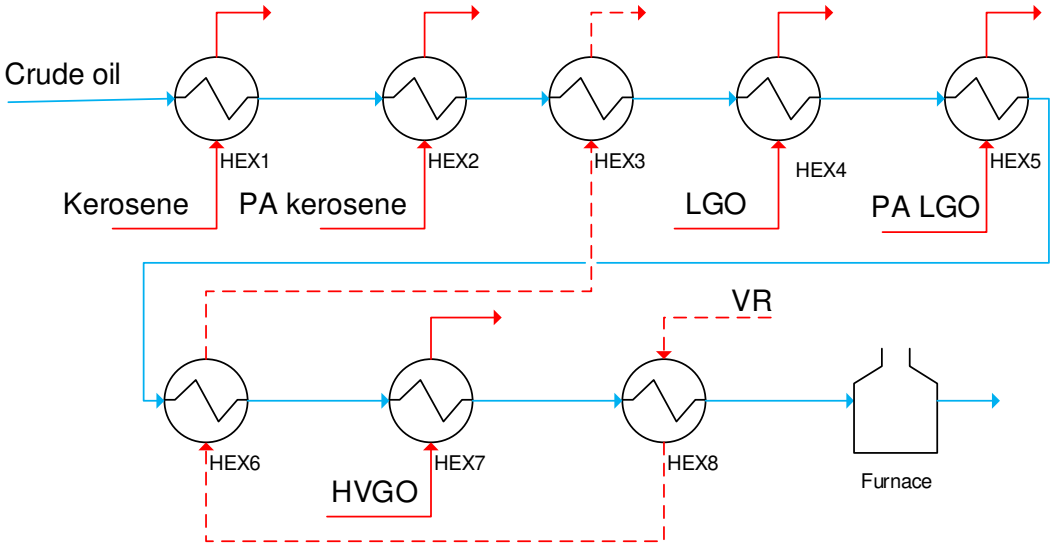

Figure A.6. Network representation of case "LN-S1".

Table A.12. Heat exchangers specifications for case “LN-S1”

	HEX1	HEX2	HEX3	HEX4	HEX5	HEX6	HEX7	HEX8
Shell diameter [mm]	890	1016	848	1296	1296	940	940	940
Tube inner diameter [mm]	16.35	16.35	16.35	16.35	16.35	16.35	16.35	16.35
Tube outer diameter [mm]	19.05	19.05	19.05	19.05	19.05	19.05	19.05	19.05
Tube length [m]	4850	4450	4450	6100	6100	6100	6100	6100
Number of tubes [-]	810	1020	900	1810	1810	1032	848	1032
Number of passes [-]	2	2	2	2	2	2	2	2
Baffle cut [%]	25	25	25	25	25	25	25	25
Tube layout [°]	45	45	45	45	45	45	45	45
Number of baffles [-]	5	5	5	8	8	8	8	8
Surface roughness	0.150	0.150	0.150	0.150	0.150	0.150	0.150	0.150
Deposition constant [$m^2K/Wday$]	138.2	138.2	138.2	138.2	138.2	138.2	138.2	138.2
Removal constant [$m^4K/NWday$]	0	0	0	$8.02x10^{-8}$	$8.02x10^{-8}$	$8.02x10^{-8}$	$8.02x10^{-8}$	$8.02x10^{-8}$
Fouling activation energy [J/mol]	28500	28500	28500	28500	28500	28500	28500	28500
Ageing frequency factor [1/day]	8.64	8.64	8.64	8.64	8.64	8.64	8.64	8.64
Ageing activation energy [J/mol]	50000	50000	50000	50000	50000	50000	50000	50000
Cleaning time [days]	10	10	10	10	10	10	10	10
Cleaning cost [$]	30000	30000	30000	30000	30000	30000	30000	30000

Table A.13. Stream specifications and physical properties for case “LN-S1”

	Crude	**VR**	**HVGO**	**PA LGO**	**LGO**	**Kerosene**	**PA Kero**
Flow rate [kg/s]	88.0	44.0	80.0	70.0	20.0	63.0	6.0
Inlet temperature [K]	403.15	633.15	573.15	530.15	528.15	448.15	475.15
k_1^{ρ}[kg/m^{3}K]	-0.690	-0.600	-0.600	-0.620	-0.620	-0.730	-0.730
k_0^{ρ}[kg/m^3]	1071.5	1233.9	1078.9	1039.4	1039.4	1019.5	1019.5
k_1^{λ}[W/mK^2]	0.0	0.0	0.0	0.0	0.0	0.0	0.0
k_0^{λ}[W/mK]	0.110	0.150	0.110	0.110	0.110	0.120	0.120
k_1^{Cp}[J/kgK^2]	3.950	3.810	3.810	3.840	3.840	4.090	4.090
k_0^{Cp}[J/kgK]	674.1	659.3	659.3	701.1	701.1	662.8	662.8
k_1^{μ}[K]	1477.0	2191.2	2191.2	1907.3	1907.3	1372.1	1372.1
k_0^{μ}[Pa s]	1.20x10^{-5}	7.00x10^{-6}	7.00x10^{-6}	8.20x10^{-6}	8.20x10^{-6}	1.31x10^{-5}	1.31x10^{-5}

A.2.7. Case 7: "LN-S2"

This case study is a network with seven heat exchangers in series, where some of them interact though the hot stream. It is adapted from the units of the network and operating conditions presented in Coletti and Macchietto (2011b). Figure A.7 shows the network structure, Table A.14 presents the configuration of the exchangers, fouling and cleaning parameters, and Table A.15 the streams conditions and physical properties parameters.

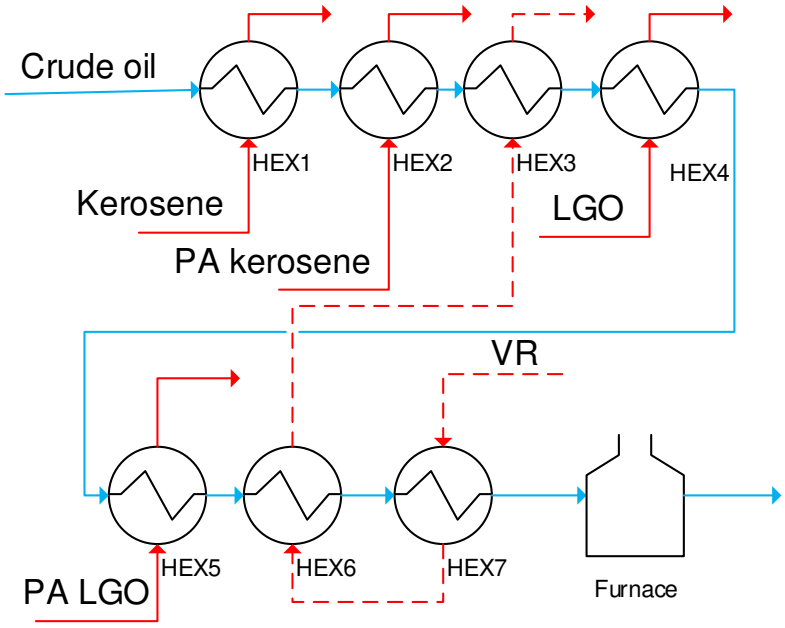

Figure A.7. Network representation of case "LN-S2".

Table A.14. Heat exchangers specifications for case “LN-S2”

	HEX1	**HEX2**	**HEX3**	**HEX4**	**HEX5**	**HEX6**	**HEX7**
Shell diameter [mm]	1295	1295	1295	1295	990	800	800
Tube inner diameter [mm]	19.86	19.86	19.86	19.86	19.86	16.35	16.35
Tube outer diameter [mm]	25.40	25.40	25.40	25.40	25.40	19.05	19.05
Tube length [m]	6100	6100	6100	6100	6100	6100	6100
Number of tubes [-]	800	764	764	500	630	630	630
Number of passes [-]	2	2	2	2	2	2	2
Baffle cut [%]	25	25	25	25	25	25	25
Tube layout [°]	45	45	45	45	45	45	45
Number of baffles [-]	8	8	8	8	16	16	14
Surface roughness	0.046	0.046	0.046	0.046	0.046	0.046	0.046
Deposition constant [$m^2K/Wday$]	138.2	138.2	138.2	138.2	138.2	138.2	138.2
Removal constant [$m^4K/NWday$]	0	0	0	$8.02x10^{-8}$	$8.02x10^{-8}$	$8.02x10^{-8}$	$8.02x10^{-8}$
Fouling activation energy [J/mol]	35000	35000	35000	35000	35000	30000	30000
Ageing frequency factor [1/day]	0.00	0.00	0.00	0.00	0.00	0.00	0.00
Ageing activation energy [J/mol]	50000	50000	50000	50000	50000	50000	50000
Cleaning time [days]	10	10	10	10	10	10	10
Cleaning cost [$]	30000	30000	30000	30000	30000	30000	30000

Table A.15. Stream specifications and physical properties for case “LN-S2”

	Crude	**Kerosene**	**PA Kerosene**	**LGO**	**PA LGO**	**VR**
Flow rate [kg/s]	88.0	63.0	30.0	20.0	70.0	70.0
Inlet temperature [K]	403.15	448.15	475.15	493.15	495.15	523.15
k_1^{ρ}[kg/m^{3}K]	-1.284	-0.660	-0.690	-0.650	-0.654	-0.492
k_0^{ρ}[kg/m^3]	1103.0	1030.3	1069.7	1084.7	1088.4	1195.6
k_1^{λ}[W/mK^2]	-1.06x10^{-4}	-1.30x10^{-4}	-1.30x10^{-4}	-1.34x10^{-4}	-1.34x10^{-4}	-1.48x10^{-4}
k_0^{λ}[W/mK]	0.136	0.168	0.167	0.172	0.172	0.191
k_1^{Cp}[J/kgK^2]	3.400	4.024	3.828	3.745	3.698	3.745
k_0^{Cp}[J/kgK]	1271.5	877.7	879.3	901.6	919.7	716.8
k_1^{μ}[K]	1346.7	1057.4	1152.1	1474.9	1474.6	-391.6
k_0^{μ}[Pa s]	9.71x10^{-6}	2.64x10^{-5}	2.48x10^{-5}	1.82x10^{-5}	1.85x10^{-5}	1.39x10^{-4}

A.2.8. Case 8: "LN-S3"

This case study is a network with six heat exchangers in series, where only two interact though the hot stream of the shell side. It is adapted from the units of the network and operating conditions presented in Diaz-Bejarano, Coletti, and Macchietto (2017). Figure A.8 shows the network structure, Table A.16 presents the configuration of the exchangers, fouling and cleaning parameters, and Table A.17 the streams conditions and physical properties parameters.

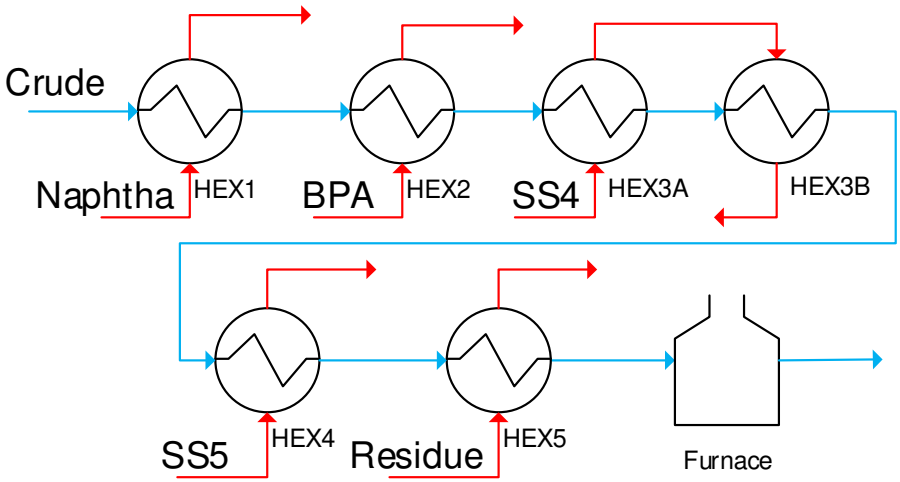

Figure A.8. Network representation of case "LN-S3".

Table A.16. Heat exchangers specifications for case “LN-S3”

	HEX1	**HEX2**	**HEX3A**	**HEX3B**	**HEX4**	**HEX5**
Shell diameter [mm]	1295	1295	1295	1295	990	990
Tube inner diameter [mm]	19.86	19.86	19.86	19.86	19.86	19.86
Tube outer diameter [mm]	25.4	25.4	25.4	25.4	25.4	25.4
Tube length [m]	6100	6100	6100	6100	6100	6100
Number of tubes [-]	800	764	764	382	630	1260
Number of passes [-]	2	2	2	2	2	4
Baffle cut [%]	25	25	25	25	25	25
Tube layout [°]	45	45	45	45	45	45
Number of baffles [-]	8	8	8	8	16	18
Surface roughness	0.046	0.046	0.046	0.046	0.046	0.046
Deposition constant [$m^2K/Wday$]	648	648	648	648	648	648
Removal constant [$m^4K/NWday$]	$3.89x10^{-7}$	$3.89x10^{-7}$	$3.89x10^{-7}$	$3.89x10^{-7}$	$3.89x10^{-7}$	$3.89x10^{-7}$
Fouling activation energy [J/mol]	35000	35000	35000	35000	35000	35000
Ageing frequency factor [1/day]	0.00	0.00	0.00	0.00	0.00	0.00
Ageing activation energy [J/mol]	50000	50000	50000	50000	50000	50000
Cleaning time [days]	10	10	10	10	10	10
Cleaning cost [$]	30000	30000	30000	30000	30000	30000

Table A.17. Stream specifications and physical properties for case “LN-S3”

	Crude	**Naphtha**	**BPA**	**SS4**	**SS5**	**Residue**
Flow rate [kg/s]	90.0	37.7	28.2	50.0	50.1	49.0
Inlet temperature [K]	463.15	483.15	523.15	563.15	593.15	633.15
k_1^{ρ}[kg/m^{3}K]	-0.812	-1.254	-0.881	-0.789	-0.828	-0.521
k_0^{ρ}[kg/m^3]	1090.4	1148.4	1096.3	1119.0	1140.5	1114.3
k_1^{λ}[W/mK^2]	-1.25x10^{-4}	-1.09x10^{-4}	-1.22x10^{-4}	-1.28x10^{-4}	-1.28x10^{-4}	-1.48x10^{-4}
k_0^{λ}[W/mK]	0.161	0.141	0.158	0.165	0.165	0.190
k_1^{Cp}[J/kgK^2]	3.483	3.286	3.370	3.264	3.019	3.110
k_0^{Cp}[J/kgK]	1037.5	1207.2	1117.8	1112.4	1248.7	1344.2
k_1^{μ}[K]	2111.5	2276.0	2388.8	2396.5	1933.0	2805.7
k_0^{μ}[Pa s]	7.03x10^{-6}	3.52x10^{-6}	4.66x10^{-6}	5.63x10^{-6}	1.05x10^{-6}	4.77x10^{-6}

A.2.9. Case 9: "LN-B1"

This case study is a network with six heat exchangers, and some of them are distributed in two parallel branches. It is adapted from the units of the network and operating conditions presented in Coletti and Macchietto (2011b) and Ishiyama et al. (2015). The cold stream is split in two branches, as well as two of the hot streams of the network, which introduces additional degrees of freedom of control. In this case, the exchangers on each branch are different, so that the branches are not balanced and there is a potential benefit if the split fraction is controlled optimally to mitigate fouling. Figure A.9 shows the network structure, Table A.18 presents the configuration of the exchangers, fouling and cleaning parameters, and Table A.19 the streams conditions and physical properties parameters.

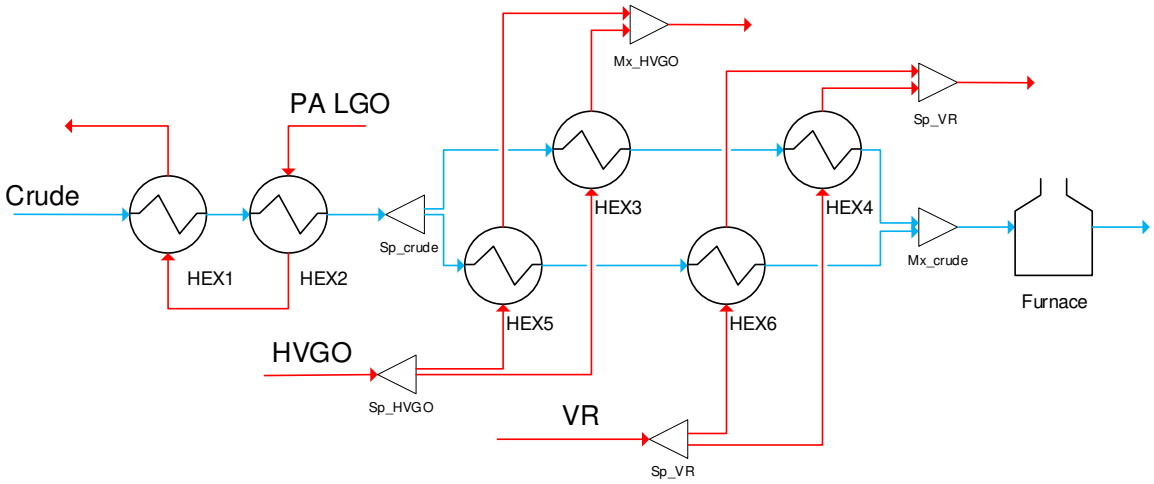

Figure A.9. Network representation of case "LN-B1".

Table A.18. Heat exchangers specifications for case “LN-B1”

	HEX1	**HEX2**	**HEX3**	**HEX4**	**HEX5**	**HEX6**
Shell diameter [mm]	584	798	1100	740	520	740
Tube inner diameter [mm]	19.05	19.05	19.05	19.05	19.05	19.05
Tube outer diameter [mm]	24.86	24.86	24.86	24.86	24.86	24.86
Tube length [m]	6100	6100	6100	6100	6100	6100
Number of tubes [-]	336	620	1130	968	240	968
Number of passes [-]	2	4	6	4	2	4
Baffle cut [%]	25	25	25	25	25	25
Tube layout [°]	45	45	45	45	45	45
Number of baffles [-]	8	8	8	8	8	8
Surface roughness	0.150	0.150	0.150	0.150	0.150	0.150
Deposition constant [$m^2K/Wday$]	138.2	138.2	138.2	138.2	138.2	138.2
Removal constant [$m^4K/NWday$]	$8.02x10^{-8}$	$8.02x10^{-8}$	$8.02x10^{-8}$	$8.02x10^{-8}$	$8.02x10^{-8}$	$8.02x10^{-8}$
Fouling activation energy [J/mol]	28500	28500	28500	28500	28500	28500
Ageing frequency factor [1/day]	8.64	8.64	8.64	8.64	8.64	8.64
Ageing activation energy [J/mol]	50000	50000	50000	50000	50000	50000
Cleaning time [days]	10	10	10	10	10	10
Cleaning cost [$]	30000	30000	30000	30000	30000	30000

Table A.19. Stream specifications and physical properties for case "LN-B1"

	Crude	VR	HVGO	PA LGO
Flow rate [kg/s]	88.0	44.0	80.0	70.0
Inlet temperature [K]	403.15	633.15	573.15	530.15
k_1^{ρ}[kg/m^{3}K]	-0.690	-0.600	-0.600	-0.620
k_0^{ρ}[kg/m^3]	1071.5	1233.9	1078.9	1039.4
k_1^{λ}[W/mK^2]	0.0	0.0	0.0	0.0
k_0^{λ}[W/mK]	0.110	0.150	0.110	0.110
k_1^{Cp}[J/kgK^2]	3.950	3.810	3.810	3.840
k_0^{Cp}[J/kgK]	674.1	659.3	659.3	701.1
k_1^{μ}[K]	1477.0	2191.2	2191.2	1907.3
k_0^{μ}[Pa s]	1.20x10^{-5}	7.00x10^{-6}	7.00x10^{-6}	8.20x10^{-6}

A.2.10. Case 10: "LN-B2"

This case study is a network with six heat exchangers, and some of them are distributed in two parallel branches. It is adapted from the units of the network and operating conditions presented in Coletti and Macchietto (2011b) and Ishiyama et al. (2015). The cold stream is split in two branches, as well as one of the hot streams of the network. This case is similar to the case "LN-B1", but one of the hot streams interacts with two exchangers in series instead of being split. Figure A.10 shows the network structure, Table A.20 presents the configuration of the exchangers, fouling and cleaning parameters, and Table A.21 the streams conditions and physical properties parameters.

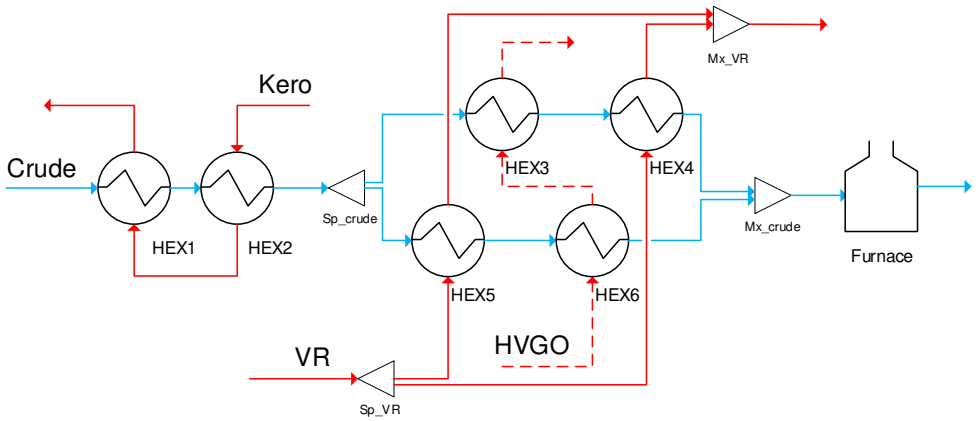

Figure A.10. Network representation of case "LN-B2".

Table A.20. Heat exchangers specifications for case “LN-B2”

	HEX1	**HEX2**	**HEX3**	**HEX4**	**HEX5**	**HEX6**
Shell diameter [mm]	1295	1295	1295	990	990	1295
Tube inner diameter [mm]	19.86	19.86	19.86	19.86	19.86	19.86
Tube outer diameter [mm]	25.40	25.40	25.40	25.40	25.40	25.40
Tube length [m]	6100	6100	6100	6100	6100	6100
Number of tubes [-]	800	764	480	500	500	480
Number of passes [-]	2	2	4	2	2	4
Baffle cut [%]	25	25	25	25	25	25
Tube layout [°]	45	45	45	30	30	45
Number of baffles [-]	8	8	8	8	8	8
Surface roughness	0.046	0.046	0.046	0.046	0.046	0.046
Deposition constant [$m^2K/Wday$]	138.2	138.2	138.2	138.2	138.2	138.2
Removal constant [$m^4K/NWday$]	$8.02x10^{-8}$	$8.02x10^{-8}$	$8.02x10^{-8}$	$8.02x10^{-8}$	$8.02x10^{-8}$	$8.02x10^{-8}$
Fouling activation energy [J/mol]	28500	28500	28500	28500	28500	28500
Ageing frequency factor [1/day]	0.00	0.00	0.00	0.00	0.00	0.00
Ageing activation energy [J/mol]	50000	50000	50000	50000	50000	50000
Cleaning time [days]	10	10	10	10	10	10
Cleaning cost [$]	30000	30000	30000	30000	30000	30000

Table A.21. Stream specifications and physical properties for case "LN-B2"

	Crude	**Kero**	**VR**	**HVGO**
Flow rate [kg/s]	88.0	63.0	80.0	65.0
Inlet temperature [K]	403.15	448.15	523.15	503.15
k_1^{ρ}[kg/m^{3}K]	-1.270	-0.656	-0.494	-0.582
k_0^{ρ}[kg/m^3]	1096.9	1028.5	1196.2	1105.3
k_1^{λ}[W/mK^2]	-1.06x10^{-4}	-1.30x10^{-4}	-1.48x10^{-4}	-1.39x10^{-4}
k_0^{λ}[W/mK]	0.136	0.168	0.191	0.179
k_1^{Cp}[J/kgK^2]	3.423	4.069	3.712	3.778
k_0^{Cp}[J/kgK]	1261.5	858.1	732.9	859.6
k_1^{μ}[K]	1333.4	1063.0	-385.7	-179.0
k_0^{μ}[Pa s]	1.00x10^{-5}	2.61x10^{-5}	1.38x10^{-4}	1.00x10^{-4}

A.2.11. Case 11: "REF-X"

This case study is a network with five heat exchangers of which four are double shells. It is adapted based on the network and operating conditions presented in Coletti and Macchietto (2011a); Coletti (2010); and Lanchas-Fuentes et al. (2016), and it corresponds to the hot-end of a real refinery preheat train. It has control degrees of freedom as the flow thought the parallel branches is not constrained. For this case, plant measurements of the flow rates, and streams temperature are available for model validation, characterization of the process variability, and testing of the algorithms and methodology. The data were collected as the daily average of the characteristic measure over 1240 days.

This case study is widely used in this thesis for: model validation on a realistic scenario with plant variability, testing solution algorithms for the optimal cleaning scheduling problem in realistic settings, comparing the actual operation of the refinery with the potential of an optimal decision making approach, and implementing and validating an online fouling mitigation strategy based on flow control and cleaning scheduling.

Figure A.11 shows the network structure, Table A.22 presents the configuration of the exchangers, fouling and cleaning parameters, and Table A.23 the streams conditions and physical properties parameters.

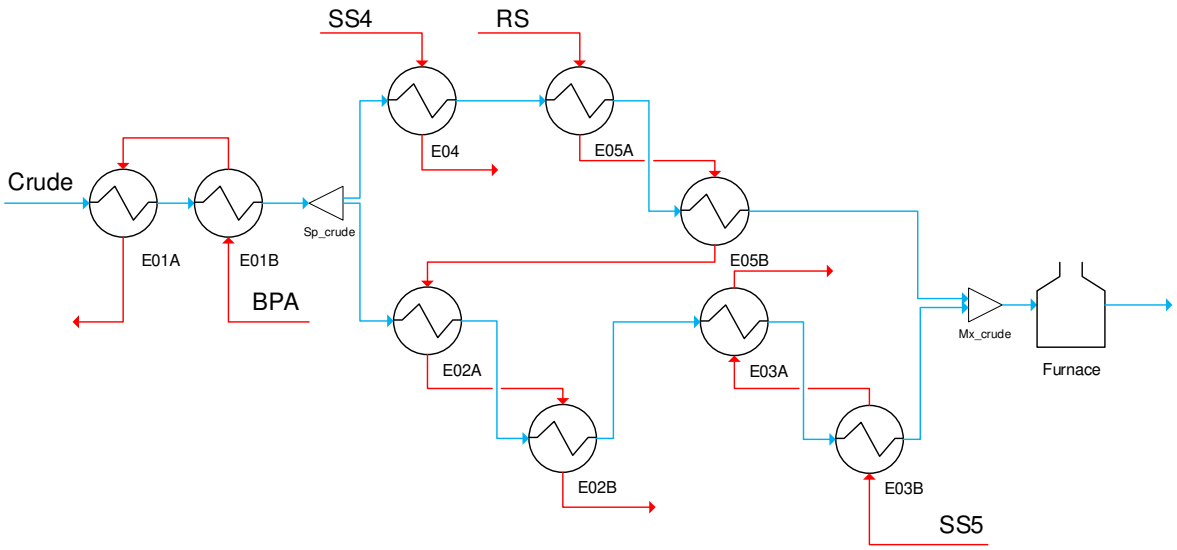

Figure A.11. Network representation of case “REF-X”.

Table A.22. Heat exchangers specifications for case “REF-X”

	E01A	**E01B**	**E02A**	**E02B**	**E03A**	**E03B**	**E04**	**E05A**	**E05B**
Shell diameter [mm]	1245	1194	1397	1397	990	990	1270	1397	1397
Tube inner diameter [mm]	19.86	19.86	19.86	19.86	13.51	13.51	19.86	19.86	19.86
Tube outer diameter [mm]	25.40	25.40	25.40	25.40	19.05	19.05	25.40	25.40	25.40
Tube length [m]	6090	6090	6090	6090	6090	6090	6090	6090	6090
Number of tubes [-]	764	850	880	880	630	630	888	880	880
Number of passes [-]	2	2	4	4	2	2	4	4	4
Baffle cut [%]	25	22.5	25	25	25	25	17	25	25
Tube layout [°]	45	45	45	45	45	45	45	45	45
Number of baffles [-]	5	7	18	18	20	20	9	18	18
Surface roughness	0.046	0.046	0.046	0.046	0.046	0.046	0.046	0.046	0.046
Deposition constant [$m^2K/Wday$]	390.9	352.1	311.3	313.3	106.9	124.9	280.7	343.3	332.1
Removal constant [$m^4K/NWday$]	$1.46x10^{-6}$	$1.32x10^{-6}$	$1.11x10^{-6}$	$1.12x10^{-6}$	$3.26x10^{-6}$	$3.92x10^{-7}$	$9.83x10^{-7}$	$1.26x10^{-6}$	$1.20x10^{-6}$
Fouling activation energy [J/mol]	28500	28500	28500	28500	28500	28500	28380	28500	28500
Ageing frequency factor [1/day]	0.00	0.00	0.00	0.00	0.00	0.00	0.00	0.00	0.00
Ageing activation energy [J/mol]	50000	50000	50000	50000	50000	50000	50000	50000	50000
Cleaning time [days]	9	9	10	10	8	8	9	16	16
Cleaning cost [$]	27000	27000	30000	30000	24000	24000	27000	48000	48000

Table A.23. Stream specifications and physical properties for case "REF-X"

	Crude	**SS4**	**BPA**	**RS**	**SS5**
Flow rate [kg/s]	150.0	22.5	180.0	22.5	22.5
Inlet temperature [K]	433.15	593.15	493.15	580.95	580.95
k_1^{ρ}[kg/m^{3}K]	-0.975	-0.733	-0.737	-0.565	-0.581
k_0^{ρ}[kg/m^3]	1156.3	1125.7	1100.6	1113.9	1127.6
k_1^{λ}[W/mK^2]	-1.21x10^{-4}	-1.31x10^{-4}	-1.29x10^{-4}	-1.41x10^{-4}	-1.40x10^{-4}
k_0^{λ}[W/mK]	0.156	0.169	0.166	0.182	0.181
k_1^{Cp}[J/kgK^2]	3.192	3.284	3.598	3.667	3.595
k_0^{Cp}[J/kgK]	1064.7	1076.3	929.4	917.3	913.2
k_1^{μ}[K]	1815.7	2190.8	2100.3	2979.6	2914.4
k_0^{μ}[Pa s]	9.69x10^{-6}	7.95x10^{-6}	7.67x10^{-6}	2.68x10^{-6}	3.07x10^{-6}

A.2.12. Case 12: "NR-S"

This case study is a retrofit network with seven fixed heat exchangers, and one potential unit (HEX7x) to include in three locations of the network. This network is adapted from the retrofit problem presented in Coletti, Macchietto, and Polley (2011), and three alternatives considered there are included in the superstructure representing the network. This is a network where all units are arranged in series, and the splitter and mixers of the hot and cold streams are only used to define a super structure that includes all three retrofit alternatives considered in the problem. In addition, this case includes a desalter which introduces a temperature drop of 4.5K, and defines two zones of the network: before the desalter where there is no fouling – low temperature – and after the desalter where fouling occurs as a consequence of high temperatures.

This case does not include control degrees of freedom as there are no parallel branches, so it only integrates the optimal retrofit problem and the optimal cleaning scheduling problem.

Figure A.12 shows the superstructure used to represent the network and retrofit alternatives. The exchangers that can be added or removed from the network are shown with a hash pattern. Table A.24 presents the configuration of the exchangers, fouling and cleaning parameters, and Table A.25 the streams conditions and physical properties parameters.

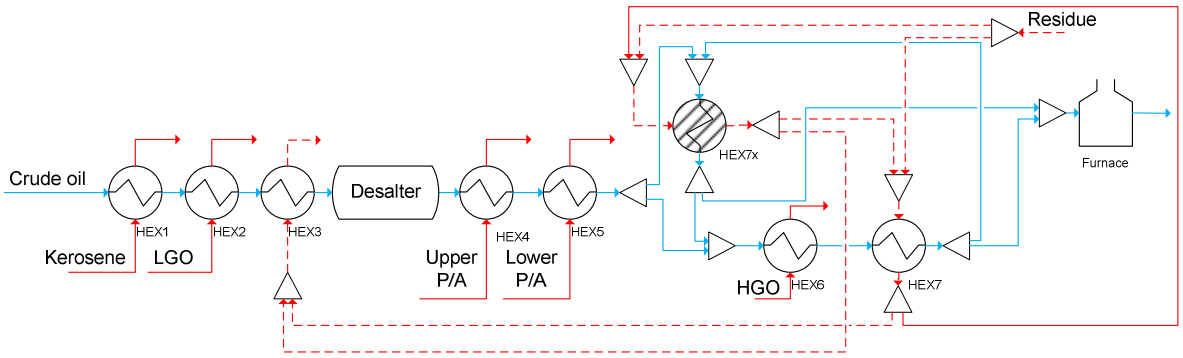

Figure A.12. Network representation of case "NR-S".

The three original retrofit alternatives considered by Coletti, Macchietto, and Polley (2011) are represented in Figure A.13. It is also shown (thick lines) how these alternatives are obtained from the superstructure representation used in the optimal retrofit problem. The superstructure used to represent the retrofit alternatives can include other network representations than those three considered. For example, a network where HEX7x is in parallel with HEX6 and HEX7 is feasible using the superstructure representation.

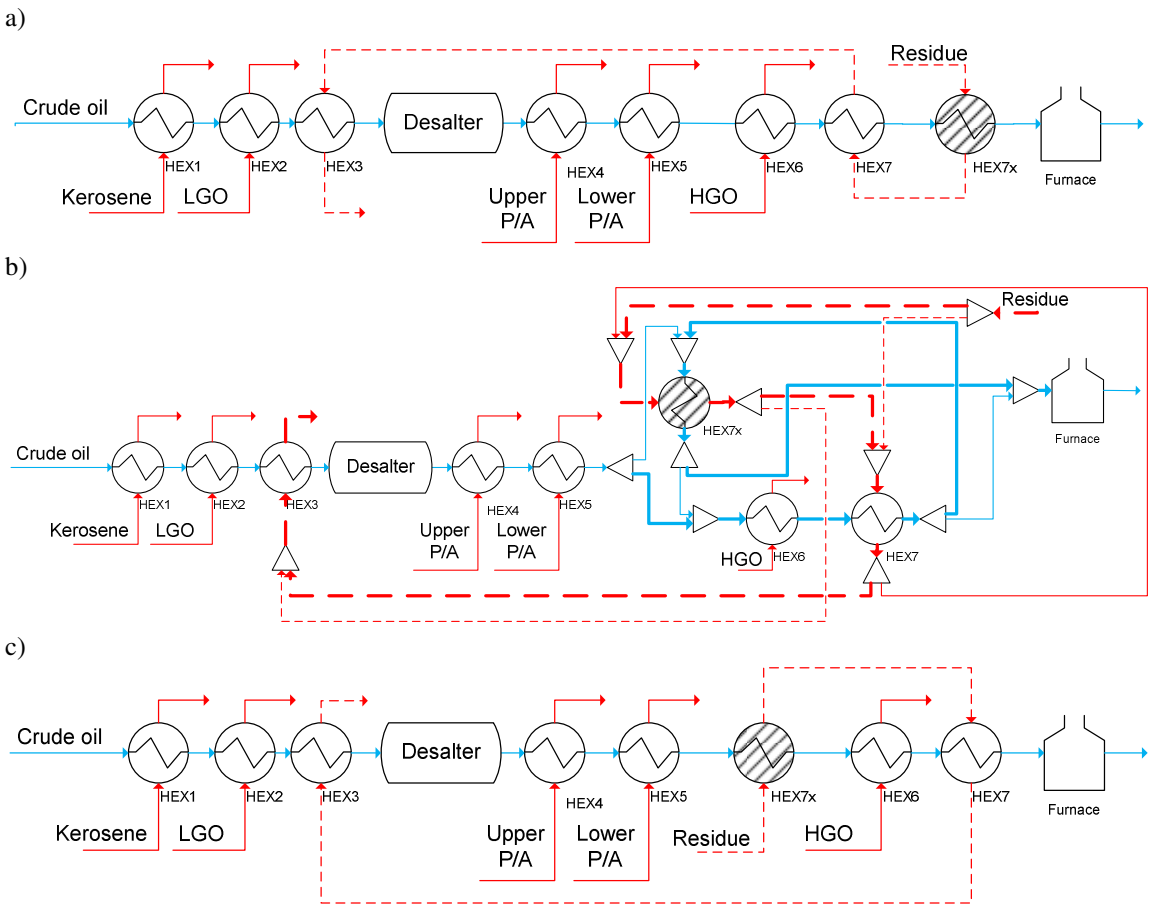

d)

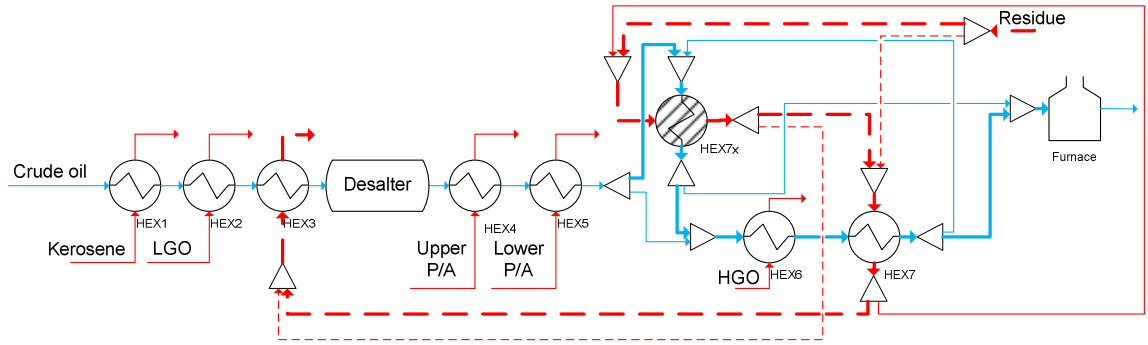

e)

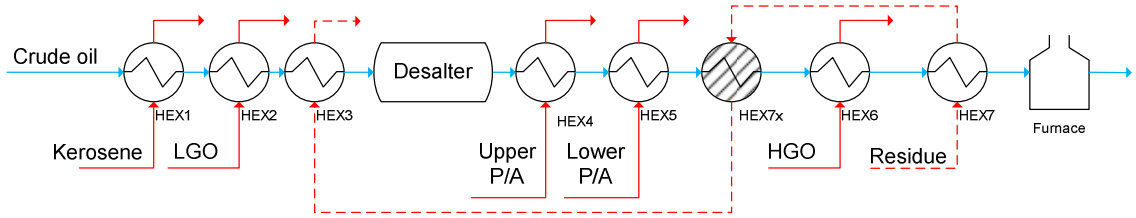

f)

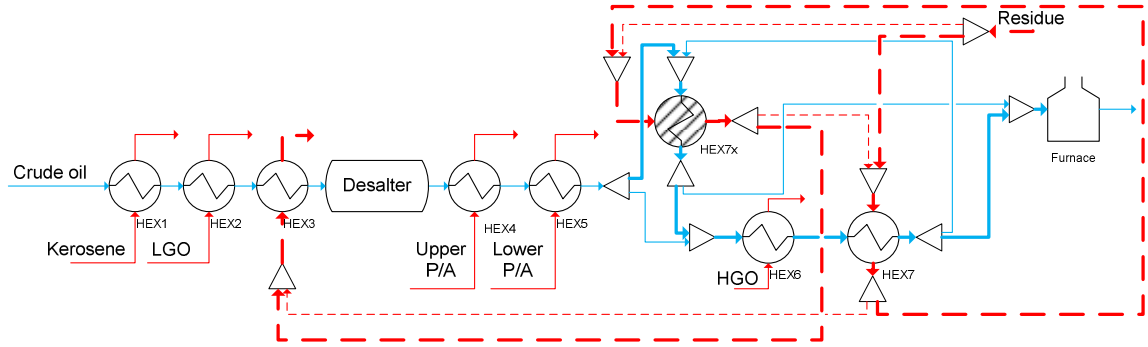

Figure A.13. Original retrofit alternatives of case "NR-S" and their representation in the network superstructure. a, b) C2, c, d) C3, e, f) C4. (Coletti, Macchietto, and Polley 2011)

Table A.24. Heat exchangers specifications for case “NR-S”

	HEX1	**HEX2**	**HEX3**	**HEX4**	**HEX5**	**HEX6**	**HEX7**	**HEX7x**
Shell diameter [mm]	444	584	584	798	1100	520	740	740
Tube inner diameter [mm]	20.90	20.90	20.90	20.90	20.90	20.90	20.90	20.90
Tube outer diameter [mm]	26.70	26.70	26.70	26.70	26.70	26.70	26.70	26.70
Tube length [m]	6100	6100	6100	6100	6100	6100	6100	6100
Number of tubes [-]	152	308	336	620	1130	240	968	968
Number of passes [-]	6	8	2	4	6	2	4	4
Baffle cut [%]	22	17	17	17	17	17	17	17
Tube layout [°]	45	45	45	45	45	45	45	45
Number of baffles [-]	32	40	43	37	41	41	41	41
Surface roughness	0.046	0.046	0.046	0.046	0.046	0.046	0.046	0.046
Deposition constant [$m^2K/Wday$]	0.0	0.0	0.0	788.4	788.4	788.4	788.4	788.4
Removal constant [$m^4K/NWday$]	0	0	0	$3.42x10^{-7}$	$3.42x10^{-7}$	$3.42x10^{-7}$	$3.42x10^{-7}$	$3.42x10^{-7}$
Fouling activation energy [J/mol]	38500	38500	38500	38500	38500	38500	38500	38500
Ageing frequency factor [1/day]	8.64	8.64	8.64	8.64	8.64	8.64	8.64	8.64
Ageing activation energy [J/mol]	50000	50000	50000	50000	50000	50000	50000	50000
Cleaning time [days]	10	10	10	10	10	10	10	10
Cleaning cost [$]	30000	30000	30000	30000	30000	30000	30000	30000

Table A.25. Stream specifications and physical properties for case "NR-S"

	Crude	**Kerosene**	**Upper P/A**	**Lower P/A**	**LGO**	**HVGO**	**Residue**
Flow rate [kg/s]	27.8	2.8	11.1	16.7	5.6	2.8	13.9
Inlet temperature [K]	305.15	478.15	493.15	553.15	563.15	553.15	633.15
k_1^{ρ}[kg/m^{3}K]	-0.690	-0.730	-0.730	-0.620	-0.620	-0.600	-0.600
k_0^{ρ}[kg/m^3]	1071.5	1019.5	1019.5	1039.4	1039.4	1078.9	1233.9
k_1^{λ}[W/mK^2]	0.0	0.0	0.0	0.0	0.0	0.0	0.0
k_0^{λ}[W/mK]	0.110	0.120	0.120	0.110	0.110	0.110	0.150
k_1^{Cp}[J/kgK^2]	3.950	4.090	4.090	3.840	3.840	3.810	3.810
k_0^{Cp}[J/kgK]	674.1	662.8	662.8	701.1	701.1	659.3	659.3
k_1^{μ}[K]	1477.0	1372.1	1372.1	1907.3	1907.3	2191.2	2191.2
k_0^{μ}[Pa s]	1.20x10^{-5}	1.31x10^{-5}	1.31x10^{-5}	8.20x10^{-6}	8.20x10^{-6}	7.00x10^{-6}	7.00x10^{-6}

A.2.13. Case 13: "NR-B"

This case study is a retrofit network with five fixed heat exchangers, one that can be removed from the original network (E2), and five that can be used for retrofitting in different locations. This network is adapted from the retrofit problem presented in Yeap et al. (2005), and three alternatives considered there are included in the superstructure representing the network. This network includes control elements as there is the possibility to have parallel branches in the network, and one of the alternatives considered in Yeap et al. (2005) has this type of structure. Additional splitters and mixers for the hot and cold streams are used in the superstructure to define those retrofitting alternatives, and many new ones.

Figure A.14 shows the superstructure of the network that defines all retrofit alternatives. The exchangers that can be added or removed from the network are shown with a hash pattern. The superstructure shows all possible connections for the exchangers, and the streams that can be redistributed are colour coded for clarity, so that the crude oil stream (blue), the VR stream (yellow), and the OR stream (dashed red) can be differentiated. Table A.26 presents the configuration of the exchangers, fouling and cleaning parameters, and Table A.27 the streams conditions and physical properties parameters.

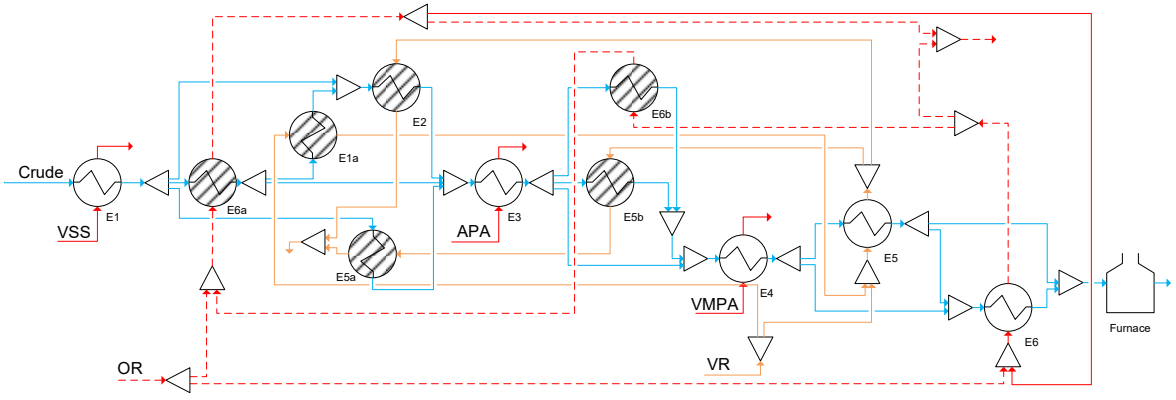

Figure A.14. Network representation of case "NR-B".

The original three alternatives considered in Yeap et al. (2005) are shown in Figure A.15 as well as their representation in the superstructure of the network (thick lines). The superstructure representation includes these three alternatives and many others that can perform even better. Note that the retrofit alternative III has been modified with respect to that of the original reference as temperature crossing in some exchangers was observed

probably because of the physical properties model or some specifications of the exchangers that were not reported in the original reference and had to be assumed.

a)

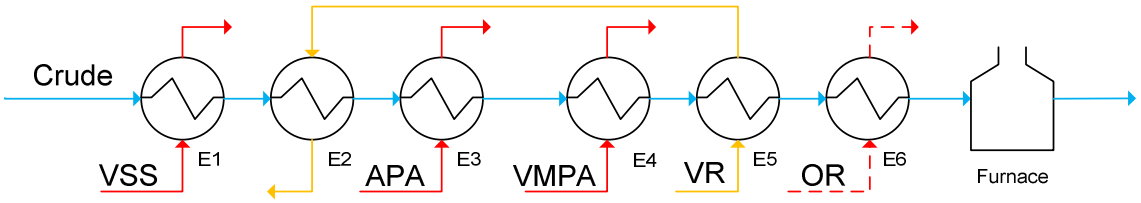

b)

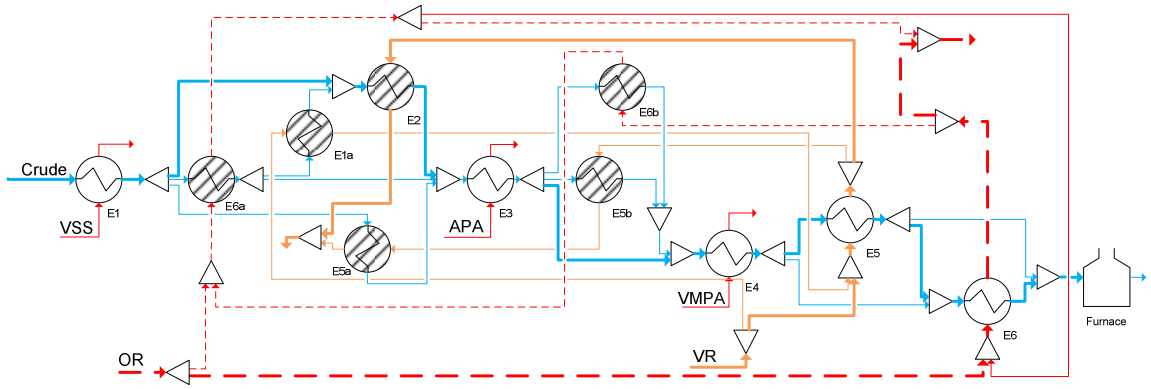

c)

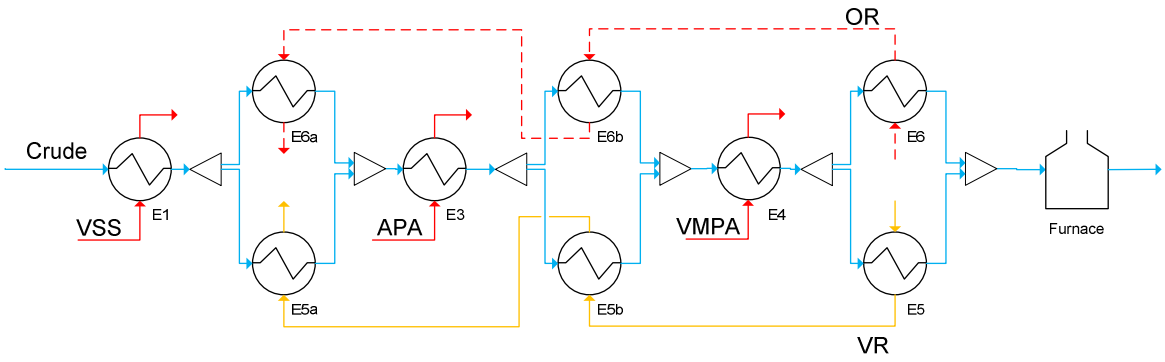

d)

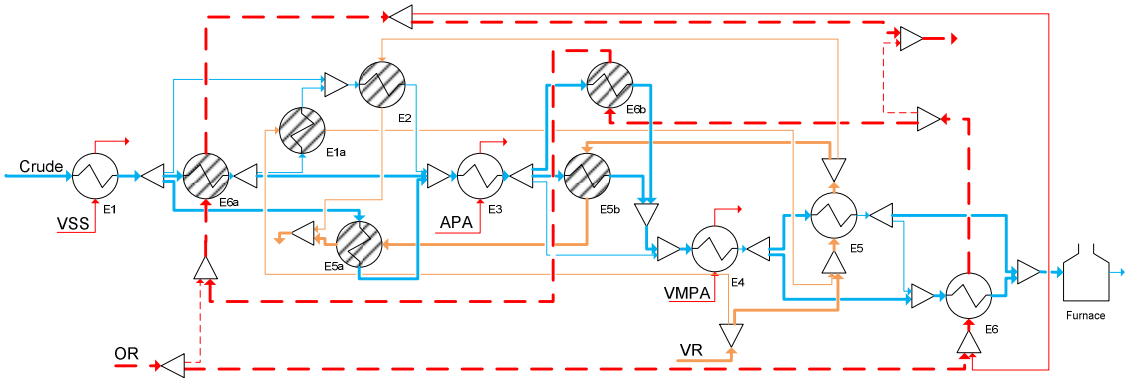

e)

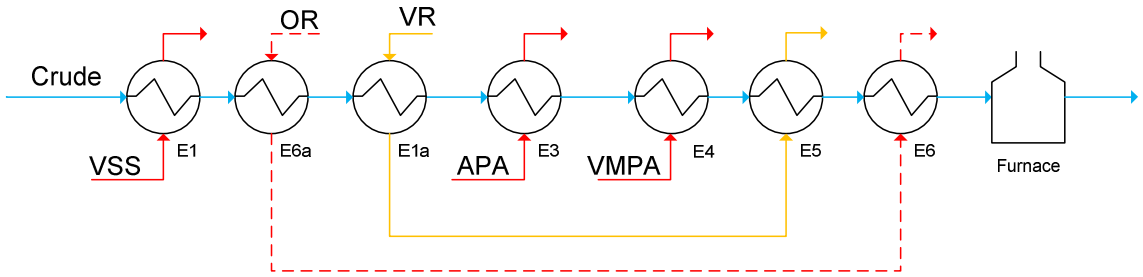

f)

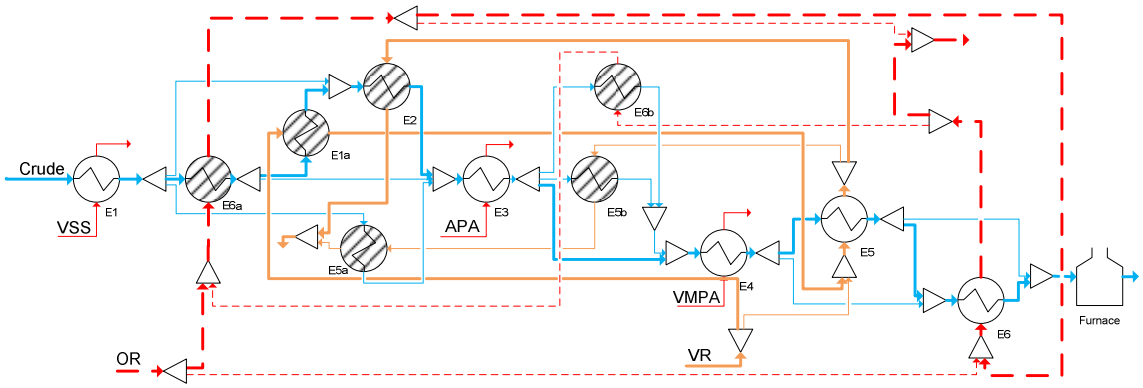

Figure A.15. Original retrofit alternatives of case “NR-B” and their representation in the network superstructure. a, b) I, c, d) II, e, f) III. (Yeap et al. 2005)

Table A.26. Heat exchangers specifications for case “NR-B”

	E1	**E2**	**E3**	**E4**	**E5**	**E6**	**E1a**	**E5a**	**E5b**	**E6a**	**E6b**
Shell diameter [mm]	1220	510	970	480	540	540	970	540	340	730	340
Tube inner diameter [mm]	19.86	19.86	19.86	19.86	19.86	19.86	19.86	19.86	19.86	19.86	19.86
Tube outer diameter [mm]	25.4	25.4	25.4	25.4	25.4	25.4	25.4	25.4	25.4	25.4	25.4
Tube length [m]	6090	6090	6090	6090	6090	6090	6090	6090	6090	6090	6090
Number of tubes [-]	724	388	962	470	388	388	486	196	128	822	128
Number of passes [-]	2	2	2	2	2	2	2	2	2	2	2
Baffle cut [%]	25	25	25	25	25	25	25	25	25	25	25
Tube layout [°]	45	45	45	45	45	45	45	45	45	45	45
Number of baffles [-]	10	8	8	12	8	16	8	12	16	12	8
Surface roughness	0.046	0.046	0.046	0.046	0.046	0.046	0.046	0.046	0.046	0.046	0.046
Deposition constant [$m^2K/Wday$]	$1.85x10^7$	$1.85x10^7$	$1.85x10^7$	$1.85x10^7$	$1.85x10^7$	$1.85x10^7$	$1.85x10^7$	$1.85x10^7$	$1.85x10^7$	$1.85x10^7$	$1.85x10^7$
Removal constant [$m^4K/NWday$]	$2.9x10^{-10}$	$2.9x10^{-10}$	$2.9x10^{-10}$	$2.9x10^{-10}$	$2.9x10^{-10}$	$2.9x10^{-10}$	$2.9x10^{-10}$	$2.9x10^{-10}$	$2.9x10^{-10}$	$2.9x10^{-10}$	$2.9x10^{-10}$
Fouling activation energy [J/mol]	76000	76000	76000	76000	76000	76000	76000	76000	76000	76000	76000
Ageing frequency factor [1/day]	0	0	0	0	0	0	0	0	0	0	0
Ageing activation energy [J/mol]	50000	50000	50000	50000	50000	50000	50000	50000	50000	50000	50000
Cleaning time [days]	10	10	10	10	10	10	10	10	10	10	10
Cleaning cost [$]	30000	30000	30000	30000	30000	30000	30000	30000	30000	30000	30000

Table A.27. Stream specifications and physical properties for case “NR-B”*

	Crude	**VSS**	**APA**	**VMPA**	**VR**	**OR**
Flow rate [kg/s]	105.0	13.0	70.0	106.0	18.0	52.0
Inlet temperature [K]	393.15	488.15	540.15	557.15	574.15	577.15
k_1^{ρ}[kg/m^{3}K]	-0.975	-0.565	-0.733	-0.581	-0.492	-0.529
k_0^{ρ}[kg/m^3]	1156.3	1113.9	1125.7	1127.6	1195.6	1154.7
k_1^{λ}[W/mK^2]	-1.21x10^{-4}	-1.41x10^{-4}	-1.31x10^{-4}	-1.40x10^{-4}	-1.48x10^{-4}	-1.45x10^{-4}
k_0^{λ}[W/mK]	0.156	0.182	0.169	0.181	0.191	0.186
k_1^{Cp}[J/kgK^2]	3.192	3.667	3.284	3.595	3.745	3.706
k_0^{Cp}[J/kgK]	1064.7	917.3	1076.3	913.2	716.8	817.0
k_1^{μ}[K]	1815.7	2979.6	2190.8	2914.4	-391.6	1294.0
k_0^{μ}[Pa s]	9.69x10^{-6}	2.68x10^{-6}	7.95x10^{-6}	3.07x10^{-6}	1.39x10^{-4}	7.09x10^{-5}

VSS: vacuum side stream
APA: atmospheric pump around
VMPA: vacuum mid pump around
VR: vacuum residue
OR: other residue stream

Appendix B.

Dynamic and distributed model for shell and tube heat exchangers

This appendix introduces a dynamic and distributed model for shell and tube heat exchangers developed previously at Imperial College (Coletti and Macchietto 2011b; Diaz-Bejarano, Coletti, and Macchietto 2016). This model is commercially available in *Hexxcell Studio*^{TM}, and the platform offers a wide range of tools for thermo hydraulic analysis and fouling diagnostic of heat exchangers (Hexxcell Ltd. 2016). This tool is used in Chapter 5 to validate the modelling approach developed in this thesis, and in Chapter 6 to demonstrate that the benefits achieved optimizing heat exchanger networks with lumped models are still observed using other more detailed modelling approaches.

B.1. Modelling framework and constituent equations

The model presented here for heat exchangers under fouling is dynamic and distributed in the axial and radial directions. Similarly to the heat exchanger model presented in Chapter 3, this model also considers heat transfer among various domains: shell side, tube wall, deposit layer, and tube side; but it includes the axial distribution of the variables. It also considers explicitly each tube pass within the shell, and exchangers with multiple shell passes or different arrangements are modelled as individual shells connected by their inlet/outlet streams. Figure B.1 shows the schematic representation of a shell and tube heat exchanger used in this modelling framework. There is one tube domain per pass which flow can be co-current or counter-current with respect to that of the shell side. The tube domain is represented by a single characteristic tube of the bundle assuming all tubes behave identically, although there are many more tubes per pass. In Figure B.1b all the different

domains involved in a single pass are observed. This also shows the general assumptions of the domains, their flow pattern, their interactions, and the boundary conditions (BC) used to link all of them.

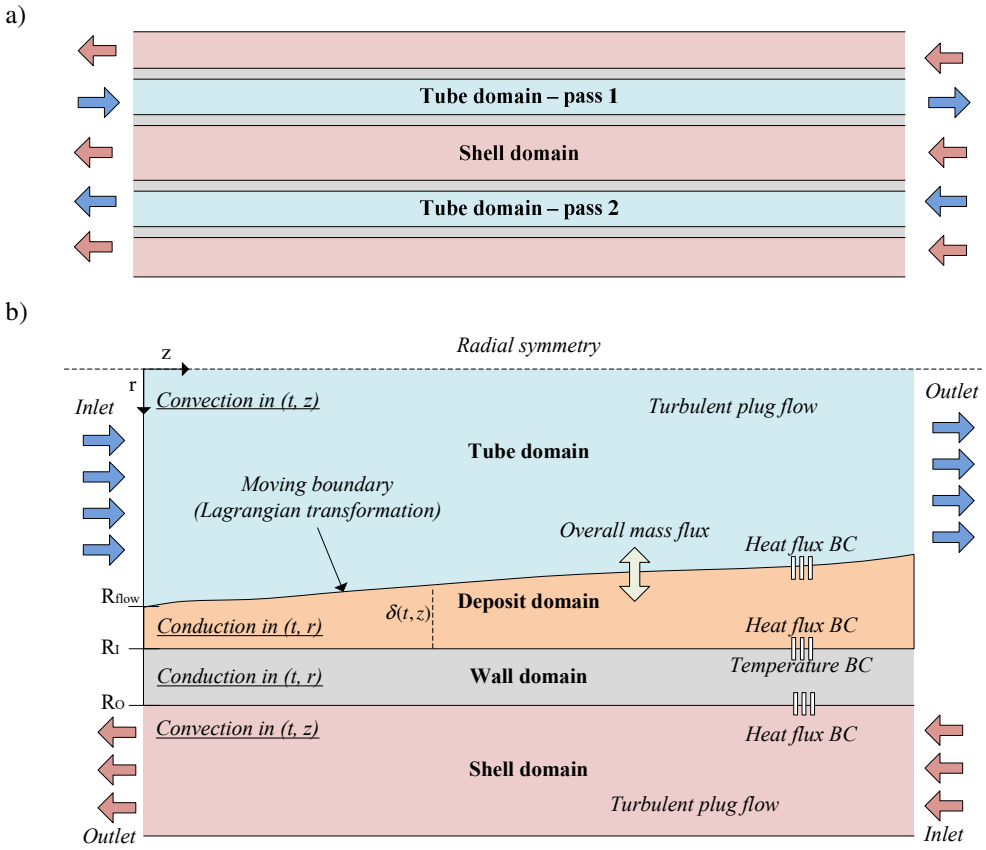

Figure B.1. Dynamic and distributed modelling framework. a) Shell and tube exchanger representation, b) Heat transfer domains in a single tube

The main assumptions of this modelling framework are:

- TEMA type AET shell
- Negligible heat losses
- Fouling only on tube side
- Plug flow on the shell side (perfectly mixed radially)
- Bell-Delaware method for the local heat transfer of the shell side
- All tubes in a pass have the same behaviour
- Tube and shell domains are axial distributed, radial averaged
- Deposit and wall domains are axial and radial distributed
- Physical properties are function of the local temperature

- Constant roughness of the deposit
- Dynamic growth of the deposit captured using a moving boundary

A more complete discussion of the model assumptions, limitations, and advantages can be found in Coletti and Macchietto (2011b; and Diaz-Bejarano, Coletti, and Macchietto (2016). Based on these assumptions the model is developed using conservation equations for each domain, and it is formulated as a large set of partial differential equations. Table B.1 summarizes the model equations and classifies them depending on the domain where they are applicable. It also shows the boundary and initial conditions. The dir variable is used to indicate the relative direction of the flow with respect to the inlet to the exchanger. A heat exchanger has as many tube side domains as tube passes, and each domain equations have different parameters and operating conditions. However, the overall effect of all tube passes is account for in the shell side energy balance. Finally, note that the deposit domain constituent equations are expressed in terms of dimensionless quantities to explicitly consider the moving boundary and how the deposit thickness changes over time and over the axial position in the tube; also, the fouling model is the Ebert-Panchal model evaluated at the local conditions.

Table B.1. Main constituent equations of the distributed and dynamic model

Shell side	
Energy balance	$\rho^S Cp^S \frac{\partial T^S}{\partial t} = -(dir^S)u^S \rho^S Cp^S \frac{\partial T^S}{\partial z} + \sum_{n=1}^{N_P} \frac{p_n^S}{A^S} h^S (T^S - T_n^{ws})$
	$BC. If\ dir^S = 1 \rightarrow T^S(z=0) = T_{in}^S; If\ dir^S = -1 \rightarrow T^S(z=L) = T_{in}^S$
Tube side	
Energy balance	$\rho_n^T Cp_n^T \frac{\partial T_n^T}{\partial t} = -(dir^T)u_n^T \rho_n^T Cp_n^T \frac{\partial T_n^T}{\partial z} + \frac{p_n^T}{A_n^T} h_n^T (T_n^{aw} - T_n^T), \quad \forall n \in N_P$
	$BC. If\ dir^S = 1 \rightarrow T_n^T(z=0) = T_{in}^T; If\ dir^S = -1 \rightarrow T_n^T(z=L) = T_{in}^T$
Mass balance	$m^T = u_n^T A_n^T \rho_n^T \frac{N_T}{N_P}, \quad \forall n \in N_P$
Pressure drop	$-dir_n \frac{dP_n}{dz} = \frac{f_n \rho_n^T (u_n^T)^2}{2(d_I - 2\delta_n)}, \quad \forall n \in N_P$
	$BC. If\ dir_n = 1 \rightarrow P_n(z=0) = P_{in}; If\ dir_n = -1 \rightarrow P_n(z=L) = P_n$

Table B.1. Main constituent equations of the distributed and dynamic model (cont.)

Tube wall	
Energy balance	$\rho_n^W Cp_n^W \frac{\partial T_n^W}{\partial t} = \frac{1}{r}\frac{\partial}{\partial r}\left(r\lambda^W \frac{\partial T_n^W}{\partial r}\right), \quad \forall n \in N_P$ $BC.\, at\ r = d/2 \colon q^W = -h^S(T^S - T^{ws}); at\ r = d_I/2 : q^W = q^D$
Deposit layer	
Domain transformation	$\tilde{r} = \frac{d_I/2 - r}{\delta}$
Energy balance	$\rho^D Cp^D \frac{\partial T^D}{\partial t} - \rho^D Cp^D \frac{\tilde{r}}{\delta}\frac{d\delta}{dt}\frac{\partial T^D}{\partial \tilde{r}} = \frac{\lambda^D}{(d_I/2 - \tilde{r}\delta)\delta^2}\frac{\partial}{\partial \tilde{r}}\left((d_I/2 - \tilde{r}\delta)\frac{\partial T^D}{\partial \tilde{r}}\right)$ $BC.\, at\ \tilde{r} = 0 \colon T^D = T^{aw}\ ; at\ \tilde{r} = 1 \colon q^D = -h^T(T^T - T^{tf})$
Fouling rate	$\frac{dR_f}{dt} = \alpha Re^{-0.66} Pr^{-0.33} \exp\left(-\frac{E_f}{RT^f}\right) - \gamma\tau$
Deposition rate	$\frac{d\delta}{dt} = \lambda^D \frac{dR_f}{dt}$

This modelling framework described for a single exchanger can be expanded to model heat exchanger networks easily, and all these features are available in *Hexxcell Studio*^{TM}. In addition, other elements of the network such as furnace, mixers, splitters, and pumps can be included using the software. Hence, all case studies considered in this thesis can be also modelled and solved using this framework – only for simulation purposes.

Appendix C.

Heuristic algorithms for online cleaning scheduling of preheat trains

This appendix introduces heuristic algorithms developed for the online cleaning scheduling of heat exchanger networks under fouling. It aims to be a preliminary study of online fouling mitigation that is not based on optimization methods. It also serves as a reference point to compare and validate the performance of online optimization based algorithms for fouling mitigation and preheat train optimization. The algorithms are based on the definition of conditional cleanings on a rolling horizon using an economic criteria, and are implemented in gPROMS using the libraries of *Hexxcell studio*^{TM}.

C.1. Heuristic algorithms for online cleaning scheduling

The heuristic algorithms described next are implemented in gPROMS using the libraries of *Hexxcell Studio*^{TM} (Hexxcell Ltd. 2016) to model the performance of the heat exchangers and the network configuration. Therefore, these algorithms use a detail distributed model to define the cleaning scheduling of the network. They are based on an approximation of the dynamic decay of the heat duty of each exchanger caused by fouling. This approximation is used to predict the economic benefits of cleaning actions in a future time window. The trade-off between cleaning cost and future energy savings is used a decisions criterion to define the sequence and frequency of the cleanings, but it is limited to define one cleaning at the time. Variations of this heuristic are considered depending on the function used to estimate the performance decay of the exchangers, which can be: constant, linear, or quadratic.

The heuristic algorithm is presented in Figure C.1. The prerequisites for these algorithm are: a dynamic model for the heat exchanger network that considers fouling, and

the economic indicators to estimate the cost of cleanings and the energy costs associated with the loss of performance of the network. The algorithm starts by estimating the heat duty for each exchanger under cleaned conditions ($Q_i^0,\ \forall i \in HEX$), then it requires an estimation of the performance decay of each exchanger, which is the heat duty loss because of fouling per unit. At this step is where the algorithm may vary, and here three prediction alternatives of the performance decay are considered: constant heat duty, linear decay of the heat duty, and quadratic approximation of the heat duty decay. Figure C.2 illustrates theses prediction approaches. The linear, and quadratic approximations of the performance decay are based on a Taylor series expansion of the function at $t = t^*$, so that the constant term correspond to the current value of the function, the slope (m, b) to the first derivate, and the constant of the quadratic term (a) to the second derivative. The derivatives of the function are estimated from a simulation of the network performance which is done before the beginning of the operation. Note that these models are predicting how the heat duty of the exchangers decreases because of fouling and the interactions of the units in the network, and they use as starting point the current state of the exchanger at time t^*. For the linear and quadratic approximations, it is assumed that the rate of change of the heat duty is constant, in other words the model parameters (m, a, b) are constant and only determined with respect to the cleaned conditions. These parameters do not capture the effect of different flow rates, or inlet temperatures, although in principle they could be updated online as more data and information about the process operation is collected.

It is important to mention that the algorithm can consider simultaneous cleanings of subsets of heat exchangers as long as the subsets are defined a priori. To consider this, the set of cleaning arrangements (exchangers that can be cleaned simultaneously) is defined: $SC = \{1,2, \dots, N_{SC}\}$. The number of elements of this set does not have to be the same number of exchangers in the network, it can have more or fewer elements. The parameter $C_{j,i} \forall i \in HEX, j \in SC$ is used to define the exchangers that are cleaned simultaneously for each cleaning arrangement defined. For example, if only individual cleanings of all the exchangers in the network are considered, the parameter $C_{j,i}$ is an identity matrix with dimension $N_{HEX} \times N_{HEX}$. In the case that more than one exchanger can be cleaned simultaneously, the row of the parameter $C_{j,i}$ corresponding to that cleaning arrangement will have at least two nonzero entries.

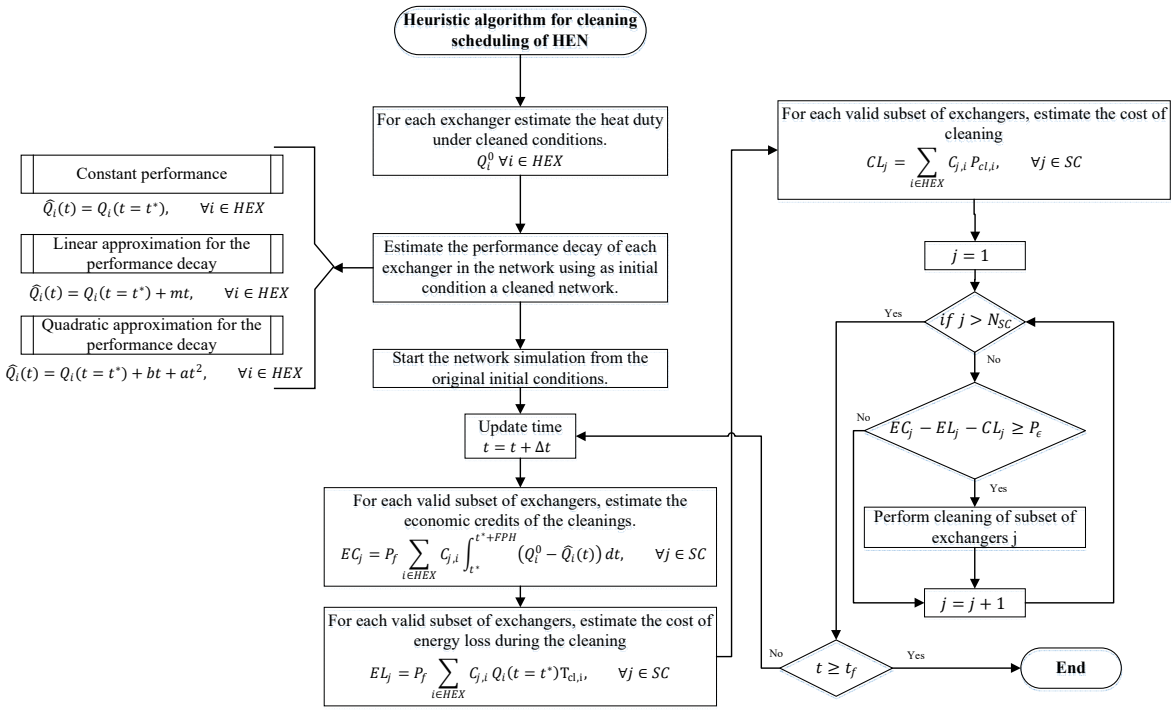

Figure C.1. Heuristic algorithm for online cleaning schedule of HEN.

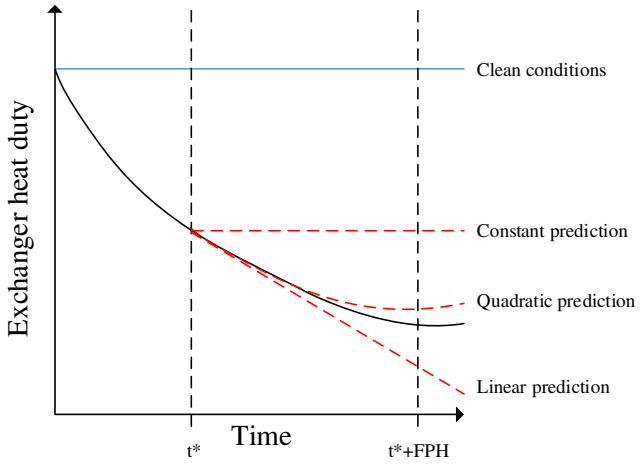

Figure C.2. Estimation of the heat duty decay for individual exchangers using three approximations.

The algorithm uses a fixed time step (Δt) at which the conditions to perform a cleaning are evaluated, and this time step can be as small as to evaluate the cleaning conditions continuously, $\Delta t \to 0$. The conditions that define when a cleaning is performed are based on an economic criterion that represents the trade-off between the energy recover in monetary value and the cleaning cost. This economic threshold is defined in Eq. (C.1). EC represents the economic credits measured as the difference between the predicted heat duty after

cleaning, and the predicted heat duty from the current conditions of the unit over a future prediction horizon FPH, Eq. (C.2). EL represents the energy loss during the cleaning for not having that exchanger or subset of exchangers operating, Eq. (C.3). CL is the cleaning cost, Eq. (C.4); and P_ϵ is the economic threshold defined by the analyst for the cleanings, in this case is zero which means that cleaning accepted are those with a break even period of FPH – the cost of the cleaning is equal to the energy recovery benefits over this time.

$$EC_j - EL_j - CL_j \geq P_\epsilon, \qquad \forall j \in SC \tag{C.1}$$

$$EC_j = P_f \sum_{i \in HEX} C_{j,i} \int_{t^*}^{t^*+FPH} \left(Q_i^0 - \widehat{Q}_\iota(t)\right) dt, \qquad \forall j \in SC \tag{C.2}$$

$$EL_j = P_f \sum_{i \in HEX} C_{j,i}\, Q_i(t = t^*)\mathrm{T}_{\mathrm{cl,i}}, \qquad \forall j \in SC \tag{C.3}$$

$$CL_j = \sum_{i \in HEX} C_{j,i}\, P_{cl,i}, \qquad \forall j \in SC \tag{C.4}$$

The algorithm finishes when the final operating time is reached. In summary, this heuristic algorithm uses an approximation of the heat duty decrease cause by fouling to predict the economic trade-off of the cleanings at each time instance. The algorithms consider network interactions and economic trade-off for defining the cleaning schedule, but it ignores the operational limits such as temperature and pressure drop limitations, and the effect of variable flow rates and stream temperatures on the performance prediction of the system.

C.2. Application to a real case study

The heuristic algorithm is used to solve the cleaning scheduling problem of the case study REF-X. This is a case study of an actual refinery for which the actual cleaning schedule is available, so that the benefits of alternative approaches can be directly compared. The specifications of the case are presented in Appendix A, and the optimal cleanings scheduling with and without control actions was obtained in Chapter 5.

The HEN has five exchangers, and four of them are double shell. For those units with multiple shells, all the shells have to be cleaned simultaneously and these constraints are imposed in the heuristic algorithms by the definition of the set of cleaning arrangements SC and of the matrix $C_{j,i}$.

C.2.1. Online cleaning scheduling

The cleaning scheduling of the case study is defined online using the heuristic algorithms, and its various ways to predict the decay of the heat duty of individual exchangers. Although the network has parallel branches, the flow split is assumed fixed at 50% for all the scenarios considered in this section.

Figure C.3 shows the Gantt charts for all the cleaning schedules considered here. They are significantly different in terms of number of cleanings, frequency of cleanings, and exchanges cleaned. For example, only in the actual cleaning schedule E05A/B is cleaned, while the other algorithms never predict a cleaning for this unit because the economic credits are not enough to compensate for the cleaning cost. For all other cleaning schedules, a pattern and constant frequency in the cleanings can be observed, which indicates the limits of the operation and the points in time at which it is beneficial to perform cleanings. While the optimal cleaning schedule – obtained in Chapter 5, Figure 5.11, for REF-X case – predicts cleanings for most of the exchangers at least once, the heuristic algorithms only predict cleanings for E01A/B and exchanger E04, and the only difference among them is the frequency and starting time of the cleanings. While the optimal alternative can capture the effects over the whole prediction horizon, the heuristic algorithms are limited to the future prediction horizon defined and the results depend on the value of this parameter. However, exchangers E01A/B and E04 are those with the highest fouling rate, therefore it is expected that their cleanings are more frequent than those of the rest.

a)

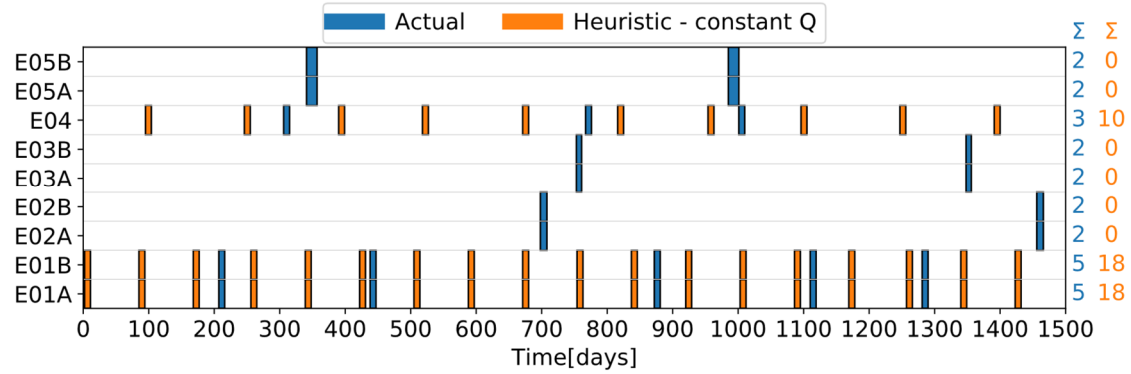

b)

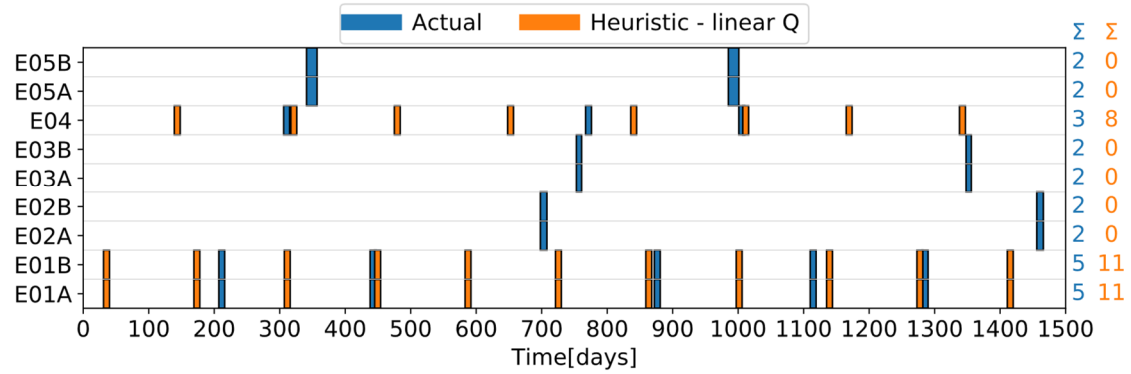

c)

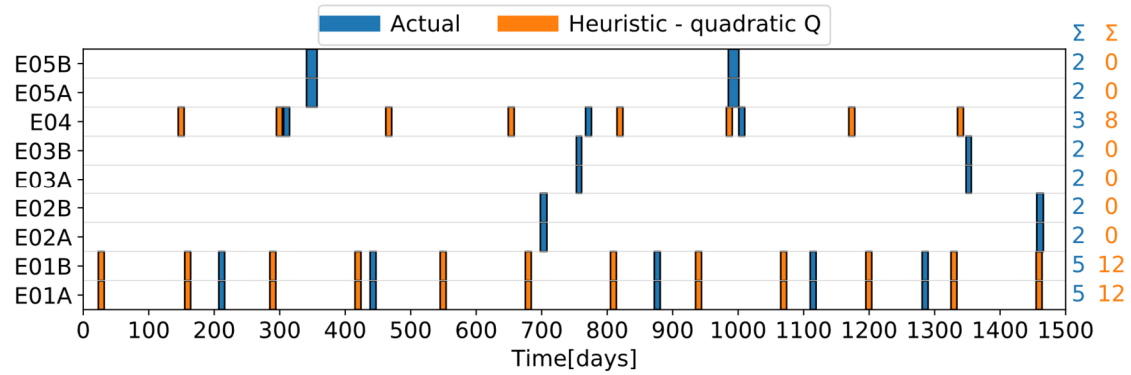

Figure C.3. Cleaning schedule of case REF-X determined by heuristic algorithms that can be applied online.

All the alternative schedules obtained from using heuristics perform better than the actual cleaning schedule, and they reduce the operational cost from $ 0.8 M to $ 1.2 M for an operation horizon of 4 years. Although all alternatives improve the operation, there is no significant difference between the benefits obtained with the linear approximation and the quadratic approximation of the heat duty decay. The predictions obtained with these two approaches are similar, and there are only small variations on the cleaning time of the exchangers.

For longer operational times the heuristic algorithms may predict the cleanings of other exchangers because the economic credits of their cleanings increase with time as the fouling thermal resistance increases. For example, Figure C.4 shows how the economic credits for each set of possible cleanings evolve with time, and it explicitly shows when certain units cross the threshold defined for the cleanings. A cleaning action in this plot is identified by the discontinuities and jumps in the value of the function, and it is defined each time a

threshold is reached. Note that the value presented include the cleaning cost, the energy cost of a unit out of service, and the potential future energy recovery of a cleaned unit, which are different for each exchanger. Finally, note that for those exchangers that are not cleaned in this operating horizon, the economic credits have an increasing trend, although it is affected by the cleanings of other units in the network.

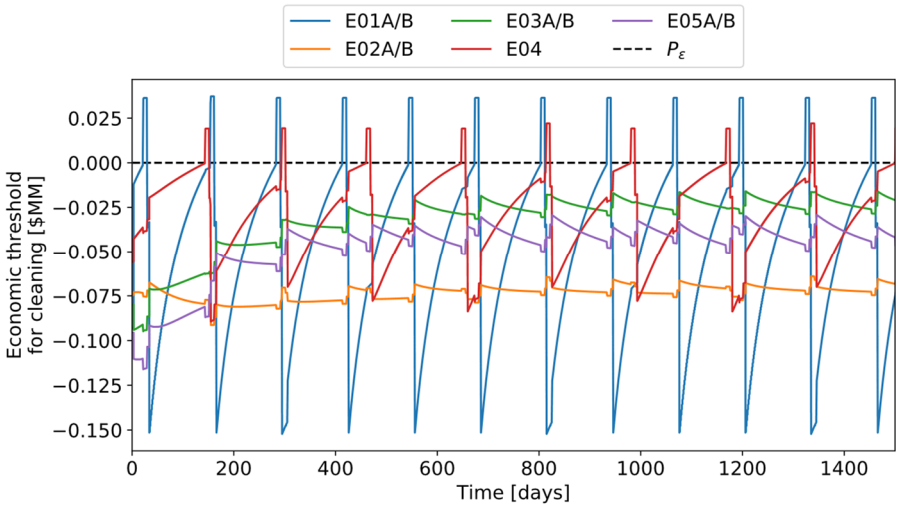

Figure C.4. Evolution of the overall benefits of cleanings – LHS of Eq. (C.1) for the case study using a quadratic approximation for the heat duty.

C.2.2. Introducing control elements

The use of heuristics can be integrated with the optimal flow distribution of the network aiming to minimize the total operating cost. To illustrate the potential of incorporating control decisions in the cleaning schedule definition, for each cleaning schedule obtained using heuristics an optimal control problem is solved to define the optimal flow distribution profiles for the network. Although this procedure is done offline after applying the heuristic algorithm and it is only done for illustration purposes, in principle a steady state optimization could be performed to optimally determine the split fraction at every sampling time.

Figure C.5 shows the furnace duty and the split fraction for those cleaning schedules obtained using the heuristic algorithm. Although the flow control is optimally defined in a sequential fashion, these results serve to illustrate the importance of the interactions between scheduling and control, and that they can both be defined online and using heuristic approximations. Regardless of the heuristic method use for predicting the duty decay, when it is coupled with the control decisions the furnace duty decreases significantly, and

reductions of up to 2.2 MW can be achieved. These important benefits are realized because the flow distribution reacts to the cleanings, so that when a unit is idle the flow is diverted from that unit if possible, and also because the flow rates are adapted dynamically to recover more energy and make the most of units with the lowest fouling resistance.

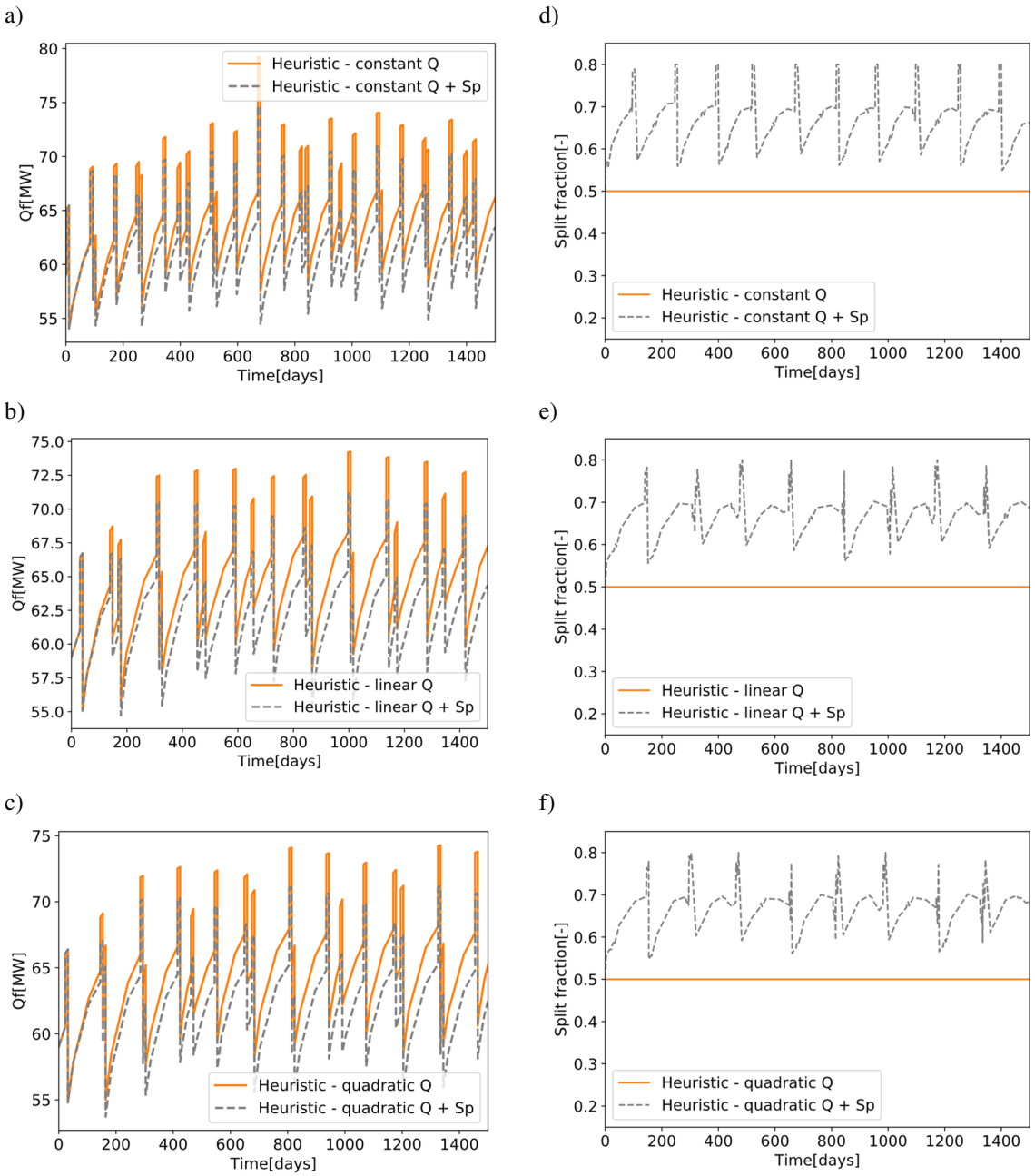

Figure C.5. Furnace duty (column 1), and split fraction to E02 branch (column 2) of the case study when the cleaning schedule is defined using heuristics (row 1: constant duty prediction, row 2: linear duty prediction, row 3: quadratic duty prediction).

The total operating cost of each cleaning schedule determine with the heuristic algorithm is compared against the actual operation, and against the optimal operation of the network – Chapter 5. Figure C.6 illustrates the cost of these alternatives, indicates the cleaning and energy cost associated with each, and demonstrates the improvements obtained when control decisions are integrated in the definition of the cleaning schedule.

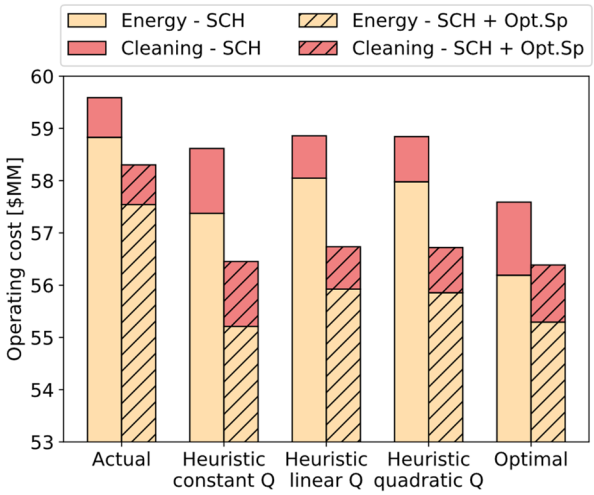

Figure C.6. Cost comparison of all alternatives for REF-X case. Using heuristics vs optimization to define the cleaning schedule of the network.

The cleaning schedules obtained with the heuristic algorithm perform better than the actual one, and worse than the optimal one. An expected result since the optimization formulation considers all possible interactions during the whole operating time. It is interesting to note that the heuristic that uses a constant prediction of the heat duty decay is the one with the lowest operational cost among all the schedules defined by heuristics, but the one with the highest cleaning cost. Although the instant economic credits are over predicted in the future prediction horizon, the overall cost during the whole operating time is greater because of the frequent cleanings. Nevertheless, there is not a large difference between this alternative and the other heuristics that use a linear or quadratic prediction of the heat duty decay. The total operational cost predicted by these alternatives differ in less than $ 0.3 M, and there is no significant difference between the schedule defined with the linear prediction of the duty, and that defined with the quadratic prediction of the duty.

Introducing optimal flow distribution on a given cleaning schedule – or done online and simultaneously – have large benefits for the operation. Even for the actual cleaning

schedule there are potential savings of $ 1.3 M by only manipulating the dynamic flow distribution. Similar cost reductions are observed when control decisions are included in the heuristic algorithms that define the cleaning schedule. The operating cost can be reduced from $ 1.8 M up to $ 2.3 M in these cases. However, none of these heuristic algorithms perform better than the optimal solution of cleaning scheduling and flow distribution. In Figure C.6 the minimum cost is observed for the optimal alternatives despite being a solution with a fixed operating horizon, instead of a online one using a rolling horizon as the heuristic approaches. No individual fouling mitigation approach can produce this reduction of the total operating cost, which shows the importance of considering both alternatives. Moreover, the simultaneous optimization of the cleaning scheduling and flow distribution control has the lowest total operating cost for the surrogate model because it considers both decisions at the same level and can exploit the synergy between them.

The use of heuristic algorithms based on a receding horizon is a preliminary study for the online fouling mitigation of HEN. The algorithms developed demonstrated that decisions involving cleaning of units can be taken on real time based on appropriate predictions of the future performance of the units, and that integrating control and scheduling decisions should be a priority to minimize the operating cost of the system. The heuristics allows a quick definition of the cleanings and cleaning sequence, although it is not optimal and does not considered all the interactions and effects in the network. More rigorous optimization based approaches are required to exploit the synergies and interactions presented in large industrial networks. Also, accurate models should be used for predicting the performance of the system so that all dynamic effects, such as changes in flow rates and stream temperatures, can be captured.

Appendix D.

Dissemination record

Journal peer-reviewed articles

Lozano Santamaría, F., Macchietto, S. Online integration of optimal cleaning scheduling and control of heat exchanger networks under fouling. Industrial & Engineering Chemistry Research 2020, 59, 2471 – 2490.

DOI: https://doi.org/10.1021/acs.iecr.9b04531

Lozano Santamaría, F, Macchietto, S. Integration of optimal cleaning scheduling and control of heat exchanger networks under fouling: MPCC solution. Computers & Chemical Engineering. 2019, 126, 128–146.

DOI: https://doi.org/10.1016/j.compchemeng.2019.04.012

Lozano Santamaría, F; Macchietto, S. Integration of Optimal Cleaning Scheduling and Control of Heat Exchanger Networks Undergoing Fouling: Model and Formulation. Industrial & Engineering Chemistry Research 2018, 57, 12842 – 12860.

DOI: https://doi.org/10.1021/acs.iecr.8b01701

Lozano Santamaría, F., Macchietto, S. Refinery preheat train network modelling and optimization: validation of surrogate model for process optimization purposes. 2020. Ready for submission to publication to Industrial and Engineering Chemistry Research journal.

Lozano Santamaría, F., Macchietto, S. Optimal heat exchanger network retrofit including fouling dynamics and cleaning scheduling. 2020. In preparation

Lozano Santamaría, F., Macchietto, S. Online control and cleaning scheduling of heat exchanger networks considering schedule stability. 2020. In preparation

Refereed conferences proceedings

Lozano Santamaría, F, Macchietto, S. Online optimal cleaning scheduling and control of heat exchanger networks under fouling with large disturbances. In proceedings of the 30th European Symposium on Computer Aided Process Engineering (ESCAPE30), 24 – 27, May 2020, Milan, Italy. Elsevier.

Lozano Santamaría, F, Honein, E, Macchietto, S. Simultaneous optimization of retrofit, cleaning schedule, and control of heat exchanger networks subject to fouling. In proceedings of the 30th European Symposium on Computer Aided Process Engineering (ESCAPE30), 24 – 27, May 2020, Milan, Italy. Elsevier.

Lozano Santamaría, F, Macchietto, S. Integration of optimal cleaning scheduling and control for fouling mitigation in heat exchanger networks: a receding horizon approach. Heat exchanger fouling & cleaning conference XIII, 2 – 7 June 2019, Josefow, Poland.

DOI: http://www.heatexchanger-fouling.com/proceedings19.htm

Lozano Santamaría, F, Macchietto, S. Model validation for the optimization of refinery preheat trains under fouling. Heat exchanger fouling & cleaning conference XIII, 2 – 7 June 2019, Josefow, Poland.

DOI: http://www.heatexchanger-fouling.com/proceedings19.htm

Lozano Santamaría, F; Macchietto, S. Integration of Optimal Cleaning Scheduling and Flow Split control for crude oil fouling mitigation in the operation of refinery heat exchanger networks. In M. R. Eden, M. Ierapetritou and G. P. Towler (Editors), Proceedings of the 13th International Symposium on Process Systems Engineering (PSE 2018), Part B, pp.1087-1092, Elsevier

DOI: https://doi.org/10.1016/B978-0-444-64241-7.50176-2

Lozano Santamaría, F; Macchietto, S. Simultaneous optimal control and optimal scheduling of heat exchanger networks subject to fouling. 13th international conference on heat transfer, fluid mechanics and thermodynamics, Portoroz, Slovenia, 2017.

DOI: http://hdl.handle.net/2263/62467

Conference presentations without proceedings

Lozano Santamaría, F; Macchietto, S. Optimal cleaning scheduling and control of heat exchanger networks: problem formulation and solution strategy. AIChE Annual meeting 2018. Pittsburgh, Pennsylvania, USA. 27 October – 2 November, 2018.

Lozano Santamaría, F; Macchietto, S. Optimal cleaning scheduling and control of heat exchanger networks: an industrial case study. AIChE Annual meeting 2018. Pittsburgh, Pennsylvania, USA. 27 October – 2 November, 2018.

Coletti, F; Lozano Santamaria, F; Diaz-Bejarano, E; Macchietto, S. Optimization of refinery preheat trains: Predictive maintenance and operations improvement. AIChE spring meeting and 14th global congress on process safety, Orlando, USA 22 – 26 April, 2018.

Lozano Santamaría, F; Macchietto, S. Reaction engineering approach to model the deposition and transformation of unwanted material in heat exchanger surfaces with refinery applications. ChemEngDay UK 2018, Molecules to Manufacturing. Leeds, UK, 2018.

Seminars and talks

Lozano Santamaría, F; Macchietto, S. Online optimal cleaning scheduling and control of heat exchanger networks under fouling. PhD Symposium, Department of Chemical Engineering, Imperial College, London, UK, 1 July, 2019.

References

Abdul-Manan, Amir F.N., Abdullah Arfaj, and Hassan Babiker. 2017. "Oil Refining in a CO2 Constrained World: Effects of Carbon Pricing on Refineries Globally." *Energy* 121 (February): 264–75. https://doi.org/10.1016/J.ENERGY.2017.01.046.

Alimohammadi, Sepideh, Sohrab Zendehboudi, and Lesley James. 2019. "A Comprehensive Review of Asphaltene Deposition in Petroleum Reservoirs: Theory, Challenges, and Tips." *Fuel* 252: 753–91. https://doi.org/https://doi.org/10.1016/j.fuel.2019.03.016.

Allgöwer, F, T A Badgwell, J S Qin, J B Rawlings, and S J Wright. 1999. "Nonlinear Predictive Control and Moving Horizon Estimation — An Introductory Overview BT - Advances in Control." In , edited by Paul M Frank, 391–449. London: Springer London.

Aminian, Javad, and Shahrokh Shahhosseini. 2009. "Neuro-Based Formulation to Predict Fouling Threshold in Crude Preheaters." *International Communications in Heat and Mass Transfer* 36 (5): 525–31. https://doi.org/10.1016/j.icheatmasstransfer.2009.01.020.

Angsutorn, Natchanon, Kitipat Siemanond, and Rungroj Chuvaree. 2014. "Heat Exchanger Network Synthesis Using MINLP Stage-Wise Model with Pinch Analysis and Relaxation." In *24 European Symposium on Computer Aided Process Engineering*, edited by Jiří Jaromír Klemeš, Petar Sabev Varbanov, and Peng Yen B T - Computer Aided Chemical Engineering Liew, 33:139–44. Elsevier. https://doi.org/https://doi.org/10.1016/B978-0-444-63456-6.50024-7.

Assis, Bruna C.G., Caroline de O. Gonçalves, Fábio S. Liporace, Sérgio G. Oliveira, Eduardo M. Queiroz, Fernando L.P. Pessoa, and André L.H. Costa. 2013. "Constrained Thermohydraulic Optimization of the Flow Rate Distribution in Crude Preheat Trains." *Chemical Engineering Research and Design* 91 (8): 1517–26. https://doi.org/10.1016/J.CHERD.2013.06.005.

Assis, Bruna C G, Julia C Lemos, Fábio S Liporace, Sérgio G Oliveira, Eduardo M Queiroz, Fernando L P Pessoa, and André L H Costa. 2015. "Dynamic Optimization of the Flow Rate Distribution in Heat Exchanger Networks for Fouling Mitigation." *Industrial &*

Engineering Chemistry Research 54 (25): 6497–6507. https://doi.org/10.1021/acs.iecr.5b00453.

Ave, Giancarlo Dalle, Mert Alici, Iiro Harjunkoski, and Sebastian Engell. 2019. "An Explicit Online Resource-Task Network Scheduling Formulation to Avoid Scheduling Nervousness." *Computer Aided Chemical Engineering* 46 (January): 61–66. https://doi.org/10.1016/B978-0-12-818634-3.50011-4.

Baldea, Michael, and Iiro Harjunkoski. 2014. "Integrated Production Scheduling and Process Control: A Systematic Review." *Computers & Chemical Engineering* 71 (December): 377–90. https://doi.org/10.1016/j.compchemeng.2014.09.002.

Banerjee, Indrani, Ravindra C Pangule, and Ravi S Kane. 2011. "Antifouling Coatings: Recent Developments in the Design of Surfaces That Prevent Fouling by Proteins, Bacteria, and Marine Organisms." *Advanced Materials* 23 (6): 690–718. https://doi.org/10.1002/adma.201001215.

Bassett, Matthew H., Joseph F. Pekny, and Gintaras V. Reklaitis. 1996. "Decomposition Techniques for the Solution of Large-Scale Scheduling Problems." *AIChE Journal* 42 (12): 3373–87. https://doi.org/10.1002/aic.690421209.

Bell, K.J. 1963. "Final Report of the Cooperative Research Program on Shell and Tube Heat Exchangers." *Engineering Experimental Station* 5.

———. 1981. "Delaware Method for Shell Side Design." In *Heat Exchangers: Thermal-Hydraulic Fundamentals and Design*, edited by S Kakac, A. E Bergles, and F Mayinger. Washington, D.C: McGraw-Hill.

Bemporad, A. 2009. "Model Predictive Control: Basic Concepts." University of Pennsylvania: University of Pennsylvania.

Bennett, Christopher A. 2012. "A Theory Describing Asphaltene Adhesion Fouling Inside Heat Exchanger Tubes." *Heat Transfer Engineering* 33 (15): 1246–50. https://doi.org/10.1080/01457632.2012.692295.

Biegler, Lorenz T. 2010. *Nonlinear Programming. Concepts, Algorithms and Applications to Chemical Process*. Edited by MOS-SIAM Series on Optimization. Philadelphi: SIAM, Society for Industrial and Applied Mathematics.

Biyanto, Totok R., M. Ramasamy, Azamuddin B. Jameran, and Henokh Y. Fibrianto. 2016. "Thermal and Hydraulic Impacts Consideration in Refinery Crude Preheat Train

Cleaning Scheduling Using Recent Stochastic Optimization Methods." *Applied Thermal Engineering* 108 (September): 1436–50. https://doi.org/10.1016/J.APPLTHERMALENG.2016.05.068.

Blackburn, Joseph D, Dean H Kropp, and Robert A Millen. 1986. "A Comparison of Strategies to Dampen Nervousness in MRP Systems." *Management Science* 32 (4): 413–29. https://doi.org/10.1287/mnsc.32.4.413.

Bott, T.R. 1990. *Fouling Notebook*. Rugby: Institution of Chemical Engineers.

———. 1995. *Fouling of Heat Exchangers*. Elsevier Science. https://doi.org/https://doi.org/10.1016/B978-0-444-82186-7.X5000-3.

Brodowicz, Kazimierz, and Mariusz Markowski. 2003. "Calculation of Heat Exchanger Networks for Limiting Fouling Effects in the Petrochemical Industry." *Applied Thermal Engineering* 23 (17): 2241–53. https://doi.org/https://doi.org/10.1016/S1359-4311(03)00190-X.

Burnham, Alison J, John F MacGregor, and Román Viveros. 1999. "Latent Variable Multivariate Regression Modeling." *Chemometrics and Intelligent Laboratory Systems* 48 (2): 167–80. https://doi.org/https://doi.org/10.1016/S0169-7439(99)00018-0.

Burnham, Alison J, Roman Viveros, and John F MacGregor. 1996. "Frameworks for Latent Variable Multivariate Regression." *Journal of Chemometrics* 10 (1): 31–45. https://doi.org/10.1002/(SICI)1099-128X(199601)10:1<31::AID-CEM398>3.0.CO;2-1.

Charnes, A, W W Cooper, and E Rhodes. 1978. "Measuring the Efficiency of Decision Making Units." *European Journal of Operational Research* 2 (6): 429–44. https://doi.org/https://doi.org/10.1016/0377-2217(78)90138-8.

Chen, Heng, Peiyuan Pan, Xiaolu Chen, Yungang Wang, and Qinxin Zhao. 2017. "Fouling of the Flue Gas Cooler in a Large-Scale Coal-Fired Power Plant." *Applied Thermal Engineering* 117: 698–707. https://doi.org/10.1016/j.applthermaleng.2017.02.048.

Chu, Yunfei, and Fengqi You. 2012. "Integration of Scheduling and Control with Online Closed-Loop Implementation: Fast Computational Strategy and Large-Scale Global Optimization Algorithm." *Computers & Chemical Engineering* 47 (December): 248–68. https://doi.org/10.1016/J.COMPCHEMENG.2012.06.035.

Ciric, A R, and C A Floudas. 1989. “A Retrofit Approach for Heat Exchanger Networks.” *Computers & Chemical Engineering* 13 (6): 703–15. https://doi.org/https://doi.org/10.1016/0098-1354(89)80008-0.

Coletti, F., E. M. Ishiyama, W. R. Paterson, D. I. Wilson, and S. Macchietto. 2010. “Impact of Deposit Aging and Surface Roughness on Thermal Fouling: Distributed Model.” *AIChE Journal* 56 (12): 3257–73. https://doi.org/10.1002/aic.12221.

Coletti, F, B.D Crittenden, and S Macchietto. 2015. “Chapter Two – Basic Science of the Fouling Process.” In *Crude Oil Fouling*, 23–50. https://doi.org/10.1016/B978-0-12-801256-7.00002-6.

Coletti, F, H M Joshi, S Macchietto, and G F Hewitt. 2015. “Chapter One – Introduction.” In *Crude Oil Fouling*, 1–22. https://doi.org/10.1016/B978-0-12-801256-7.00001-4.

Coletti, Francesco. 2010. “Multi-Scale Modelling of Refinery Pre-Heat Trains Undergoing Fouling for Improved Energy Efficiency.” Imperial College of London.

Coletti, Francesco, and G F Hewitt. 2015. *Crude Oil Fouling. Deposit Characterization, Measurements, and Modelling*. Edited by Francesco Coletti and G F Hewitt. 1st editio. London: Gulf Professional Publishing.

Coletti, Francesco, and Sandro Macchietto. 2011a. “Refinery Pre-Heat Train Network Simulation Undergoing Fouling: Assessment of Energy Efficiency and Carbon Emissions.” *Heat Transfer Engineering* 32 (3–4): 228–36. https://doi.org/10.1080/01457632.2010.495606.

———. 2011b. “A Dynamic, Distributed Model of Shell-and-Tube Heat Exchangers Undergoing Crude Oil Fouling.” *Industrial & Engineering Chemistry Research* 50 (8): 4515–33. https://doi.org/10.1021/ie901991g.

Coletti, Francesco, Sandro Macchietto, and Graham T Polley. 2011. “Effects of Fouling on Performance of Retrofitted Heat Exchanger Networks: A Thermo-Hydraulic Based Analysis.” *Computers & Chemical Engineering* 35 (5): 907–17. https://doi.org/https://doi.org/10.1016/j.compchemeng.2011.01.027.

Costa, André Luiz Hemerly, Viviane Barbosa Guimarães Tavares, Joana Lopes Borges, Eduardo Mach Queiroz, Fernando Luiz Pellegrini Pessoa, Fábio dos Santos Liporace, and Sergio Gregório de Oliveira. 2013. “Parameter Estimation of Fouling Models in

Crude Preheat Trains." *Heat Transfer Engineering* 34 (8–9): 683–91. https://doi.org/10.1080/01457632.2012.738566.

Cott, B J, and S Macchietto. 1989. "Minimizing the Effects of Batch Process Variability Using Online Schedule Modification." *Computers & Chemical Engineering* 13 (1): 105–13. https://doi.org/https://doi.org/10.1016/0098-1354(89)89011-8.

Deka, Dimbalita, and Dilip Datta. 2017. "Multi-Objective Optimization of the Scheduling of a Heat Exchanger Network under Milk Fouling." *Knowledge-Based Systems* 121 (April): 71–82. https://doi.org/10.1016/j.knosys.2016.12.027.

Deshannvar, U. B., M. S. Rafeen, M. Ramasamy, and D. Subbarao. 2010. "Crude Oil Fouling: A Review." *Journal of Applied Sciences* 10 (24): 3167–74.

Diaby, Abdullatif Lacina, Lee Luong, Amer Yousef, and Jonas Addai Mensah. 2012. "A Review of Optimal Scheduling Cleaning of Refinery Crude Preheat Trains Subject to Fouling and Ageing." *Applied Mechanics and Materials* 148–149: 643–51. https://doi.org/10.4028/www.scientific.net/AMM.148-149.643.

Diaby, Abdullatif Lacina, Stanley Joseph Miklavcic, and Jonas Addai-Mensah. 2016. "Optimization of Scheduled Cleaning of Fouled Heat Exchanger Network under Ageing Using Genetic Algorithm." *Chemical Engineering Research and Design* 113 (September): 223–40. https://doi.org/10.1016/j.cherd.2016.07.013.

Diaby, Abdullatif Lacina, Stanley Joseph Miklavcic, Saiful Bari, and Jonas Addai-Mensah. 2016. "Evaluation of Crude Oil Heat Exchanger Network Fouling Behavior Under Aging Conditions for Scheduled Cleaning." *Heat Transfer Engineering* 37 (15): 1211–30. https://doi.org/10.1080/01457632.2015.1119583.

Dias, Lisia S, and Marianthi G Ierapetritou. 2016. "Integration of Scheduling and Control under Uncertainties: Review and Challenges." *Chemical Engineering Research and Design*, November. https://doi.org/10.1016/j.cherd.2016.10.047.

———. 2020a. "Integration of Planning, Scheduling and Control Problems Using Data-Driven Feasibility Analysis and Surrogate Models." *Computers & Chemical Engineering* 134: 106714. https://doi.org/https://doi.org/10.1016/j.compchemeng.2019.106714.

———. 2020b. “110th Anniversary: Integration of Scheduling and Robust Model Predictive Control.” *Industrial & Engineering Chemistry Research* 59 (1): 265–80. https://doi.org/10.1021/acs.iecr.9b02545.

Diaz-Bejarano, E., E. Behranvand, F. Coletti, M.R. Mozdianfard, and S. Macchietto. 2017. “Organic and Inorganic Fouling in Heat Exchangers – Industrial Case Study: Analysis of Fouling State.” *Applied Energy* 206 (November): 1250–66. https://doi.org/10.1016/J.APENERGY.2017.10.018.

Diaz-Bejarano, E., F. Coletti, and S. Macchietto. 2017. “Thermo-Hydraulic Analysis of Refinery Heat Exchangers Undergoing Fouling.” *AIChE Journal* 63 (3): 984–1001. https://doi.org/10.1002/aic.15457.

Diaz-Bejarano, Emilio, Francesco Coletti, and Sandro Macchietto. 2015. “Beyond Fouling Factors: A Reaction Engineering Approach to Crude Oil Fouling Modelling.” In *Proceedings of International Conference on Heat Exchanger Fouling and Cleaning2*, edited by M R Malayeri, H Muller-Steinhagen, and A P Watkinson, 89–96. PP Publico Publications.

———. 2016. “A New Dynamic Model of Crude Oil Fouling Deposits and Its Application to the Simulation of Fouling-Cleaning Cycles.” *AIChE Journal* 62 (1): 90–107. https://doi.org/10.1002/aic.15036.

———. 2017. “Crude Oil Fouling Deposition, Suppression, Removal, and Consolidation—and How to Tell the Difference.” *Heat Transfer Engineering* 38 (7–8): 681–93. https://doi.org/10.1080/01457632.2016.1206408.

———. 2018. “Complex Crude Oil Fouling Layers: Use of Model Predictions to Detect Inorganics Breakthrough.” *Applied Thermal Engineering* 141: 666–74. https://doi.org/https://doi.org/10.1016/j.applthermaleng.2018.05.097.

Díaz-Bejarano, Emilio, Francesco Coletti, and Sandro Macchietto. 2015. “Detection of Changes in Fouling Behavior by Simultaneous Monitoring of Thermal and Hydraulic Performance of Refinery Heat Exchangers.” *Computer Aided Chemical Engineering* 37 (January): 1649–54. https://doi.org/10.1016/B978-0-444-63577-8.50120-0.

Donselaar, K van, J van den Nieuwenhof, and J Visschers. 2000. “The Impact of Material Coordination Concepts on Planning Stability in Supply Chains.” *International Journal*

of Production Economics 68 (2): 169–76. https://doi.org/10.1016/S0925-5273(00)00033-5.

Ebert, Richmond, and IL Panchal. 1995. “Analysis of Exxon Crude-Oil-Slip Stream Coking Data.” In . United States. http://www.osti.gov/scitech/servlets/purl/453433.

Ellis, Matthew, and Panagiotis D Christofides. 2014. “Integrating Dynamic Economic Optimization and Model Predictive Control for Optimal Operation of Nonlinear Process Systems.” *Control Engineering Practice* 22 (0): 242–51. https://doi.org/http://dx.doi.org/10.1016/j.conengprac.2013.02.016.

Ellis, Matthew, and Helen Durand. 2014. “A Tutorial Review of Economic Model Predictive Control Methods.” *Journal of Process Control* 24 (8): 1156–78. https://doi.org/10.1016/J.JPROCONT.2014.03.010.

Ellis, Matthew, Helen Durand, and Panagiotis D Christofides. 2016. “Elucidation of the Role of Constraints in Economic Model Predictive Control.” *Annual Reviews in Control* 41: 208–17. https://doi.org/https://doi.org/10.1016/j.arcontrol.2016.04.004.

Ellis, Matthew, Jinfeng Liu, and Panagiotis D Christofides. 2017. *Economic Model Predictive Control. Theory, Formulations and Chemical Process Applications*. Springer Nature Switzerland.

Emani, Sampath, M. Ramasamy, and Ku Zilati Ku Shaari. 2019. “Discrete Phase-CFD Simulations of Asphaltenes Particles Deposition from Crude Oil in Shell and Tube Heat Exchangers.” *Applied Thermal Engineering* 149 (February): 105–18. https://doi.org/10.1016/J.APPLTHERMALENG.2018.12.008.

Epstein, N. 1983. “Thinking about Heat Transfer Fouling: A 5 × 5 Matrix AU - EPSTEIN, NORMAN.” *Heat Transfer Engineering* 4 (1): 43–56. https://doi.org/10.1080/01457638108939594.

Farrell, M J. 1957. “The Measurement of Productive Efficiency.” *Journal of the Royal Statistical Society. Series A (General)* 120 (3): 253–90. https://doi.org/10.2307/2343100.

Fletcher, Roger, and Leyffer Sven. 2004. “Solving Mathematical Programs with Complementarity Constraints as Nonlinear Programs.” *Optimization Methods and Software* 19 (1): 15–40. https://doi.org/10.1080/10556780410001654241.

Flores-Tlacuahuac, Antonio, and Ignacio E Grossmann. 2006. “Simultaneous Cyclic Scheduling and Control of a Multiproduct CSTR.” *Industrial & Engineering Chemistry Research* 45 (20): 6698–6712. https://doi.org/10.1021/ie051293d.

Floudas, C A, A R Ciric, and I E Grossmann. 1986. “Automatic Synthesis of Optimum Heat Exchanger Network Configurations.” *AIChE Journal* 32 (2): 276–90. https://doi.org/10.1002/aic.690320215.

Floudas, C A, and I E Grossmann. 1987. “Synthesis of Flexible Heat Exchanger Networks with Uncertain Flowrates and Temperatures.” *Computers & Chemical Engineering* 11 (4): 319–36. https://doi.org/https://doi.org/10.1016/0098-1354(87)85014-7.

Floudas, Christodoulos A., and Xiaoxia Lin. 2004. “Continuous-Time versus Discrete-Time Approaches for Scheduling of Chemical Processes: A Review.” *Computers & Chemical Engineering* 28 (11): 2109–29. https://doi.org/10.1016/j.compchemeng.2004.05.002.

Flower, John R, and Bodo Linnhoff. 1980. “A Thermodynamic-Combinatorial Approach to the Design of Optimum Heat Exchanger Networks.” *AIChE Journal* 26 (1): 1–9. https://doi.org/10.1002/aic.690260102.

Georgiadis, Michael C, Lazaros G Papageorgiou, and Sandro Macchietto. 2000. “Optimal Cleaning Policies in Heat Exchanger Networks under Rapid Fouling.” *Industrial & Engineering Chemistry Research* 39 (2): 441–54. https://doi.org/10.1021/ie990166c.

Georgiadis, Michael C, Guillermo E Rotstein, and Sandro Macchietto. 1998. “Optimal Design and Operation of Heat Exchangers under Milk Fouling.” *AIChE Journal* 44 (9): 2099–2111. https://doi.org/10.1002/aic.690440917.

Gerrard, A. M. 2000. *Guide to Capital Cost Estimating*. 4th ed. Rugby: Institution of Chemical Engineers.

Gomes da Cruz, L, E M Ishiyama, C Boxler, W Augustin, S Scholl, and D I Wilson. 2015. “Value Pricing of Surface Coatings for Mitigating Heat Exchanger Fouling.” *Food and Bioproducts Processing* 93: 343–63. https://doi.org/https://doi.org/10.1016/j.fbp.2014.05.003.

Gonçalves, Caroline de O., Eduardo M. Queiroz, Fernando L.P. Pessoa, Fábio S. Liporace, Sérgio G. Oliveira, and André L.H. Costa. 2014. “Heuristic Optimization of the

Cleaning Schedule of Crude Preheat Trains." *Applied Thermal Engineering* 73 (1): 3–14. https://doi.org/10.1016/j.applthermaleng.2014.07.036.

Gounder, Ramasamy Marappa, and Sampath Emani. 2017. "CFD Simulation of Crude Oil Fouling on Heat Transfer Surfaces." In *Computational Fluid Dynamics - Basic Instruments and Applications in Science*, edited by Adela Ionescu, 357–75. intechopen. https://doi.org/10.5772/intechopen.71886.

Graves, Stephen C. 1981. "A Review of Production Scheduling." *Operations Research* 29 (4): 646–75. https://doi.org/10.1287/opre.29.4.646.

Gupta, Dhruv, and Christos T. Maravelias. 2016. "On Deterministic Online Scheduling: Major Considerations, Paradoxes and Remedies." *Computers & Chemical Engineering* 94 (November): 312–30. https://doi.org/10.1016/J.COMPCHEMENG.2016.08.006.

Han, Jeongwoo, Grant S. Forman, Amgad Elgowainy, Hao Cai, Michael Wang, and Vincent B. DiVita. 2015. "A Comparative Assessment of Resource Efficiency in Petroleum Refining." *Fuel* 157: 292–98. https://doi.org/10.1016/j.fuel.2015.03.038.

Hart, William E, Jean-Paul Watson, and David L Woodruff. 2011. "Pyomo: Modeling and Solving Mathematical Programs in Python." *Mathematical Programming Computation* 3: 219–60.

Herty, M, and S Steffensen. 2012. "MPCC Solution Approaches for a Class of MINLPs with Application in Chemical Engineering."

Hewitt, G F, G L Shires, and T R Bott. 1994. *Process Heat Transfer*. Boca raton, Florida: CRC PRESS.

Hexxcell Ltd. 2016. "Hexxcell Studio." 2016. http://www.hexxcell.com/technology/software/.

Ho, Teh C. 2016a. "A Study of Crude Oil Fouling Propensity." *International Journal of Heat and Mass Transfer* 95: 62–68. https://doi.org/10.1016/j.ijheatmasstransfer.2015.11.086.

———. 2016b. "A Study of Crude Oil Fouling Propensity." *International Journal of Heat and Mass Transfer* 95 (April): 62–68. https://doi.org/10.1016/J.IJHEATMASSTRANSFER.2015.11.086.

Hodrick, Robert J, and Edward Prescott. 1981. “Post-War U.S. Business Cycles: An Empirical Investigation.” Discussion Papers. Northwestern University, Center for Mathematical Studies in Economics and Management Science. https://doi.org/DOI:

International Panel on Climate Change IPCC. 2014. “Climate Change 2014: Mitigation of Climate Change.” https://www.ipcc.ch/report/ar5/wg3/.

Ishiyama, E M, A V Heins, W R Paterson, L Spinelli, and D I Wilson. 2010. “Scheduling Cleaning in a Crude Oil Preheat Train Subject to Fouling: Incorporating Desalter Control.” *Applied Thermal Engineering* 30 (13): 1852–62. https://doi.org/http://dx.doi.org/10.1016/j.applthermaleng.2010.04.027.

Ishiyama, E M, W R Paterson, and D I Wilson. 2009. “Platform for Techno-Economic Analysis of Fouling Mitigation Options in Refinery Preheat Trains.” *Energy & Fuels* 23 (3): 1323–37. https://doi.org/10.1021/ef8005614.

Ishiyama, Edward. M, Francesco Coletti, Sandro Macchietto, W R Paterson, and D I Wilson. 2010. “Impact of Deposit Ageing on Thermal Fouling: Lumped Parameter Model.” *AIChE Journal* 56 (2): 531–45. https://doi.org/10.1002/aic.11978.

Ishiyama, Edward. M, Simon J Pugh, J Kennedy, D.I. Wilson, A Ogden-Quin, and G Birch. 2013. “An Industrial Case Study on Retrofitting Heat Exchangers and Revamping Preheat Trains Subject to Fouling.” In *Proceedings of International Conference on Heat Exchanger Fouling and Cleaning*, edited by Mohamamd Reza Malayeri, H Muller-Steinhagen, and A P Watkinson.

Ishiyama, Edward M., William R. Paterson, and D. Ian Wilson. 2011. “Optimum Cleaning Cycles for Heat Transfer Equipment Undergoing Fouling and Ageing.” *Chemical Engineering Science* 66 (4): 604–12. https://doi.org/10.1016/j.ces.2010.10.036.

Ishiyama, Edward M, William R. Paterson, and D. Ian Wilson. 2010. “Exploration of Alternative Models for the Aging of Fouling Deposits.” *AIChE Journal* 57 (11): 3199–3209. https://doi.org/10.1002/aic.12514.

Ishiyama, Edward M, William R Paterson, and D Ian Wilson. 2014. “Aging Is Important: Closing the Fouling–Cleaning Loop.” *Heat Transfer Engineering* 35 (3): 311–26. https://doi.org/10.1080/01457632.2013.825192.

Ishiyama, Edward M, S.J. Pugh, J Kennedy, and D.I. Wilson. 2015. “Effect of Scheduling Cleaning of Crude Preheat Train Exchangers on the Operating Conditions of Fired

Heaters." In *International Conference on Heat Exchanger Fouling and Cleaning*, edited by M R Malayeri, H Muller-Steinhagen, and A P Watkinson, 435–44. Dublin, Ireland.

Ismaili, Riham Al, Min Woo Lee, D Ian Wilson, and Vassilios S Vassiliadis. 2018. "Heat Exchanger Network Cleaning Scheduling: From Optimal Control to Mixed-Integer Decision Making." *Computers & Chemical Engineering* 111: 1–15. https://doi.org/https://doi.org/10.1016/j.compchemeng.2017.12.004.

———. 2019. "Optimisation of Heat Exchanger Network Cleaning Schedules: Incorporating Uncertainty in Fouling and Cleaning Model Parameters." *Computers & Chemical Engineering* 121: 409–21. https://doi.org/https://doi.org/10.1016/j.compchemeng.2018.11.009.

Jacobs, F.R, W.L Berry, D.C Whybark, and T.E Vollmann. 2005. "Advanced MRP." In *Manufacturing Planning and Control for Supply Chain Management*. New York: McGraw-Hill.

Kadam, J V, M Schlegel, W Marquardt, R L Tousain, D H van Hessem, J van den Berg, and O H Bosgra. 2002. "A Two-Level Strategy of Integrated Dynamic Optimization and Control of Industrial Processes—a Case Study." In *European Symposium on Computer Aided Process Engineering-12*, edited by Johan Grievink and Jan B T - Computer Aided Chemical Engineering van Schijndel, 10:511–16. Elsevier. https://doi.org/https://doi.org/10.1016/S1570-7946(02)80113-4.

Kadam, Jitendra, Martin Schlegel, Wolfgang Marquardt, Okko H Bosgra, A Dunnebier, A A Tiagounov, A.C.P.M. Backx, and Philip J M Brouwer. 2003. "Towards Integrated Dynamic Real-Time Optimization and Control of Industrial Processes." In .

Kadipasaoglu, S N, and S V Sridharan. 1997. "Measurement of Instability in Multi-Level MRP Systems." *International Journal of Production Research* 35 (3): 713–37. https://doi.org/10.1080/002075497195678.

Kemp, I.C. 2006. *Pinch Analysis and Process Integration. A User Guide on Process Integration for the Efficient Use of Energy*. Butterworth-Heinemann.

Lachas-Fuentes, Laura. 2015. "Optimal Operation of Heat Exchanger Networks." Imperial College of London.

Lal, Nathan S, Timothy G Walmsley, Michael R W Walmsley, Martin J Atkins, and James R Neale. 2018. “A Novel Heat Exchanger Network Bridge Retrofit Method Using the Modified Energy Transfer Diagram.” *Energy* 155: 190–204. https://doi.org/https://doi.org/10.1016/j.energy.2018.05.019.

Lanchas-Fuentes, L, E Dias-Bejarano, F Coletti, and S Macchietto. 2016. “Management of Cleaning Types and Schedules in Refinery Heat Exchangers.” In *12th International Conference on Heat Transfer, Fluid Mechanics and Thermodynamics. HEFAT2016*. Costa del Sol, Spain.

Laouini, A., C. Charcosset, H. Fessi, and K. Schroen. 2014. “Use of Dynamic Membranes for the Preparation of Vitamin E-Loaded Lipid Particles: An Alternative to Prevent Fouling Observed in Classical Cross-Flow Emulsification.” *Chemical Engineering Journal* 236: 498–505. https://doi.org/10.1016/j.cej.2013.10.053.

Lavaja, Javier H, and Miguel J Bagajewicz. 2004. “On a New MILP Model for the Planning of Heat-Exchanger Network Cleaning.” *Industrial & Engineering Chemistry Research* 43 (14): 3924–38. https://doi.org/10.1021/ie034178g.

———. 2005a. “On a New MILP Model for the Planning of Heat-Exchanger Network Cleaning. Part II: Throughput Loss Considerations.” *Industrial & Engineering Chemistry Research* 44 (21): 8046–56. https://doi.org/10.1021/ie0503186.

———. 2005b. “On a New MILP Model for the Planning of Heat-Exchanger Network Cleaning. Part III: Multiperiod Cleaning under Uncertainty with Financial Risk Management.” *Industrial & Engineering Chemistry Research* 44 (21): 8136–46. https://doi.org/10.1021/ie050319y.

Lemos, Julia Coelho, Bruna Carla Gonçalves Assis, André Luiz Hemerly Costa, Eduardo Mach Queiroz, Fernando Luiz Pellegrini Pessoa, Fábio dos Santos Liporace, and Séergio Gregório de Oliveira. 2015. “A Sliding Mixed-Integer Linear Programming Approach for the Optimization of the Cleaning Schedule of Crude Preheat Trains.” *Heat Transfer Engineering* 36 (7–8): 642–51. https://doi.org/10.1080/01457632.2015.954920.

Li, Bao-Hong, and Chuei-Tin Chang. 2010. “Retrofitting Heat Exchanger Networks Based on Simple Pinch Analysis.” *Industrial & Engineering Chemistry Research* 49 (8): 3967–71. https://doi.org/10.1021/ie9016607.

Li, Zukui, and Marianthi Ierapetritou. 2008. “Process Scheduling under Uncertainty: Review and Challenges.” *Computers & Chemical Engineering* 32 (4): 715–27. https://doi.org/https://doi.org/10.1016/j.compchemeng.2007.03.001.

Liu, Xin-wen, Xing Luo, and Hu-gen Ma. 2014. “Studies on the Retrofit of Heat Exchanger Network Based on the Hybrid Genetic Algorithm.” *Applied Thermal Engineering* 62 (2): 785–90. https://doi.org/https://doi.org/10.1016/j.applthermaleng.2013.10.036.

Macchietto, S, G F Hewitt, F Coletti, B D Crittenden, D R Dugwell, A Galindo, G Jackson, et al. 2011. “Fouling in Crude Oil Preheat Trains: A Systematic Solution to an Old Problem.” *Heat Transfer Engineering* 32 (3–4): 197–215. https://doi.org/10.1080/01457632.2010.495579.

Maciejowski, J M. 2002. *Predictive Control with Constraints*. Prentice Hall.

Markowski, M. 2000. “Reconstruction of a Heat Exchanger Network under Industrial Constraints — the Case of a Crude Distillation Unit.” *Applied Thermal Engineering* 20 (15): 1535–44. https://doi.org/https://doi.org/10.1016/S1359-4311(00)00022-3.

Marquardt, Wolfgang. 2002. “Nonlinear Model Reduction for Optimization Based Control of Transient Chemical Processes.” In .

Master, B.I., K.S. Chunangad, and V. Pushpanathan. 2003. “Fouling Mitigation Using Helix-Changer Heat Exchangers.” In *Proceedings of the ECI Conference on Heat Exchanger Fouling and Cleaning: Fundamentals and Applications*, 317–22. Santa Fe, US.

McAdams, W. H. 1954. *Heat Transmission*. 3rd ed. New York: McGraw-Hill.

Meadows, Edward, and J Rawlings. 1997. “Model Predictive Control.” In *Nonlinear Process Control*, 233–310.

Méndez, Carlos A, Jaime Cerdá, Ignacio E Grossmann, Iiro Harjunkoski, and Marco Fahl. 2006. “State-of-the-Art Review of Optimization Methods for Short-Term Scheduling of Batch Processes.” *Computers & Chemical Engineering* 30 (6): 913–46. https://doi.org/https://doi.org/10.1016/j.compchemeng.2006.02.008.

Mouret, Sylvain, Ignacio E Grossmann, and Pierre Pestiaux. 2011. “Time Representations and Mathematical Models for Process Scheduling Problems.” *Computers & Chemical Engineering* 35 (6): 1038–63. https://doi.org/https://doi.org/10.1016/j.compchemeng.2010.07.007.

Mozdianfard, Mohammad Reza, and Elaheh Behranvand. 2013. “A Field Study of Fouling in CDU Preheaters at Esfahan Refinery.” *Applied Thermal Engineering* 50 (1): 908–17. https://doi.org/10.1016/J.APPLTHERMALENG.2012.08.025.

———. 2015. “Fouling at Post Desalter and Preflash Drum Heat Exchangers of CDU Preheat Train.” *Applied Thermal Engineering* 89 (October): 783–94. https://doi.org/10.1016/J.APPLTHERMALENG.2015.06.045.

Muller-Steinhagen, H. 2000. *Handbook of Heat Exchanger Fouling: Mitigation and Cleaning Technologies*. Essen: Publico Publications.

Müller-Steinhagen, H, M R Malayeri, and A P Watkinson. 2011. “Heat Exchanger Fouling: Mitigation and Cleaning Strategies.” *Heat Transfer Engineering* 32 (3–4): 189–96. https://doi.org/10.1080/01457632.2010.503108.

Muller-Steinhagen, H, and H.U Zettler. 2011. *Heat Exchanger Fouling. Mitigation and Cleaning Technologies*. 2do ed. Essen: PP Publico.

Müller-Steinhagen, Hans. 2011. “Heat Transfer Fouling: 50 Years After the Kern and Seaton Model.” *Heat Transfer Engineering* 32 (1): 1–13. https://doi.org/10.1080/01457632.2010.505127.

Nategh, Mahshid, Mohamamd Reza Malayeri, and Hojjat Mahdiyar. 2017. “A Review on Crude Oil Fouling and Mitigation Methods in Pre-Heat Trains of Iranian Oil Refineries.” *Journal of Oil, Gas and Petrochemical Technology* 4 (Number 1): 1–17. https://doi.org/10.22034/jogpt.2017.58055.

Navvab Kashani, Moein, Javad Aminian, Shahrokh Shahhosseini, and Mohammad Farrokhi. 2012. “Dynamic Crude Oil Fouling Prediction in Industrial Preheaters Using Optimized ANN Based Moving Window Technique.” *Chemical Engineering Research and Design* 90 (7): 938–49. https://doi.org/https://doi.org/10.1016/j.cherd.2011.10.013.

Nguyen, Duy Quang, Andres Barbaro, Narumon Vipanurat, and Miguel J Bagajewicz. 2010. “All-At-Once and Step-Wise Detailed Retrofit of Heat Exchanger Networks Using an MILP Model.” *Industrial & Engineering Chemistry Research* 49 (13): 6080–6103. https://doi.org/10.1021/ie901235c.

Nie, Yisu, Lorenz T Biegler, Carlos M Villa, and John M Wassick. 2015. “Discrete Time Formulation for the Integration of Scheduling and Dynamic Optimization.” *Industrial*

& Engineering Chemistry Research 54 (16): 4303–15. https://doi.org/10.1021/ie502960p.

Pahlavanzadeh, H, M R Jafari Nasr, and S H Mozaffari. 2007. "Experimental Study of Thermo-Hydraulic and Fouling Performance of Enhanced Heat Exchangers." *International Communications in Heat and Mass Transfer* 34 (7): 907–16. https://doi.org/https://doi.org/10.1016/j.icheatmasstransfer.2007.04.002.

Pan, Ming, Igor Bulatov, and Robin Smith. 2013a. "New MILP-Based Iterative Approach for Retrofitting Heat Exchanger Networks with Conventional Network Structure Modifications." *Chemical Engineering Science* 104: 498–524. https://doi.org/https://doi.org/10.1016/j.ces.2013.09.049.

———. 2013b. "Exploiting Tube Inserts to Intensify Heat Transfer for the Retrofit of Heat Exchanger Networks Considering Fouling Mitigation." *Industrial & Engineering Chemistry Research* 52 (8): 2925–43. https://doi.org/10.1021/ie303020m.

———. 2016. "Improving Heat Recovery in Retrofitting Heat Exchanger Networks with Heat Transfer Intensification, Pressure Drop Constraint and Fouling Mitigation." *Applied Energy* 161: 611–26. https://doi.org/https://doi.org/10.1016/j.apenergy.2015.09.073.

Panchal, C B, and Ehr-Ping Huangfu. 2000. "Effects of Mitigating Fouling on the Energy Efficiency of Crude-Oil Distillation." *Heat Transfer Engineering* 21 (3): 3–9. https://doi.org/10.1080/014576300270843.

Papoulias, Soterios A, and Ignacio E Grossmann. 1983a. "A Structural Optimization Approach in Process Synthesis—I: Utility Systems." *Computers & Chemical Engineering* 7 (6): 695–706. https://doi.org/https://doi.org/10.1016/0098-1354(83)85022-4.

———. 1983b. "A Structural Optimization Approach in Process Synthesis—II: Heat Recovery Networks." *Computers & Chemical Engineering* 7 (6): 707–21. https://doi.org/https://doi.org/10.1016/0098-1354(83)85023-6.

Paterson, W.R., and P.J. Fryer. 1988. "A Reaction Engineering Approach to the Analysis of Fouling." *Chemical Engineering Science* 43 (7): 1714–17. https://doi.org/10.1016/0009-2509(88)85166-2.

Pinto, Jose M, and Ignacio E Grossmann. 1998. “Assignment and Sequencing Models for Thescheduling of Process Systems.” *Annals of Operations Research* 81 (0): 433–66. https://doi.org/10.1023/A:1018929829086.

Pistikopoulos, Efstratios N., and Nikolaos A. Diangelakis. 2016. “Towards the Integration of Process Design, Control and Scheduling: Are We Getting Closer?” *Computers & Chemical Engineering* 91 (August): 85–92. https://doi.org/10.1016/J.COMPCHEMENG.2015.11.002.

Pitarch, J L, C G Palacín, C De Prada, B Voglauer, and G Seyfriedsberger. 2017. “Optimisation of the Resource Efficiency in an Industrial Evaporation System.” *Journal of Process Control* 56: 1–12. https://doi.org/https://doi.org/10.1016/j.jprocont.2017.04.002.

Pitarch Pérez, José Luis, Carlos Gomez Palacin, and César de Prada Moraga. 2017. “Online Decision Support for an Evaporation Network.” In *XXXVIII Jornadas de Automatica*, 575–81. Servicio de Publicaciones de la Universidad de Oviedo.

Pogiatzis, Thomas A, D Ian Wilson, and Vassilios S Vassiliadis. 2012. “Scheduling the Cleaning Actions for a Fouled Heat Exchanger Subject to Ageing: MINLP Formulation.” *Computers & Chemical Engineering* 39: 179–85. https://doi.org/https://doi.org/10.1016/j.compchemeng.2011.12.012.

Powell, M Kody, N Ammon Eaton, D John Hedengren, and F Thomas Edgar. 2016. “A Continuous Formulation for Logical Decisions in Differential Algebraic Systems Using Mathematical Programs with Complementarity Constraints.” *Processes* . https://doi.org/10.3390/pr4010007.

Prakash, Sangeeta, Olena Kravchuk, and Hilton Deeth. 2015. “Influence of Pre-Heat Temperature, Pre-Heat Holding Time and High-Heat Temperature on Fouling of Reconstituted Skim Milk during UHT Processing.” *Journal of Food Engineering* 153: 45–52. https://doi.org/10.1016/j.jfoodeng.2014.12.009.

Puhakka, Eini, Markus Riihimäki, and Riitta L Keiski. 2007. “Molecular Modeling Approach on Fouling of the Plate Heat Exchanger: Titanium Hydroxyls, Silanols, and Sulphates on TiO2 Surfaces.” *Heat Transfer Engineering* 28 (3): 248–54. https://doi.org/10.1080/01457630601066921.

Pujawan, I Nyoman. 2004. “Schedule Nervousness in a Manufacturing System: A Case Study.” *Production Planning & Control* 15 (5): 515–24. https://doi.org/10.1080/09537280410001726320.

Qian, Zhiguang, Carolyn Conner Seepersad, V Roshan Joseph, Janet K Allen, and C F Jeff Wu. 2005. “Building Surrogate Models Based on Detailed and Approximate Simulations.” *Journal of Mechanical Design* 128 (4): 668–77. https://doi.org/10.1115/1.2179459.

Qin, S.Joe, and Thomas A Badgwell. 2003. “A Survey of Industrial Model Predictive Control Technology.” *Control Engineering Practice* 11 (7): 733–64. https://doi.org/http://dx.doi.org/10.1016/S0967-0661(02)00186-7.

Raghunathan, Arvind U, and Lorenz T Biegler. 2003. “Mathematical Programs with Equilibrium Constraints (MPECs) in Process Engineering.” *Computers & Chemical Engineering* 27 (10): 1381–92. https://doi.org/10.1016/S0098-1354(03)00092-9.

Raghunathan, Arvind U, M Soledad Diaz, and Lorenz T Biegler. 2004. “An MPEC Formulation for Dynamic Optimization of Distillation Operations.” *Computers & Chemical Engineering* 28 (10): 2037–52. https://doi.org/10.1016/j.compchemeng.2004.03.015.

Ramos, Manuel A, Jorge M Gómez, and Jean-Michel Reneaume. 2014. “Simultaneous Optimal Design and Control of an Extractive Distillation System for the Production of Fuel Grade Ethanol Using a Mathematical Program with Complementarity Constraints.” *Industrial & Engineering Chemistry Research* 53 (2): 752–64. https://doi.org/10.1021/ie402232w.

Ravn, Morten O, and Harald Uhlig. 2002. “On Adjusting the Hodrick-Prescott Filter for the Frequency of Observations.” *The Review of Economics and Statistics* 84 (2): 371–76. https://doi.org/10.1162/003465302317411604.

Rawlings, J B, D Angeli, and C N Bates. 2012. “Fundamentals of Economic Model Predictive Control.” In *2012 IEEE 51st IEEE Conference on Decision and Control (CDC)*, 3851–61. https://doi.org/10.1109/CDC.2012.6425822.

Rennard, Jean’Philippe. 2006. “Stochastic Optimization Algorithms.” In *Handbook of Research on Nature Inspired Computing for Economics and Management*. Hershey, IGR.

Riazi, M.R. 2005. *Characterization and Properties of Petroleum Fractions*. 1st ed. Philadelphia: ASTM manual series MNL50.

Risbeck, Michael J., Christos T. Maravelias, and James B. Rawlings. 2019. "Unification of Closed-Loop Scheduling and Control: State-Space Formulations, Terminal Constraints, and Nominal Theoretical Properties." *Computers & Chemical Engineering* 129 (October): 106496. https://doi.org/10.1016/J.COMPCHEMENG.2019.06.021.

Robertson, Douglas G, Jay H Lee, and James B Rawlings. 1996. "A Moving Horizon-Based Approach for Least-Squares Estimation." *AIChE Journal* 42 (8): 2209–24. https://doi.org/10.1002/aic.690420811.

Rodriguez, C., and R. Smith. 2007. "Optimization of Operating Conditions for Mitigating Fouling in Heat Exchanger Networks." *Chemical Engineering Research and Design* 85 (6): 839–51. https://doi.org/10.1205/cherd06046.

Scarborough, C.E., D.C. Cherrington, R. Diener, and L.P. Golan. 1979. "Cokinf of Crude Oil at High Heat Flux Levels." *Chemical Engineering Processing* 75: 41–46.

Sheikh, Anwar K, Syed M Zubair, Muhammad Younas, and M.O Budair. 2000. "A Risk Based Heat Exchanger Analysis Subject to Fouling: Part II: Economics of Heat Exchangers Cleaning." *Energy* 25 (5): 445–61. https://doi.org/10.1016/S0360-5442(99)00081-X.

Shi, Hanyu, Yunfei Chu, and Fengqi You. 2015. "Novel Optimization Model and Efficient Solution Method for Integrating Dynamic Optimization with Process Operations of Continuous Manufacturing Processes." *Industrial & Engineering Chemistry Research* 54 (7): 2167–87. https://doi.org/10.1021/ie503857r.

Simkoff, Jodie M., and Michael Baldea. 2019. "Production Scheduling and Linear MPC: Complete Integration via Complementarity Conditions." *Computers & Chemical Engineering* 125 (June): 287–305. https://doi.org/10.1016/J.COMPCHEMENG.2019.01.024.

Smaïli, F, V S Vassiliadis, and D I Wilson. 2001. "Mitigation of Fouling in Refinery Heat Exchanger Networks by Optimal Management of Cleaning." *Energy & Fuels* 15 (5): 1038–56. https://doi.org/10.1021/ef010052p.

———. 2002. “Optimization of Cleaning Schedulesin Heat Exchanger Networkssubject to Fouling.” *Chemical Engineering Communications* 189 (11): 1517–49. https://doi.org/10.1080/00986440214999.

Somerscales, Euan F C, and Arthur E Bergles. 1997. “Enhancement of Heat Transfer and Fouling Mitigation.” In , edited by James P Hartnett, Jr. Irvine Thomas F., Young I Cho, and George A B T - Advances in Heat Transfer Greene, 30:197–253. Elsevier. https://doi.org/https://doi.org/10.1016/S0065-2717(08)70252-1.

Sridharan, Sri V, William L Berry, and V Udayabhanu. 1988. “MEASURING MASTER PRODUCTION SCHEDULE STABILITY UNDER ROLLING PLANNING HORIZONS.” *Decision Sciences* 19 (1): 147–66. https://doi.org/10.1111/j.1540-5915.1988.tb00259.x.

Stan Jones, D, and P Pujado. 2006. *Handbook of Petroleum Processing*. Springer, Dordrecht.

Subramanian, Kaushik, James B. Rawlings, and Christos T. Maravelias. 2014. “Economic Model Predictive Control for Inventory Management in Supply Chains.” *Computers & Chemical Engineering* 64 (May): 71–80. https://doi.org/10.1016/J.COMPCHEMENG.2014.01.003.

Sundaramoorthy, Arul, and Christos T Maravelias. 2011. “Computational Study of Network-Based Mixed-Integer Programming Approaches for Chemical Production Scheduling.” *Industrial & Engineering Chemistry Research* 50 (9): 5023–40. https://doi.org/10.1021/ie101419z.

Tavares, Viviane Barbosa Guimarães, Joana Lopes Borges, Eduardo Mach Queiroz, Fernando Luiz Pellegrini Pessoa, Fábio dos Santos Liporace, and Sergio Gregório de Oliveira. 2013. “Parameter Estimation of Fouling Models in Crude Preheat Trains AU - Costa, André Luiz Hemerly.” *Heat Transfer Engineering* 34 (8–9): 683–91. https://doi.org/10.1080/01457632.2012.738566.

TEMA. 2007. *Standards of the Tubular Exchanger Manufacturers Association*. 9th ed. New York.

Thulukkanam, Kuppan. 2013. “Shell and Tube Heat Exchanger Design.” In *Heat Exchanger Design Handbook*, 237–336. CRC PRESS.

Tian, Jiayang, Yufei Wang, and Xiao Feng. 2016. “Simultaneous Optimization of Flow Velocity and Cleaning Schedule for Mitigating Fouling in Refinery Heat Exchanger Networks.” *Energy* 109: 1118–29. https://doi.org/10.1016/j.energy.2016.05.053.

Tjoe, T.N, and B Linnhoff. 1986. “Using Pinch Technology for Process Retrofit.” *Chemical Engineering*, 47–60.

Trafczynski, M., M. Markowski, S. Alabrudzinski, and K. Urbaniec. 2016. “The Influence of Fouling on the Dynamic Behavior of PID-Controlled Heat Exchangers.” *Applied Thermal Engineering* 109 (October): 727–38. https://doi.org/10.1016/j.applthermaleng.2016.08.142.

U.S. Energy Information Administration. 2016. “International Energy Outlook 2016.” Washington, D.C. http://www.eia.gov/forecasts/ieo/.

Varbanov, Petar Sabev, Jiří Jaromír Klemeš, and Ferenc Friedler. 2011. “Cell-Based Dynamic Heat Exchanger Models—Direct Determination of the Cell Number and Size.” *Computers & Chemical Engineering* 35 (5): 943–48. https://doi.org/10.1016/j.compchemeng.2011.01.033.

Wächter, Andreas, and T Lorenz Biegler. 2006. “On the Implementation of an Interior-Point Filter Line-Search Algorithm for Large-Scale Nonlinear Programming.” *Mathematical Programming* 106 (1): 25–57. https://doi.org/10.1007/s10107-004-0559-y.

Walmsley, Timothy G, Nathan S Lal, Petar S Varbanov, and Jiří J Klemeš. 2018. “Automated Retrofit Targeting of Heat Exchanger Networks.” *Frontiers of Chemical Science and Engineering* 12 (4): 630–42. https://doi.org/10.1007/s11705-018-1747-2.

Wang, Yong, Zongming Yuan, Ying Liang, Ying Xie, Xingyi Chen, and Xiaoqing Li. 2015. “A Review of Experimental Measurement and Prediction Models of Crude Oil Fouling Rate in Crude Refinery Preheat Trains.” *Asia-Pacific Journal of Chemical Engineering* 10 (4): 607–25. https://doi.org/10.1002/apj.1895.

Wang, Yufei, and Robin Smith. 2013. “Retrofit of a Heat-Exchanger Network by Considering Heat-Transfer Enhancement and Fouling.” *Industrial & Engineering Chemistry Research* 52 (25): 8527–37. https://doi.org/10.1021/ie4000097.

Wang, Yufei, Shihui Zhan, and Xiao Feng. 2015. “Optimization of Velocity for Energy Saving and Mitigating Fouling in a Crude Oil Preheat Train with Fixed Network

Structure." *Energy* 93 (December): 1478–88. https://doi.org/10.1016/j.energy.2015.09.130.

Wansaseub, Kittinan, Nantiwat Pholdee, and Sujin Bureerat. 2017. "Optimal U-Shaped Baffle Square-Duct Heat Exchanger through Surrogate-Assisted Self-Adaptive Differential Evolution with Neighbourhood Search and Weighted Exploitation-Exploration." *Applied Thermal Engineering* 118: 455–63. https://doi.org/https://doi.org/10.1016/j.applthermaleng.2017.02.100.

Watkinson, A P, and D I Wilson. 1997. "Chemical Reaction Fouling: A Review." *Experimental Thermal and Fluid Science* 14 (4): 361–74. https://doi.org/https://doi.org/10.1016/S0894-1777(96)00138-0.

Wiehe, Irwin A, and Raymond J Kennedy. 2000. "The Oil Compatibility Model and Crude Oil Incompatibility." *Energy & Fuels* 14 (1): 56–59. https://doi.org/10.1021/ef990133+.

Wilson, D.I., G.T. Polley, and S.J. Pugh. 2005. "Ten Years of Ebert, Panchal and the Threshold Fouling Concept." In *Heat Exchanger Fouling and Cleaning - Challenges and Opportunities*, edited by Hans Muller-Steinhagen, M. Reza Malayeri, and A. Paul Watkinson. Kloster Irsee, Germany.

Wilson, D Ian, Edward M Ishiyama, and Graham T Polley. 2017. "Twenty Years of Ebert and Panchal—What Next?" *Heat Transfer Engineering* 38 (7–8): 669–80. https://doi.org/10.1080/01457632.2016.1206407.

Yang, Junfeng, Maria G.Jimenez Serratos, Damilola S. Fari-Arole, Erich A. Müller, and Omar K. Matar. 2015. "Crude Oil Fouling: Fluid Dynamics, Reactions and Phase Change." In *Procedia IUTAM*, 15:186–93. Elsevier. https://doi.org/10.1016/j.piutam.2015.04.026.

Yeap, B.L., D.I. Wilson, G.T. Polley, and S.J. Pugh. 2004. "Mitigation of Crude Oil Refinery Heat Exchanger Fouling Through Retrofits Based on Thermo-Hydraulic Fouling Models." *Chemical Engineering Research and Design* 82 (1): 53–71. https://doi.org/10.1205/026387604772803070.

Yeap, B L, G T Polley, S J Pugh, and D I Wilson. 2005. "Retrofitting Crude Oil Refinery Heat Exchanger Networks to Minimize Fouling While Maximizing Heat Recovery."

Heat Transfer Engineering 26 (1): 23–34. https://doi.org/10.1080/01457630590890139.

Yee, T F, and I E Grossmann. 1990. “Simultaneous Optimization Models for Heat Integration—II. Heat Exchanger Network Synthesis.” *Computers & Chemical Engineering* 14 (10): 1165–84. https://doi.org/https://doi.org/10.1016/0098-1354(90)85010-8.

Yee, Terrence F, and Ignacio E Grossmann. 1991. “A Screening and Optimization Approach for the Retrofit of Heat-Exchanger Networks.” *Industrial & Engineering Chemistry Research* 30 (1): 146–62. https://doi.org/10.1021/ie00049a023.

Zavala, Victor M, and Lorenz T Biegler. 2009. “Nonlinear Programming Strategies for State Estimation and Model Predictive Control BT - Nonlinear Model Predictive Control: Towards New Challenging Applications.” In , edited by Lalo Magni, Davide Martino Raimondo, and Frank Allgöwer, 419–32. Berlin, Heidelberg: Springer Berlin Heidelberg. https://doi.org/10.1007/978-3-642-01094-1_33.